Fátima
Mariño Fernández

PhD Thesis

Design and Characterization of Lubricants Based on Functionalized Nanoparticles

Santiago de Compostela, 2023

DOCTORAL THESIS

DESIGN AND CHARACTERIZATION OF LUBRICANTS BASED ON FUNCTIONALIZED NANOPARTICLES

Fátima Mariño Fernández

INTERNATIONAL PHD SCHOOL OF THE UNIVERSITY OF SANTIAGO DE COMPOSTELA

PHD PROGRAMME IN FLUID THERMODYNAMICS ENGINEERING

SANTIAGO DE COMPOSTELA

2023

D./Dña. **Fátima Mariño Fernández**

Título de la tesis: **Design and characterization of lubricants based on functionalized nanoparticles**

Presento mi tesis, siguiendo el procedimiento adecuado al Reglamento y declaro que:

1) La tesis abarca los resultados de la elaboración de mi trabajo.
2) De ser el caso, en la tesis se hace referencia a las colaboraciones que tuvo este trabajo.
3) Confirmo que la tesis no incurre en ningún tipo de plagio de otros autores ni de trabajos presentados por mí para la obtención de otros títulos.
4) La tesis es la versión definitiva presentada para su defensa y coincide la versión impresa con la presentada en formato electrónico.

Y me comprometo a presentar el Compromiso Documental de Supervisión en el caso que el original no esté depositado en la Escuela.

En **Santiago de Compostela**, **25 de agosto de 2023**.

Firma electrónica

AUTORIZACIÓN DEL DIRECTOR / TUTOR DE LA TESIS

Design and characterization of lubricants based on
functionalized nanoparticles

D./Dª. Josefa Fernández Pérez
D./Dª. Enriqueta R. López Iglesias

INFORMAN:

Que la presente tesis, se corresponde con el trabajo realizado por Dª. Fátima Mariño Fernández, bajo nuestra dirección, y autorizamos su presentación, considerando que reúne los requisitos exigidos en el Reglamento de Estudios de Doctorado de la USC, y que como directoras de esta no incurre en las causas de abstención establecidas en la Ley 40/2015.

De acuerdo con lo indicado en el Reglamento de Estudios de Doctorado, declaramos también que la presente tesis doctoral es idónea para ser defendida en base a la modalidad de Monográfica con reproducción de publicaciones, en los que la participación de la doctoranda fue decisiva para su elaboración y las publicaciones se ajustan al Plan de Investigación.

En Santiago de Compostela, 23 de Agosto de 2023

ABSTRACT

The main objective of this PhD Thesis is to design and characterize efficient nanolubricants based on three polyalphaolefins (PAOs) and functionalized nanoparticles (NPs) for wind turbine gearboxes and transmissions of electric vehicles, EV. Preliminary tests and an in-depth study of the literature on time stability of nanodispersions containing chemically modified nanoadditives were carried out to analyze factors such as morphology, size and coating type, concluding that organic acid coated spherical metallic or ceramic oxide NPs with diameters lower than 20 nm show longer stability times and enhanced tribological results. Another analyzed factor was preparation method of the nanolubricant, finding that the evaporation method leads to long-lasting dispersions.

Therefore, three NPs (ZnO-OA, 10 nm, TiO_2, 5 nm, and SiO_2, 8 nm) and two modifying agents (oleic acid, OA, and stearic acid, SA) were selected, to synthetize three coated spherical NPs: ZnO-OA, TiO_2-OA and SiO_2-SA NPs. All the coated NPs were morphologically characterized (TEM or SEM) and the coatings were verified by Fourier transform infrared spectroscopy and Raman. Polyalphaolefin base oils were selected for the preparation of the nanolubricants due to the excellent physical and chemical properties compared to other types of base oils. The specific PAOs used were chosen to match the needed working conditions of the applications; a high-viscosity PAO, PAO40, for the gearboxes, and low-viscosity PAOs, PAO6 and PAO8, for the EV electric drivetrains.

Tribological and thermophysical properties of PAO40 + ZnO-OA NPs nanolubricants were evaluated. The OA coating made possible the preparation of homogeneous nanodispersions at different concentrations (0.10-1.00 wt%) of ZnO-OA NPs in PAO40 oil, reaching 29 days of stability (0.25 wt%). Both density and viscosity values increased with the concentration of NPs, furthermore, the experimental results were compared with predictive models. Pure-sliding tribological tests were performed at 80 °C using an Anton Paar MCR 302 rheometer equipped with a tribological ball-on-three-pins configuration testing module. The optimal concentration was 0.25 wt% of ZnO-OA, with 25 % coefficient of friction (COF) reduction and 82 % cross-sectional area reduction, respect to those obtained with the neat base oil. Rolling, mending, polishing, and tribofilm formation mechanisms owing to the spherical shape of the nanoadditives, the reduced roughness and the presence of PAO40, ZnO-OA NPs and iron oxides, that was evidenced from confocal Raman microscopy on the worn surfaces, explain the better tribological performance of the optimal nanolubricant with respect to that of neat PAO40.

PAO8 nanodispersions of TiO_2-OA were formulated with concentrations between 0.10 wt% and 0.50 wt% of TiO_2-OA NPs, all of them also contained 0.20 wt% OA as a dispersant to enhance stability. The OA coating and dispersant increased the stability times from 24 h (TiO_2 NPs) to at least 4 weeks (until 0.35 wt% TiO_2-OA). The thermophysical analysis of PAO8 + 0.35 wt% + 0.20 wt% OA showed almost no variation on the density values, and an increment up to 15 % on the dynamic viscosity due to the addition of both additives. Tribological experiments were performed under pure sliding and rolling-sliding conditions at 120 °C. All

the nanolubricants showed lower friction coefficients than that obtained with the PAO8 base oil, reaching maximum reductions for the 0.35 wt% TiO_2-OA nanolubricant, for both types of test conditions. Under pure sliding conditions the highest wear reductions were 26 %, 65 % and 73 %, in wear track width (WTW), wear track depth (WTD) and cross-sectional area, respectively. Through confocal Raman microscopy and roughness study of the worn samples, it can be inferred that tribofilm, mending and polishing mechanisms occur. On the other hand, nanodispersions of (0.05–0.30 wt%) SiO_2-SA NPs in PAO6, that also contained SA as a dispersant, were studied. The stability reached up to 100 days for the nanodispersion of PAO6 + SiO_2-SA NPs + SA, while only having 48 h stability the nanodispersions of PAO6 + SiO_2 NPs. Concerning the thermophysical characterization, the PAO6 + 0.20 wt% SiO_2-SA + 0.20 wt% SA had no effect on the density of PAO6 and a maximum increment of 13 % in the dynamic viscosity. The same tribological tests as in the TiO_2-OA work were performed. The optimum concentration for COF reduction was 0.30 wt% for both tribological conditions. The best antiwear results were achieved with PAO6 + 0.20 wt% SiO_2-SA + 0.20 wt% SA with reductions of 55%, 86% and 92%, in WTW, WTD and wear area, respectively. Tribological mechanisms of the nanoparticles have been analyzed through roughness measurements, concluding that polishing, mending, and tribofilm formation occur. Moreover, the effect of the coating and the dispersant were evaluated separately, concluding that the SA dispersant can act as an antifriction additive but does not reduce wear, additionally, there is a synergistic effect between the SA and the SiO_2-SA NPs; concerning the effect of the coating, it was verified that the presence of a SA layer can help the SiO_2 NPs enhance the tribological properties. Finally, the nanodispersion PAO6 + 0.20 wt% SiO_2-SA + 0.20 wt% SA, was compared to PAO6 + 0.20 wt% zinc dialkyl dithiophosphate, proving that the nanodispersion has better tribological properties than the mixture containing the commercial additive.

In conclusion, this thesis fulfilled its objectives, developing potential nanolubricants based on PAOs formulated NPs chemically modified with amphiphilic molecules that improved the stability of the nanodispersions compared to the corresponding ones with bare NPs and effectively reduce friction and wear in tests under laboratory conditions. It is also found that the addition of the same organic acid as dispersant as well as modifying agent leads to excellent synergies for tribological enhancements and long-lasting stabilities.

RESUMEN

El objetivo principal de esta Tesis Doctoral es diseñar y caracterizar nanolubricantes eficientes basados en tres polialfaolefinas (PAOs) y nanopartículas (NPs) funcionalizadas para multiplicadoras de aerogeneradores y transmisiones eléctricas de vehículos eléctricos, VE. Se realizaron ensayos preliminares y un estudio en profundidad de la bibliografía sobre la estabilidad en el tiempo de nanodispersiones que contienen nanoaditivos modificados químicamente para analizar factores como la morfología, el tamaño y el tipo de recubrimiento, concluyendo que las NPs esféricas de óxidos metálicos o cerámicos recubiertas de ácidos orgánicos con diámetros inferiores a 20 nm muestran mayores tiempos de estabilidad y mejores resultados tribológicos. Otro factor analizado fue el método de preparación del nanolubricante, encontrándose que el método de evaporación conduce a dispersiones de larga duración.

Por lo tanto, se seleccionaron tres NPs (ZnO-OA, 10 nm, TiO_2, 5 nm, y SiO_2, 8 nm) y dos agentes modificadores (ácido oleico, OA, y ácido esteárico, SA), para sintetizar tres NPs esféricas recubiertas: ZnO-OA, TiO_2-OA y SiO_2-SA. Todas las NPs recubiertas se caracterizaron morfológicamente (TEM o SEM) y los recubrimientos se verificaron por espectroscopía infrarroja de transformada de Fourier y Raman. Para la preparación de los nanolubricantes se seleccionaron aceites base de polialfaolefina debido a sus excelentes propiedades físicas y químicas en comparación con otros tipos de aceites base. Las PAO específicas utilizadas se eligieron para ajustarse a las condiciones de trabajo necesarias de las aplicaciones; una PAO de alta viscosidad, PAO40, para multiplicadoras, y PAO de baja viscosidad, PAO6 y PAO8, para las transmisiones eléctricas de los VE.

Se evaluaron las propiedades tribológicas y termofísicas de los nanolubricantes PAO40 + ZnO-OA NPs. El recubrimiento de OA hizo posible la preparación de nanodispersiones homogéneas a diferentes concentraciones (0,10-1,00 % en peso) de NPs de ZnO-OA en aceite PAO40, alcanzando 29 días de estabilidad (0,25 % en peso). Tanto los valores de densidad como de viscosidad aumentaron con la concentración de NPs, además, los resultados experimentales se compararon con modelos predictivos. Se realizaron pruebas tribológicas de deslizamiento puro a 80 ºC utilizando un reómetro Anton Paar MCR 302 equipado con un módulo de pruebas tribológicas de configuración de bola sobre tres pines. La concentración óptima fue del 0,25 % en peso de ZnO-OA, con una reducción del 25 % del coeficiente de fricción (COF) y del 82 % del área de la sección transversal, respecto a las obtenidas con el aceite base puro. Los mecanismos de rodadura, reparación, pulido y formación de tribofilm debidos a la forma esférica de los nanoaditivos, la rugosidad reducida y la presencia de PAO40, NPs de ZnO-OA y óxidos de hierro, que se evidenció a partir de microscopía confocal Raman en las superficies desgastadas, explican el mejor rendimiento tribológico del nanolubricante óptimo con respecto al del PAO40 puro.

Se formularon nanodispersiones de PAO8 y TiO_2-OA con concentraciones comprendidas entre el 0,10 % en peso y el 0,50 % en peso de NPs de TiO_2-OA, todas ellas contenían también 0,20 % en peso de OA como dispersante para mejorar la estabilidad. El recubrimiento de OA y el

dispersante aumentaron los tiempos de estabilidad desde 24 h (TiO$_2$ NPs) hasta al menos 4 semanas (hasta 0,35 % en peso de TiO$_2$-OA NPs). El análisis termofísico de PAO8 + 0,35 % en peso + 0,20 % en peso de OA no mostró prácticamente ninguna variación en los valores de densidad, y un incremento de hasta el 15 % en la viscosidad dinámica debido a la adición de ambos aditivos. Se realizaron experimentos tribológicos en condiciones de deslizamiento puro y de rodadura-deslizamiento a 120 °C. Todos los nanolubricantes mostraron coeficientes de fricción inferiores a los obtenidos con el aceite base PAO8, alcanzando reducciones máximas en el caso del nanolubricante TiO$_2$-OA al 0,35 % en peso, para ambos tipos de condiciones de ensayo. En condiciones de deslizamiento puro, las mayores reducciones de desgaste fueron del 26 %, 65 % y 73 %, en ancho de huella de desgaste (WTW), profundidad de huella de desgaste (WTD) y área transversal, respectivamente. Mediante microscopía confocal Raman y estudio de rugosidad de las muestras desgastadas, se puede inferir que se producen mecanismos de tribofilm, reparación y pulido. Por otro lado, se estudiaron nanodispersiones de (0,05-0,30 wt%) NPs de SiO$_2$-SA en PAO6, que también contenían SA como dispersante. La estabilidad alcanzó hasta 100 días para la nanodispersión de PAO6 + SiO$_2$-SA NPs + SA, mientras que sólo tuvieron 48 h de estabilidad las nanodispersiones de PAO6 + SiO$_2$ NPs. En cuanto a la caracterización termofísica, la PAO6 + 0,20 % en peso de SiO$_2$-SA + 0,20 % en peso de SA no tuvo ningún efecto sobre la densidad de la PAO6 y un incremento máximo del 13 % en la viscosidad dinámica. Se realizaron las mismas pruebas tribológicas que en el trabajo de TiO$_2$-OA. La concentración óptima para la reducción del COF fue del 0,30 % en peso para ambas condiciones tribológicas. Los mejores resultados antidesgaste se obtuvieron con PAO6 + 0,20 wt% SiO$_2$-SA + 0,20 wt% SA con reducciones del 55%, 86% y 92%, en WTW, WTD y área de desgaste, respectivamente. Se han analizado los mecanismos tribológicos de las nanopartículas mediante mediciones de rugosidad, concluyendo que se produce pulido, reparación y formación de tribofilm. Además, se evaluó el efecto del recubrimiento y del dispersante por separado, concluyendo que el dispersante SA puede actuar como aditivo antifricción, pero no reduce el desgaste, además, existe un efecto sinérgico entre el SA y las NPs de SiO$_2$-SA; en cuanto al efecto del recubrimiento, se verificó que la presencia de una capa de SA puede ayudar a las NPs de SiO$_2$ a mejorar las propiedades tribológicas. Por último, la nanodispersión PAO6 + 0,20 wt% SiO$_2$-SA + 0,20 wt% SA, se comparó con PAO6 + 0,20 wt% dialquilditiofosfato de zinc (ZDDP), demostrando que la nanodispersión tiene mejores propiedades tribológicas que la mezcla que contiene el aditivo comercial.

En conclusión, esta tesis cumplió sus objetivos, desarrollando potenciales nanolubricantes basados en NPs formuladas con PAOs modificados químicamente con moléculas anfifílicas que mejoraron la estabilidad de las nanodispersiones en comparación con las correspondientes con NPs sin recubrir y reducen eficazmente la fricción y el desgaste en ensayos bajo condiciones de laboratorio. También se ha comprobado que la adición del mismo ácido orgánico como dispersante y como agente modificador da lugar a excelentes sinergias para mejoras tribológicas y estabilidades duraderas.

AGRADECIMIENTOS

Quería agradecer a todas las personas e instituciones que me han acompañado durante los pasados cuatro años y han hecho posible el desarrollo de este trabajo.

En primer lugar, a mis directoras de tesis, Prof. Josefa Fernández Pérez y Prof. Enriqueta R. López, por darme la posibilidad de llegar hasta aquí. Sin su ayuda y enseñanzas a lo largo de estos años no habría sido posible. También a los demás miembros de nuestro grupo de investigación por haber estado ahí.

A todos los profesores y compañeros del departamento de Física Aplicada y del grupo NaFoMat, por su compañía en los descansos del café con los que he podido pasar muy buenos ratos.

A los miembros del iMATUS con los que he tenido la oportunidad de colaborar y de los que he aprendido mucho, en especial a los grupos NANOMAG (Prof. José Rivas y Dr. Yolanda Piñeiro) e I+D Farma (Prof. Carlos A. García González y Prof. Carmen Isabel Álvarez Lorenzo).

Al servicio de apoyo a la investigación de la Universidad de Santiago de Compostela, RIAIDT, sobre todo a la Ezequiel Vázquez, por su ayuda en la caracterización de las muestras. También a María Herrero por enseñarme a utilizar el perfilómetro. Así como a Prof. Juan Manuel Ruso Veiras y a Prof. Carmen Isabel Álvarez Lorenzo, por darme acceso a sus reómetros Anton Paar MCR 302.

Al programa IACOBUS y al Prof. Jorge H. O. Seabra por brindarme la oportunidad de realizar una estancia de investigación en su grupo en la Universidad de Porto y al Dr. David E. P. Gonçalves por enseñarme a utilizar el tribómetro EHD2.

Y, por último, el más profundo agradecimiento a mis padres y a mi pareja por apoyarme siempre, animarme en mis momentos de duda y celebrar conmigo los logros conseguidos por el camino, esta tesis no habría sido posible sin vosotros.

ACRONYM LIST

Acronym	Meaning
3-MPS	3-(Trimethoxysilyl)propyl methacrylate
AAD%	Absolute average deviation
AEAPS	3-(2-Aminoethylamino)propyldimethoxymethylsilane
API	American Petroleum Institute
APTES	(3-Aminopropyl)triethoxysilane
ATR	Attenuated total reflectance
BA	Benzoic acid
BHSN	Bifunctional hairy silica nanoparticle
CDs	Carbon dots
CNPs	Carbon nanoparticles
CQDs	Carbon quantum dots
COF	Coefficient of friction
CTAB	Cetrimonium bromide
CVT	Automatic continuously variable transmissions
DDA	Dodecylamine
DDP	Dodecylphosphate
DETAS	N1-(3-trimethoxysilylpropyl)diethylenetriamine)
DCT	Automatic dual-clutch transmissions
DIOS	Dioctyl sebacate
DLS	Dynamic light scattering
DPA	Diphenylamine
DSG	Automatic direct-shift gearbox
DTS	Dodecyltrichlorosilane
EHD	Elastohydrodynamic
ERDF	European Regional Development Fund
ETF	Electric transmission fluids
EV	Electric vehicle
F	Axial force
FEUP	Faculdade de Engenharia da Universidade do Porto
F_N	Normal force
FTIR	Fourier transform infrared spectroscopy
GO	Graphene oxide
GOPS	3-Glycidoxypropyltrimethoxysilane
h-BN	Hexagonal boron nitride
HDA	Hexadecylamine
HSNs	Hairy silica nanoparticles

h_t	Theoretical central film thickness
HTS	Hexyltrichlorosilane
ICE	Internal combustion engine
ICP-MS	Inductively coupled plasma mass spectrometry
IF	Inorganic fullerene-like
IL	Ionic liquid
iMATUS	Institute of Materials of the University of Santiago de Compostela
INEGI	Instituto de Ciência e Inovação em Engenharia Mecânica e Engenharia Industrial
k	Coverage factor of the standard deviation
LA	Lauric acid
LTTP	Laboratory of Thermophysical and Tribological Properties
MADE	Maleic anhydride dodecyl ester
MALDI-TOF	Matrix-Assisted Laser Desorption/Ionization coupled with a Time-of-flight ion detector
MTT	Montmorillonite
MWCNTs	Multi walled carbon nanotubes
n	Refractive index
NaFoMat	Nanomaterials, Photonics and Soft Matter Laboratory
NanoMag	Research group on magnetism and nanotechnology from the University of Santiago de Compostela
NOM	Natural organic matter
NPs	Nanoparticles
OA	Oleic acid
ODA	Octadecylamine
OM	Oleylamine
OTES	Octadecyltriethoxysilane
OTS	Trichloro(octadecyl)silane
PAA	Poly(acrylic acid sodium salt)
PAO	Polyalphaolefin
PEG	Polyethyleneglycol
PEI	Polyethylenimine
PLMA	Poly(lauryl methacrylate)
PSS	Poly(sodium 4-styrenesulfonate)
PVD	Physical vapor deposition
R_a	Average roughness
R+D Pharma	Department of Pharmacy and Pharmaceutical Technology
rGO	Reduced graphene oxide
RIAIDT	Network of Infrastructures to Support Research and Technological Development
R_{ku}	Kurtosis
R_q	Root mean square roughness
R_{sk}	Skewness
SA	Stearic acid
ScA	Succinic acid
SEM	Scanning electron microscope

SPAN 80	Sorbitan monooleate
SRR	Slide-to-roll ratio
TEM	Transmission electron microscope
TGA	Thermogravimetric analysis
TMPTO	Trimethylolpropane trioleate
TOA	N,N-dioctyl-1-octanamine
U	Expanded uncertainties
U_s	Entrainment speed
USC	University of Santiago de Compostela
UV-Vis	Ultraviolet-visible
VFT	Vogel-Fulcher-Tammann
VI	Viscosity index
W_{rate}	Wear rate
WTD	Wear track depth
WTW	Wear track width
W_{Vol}	Wear volume
XRD	X-ray diffraction
ZDDP	Zinc dialkyl dithiophosphate
η	Dynamic viscosity
ϕ	Volume fraction
ϕ	Mass fraction
Λ	Specific film thickness
ρ	Density

INDEX

1 INTRODUCTION, STATE OF ART AND OBJETIVES

The results presented in this chapter are mainly related to the following publication (the publisher authorization for the use of this publication is in the Appendix A):

F. Mariño[a], J. M. Liñeira del Río[a,b], E. R. López[a], J. Fernández[a]. Chemically modified nanomaterials as lubricant additive: Time stability, friction, and wear. *Journal of Molecular Liquids*, (2023) 382, 121913. (Open access) https://doi.org/10.1016/j.molliq.2023.121913

[a] Laboratory of Thermophysical and Tribological Properties, Nafomat Group, Department of Applied Physics, Faculty of Physics and Institute of Materials (iMATUS), Universidade de Santiago de Compostela, 15782 Santiago de Compostela, Spain

[b] Unidade de tribologia, vibraçoes e manutençao industrial, INEGI, Universidade do Porto, Porto, Portugal

The main contributions of the PhD student to this study are explicitly indicated below:

Experimental: Data curation, Investigation, Methodology

Manuscript: Writing original draft, Writing – review & editing, Formal analysis

Some conclusions of this chapter related with low viscosity nanolubricants are included in:

F. Mariño[a], J. M. Liñeira del Río[a,b], E. R. López[a], J. Fernández[a]. Influence of the nanoparticle coating agent on stability time and tribological performance on potential e-transmission nanofluids, Proceedings of the eight[th] "International Conference on Lubrication, Maintenance and Tribotechnology", LUBMAT 2023, Preston, UK, 17th - 19th July 2023.

[a] Laboratory of Thermophysical and Tribological Properties, Nafomat Group, Department of Applied Physics, Faculty of Physics and Institute of Materials (iMATUS), Universidade de Santiago de Compostela, 15782 Santiago de Compostela, Spain

[b] Unidade de tribologia, vibraçoes e manutençao industrial, INEGI, Universidade do Porto, Porto, Portugal

The main contributions of the PhD student to this study are explicitly indicated below:

Experimental: Data curation, Investigation, Methodology

Manuscript: Writing original draft, Writing – review & editing, Formal analysis

1.1 INTRODUCTION

At present, around 23 % of the total energy consumed in the world is owing to friction and wear occurring in the tribological contacts of mechanical elements [1]. Of that, around 87 % is used to overcome friction, and around 13 % is used to remanufacture worn parts and spare equipment owing to the wear. According to Holmberg and Erdermir [1] calculations, worldwide, the overall economic costs due to tribological contacts in all societal sectors in 2017 were around

2500 billion euros/year of that around ¾ are owing to friction and ¼ is owing to wear. Furthermore, the amount of CO_2 emissions generated from friction and wear was estimated in more than 8000 $MtCO_2$/year. The friction loss of the total energy used in the transportation sector is the greatest, being about 30 % of the total energy use, in comparison with 20 % in the manufacturing and power-generating industry and just 10 % in the residential sector. Moreover, friction also causes several problems, such as environmental contamination, and might contribute to increased corrosion. Consequently, the reduction of friction and wear plays a crucial role in the extension of mechanical equipment service life, in saving energy and decreasing emissions [1]. Lubrication is considered one of the most effective ways to save energy and increase the effectiveness of devices used in industries of different sectors [1,2]. Thus, lubrication is the procedure used to reduce friction and wear between two surfaces that move at a very short distance from each other, through the interposition of a substance called lubricant. A lubricant is a multicomponent chemical mixture of different base oils and additives in a proportion around 90 % and 10 %, respectively. Many researchers considered diverse technologies to develop new procedures to substitute traditional environmental harmful additives that cause adverse emissions and contain sulfur or phosphorous (for instance zinc dialkyldithiophosphate) studying other additives like many nanoparticles (NPs) [3-8]. However, unlike traditional additives currently used in the field of lubrication, information about the effect of NPs on the environment is still lacking. Numerous studies show that several NPs used as additives have better tribological properties than traditional additives in lubricant bases used in different applications, such as wind turbines [9,10], automobile engines [11-15], transmission fluids for electric vehicles [16,17], cutting tools [18], among others. In fact, adding a small quantity of NPs to a lubricant usually has favorable effects on both friction and wear reductions. Such improvement is owing to their small size, since nanoadditives can enter the contact area, causing a positive lubrication effect [15]. One of the main benefits of NPs as lubricant additive is their low volatility that prevents NP losses under high temperature conditions [19]. Furthermore, NPs are less chemically reactive than common additives, since their films are mechanically formed, so they do not react with other additives and, therefore, both the NPs and the other additives will be more durable [19].

Nevertheless, NPs still present several problems that limit their use in real applications in the industry. One of the main challenges of using NPs as additive is to achieve homogeneous and stable dispersions over time. The stability of a nanolubricant is the time that the NPs are suspended in the base oil without settling. Stability is a drawback that restricts both development and technical application of nanolubricants. Preparation of stable nanolubricants is a key step to achieve their use in industrial applications, such as in gearboxes or bearings of wind turbines or for lubrication of hybrid or electrical vehicles since long-term stability is needed [10,16,20-22]. After aggregation, sedimentation occurs. NPs tend to aggregate due to attractive van der Waals forces acting on each other [6,11]. To obtain a stable nanofluid, it is essential to overcome the attractive interaction between particles, which must be compensated with other types of forces [12]. A common solution is the addition of surfactants which work through two types of mechanisms: electrostatic stabilization with ionic surfactants that prevents agglomeration due to the presence of a double layer of electrical charges around the NPs, and steric stabilization in which surfactant molecules with long hydrocarbon chains surround the NPs create a steric barrier that separates the NPs from each other [23-26]. Electrostatic stabilization is the dominant mechanism of water-based dispersions. The use of surfactants may hinder the reduction of friction and wear produced by NPs [27], changes the formulation of the

lubricant, and also does not usually lead to long-term stability (several months) [28]. Regarding oils, in addition to the use of non-ionic surfactants, there is another strategy to increase the stability time of the nanodispersions, which consists of the chemical modification of the NPs [29-31]. Of these two existing strategies [28], in this work we focus on the modification through covalent bonds of the surface of NPs with molecules of different type as organic acids, amines, silanes, organic phosphates, polymers, alcohols, among others (Figure 1.1), the first three being the most common (Figure 1.2). In all these cases, the molecules are chemically bonded to the surface of the NP and, in addition to their functional group that reacts with its surface, have long nonpolar chains at the other end of the molecule, which are capable of stabilizing the NPs in the oil [28]. Among the main conclusions of Chen et al. [28] review is that chemical coating with amphiphilic molecules is appropriate for stabilizing NPs with size smaller than 50 nm whereas for larger NPs, alkoxysilanes are better. These authors also indicate, based on theoretical analysis, that steric stabilization plays a more important role than other mechanisms because of the nonpolar nature of most of lubricating oils. On the other hand, the way most solvents perform is *like dissolves like*, thus it is generally agreed that a nonpolar compound will better solubilized in a nonpolar base fluid rather than in a polar one [23], although this is not exactly the case of nanomaterials, dispersing rather than dissolving in the base fluid. This rule has been modified to *like seeks like*, then including interactions with surfaces [32]. Thus, this rule, referred to nanomaterials, means that solvents will better disperse nanomaterials with similar surface chemistry [33].
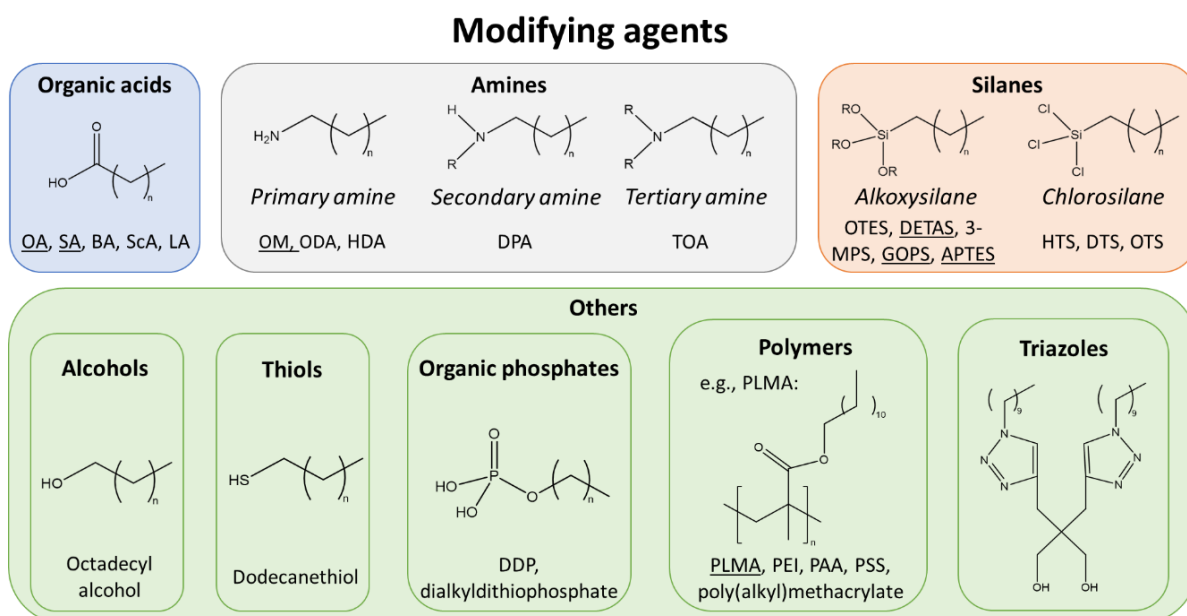

Figure 1.1 Chemical structure of different NP modifying agents used in the literature. The names of the most common of each type are underlined
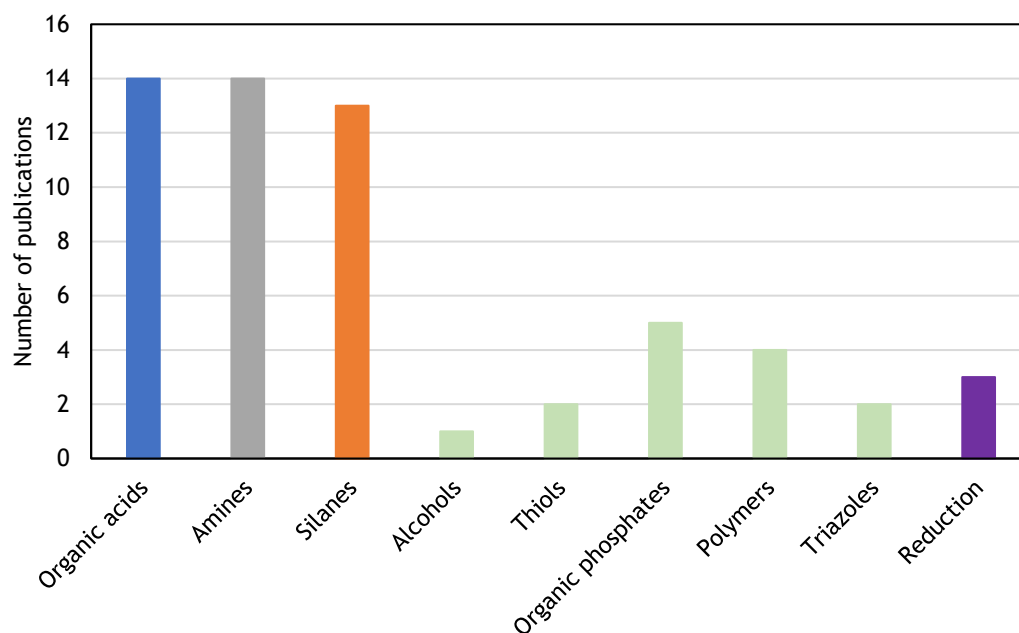
Figure 1.2 Number of publications (those until February 2022 that include information and evidence about stability time using the search engine Google Scholar) for each type of modifying agent based on the publications evaluated in Section 1.3

The base oils are categorized by the American Petroleum Institute (API) into five categories depending on their physical properties and composition [34]. The API groups I, II and III include mineral base oils refined from crude petroleum oil and are differentiated by viscosity index (VI), content of saturated carbon chains, and sulfur content. The API group I oils are obtained by solvent refining or separation processing, meanwhile those of groups II and III are obtained by conversion or hydroprocessing technologies or by a combination of solvent and hydroprocessing technologies. The API group IV designates polyalphaolefins (PAOs), which are synthetic oils. Finally, the API group V is assigned to all the base oils not covered in the other categories, including naphthenic base oils, esters, silicones, glycols, polyalkylene glycols, vegetable oils, etc.

PAOs have been used in lubrication since the 1950s and are the most common synthetic base oils nowadays [35]. They are prepared under controlled conditions from synthetic alphaolefins, mainly 1-decene. These base oils are named by their acronym followed by their viscosity grade, which is close to the kinematic viscosity in centistokes at 100 °C, i.e., PAO40 is a polyalphaolefin with a kinematic viscosity around 40 cSt at 100 °C. PAOs can overcome the limitations of mineral oils, so the industry is shifting from mineral oils to these synthetic alternatives. Moreover, PAOs have better physical and chemical properties and a wider temperature operating range comparing with those of mineral oils with similar viscosities at 100 °C. Among these properties are lower volatility, higher flash point, lower pour point, higher thermal stability, and higher oxidative stability. In addition, PAOs are non-toxic to aquatic environments (up to 49500 ppm) and low viscosity PAOs are quite biodegradable (PAO2-4) and non-toxic to mammals (PAO2-10) [36].

Regarding API group V base oils, this introduction focuses on esters, polyalkylene glycols and vegetable oils. Firstly, ester oils can be a natural or a synthetic product, natural ester oils have been used in lubrication since ancient times [37]. Esters can be synthesized by chemical reaction

of a carboxylic acid and an alcohol, both can be mono-, bi- or polyfunctional acids or alcohols, thus a broad variety of esters can be obtained. Generally, ester lubricants have long hydrocarbon groups and their properties depend on the number and structure of these groups [38,39]. The molecular weight and relative concentration of the ester groups determine the viscosity and polarity of the ester oil. Secondly, polyalkylene glycols (PAGs) are oil soluble glycols, which make them desirable components for hydrocarbon-based lubricants [40]. The VI of polyalkylene glycols are typically higher than conventional API Group I-III mineral oils with similar viscosity grades and show more favorable low-temperature properties than API group III oils. Nevertheless, antioxidant additives are required due to the poor thermal oxidative stability. In addition, compared to API groups II, III and IV base oils, the PAGs show higher volatilities for similar viscosities. Thirdly, vegetable oils are also used as lubricants [41] due to the excellent lubricity, good anticorrosion capabilities, great viscosity–temperature behavior and low evaporation losses. Important advantages of these oils are their biodegradability and environmental safety compared to mineral or synthetic oils. Nevertheless, the use of vegetable oils as base stocks is limited due to their poor cold-flow behavior and low thermal oxidative stability [42].

1.2 NANODISPERSIONS AND THEIR STABILITY

Long-term stability is a fundamental requirement for nanolubricants to be used in real applications. To obtain stable suspensions of NPs in lubricant oils, there are some strategies presented below. In addition, techniques for evaluating stability time are discussed.

1.2.1 Techniques used to improve the nanolubricant stability

-Preparation of nanodispersions: It is generally considered that there are two main methods for preparing nanolubricants: single-step method and two-step method [43-45]. In the former, the production of NPs and their dispersion in the liquid occur simultaneously [11]. Vapor deposition is the single-step method most frequently used: the raw material is heated and evaporated in a resistively heated crucible, the vapor is condensed into NPs when it contacts with a flowing low vapor pressure liquid [43,46]. If the raw material is a liquid or solid this procedure is based in physical vapor deposition (PVD), and it is named one-step *physical* method. With this method only small amounts of NPs can be synthesized, which limits their application on an industrial scale. Zhu et al. [47] developed the one-step *chemical* method by preparing nanofluids under microwave irradiation. Mineral-oil-based nanofluids including silver NPs with a narrow size distribution (9.5 ± 0.7 nm) were prepared by one-step chemical method, but surfactants were needed to stabilize the nanofluid [48]. The one-step chemical method combines the synthesis of NPs with the preparation of nanofluids. With this method it is possible to control the particle size, reduce the agglomeration of NPs, and produce nanofluids containing metallic NPs [49]. However, it is difficult to prepare nanofluids with a high concentration of NPs using this last method. Nevertheless, with the single-step methods good stability results as well as a small agglomeration of the NPs are usually achieved but they are quite expensive and if the reactants are not completely transformed into products, there will be impurities in the nanofluid [45], making difficult to clarify the effect of NPs on the nanodispersion properties without removing impurities. In addition, these residues could negatively affect the tribological behavior and dispersion stability of the formulated lubricating oil.

Alternatively, in the two-step method, the NPs in dry powder form are incorporated into the base oil and the resulting dispersion is homogenized (Figure 1.3). Such homogenization is

usually carried out by ultrasonic stirring. For this purpose, an ultrasound tip or/and bath are used and different parameters such as power, shaking mode or sonication time are modified until the optimal conditions are found. An advantage of this method is the easy control of size of the NPs, since a wide variety of NPs with different sizes are commercially available. The two-step method is the most broadly used to formulate nanolubricants and thermal nanofluids as it is the most economical [23].
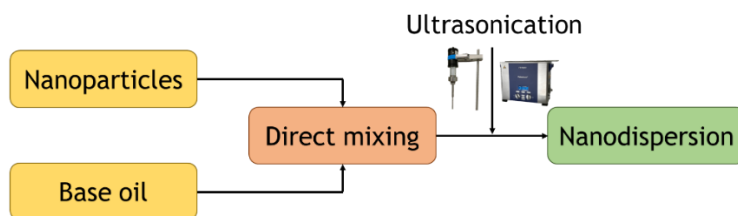

Figure 1.3 Two-step method for the preparation of nanodispersions

For nanodispersions containing ILs and NPs as hybrid additives of oils, Sanes et al. [50] designed a modified two-step method. In this case, nanopowders are added to the IL in an agate mortar being both mechanically mixed for 5 min and then mixed with the base oil. Finally, the nanodispersions are homogenized by means of an ultrasound bath. Using this method, Nasser et al. [51] obtained stabilities longer than eight months. Ali and Xianjun [52] proposed another method that includes mechanical stirring to mix the base oil and the IL with a magnetic stirrer and then adding the NPs to the liquid mixture using a probe sonicator and a ultrasonic vibration bath to disperse them. Stability times up to 70 days were obtained for the lowest concentrations of NPs.

Another interesting method to improve the dispersion stability is the *four-step method* reported by Sui et al [29,53-55], which is based on an azeotropic distillation (Figure 1.4). Firstly, a dispersion of ethanol and NPs is mixed with toluene and, after the evaporation of ethanol at 70 ºC, PAO is added to the nanodispersion with fast stirring. Finally, the dispersion of the NPs in PAO is obtained by removing toluene by evaporation in an oven [55]. The stability results obtained through this method by Sui et al. [53] were better than those of the same dispersions prepared by the two-step method.
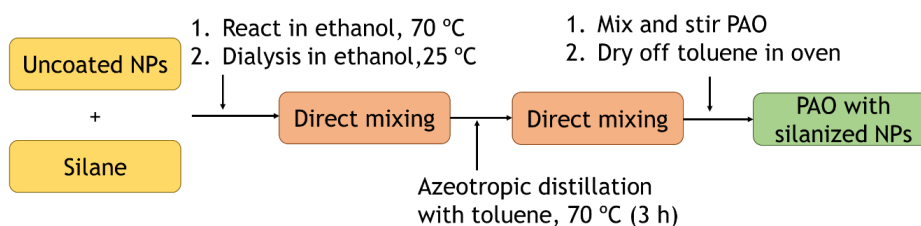
Figure 1.4 Scheme of four-step method based on azeotropic distillation

Recently, Liñeira del Río et al. [56] designed an efficient method to prepare nanodispersions (Figure 1.5), in which superparamagnetic NPs, suspended in cyclohexane after the synthesis, are transferred to another highly volatile solvent by centrifugation. Subsequently, the NP concentration was obtained by thermogravimetry, and the dispersion was added to the base oil and blended with an ultrasonic bath and an ultrasonic probe sonicator for a total time of 15 min. Then, the solvent was evaporated with a rotary evaporator, obtaining the superparamagnetic

nanolubricants. Finally, these nanolubricants were sonicated in the ultrasonic bath for 4 h. With this procedure, the nanodispersions are stable more than eleven months.
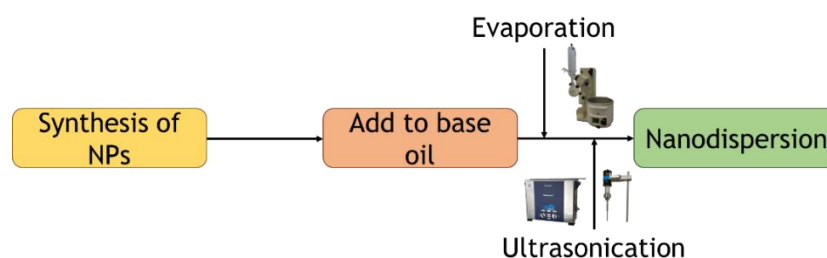

Figure 1.5 Preparation process of nanodispersions by a Liñeira del Río et al. method [56]

-Use of dispersants: As aforementioned to obtain more stable dispersions, surfactants are widely used. There are numerous different types such as oleic acid [56], alkyl phosphates [57], toluene [58,59], ionic liquids (ILs) [10,60,61], among others. Toluene can change the oil polarity of the nanodispersions, due to its small dipole moment, keeping the nonpolar base oil and NPs in a stable solution as a colloidal suspension [58]. Ionic liquids are considered outstanding dispersants for the stabilization of well-characterized nanomaterials [50,62-64], these compounds were also analyzed as hybrid lubricant additives in combination with NPs. For instance, Liñeira del Río et al. [61] examined the stability of a polyester base oil additivated with hybrid nanoadditives (hexagonal boron nitride, h-BN NPs and a phosphonium IL) obtaining temporal stabilities even longer than 3 weeks. Furthermore, Nasser et al. [51,60] studied the stability of h-BN NPs or GnP combined separately with three phosphonium ILs as hybrid nanoadditives in a polyalphaolefin (PAO32), finding stabilities longer than 150 days with the ILs based on the trihexyltetradecylphosphonium cation. It should be considered that surfactants can modify lubricant properties such as viscosity and antifriction and/or antiwear capabilities. For this reason, it is important to analyze the lubricants properties after the dispersant's addition.

-Chemical modification of NPs surface: it is the most recent strategy to stabilize the NPs in the base oil [28], which was explained in the previous section. This type of stabilization is continuously developing. Usually, organic compounds with polar groups, among them dispersants, and compounds with long hydrocarbon chains and different polar functional groups (silanes, amines, carboxylic acids, alcohols, thiols, …) are used as modifying agents of the NP surface to have good dispersibilities in base oils [56,65,66]. There are other types of chemical modifications that improve the stability against sedimentation such as a simple oxygen reduction [67,68].

1.2.2 Techniques to evaluate the nanolubricant stability

There are numerous techniques to analyze and quantify the stability of nanodispersions against sedimentation [23] such as sediment photograph capturing, refractometry, UV–Vis spectrophotometry, turbidimetry as well as dynamic light scattering (DLS). Nonetheless, most of them have some limitations due to several aspects as it is presented below.

Sediment photograph capturing: it is the easiest and most economical way to evaluate the stability of the nanolubricants. This process, also named visual inspection, is carried out taking photos of the nanodispersions over a period of time [69]. It is the most broadly used to have a

qualitative notion of the stability of the nanolubricants [70]. In this evaluation technique, the nanodispersions must be kept under controlled conditions and without any alteration during analysis. It should be noted that the only limitation of this technique is that for dark nanodispersions it is sometimes difficult to see the sedimentation clearly. Usually, authors complement this procedure with other quantitative methods.

Dynamic light scattering (DLS): this technique is used to determine the size distribution of the aggregates of NPs in the lubricant [67,70,71]. The stability of nanodispersions is given by the evolution of the average size of the aggregates: if it increases over time, agglomeration occurs while if it decreases sedimentation takes place. In the case that the average size of the aggregates remains constant it can be considered that the nanolubricant is stable. However, this technique has a limitation for opaque nanolubricants because it is difficult to obtain representative values of average particles size. Some authors analyze the size distribution of the aggregates of the nanoadditives of the formulated lubricants diluting them or transferring the NPs to a solvent in a very dilute concentration [72,73]. It is expected that the aggregate size distribution changes when both the base fluid and/or the concentration change [53,74].

Multiple Light Scattering technology consists of capturing and analyzing the intensity of the resulting light backscattered by the particles of a sample. When a liquid dispersion has a certain particle concentration, the light that hits one particle is scattered to hit nearby particles, finally being backscattered towards a backscattering detector. The intensity of light captured in this detector is directly related to the concentration, the average particle size, and the degree of dispersion of the sample. Turbiscan is a device that allows characterizing the stability of liquid dispersions, both at very low and at high concentrations, thanks to the Multiple Light Scattering technology and the two light transmission and backscattering detection systems [75,76]. It is common to use this device to characterize the coalescence, sedimentation, flotation, phase separation as well as to determine the average size of aggregates. Nevertheless, the use of this device to evaluate the stability of nanolubricants is quite scarce [76].

Evolution of refractive index is a stability characterization method developed by Guimarey et al. [77,78] based on the measurement of the refractive index of the nanodispersion over time. Nanodispersions are considered stable when the refractive index hardly varies with time, nonetheless when the NPs settle the refractive index changes [67,79].

UV–Vis spectroscopy is a conventional technique used to analyze the stability of nanodispersions. The decrease in the absorbance level indicates the sedimentation of NPs. Nevertheless, at the usual concentrations of NPs in nanolubricants for which wear and friction are considerably reduced, the signals from both devices show saturation because they are usually too opaque and absorbance is too strong [78]. To avoid this issue, some authors dilute the dispersion [23,72,80]; however, this method is not rigorous since the stability of the nanodispersions strongly depends on the concentration of NPs and the dilution will only give information about the stability of less concentrated nanodispersions [59].

1.2.3 Role of nanoparticles on the lubrication mechanism

It is crucial to understand the tribological mechanisms of NPs in tribocontacts that depend on the morphology, size, crystal structure, and compatibility of the NP and the base oil [81]. These mechanisms, which are illustrated in Figure 1.6, cause NPs to improve or worsen the

lubricating ability of the base oil. The six tribological mechanisms by which NPs display positive roles are:

- Rolling (Figure 1.6a): NPs with spherical morphology tend to roll through the tribocontact mainly when their diameter is similar to the film thickness [82].
- Protective film formation (Figure 1.6b), also referred as tribofilm formation: it consists of the formation of a layer of NPs that react with the lubricated surface [15]. The formation of these tribofilms can be confirmed by surface analysis techniques like SEM/EDS, XPS or Raman spectroscopy [83].
- Mending (Figure 1.6c): NPs with small sizes have better ability to penetrate the contact region, being able to fill the valleys from the surface, resulting in a reduced roughness which causes a reduction in friction and wear [84].
- Sliding and shearing (Figure 1.6d): plate-like NPs tend to slide and shear their layers, that are weakly bonded through van der Waals forces, resulting in an improvement of the lubrication by avoiding direct contact with the surfaces [85].
- Sintering onto surfaces (Figure 1.6e): small NPs have lower melting points compared to bigger NPs, making them more prone to weld and melt (sinter) on the surface of the tribocontact generating an intermediate layer between the rubbing surfaces [86,87].
- Polishing and smoothing (Figure 1.6f): the NPs smooth the surface by polishing the asperities of the tribocontact leading to a better lubrication [88].

Meanwhile, hard NPs may show a negative role through the abrasion mechanism (Figure 1.6g). Finally, NPs may not have any relevant interaction with surfaces (Figure 1.6h) [16].
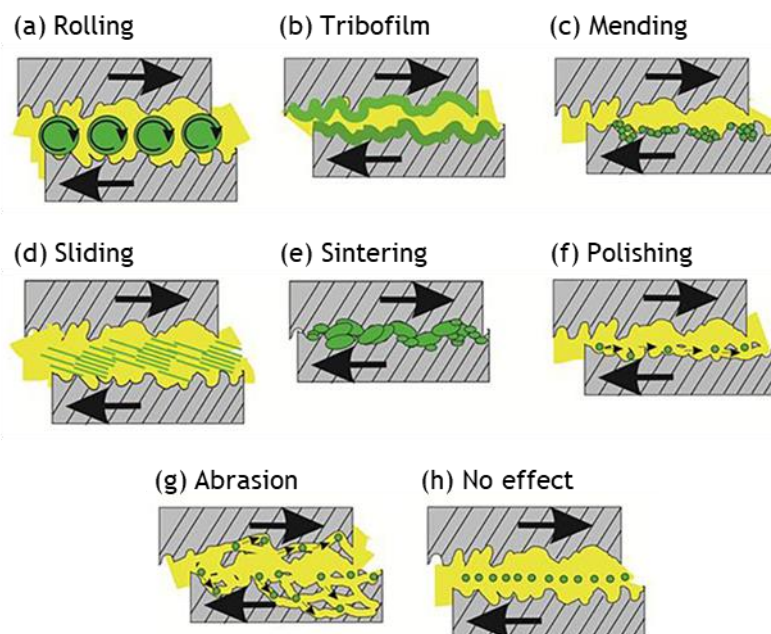

Figure 1.6 Schematic representation of the possible mechanisms of the nanoparticles in the tribocontact by Mustafa et al. [81]

1.3 Chemically Modified Nanomaterials as lubricant Additives: time stability, friction, and wear

In this section, a review of published literature on non-aqueous lubricants containing chemical modified NPs is presented. NPs are usually categorized as: carbon-based nanomaterials, metal NPs, metal oxide NPs, metal sulfide NPs, and other NPs that cannot be covered in the other categories, such as rare-earth NPs, silicon NPs, hexagonal boron nitride (h-BN) and mineral oxides [4]. The purpose of this section is to try to answer the following questions: which is the best method to obtain nanolubricants with long-term stability? Which are the best NPs to obtain efficient nanolubricants with long-term stability? Which are the best modifying agents? Thus, one of the aims of this section and this PhD thesis is to contribute to cover these research gaps. Section 1.3 is organized in two parts. In the former, a state of art of time stability of non-aqueous nanolubricants is presented. The term chemical modified NPs includes not only surface-functionalized NPs but also oxygen reduction of carbon nanomaterials [42,43]. In the second part, the tribological literature results (friction and wear) obtained with the nanolubricants with stabilities longer than four weeks are analyzed. According with the scarce literature [20,89-94], it seems that surface-functionalized NPs should have better tribological properties as additives than those of the corresponding bare NPs. The coating avoids material transfer, preventing direct contact and cold-welding between rubbing surfaces. Furthermore, the hybrid structure of functionalized NPs contains a rigid core and a soft shell which permits high load carrying capabilities and has no negative effect on lubrication [89]. Thus, the functionalized NPs maintain the rigidity of the corresponding bare NPs thanks to the rigid core, whereas the soft shell is flexible and slippery [92]. Therefore, compared to bare NPs, surface-modified NPs offer unique advantages. For instance, improvements in friction and wear properties were found by several authors [20,90-93] when functionalized NPs, compared to bare ones, were tested. Thus, Yegin et al. [92] examined how the addition of octadecyltrichlorosilane (OTS) functionalized silica NPs in an ionic liquid (IL, 1-butyl-3-methylimidazolium (trifluoromethysulfony)imide) affects the IL tribological properties under different lubrication conditions. Optimum concentrations of 0.05 wt% for uncoated silica NPs and at 0.10 wt% for OTS-functionalized silica NPs were found. These authors found that, at the optimum concentration, the IL additivated with functionalized NPs leads to a friction coefficient (COF) decrease of 37 % compared to neat IL and of 17 % compared to IL additivated with uncoated silica NPs. Srinivas et al. [91] modified multi walled carbon nanotubes (MWCNTs) with cetrimonium bromide (CTAB) or with sorbitan monooleate (SPAN 80) and tested them as additives for a diesel engine oil, finding that the surface modified nanoadditives improved the engine oil tribological properties whereas unmodified NPs lead to no improvements. Samanta et al. [90] functionalized graphene oxide (GO) with octadecylamine (ODA) finding that, when it is dispersed in heavy paraffin oil, hydrophobic GO-ODA NPs perform much better under low load conditions because of the presence of long hydrocarbon chains that act as a shield between the contact surfaces, while hydrophilic GO works better in the high load regime because it adheres onto surfaces when pressed under high pressure. Sade et al. [93] tested WS_2 nanotubes and two different grades of inorganic fullerene-like NPs (IFs), functionalized by a humin-like conformal shell, as additives for a polyalphaolefin (PAO4) oil. These authors found that the coating of WS_2 IFs leads to improvements in friction and wear comparing to the non-coated NPs, while they did not find any improvement in antifriction and antiwear capacity due to the functionalization of the WS_2 nanotubes. Saidi et al. [20], using octyl- and octadecyl-trichlorosilane as surface hydrophobization agents to improve the stability of MoS_2 nano-

additives formulations in a wind turbine oil, found that both coated additives led to a strongly better antifriction and antiwear capabilities than those of the corresponding bare MoS$_2$ NPs. Nevertheless, Viesca et al. [94] found that the addition of carbon-coated copper NPs decreases wear and increases the loading capacity of PAO6, but coated Cu NPs do not perform better than uncoated Cu NPs. Thus, the varied results indicate that this is an open field of research.

1.3.1 Stability

In this regard, stability results with different types of functionalized NPs such as: carbon-based nanomaterials (Table 1.1), metals (Table 1.2), metal oxides (Table 1.3), metal sulfides (Table 1.4), other NPs (Table 1.5) and nanocomposites (Table 1.6) are presented. The analyzed base oils include mineral (groups I, II, III), synthetic (polyalphaolefins, PAO; esters; polyethylene glycols, PEG) and vegetable oils. Fully formulated oils are included, but aqueous lubricants are not considered here. Tables 1.1-1.6 also indicate the modifying agents of the NPs surface such as amines, organic acids, alcohols, thiols, organic phosphates, polymers, and silanes. In addition, several authors obtained remarkable stabilities by reducing carbon derivative nanomaterials [95]. Apart from the presence of "functionalities", the size, and shape of the nanoadditives as well as their concentration have a great impact on the stability of the dispersions. Thus, for the spherical NPs, their sedimentation velocity is proportional to the square of the radius according to the Stokes law [96]. The smaller the radius of the NP, the lower the sedimentation rate [28,96]. Another factor that affects the nanodispersion stability is the length/diameter ratio (aspect ratio); the higher the aspect ratio of the NPs, the more likely they agglomerate [96]. However, it should be noted that some aggregation always occurs without a suitable dispersion method, regardless of the shape of the nanoadditive [28]. Furthermore, the higher the base oil viscosity, the longer the dispersion stability, according to the Stokes law.

As it was indicated, uncoated nanoadditives usually show low stabilities in nonpolar base oils due to the high van der Waals interactions between bare NPs and their lipophobicity due to their high polarity. To coat the NPs with the modifying agents it is needed to chemically activate the surface of the NPs. In the case of metal oxide NPs and SiO$_2$, liquid or vapor water interacting with them can cause their hydration and hydroxylation leading to hydroxyl groups on the NPs surface [97]. Due to the similar chemical properties of metal oxides and metal sulfides, analogous behavior can be expected in metal sulfide NPs, which have thiol groups on their surface. In the case of metal NPs, surface oxidation may also occur due to the presence of gaseous species, water vapor, and other electrolytes in the air [98]; subsequently, the hydroxylation of the oxide coating can also lead to hydroxyl functionalities on those surfaces. Similarly, carbon based nanomaterials such as graphene nanoplatelets, which are hydrophobic, can be oxidized generating a highly defective graphene that is covered more or less uniformly with hydroxyl or carboxyl groups, which lead to a hydrophilic nanomaterial [99,100]. Even after chemical reduction of graphene oxide, obtaining reduced graphene oxide, some hydroxyl or carboxyl groups may remain [101]. Both graphene oxide and reduced graphene oxide can be further functionalized. Thus, chemical reactions used in the functionalization of NPs mainly occur with amphiphilic molecules, such as oleic acid, and happen through esterification reactions with the above-indicated surface groups (hydroxyl, carboxyl, thiol…). The presence of alkyl chains covalently bonded to the NPs can prevent agglomeration by reducing their surface energy, overcoming the van der Waals interactions between NPs through steric hindrance, as well as the generation of van der Waals interactions between the alkyl chains of

the coating with those of the base oil [57,71]. If the alkyl chains of NPs slow down the sedimentation rate enough, this can be counterbalanced by Brownian motion [72,73]. In fact, the longer the alkyl chains, the longer the stability time. It should be noted that the grafting density (number of chains per NP surface unit) vary with the number of available polar moieties and the type of synthesis [102]. Regarding the NPs size, Chen et al. [28] concluded that with the same surface coating, a decrease in the size of NPs reduce the attractive van der Waals interactions among NPs and rise the repulsive steric force.

Carbon and its derivatives: Different modifying agents were investigated, such as oleic acid, OA; stearic acid, SA; dodecylamine, DDA; hexadecylamine, HDA; 1-octadecylamine, ODA; diphenylamine, DPA; oleylamine, OM; octadecyl alcohol; dodecylphosphate, DDP; OTS; or triazole. Polymers have been also used, such as polyethylenimine (PEI), poly(acrylic acid sodium salt) (PAA) and poly(sodium 4-styrenesulfonate) (PSS) (Table 1.1).

The best stability using carbon nanoadditives was achieved by Chen et al. [103] with SA functionalized MWCNTs in a paraffin oil, claiming a visual stability at ambient conditions for up to six months, meanwhile non-functionalized MWCNTs (outer diameter from 20 to 40 nm) are completely settled before two months. The alkyl chains of the coating lead to an increase of the outer diameter of 10 nm. Mungse et al. [104] achieved a slightly lower stability (1 month) with a less concentrated dispersion (0.04 g L^{-1}) of GO functionalized with ODA in a 10W40 mineral oil (104 cSt at 40 ºC). Moreover, GO can also be modified by reduction reactions, obtaining rGO. Similar results were found by the same research group with rGO functionalized with ODA [65]. Samanta and Sahoo [105] obtained dispersions of rGO functionalized with a branched PEI and PSS or PAA at 1 g L^{-1} concentration in heavy paraffin oil (viscosity 64 cSt at 37 ºC) with time stabilities of two months. In all the articles indicated in Table 1.1 the classical two-step method was used except in that of Zhu et al. [106] who used a rotary evaporator to transfer rGO functionalized with octadecyl alcohol from THF to a low viscosity mineral oil (13.2 cSt at 40 ºC), reaching a month stability.

Another type of carbon-based NPs are CDs and QCDs. Liang et al. [107] synthetized HDA modified carbon dots, CDs-HDA; their dispersions in PAO4 having stabilities of at least 3 months for the highest concentration (1 wt%). Furthermore, Shang et al. [108] synthetized hydrophilic N-doped carbon dots (4-12 nm), N-CDs, and tuned to hydrophobic N-CDs through covalent grafting of OM on the surface of N-CDs, OM-N-CDs. Hydrophilic N-CDs were dispersed in a PEG meanwhile hydrophobic OM-N-CDs were dispersed in a PAO base oil, finding in both cases stabilities of 30 days for 1 wt% N-CDs or OM-N-CDs in the corresponding base oil. Finally, Ye et al. [109] synthetized N-doped carbon quantum dots uncoated and coated with OM (N-CQDs and OM-N-CQDs with 2 nm and 4.2 nm diameter, respectively), finding that the dispersion of a castor oil with 0.2 wt% N-CQDs was still stable after 5 months, whereas the dispersion stability of PAO with 2 wt% OM-N-CQDs showed little sedimentation after 3 months. The high stability of the first dispersion can be due to the small size of the NPs and the lowest concentration.

Table 1.1 Stability of nanolubricants based on modified surface carbon-based nanomaterials

Nanoadditive	Functionalization	Concentration	Base oil	Stability	Ref.
Graphene Nanosheets	Fluorine	NA	GTL-8	7 days	[110]
GO	DDA	0.1 wt%	5W30	32 days	[80]
GO	ODA	0.04 g L^{-1}	10W40	1 month	[104]
GO	DDP	0.1–0.5 g L^{-1}	Mineral oil	10 days	[111]
GO	OA	0.5-2 wt%	PAO12	7 days	[112]
rGO	ODA	0.04 g L^{-1}	10W40	>1 month	[65]
rGO	ODA	0.05wt% + 1 wt% IL	Ester Oil	28 days	[113]
rGO	PEI-PAA or PEI-PSS	1 g L^{-1}	Paraffin oil	2 months	[105]
rGO	OTS	0.04 wt%	Polyol ester	20 days	[102]
rGO	Octadecyl alcohol	0.01 wt%	Mineral oil	1 month	[106]
rGO	Triazole	0.01 wt%	500N	1 month	[114]
rGO	Reduction	0.01 wt%	Mineral oil	45 days	[95]
rGO	Reduction	0.50 wt%	PAO6	4 days	[68]
rGO	Reduction	0.25 wt%	TMPTO and PAO40	10 days	[67]
MWCNT (20-40 nm)	SA	0.45 wt%	Paraffin oil	6 months	[103]
CNPs (25-35 nm)	OM	1 wt%	PAO10	3 months	[115]
CDs (4.2 nm)	HDA	1 wt%	PAO4	3 months	[107]
CDs (4-12 nm)	N-OM	1wt%	PAO	1 month	[108]
	N	1 wt%	PEG	1 month	[108]
CQDs (2 nm)	DPA	0.2 wt%	Castor Oil	5 months	[109]
CQDs (4 nm)	DPA and OM	2 wt%	PAO6	< 3 months	[109]

Functionalization of carbon nanomaterials leads to improve the stability of nanodispersions from days to months, mostly dispersed in mineral oils but also in ester oils, PAOs and formulated oils. Furthermore, usually reducing GO the stability increases [67,113]. Chen et al. [103] reported the highest stability time of all the nanolubricants from Table 1.1 (6 months). Nevertheless, in their article [103] the photographs included were taken two months after preparation. However, those photographs evidence that the modification of MWCNTs leads to a more stable nanodispersion, although their length/diameter ratio. This improvement can be explained by the appearance of favorable steric hindrance force, due to the alkyl chains, which reduces the unfavorable van der Waals interaction between MWCNTs.

Functionalized metal NPs: these nanoadditives were functionalized with dialkyldithiophosphate, dodecanethiol, OM or OA (Table 1.2). Li et al. [116] synthetized surface modified Ag and Cu NPs, using dialkyldithiophosphate as a coating agent, indicating that their paraffin oil dispersions (0.5 wt%) kept unchanged for several months in ambient conditions or for 3 days at 140 ºC (no images are reported). Kumara et al. [117] synthetized dodecanethiol coated silver and palladium NPs finding that the dispersions with 0.5 wt% concentration in PAO4 (17 cSt at 40 ºC) are stable for several months, whereas at higher concentrations, up to 2 wt%, the time stability is only several days (no images are reported). Briefly, all these authors got dispersions with stabilities of several months for the NPs with diameters lower than 7 nm [116,117] whereas for dialkyldithiophosphate functionalized Ag NPs (15 nm) dispersions in a paraffin oil the stability is only five days [118].

Table 1.2 Stability of nanolubricants based on modified metal NPs

Nanoadditive	Functionalization	Concentration	Base oil	Stability	Ref.
Ag (4 nm)	Dialkyldithiophosphate	0.5 wt%	Paraffin oil	Several months (r.t.)* 3 days at 140 ºC.	[116]
Ag (3-6 nm)	Dodecanethiol	0.5 wt%	PAO4	Several months	[117]
Ag (15 nm)	Dialkyldithiophosphate	0.5 wt%	Paraffin oil	5 days	[118]
Cu (5 nm)	Dialkyldithiophosphate	0.5 wt%	Paraffin oil	Several months (r.t.) 3 days at 140 ºC.	[116]
Pd (2-4 nm)	Dodecanethiol	1.0 wt%	PAO4	Several months	[117]
Ni (7 nm)	OM and OA	0.025 wt%	PAO6	1 month	[119]

*r.t.: room temperature

Functionalized metal oxide NPs: Regarding these NPs, oleic acid is the most common functionalization although poly(lauryl methacrylate) (PLMA), 3-glycidoxypropyltrimethoxysilane (GOPS) or 2-octyldodecyl gallate are also used (Table 1.3). Wright et al. [120] studied three dispersions in PAO4 of hairy TiO_2 NPs densely grafted with PLMA which remained transparent and stable after 56 days at three different temperatures, -20, 22, and 100 ºC, but the dispersion color at 100 ºC changed, which was attributed by the authors to the oxidation of a residual catalyst used in the functionalization of the hairy NPs.

Liñeira del Río et al. [56] found the best stability among metal oxides, achieving stable TMPTO dispersions of OA modified Fe_3O_4 for at least 11 months due to the mutual affinity of the base oil which contains three oleate groups and the OA coating as well as the preparation method of the nanodispersions (Figure 1.5).

Table 1.3 Stability of nanolubricants based on modified metal oxide NPs

Nanoadditive	Functionalization	Concentration	Base oil	Stability	Ref.
TiO_2 (15 nm)	PLMA	1.0 wt%	PAO4	56 days	[120]
TiO_2 (20-25 nm)	2-octyldodecyl gallate	1.0 wt%	PAO10 10W30	3 days 5 days	[121]
Al_2O_3 (78 nm)	GOPS	0.05 wt%	N.A.**	50 days	[122]
ZnO (10-30 nm)	OA	0.5 wt%	60SN	12 hours	[123]
Fe_3O_4 (6.3, 10 nm)	OA	0.015 wt%	TMPTO	11 months	[56]

**Not available

Functionalized metal sulfide NPs. Different dispersions of metal sulfides with some modifying agents were studied, such as silanes (OTS; dodecyltrichlorosilane, DTS; hexyltrichlorosilane, HTS), and OM (Table 1.4). Shahar et al. [124] investigated the dispersibility in a paraffin oil of inorganic fullerene-like tungsten disulfide (IF-WS_2) NPs with the three different alkylsilane surface modifiers: OTS, HTS and DTS. The different silanized IF-WS_2 NPs (size <150 nm) were dispersed in a paraffin oil at 1 wt%. Surprisingly, the dispersion of IF-WS_2 functionalized with the silane with the longest alkyl chains, OTS (C_{18} chain) is stable only for 4 days, whereas that of IF-WS_2 functionalized with DTS (C_{12} chain) is stable for more than 14 days and that with HTS (C_6 chain) remained stable for 8 days. This could be due to differences in grafting-density. Jiang et al. [125] studied 2 wt% dispersions of OM modified WS_2 nanosheets (size 6-8 nm with 0.276 nm between nanosheets) in PAO6 (30.6 cSt at 40 ºC), at ambient conditions the dispersions remain stable up to 6 months and, at 160 ºC, up to 7 days. Another article from Jiang et al. [126] reports studies on ultrathin WS_2 nanosheets

capped by OM and maleic anhydride dodecyl ester (MADE), being their 2 wt% dispersions in dioctyl sebacate (DIOS, 11.5 cSt at 40 ºC) stable for 6 months at room temperature. Table 1.4 shows again the relevance of the size of the NPs in the stability of the nanodispersions.

Table 1.4 Stability of nanolubricants based on modified metal sulfide NPs

Nanoadditive	Functionalization	Concentration	Base oil	Stability	Ref.
IF-WS$_2$ (< 150 nm)	OTS	1.0 wt%	Paraffin oil	4 days	[124]
	DTS			>14 days	
	HTS			8 days	
WS$_2$ (6-8 nm)	OM	2.0 wt%	PAO6	6 months	[125]
WS$_2$ (6-8 nm)	OM and MADE	2.0 wt%	DIOS	6 months	[126]

Other functionalized NPs: other compounds used as nanoadditives for lubricants are silica (SiO$_2$) NPs, h-BN, rare-earth compounds like LaF$_3$ and mineral oxides like ZnAl$_2$O$_4$. Several modifying agents are used, such as organic acids (benzoic acid, BA; succinic acid, ScA or lauric acid, LA), amines (N,N-dioctyl-1-octanamine, TOA and ODA), OA, SA, polymers (PLMA, poly(alkyl)methacrylate) and silanes (octadecyltriethoxysilane, OTES; N1-(3-trimethoxysilylpropyl)diethylenetriamine, DETAS and 3-(trimethoxysilyl)propyl methacrylate, 3-MPS) (Table 1.5). Liñeira del Río et al. [56] found the best stability, achieving stable TMPTO dispersions of OA modified Nd alloy NPs (Nd$_2$Fe$_{14}$B) for at least 11 months due to the mutual affinity of the base oil which contains three oleate groups and the OA coating as well as the preparation method of the nanodispersions (Figure 1.5). Li et al. [127] obtained a stability time even longer than 5 months for nanolubricants of three different silane-modified SiO$_2$ NPs (APTES, GOPS or 3-MPS) in a gas mobile oil (0.3 wt%). Sui et al. [55] reported the stability of a hairy SiO$_2$ NPs (HSNs) dispersed in PAO100 using an aminosilane ended in NH$_2$: DETAS. This aminosilane is not amphiphilic. After two months, the nanodispersion with HSNs remained stable but not that of unmodified SiO$_2$ NPs. Sui et al. [29,53] also investigated the effect of three different end modifications of DETAS HSNs adding BA, SA or ScA finding that their nanodispersions in PAO100 are also stable after 2 months standing. The nanodispersion of the DETAS HSNs modified with SA (18 C) presents the best optical transparency, which can be attributed to excellent affinity of the nonpolar functional groups of the NPs with PAO100. In addition, Sui et al. [54] analyzed the advantages of using silica NPs functionalized with both alkyl and amino terminated organic silanes (OTES and DETAS). The dispersibility characterized with DLS showed that as the amount of OTES increased, the dispersibility of these NPs in PAO100 improved. Seymour et al. [73] studied a series of PLMA HSNs and the effect of alkyl pendant length (6, 8, 12, 13, 16 and 18 C atoms) on their stability in PAO4. The unmodified silica NPs were not stable in this PAO. All the HSNs with alkyl pendant length of more than eight carbons were readily dispersed in PAO and presented stability at room or high temperatures such as 80 ºC for up to 60 days. However, C6- and C8-grafted silica NPs (1 wt%) are not readily dispersible in PAO4 at room temperature. The C8 HSNs suspensions in PAO4 became clear and homogeneous upon heating at 80 °C. Interestingly, this cloudy-to-clear transition is reversible. These changes in the stability behavior can be described in terms of favorable brush solvation forces, which increase with the alkyl pendant length of the HSNs as well as the unfavorable interactions a) between PAO4 and silica NPs and b) between hairy NPs.

Li et al. [116] synthesized NPs of dialkyldithiophosphate modified lanthanum trifluoride, which were dispersed in a paraffin oil (viscosity 36 mPa·s at 40 ºC) leading to a transparent lubricant with stabilities of several months in ambient conditions and for 3 days at 140 ºC.

Literature results, showed in Table 1.5, bring out that SiO_2 NPs with sizes from 15 to 200 nm led to quite stable nanodispersions when are functionalized with silanes or polymers. Generally, the longest the alkyl chain of the functionalization is, the most stable the nanodispersions. Furthermore, it is important to modulate the polarity of the coating depending on that of the base oil.

Table 1.5 Stability of nanolubricants based on other modified NPs

Nanoadditive	Functionalization	Concentration	Base oil	Stability	Ref.
LaF_3 (8 nm)	Dialkyldithiophosphate	0.5 wt%	Paraffin oil	Several months (r.t.) 3 days (140 °C)	[116]
SiO_2 (15-20 nm)	APTES	0.3 wt%	Gas mobile oil	5 months	[127]
	GOPS	0.3 wt%		5 months	
	3-MPS	0.3 wt%		5 months	
SiO_2 (<100 nm)	DETAS	1.0 wt%	PAO100	2 months	[55]
SiO_2 (<200 nm)	DETAS	0.5 wt%	PAO100	< 2 months	[29,53]
	DETAS-SA	0.5 wt%		> 2 months	
	DETAS-BA	0.5 wt%		2 months	
	DETAS-ScA	0.5 wt%		< 2 months	
SiO_2 (100 nm)	DETAS and OTES	NA	PAO100	4 months	[54]
SiO_2, (24 nm)	PLMA	1.0 wt%	PAO4	55 days	[120]
SiO_2 (23 nm)	PLMA	1.0 wt%	PAO4	2 months	[73]
SiO_2 (58 nm)	OA	NA	Paraffin oil	30 days	[128]
h-BN	OA	NA	PAO8	3 days	[129]
h-BN (70 nm)	BA	NA	SN500	5 days	[130]
	ODA	NA		1 day	
	TOA	0.25 g L^{-1}		6 days	
$ZnAl_2O_4$ (95 nm)	OA	0.5 wt%	Lubricating oil	Several days (70 °C)	[131]
Nd alloy (19 nm)	OA	0.015 wt%	TMPTO	11 months	[56]

Functionalized nanocomposites: The modifying agents are organic acids (OA, SA), silanes (GOPS and APTES), and triazole (Table 1.6). Jiao et al. [132] compared uncoated alumina/silica (Al_2O_3/SiO_2) composite NPs with GOPS modified Al_2O_3/SiO_2 NPs as additives of a mineral oil and after 3 months the uncoated nanocomposites were mostly precipitated, and the modified ones stayed homogenously dispersed in the oil. Two main factors affect the best time stability results corresponding to GOPS modified Al_2O_3/SiO_2 NPs: first the adequacy of the functionalization method (silanization) to the size of the NPs (70 nm) [28] and second, the fact that the surface properties of Al_2O_3/SiO_2 nanocomposite changed, after modification, from hydrophilicity to lipophilicity [132], showing affinity for nonpolar oils. Using click chemistry, Farsadi et al. [133] synthesized a novel friction modifier: a nanocomposite of MoS_2 NPs and a reduced graphene oxide functionalized with triazole (rGO-T). This nanocomposite was dispersed in a group II 500 N petroleum-based oil (viscosity 93 cSt at 40 °C) remaining uniformly dispersed for one month.

Regarding the lubricants containing nanocomposites, it has not broadly been investigated the stability of the nanodispersions with a given nanocomposite compared to that of the dispersions containing the corresponding separated NPs. Interestingly, Farsadi et al. [133] found that a MoS_2

nanodispersion shows sedimentation meanwhile the nanodispersion of $MoS_2/FrGO$ nanocomposite remains stable, so, the triazole modified rGO, rGO-T, is capable of stabilizing the MoS_2 NPs.

Table 1.6 Stability of nanolubricants based on modified nanocomposites

Nanoadditive	Functionalization	Concentration	Base oil	Stability	Ref.
Al_2O_3/SiO_2 (70 nm)	GOPS	1 wt%	Lubricating oil	3 months	[132]
MoS_2 (50 nm)/rGO-T	Triazole	NA	Group II oil	1 month	[133]
ZnO/Al_2O_3 (63 nm)	OA	1 wt%	Mineral oil	28 days	[134]
Graphene/MTT	APTES	0.4 g/L	15W40	1 month	[135]
Cu (5 nm)/GO	SA	0.05 wt%	Paraffin oil	10 days	[136]
Cu/rGO (50 nm)	OA	0.5 wt%	PAO10	7 days	[137]

Considering only those publications with information on the size of the NP, it is possible to relate the effect of their size, and the type of modifying agent with the stability time of the nanodispersions (Figure 1.7). For this purpose, five types of modifying molecules were considered: organic acids, amines, silanes, combinations of two types and other modifying agents. Most nanodispersions included in Tables 1.1 to 1.6 show stability times longer than 4 weeks (28 days). Among the nanodispersions with lower stabilities, more than half have NPs with sizes above 50 nm. Silanes are the most effective modifying agents for increasing the stability times for nanodispersions of NPs above 70 nm, achieving a maximum stability of 120 days for a dispersion containing OTES and DETAS silanized SiO_2 NPs (100 nm) dispersed in PAO100 [54]. Despite the small size, some of the NPs with sizes below 30 nm have poor stability times, such as 2-octadecyl gallate modified TiO_2 NPs (20-25 nm) dispersed in PAO10 or 10W30 [121], and dialkyldithiophosphate modified Ag NPs (15 nm) dispersed in paraffin oil [118], all of them with less than 5 days of stability. It is very unlikely that the three close hydroxyl groups of the 2-octadecyl gallate react with the NP surface, so the formed coated NPs have OH groups, i.e., higher polarity than PAO10 and 10W30. The polar groups of 2-octadecyl gallate and dialkyldithiophosphate are bulkier than those of organic acids or amines, which can lead to lower grafting densities. Most of the nanodispersions with stability times greater than 4 weeks contain NPs with sizes smaller than 30 nm with organic acids or amines as modifying agents, reaching stabilities of 11 months (330 days), in the case of an ester oil containing OA modified Fe_3O_4 NPs (6.3 or 10 nm) or Nd alloy NPs (19 nm) [56]. Other nanolubricants with stability times longer than 5 months are: paraffin oil + (MWCNT-SA (20-40 nm), Ag-dialkyldithiophosphate (4 nm), Cu-dialkyldithiophosphate (5 nm)), castor oil + CQD-DPA (2 nm), PAO4 + (Ag-dodecanethiol (3-6 nm), Pd-dodecanethiol (2-4 nm)), PAO6 + WS_2-OM (6-8 nm) and DIOS + WS_2-OM-MADE (6-8 nm) and gas mobile oil + SiO_2-APTES, GOPS, or 3-MPS (15-20 nm). Except MWCNT-SA, all the last nanoadditives are spherical (Tables 1.1, 1.2, 1.4 and 1.5).
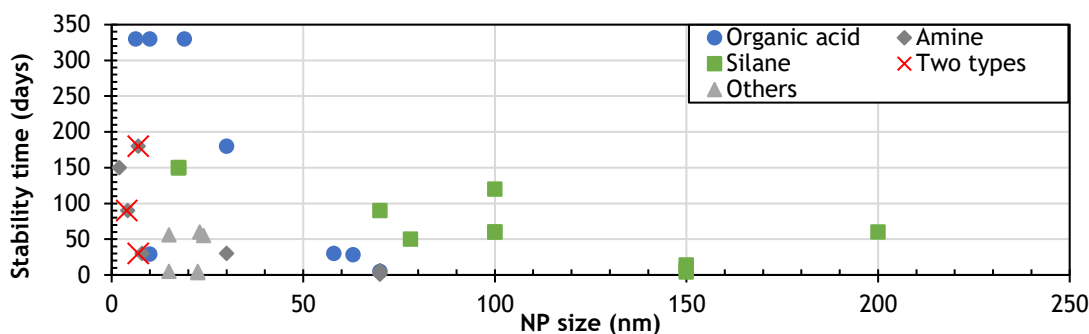
Figure 1.7 Effect of the size of the NPs and their modifying agent on the stability of their nanodispersions

Another relevant factor to choose the appropriate modifying agent is the similarity in the polarities of the agent and of the base oil. For instance, an N-doped modification of CDs is more suitable for PEG (stability time of one month) meanwhile a further modification with OM to the N-doped CDs was needed for PAO4 (stability time of one month) [108]. Similarly, in the case of OM modified WS_2 NPs [125,126] with a non-polar base oil like PAO6 a stability time of 6 months was achieved. A further modification of OM-WS_2 NPs with MADE is needed to get the same stability time with a more polar ester base oil [126].

Figure 1.8 presents the effect of the type of NPs on the stability of the nanodispersions with stabilities longer than 28 days. Metal oxide NPs, specifically Fe_3O_4-OA NPs, and Nd alloy-OA NPs show the best stability times, more than 11 months [56]. Metal sulfide NPs, specifically OM or OM/MADE modified WS_2 NPs, is the next type with the best stability, up to 180 days [125,126]. Small carbon nanomaterials, such as amine modified CQDs, also show some promising results, reaching up to 150 days of stability [109]. Other NPs, like silane modified SiO_2 NPs, can achieve long stability times remaining stable for 150 days [127].
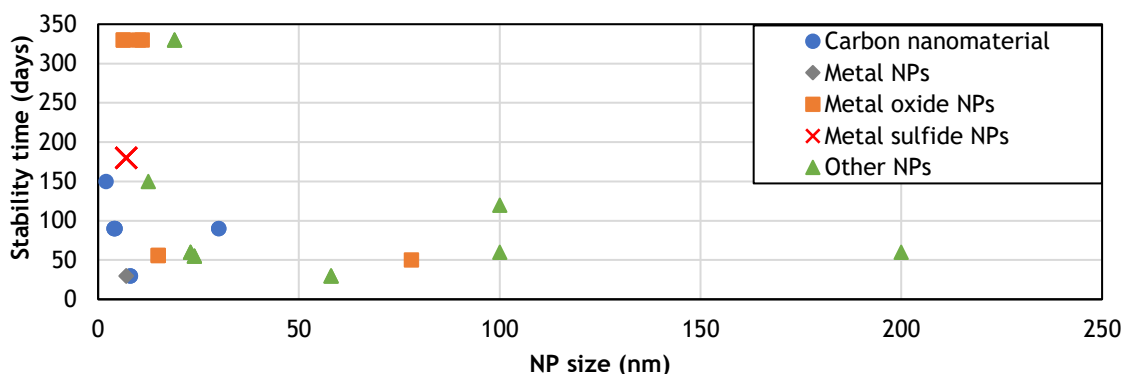
Figure 1.8 Effect of the size and type of the NPs on the stability of their nanodispersions

Regarding the base oil and limiting the analysis to those nanodispersions with stabilities longer than 28 days, Figure 1.9 shows that PAOs are the most used base oil in the study of nanolubricants. However, nanodispersions based in PAOs show poorer stabilities compared to ester oils. Mineral oil nanolubricants show similar stability results to those of PAOs. Vegetable oil nanolubricants are scarce in the literature. The best results were obtained with an ester oil, specifically TMPTO, which contains oleate, thus having great compatibility with the oleic acid coating of the nanoparticles used in these cases [56].
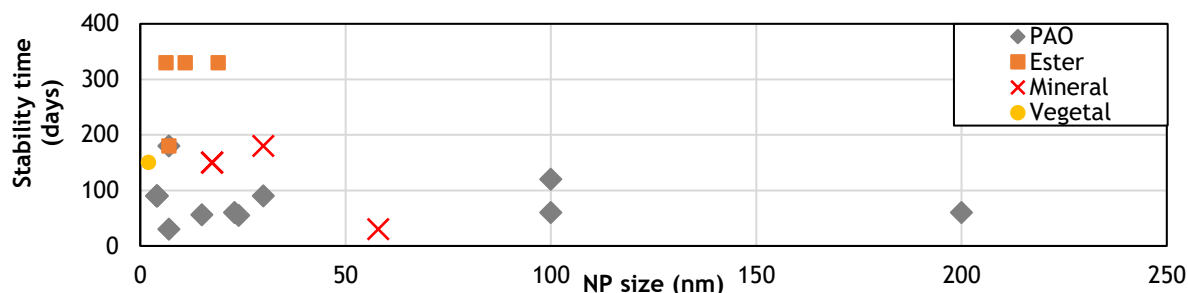
Figure 1.9 Effect of the size of the NPs and the base oil on the stability of their nanodispersions

Another factor affecting the nanolubricant stability related to the base oil is its viscosity. Figure 1.10 presents the literature stability results that include information about the dynamic viscosity of the base oil at 40 ºC. The base oils used in most of these articles have low viscosities (less than 100 mPa s at 40 ºC) and correspond to the most stable nanolubricants [56,125,126]. That of high viscosity (1100 mPa s at 40 ºC) was PAO100 and its nanodispersions remained stable up to 120 days[29,53-55]. This trend could be related to the conclusion from Figure 1.9, PAO nanolubricants show lower stabilities compared to ester oils.
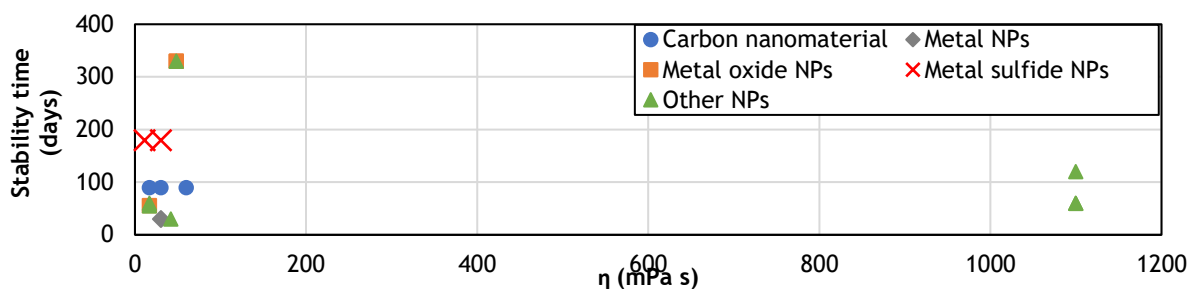
Figure 1.10 Effect of the dynamic viscosity at 40 ºC of the base oils and the NP type on the stability of their nanodispersions

In conclusion, multiple factors play a role in the stabilization of the nanoparticles, like modifying agent and base compatibility, type of base oil and its viscosity, as well as size, morphology, and concentration of the NPs. Thus, all these factors must be evaluated to reach the best possible stability results.

1.3.2 Tribology

The stability of the coated NPs in the lubricants is not the only challenge, but also their tribological behavior, which is affected by many factors such as grafting density, size, shape, concentration, or composition [116,117,119,120] of the NPs. Furthermore, when the NP coating has polar groups at its external ends, tribochemical reactions can occur between those polar moieties and the positively charged metallic surface, facilitating the adsorption of the NPs onto the metallic surface [29,114,120]. This section reviews the tribological results reported in the literature for nanolubricants, containing chemically modified NPs, with stabilities of at least four weeks, discussed in Section 1.3.1, with the objective of providing knowledge on the characteristics that the NPs must have to give rise to strong reductions in friction and wear. This is one of the tools of this PhD thesis to contribute to cover this gap in science. Thus, the friction and wear reductions due to nanoadditives of carbon and its derivatives (Table 1.7), metals (Table 1.8), metal oxides (Table 1.9), metal sulfides (Table 1.10), nanocomposites (Table 1.11) and other NPs (Table 1.12) are summarized.

The different experimental conditions of the tribological experiments significantly affect both wear and friction values and highly difficult the comparison of the literature results. Standard measurement conditions should be defined by international associations of tribologists to better compare the antiwear and antifriction capabilities of the additives and lubricants from a global perspective. However, it is very difficult to establish standards that can generalize results because most of the tribologists make friction tests with conditions as close as possible to those of the real applications, taking into account also the characteristics of their tribometers. This issue can be partially arranged because in this paper friction and wear reductions with respect to those of the base oils were used.

The dependence of the friction and wear reductions on the nanoparticle concentration, frequently shows a maximum at the usually named optimal concentration; for lower concentrations, the friction and wear reducing mechanisms due to NPs can partially (or even cannot) act since the quantity of NPs is insufficient, being the tribological behavior governed mainly by the base oil, while if the concentration is higher than the optimum one, the NPs can act as debris particles increasing friction and wear [114]. Wear can be characterized by different parameters such as wear volume (W_{Vol}), wear track width (WTW), wear track depth (WTD), or wear rate (W_{rate}). There are several tribological mechanisms by which nanoadditives improve lubrication [138], such as the formation of physical or chemical tribofilms leading to the protection of the tribopair from wear and a reduction of the COF [31,120,126]. The other mechanisms that reduce friction and wear are rolling effect, which only occurs when the NPs are spherical or cylindrical, mending effect, which consists in the introduction of NPs in micro-pits and grooves present on the metallic surface, and polishing effect, through which the lubricated surface roughness is reduced by abrasion due to NPs [4].

Carbon and its derivatives (Table 1.7): Sun and Du [139] studied the mechanisms by which graphene derivatives with two-dimensional structures, as GO or rGO, act as antifriction and antiwear nanoadditives. According to these authors, these NPs 1) can easily enter the friction pair contact region, being able to be effectively involved in lubrication because they easily shear; 2) can form friction transfer films and 3) can both fill the surface concave area, and adsorb at the roughness peaks, thus reducing the friction between the rubbing surfaces. The tribological performance of the lubricants containing this type of additives not only depends on the morphology and the type of coating but also on number of layers, and their size [140].

Paul et al. [80] analyzed the effect of applied load for a 5W30 oil and three of its nanodispersions containing DDA functionalized GO (0.01, 0.05, 0.10 wt%) obtaining the optimal concentration 0.10 wt% with reductions of 40% in COF and 50% in WTW under a load of 10 N, the lowest load analyzed.

Mungse et al. [104] studied the antifriction and antiwear properties of GO functionalized with ODA as an additive for a 10W40 oil, presenting a 25 % reduction in both COF and WTW compared to those of 10W40 oil. Several articles shown the tribological properties of lubricants using rGO as additives. Samanta and Sahoo [105] examined the effect of a polymer-grafted rGO on the tribological behavior at different contact pressures and on load-bearing capacity of a paraffin oil. The highest COF reductions achieved under 147 N were 75 % and 50 % for rGO-PEI-PSS and rGO-PEI-PAA respectively being the W_{Vol} reductions 69 % and 53 % compared to that obtained with the paraffin oil additivated with GO. Due to the higher packing density and the dispersion stability, the rGO modified with polymer brushes can more effectively reduce stress, compression, and shear than unmodified rGO, leading to improvements in antifriction, antiwear and load-bearing capabilities.

Ismail et al. [114] studied the tribological behavior of a base oil (group II 500 N petroleum-based oil) containing triazole ring-decorated rGO, FrGO, at three different concentrations, by means of four-ball tests. The nanodispersion with 0.01 wt% of FrGO led to the greatest COF and wear reductions, being respectively 16 % and 30 % (WTW) when compared to those of neat base oil. The aforementioned results show that several functionalities (ODA, PEI-PSS, octadecyl alcohol and triazole) of GO or rGO, enhance the stability of the nanoadditives in the oil and also lead to excellent tribological properties. On the other hand, Patel et al. [95] used a ball-on-disc instrument to measure the wear preventive characteristics of rGO dispersed at three different concentrations in a group II oil; the nanolubricant containing 0.05 wt% rGO nanoplatelets showed the greatest wear reduction, 52 % compared to the group base oil, as well as a reduction in friction of around 40 % at 60 rpm.

Chen et al. [103] modified MWCNTs with SA (20-40 nm), dispersed them in a liquid paraffin (being the concentration 0.45 wt%), and studied the effect of the mass ratio of SA to MWCNTs (SA:MWCNTs) on tribological properties under a load of 1000 N, finding 2:1 as the optimum ratio to improve the friction reduction and antiwear capacity of base lubricant. These could be explained because SA is also a good lubricant; during the wear test, SA forms an effective film, but, due to the high temperature reached during the tests, for high SA concentrations it is decomposed and oxidized easily, increasing COF and wear. Furthermore, these authors also examined the effect of load on tribological properties using modified and unmodified MWCNTs nanodispersions (0.45 wt% and a SA:MWCNT mass ratio 2:1) obtaining the highest friction reductions and the best antiwear capabilities with the modified MWCNTs. This fact can be explained by the better dispersibility of modified MWCNTs; the tribopair surfaces were easily filled with the dispersed modified MWCNTs during the tribological tests, and then the NPs on the wear surface could help as spacers, avoiding rough contact between the two mating surfaces, thus greatly reducing the wear loss significantly (45 % at 1000 N). Nevertheless, the friction reductions are quite small: 9 % at 500 N and 4 % at 1000 N. Liang et al. [74] analyzed the tribological behavior of CDs-HDA (4.2 nm) as additives of PAO4, observing that for the load of 20 N and the nanolubricant with the optimal concentration (1 wt%), the COF and W_{Vol} decreased by 27 % and 46 %, respectively. These authors proposed that boundary lubrication films containing iron oxides and CDs-HDA are formed on rubbing surfaces by absorption and deposition but also act through rolling, mending and polishing mechanisms. Furthermore, Shang et al. [75] analyzed the tribological behavior of dispersions of N-CDs in a PEG as well as OM-N-CDs in a PAO finding that the COF and W_{Vol} of PEG with 1.0 wt% N-CDs are reduced up to 76 % and 83 %, respectively. In addition, for the OM-N-CDs (1.0 wt% in PAO) 23 % and 46 % reductions in COF and wear were achieved. These authors suggested that N-CDs act as rolling ball bearings and could be irregularly deposited on the worn surface with mending effect and the formation of a tribochemical film which contains also Fe_2O_3 and nitrogen element, which prevented direct contact of the metal surfaces.

Likewise, Lu et al. [76] studied the mass concentration effect of OM-CDs on tribological properties of PAO10, concluding that the 1.0 wt% OM-CDs nanolubricant showed the best friction-reducing and antiwear properties. Specifically, the COF and diameter of the worn scar were reduced by 47 % and 30 %, respectively. These authors suggested that the synergistic effect of a formed tribofilm which includes PAO and the OM-CDs might account for the good antiwear and antifriction capabilities under boundary lubrication. Finally, Ye et al. [109] evaluated the tribological performance of castor oil and PAO nanooils containing N-CQDs as additives, finding that for both oils the COF is not improved by adding these nanoadditives.

Nevertheless, the wear is reduced by 45 % for the optimal concentration of 0.2 wt% N-CQDs (in comparison to the CO base oil) and 29 % for optimal addition of 0.5 wt% OM-N-CQDs (in comparison to PAO). These authors proposed that CQDs are deposited unevenly on the worn surface and form a thin protective film also containing iron oxides and nitrogen.

In conclusion, it can be inferred that nanolubricants based on functionalized carbon derivatives act as contact mitigators between rubbing surfaces through the formation of effective tribofilms, which reduce friction and protects the surfaces against undesirable wear, especially when their coating contains polar groups, which promote tribochemical reactions with the positively charged metal surfaces.

Table 1.7 Friction and wear reduction of nanolubricants based on modified carbon NPs

Nanoparticle	Functionalization	Best concentration	Base oil	Friction reduction	Wear reduction	Ref.
GO	DDA	0.1 wt%	5W30	40 %	~50 % WTW	[80]
GO	ODA	0.02 g L^{-1}	10W40	25 %	25 % WTW	[104]
rGO	ODA	0.05wt% + 1wt% IL	Ester Oil	34 %	34 % WTW	[113]
rGO	PEI-PSS	0.5 wt%	Paraffin oil	75 %	69 % W$_{Vol}$	[105]
rGO	PEI-PAA	0.5 wt%	Paraffin oil	50 %	53 % W$_{Vol}$	[105]
rGO	Octadecyl alcohol	0.005 wt%	Hydraulic oil	10 %	44 % W$_{Vol}$	[106]
rGO	Triazole	0.01wt%	Group II oil	16 %	30 % WTW	[114]
rGO	Reduction	0.050 wt%	Group II oil	40 %	52 % W$_{rate}$	[95]
MWCNT (20-40 nm)	Stearic acid	0.45 wt%	Paraffin oil	4 %	45 % wear loss	[103]
CNPs (25-35 nm)	OM	1 wt%	PAO10	47 %	30 % WTW	[115]
CDs (4.2 nm)	HDA	1 wt%	PAO4	27 %	46 % W$_{Vol}$	[107]
CDs (4-12 nm)	N	1 wt%	PEG	72 %	83 % W$_{Vol}$	[108]
CDs (4-12 nm)	N-OM	1 wt%	PAO	23 %	46 % W$_{Vol}$	[108]
CQDs (2 nm)	DPA	0.2 wt%	Castor Oil	COF increases	45 % WTW	[109]
CQDs (4 nm)	DPA and OM	0.5 wt%	PAO6	COF increases	29 % WTW	[109]

Functionalized metal NPs (Table 1.8): Li et al. [116] found improvements in the antiwear properties of a paraffin oil through the addition of dialkyldithiophosphate-coated copper or silver NPs. Wear analysis showed significant reductions with the addition of these NPs compared to that obtained using the base oil, especially at high loads. Specifically, paraffin oil nanodispersions containing 0.5 wt% dialkyldithiophosphate coated copper or silver NPs lead to WTW reductions of 58 % or 59 %, respectively. Antiwear properties of the dispersions containing dialkyldithiophosphate coated Cu NPs are better than those containing only zinc dialkyldithiophosphate (ZDDP), especially at lower concentrations. Moreover, Kumara et al. [117] performed tribological tests with dodecanethiol-modified silver or palladium NPs (Ag and Pd NPs) dispersed in PAO4 for a contact formed by a steel ball and a cast iron plate. Both Pd and Ag NPs led to substantial reductions of the COF (25–40 %) and wear of the cast iron plate (90–97 %) with the best reductions in both properties being obtained with Pd NPs,

especially with the 1.0 wt% concentration. Chen et al. [119] studied the effect of OM and OA modified Ni NPs of controlled sizes on tribological performance of PAO6, using a four-ball friction and wear tester. The authors concluded that the smallest NPs (7 nm) are more effective than the larger ones, specifically in reducing WTW, with a maximum reduction of 30 %. Nevertheless, no reduction was found in the COF for any coated Ni NPs.

The sizes of NPs contained in Table 1.8 are lower than 15 nm. For three of the five nanodispersions, friction data are not available or get worse. Nevertheless, in terms of wear, substantial reductions are achieved by using nanolubricants instead of neat oils; the most sensitive wear parameter is the worn track volume, with reductions of up to 98 %. Furthermore, in this case, under mixed and boundary lubrication conditions, the nanoadditives could easily form boundary lubricating films on the sliding surfaces. In addition, smaller NPs (high surface activity) can generate protective tribofilms through an *in situ* deposition mechanism.

Table 1.8 Friction and wear reduction of nanolubricants based on modified metal NPs

Nanoparticle	Functionalization	Best concentration	Base oil	Friction reduction	Wear reduction	Ref
Ag (4 nm)	Dialkyldithiophosphate	0.5 wt%	Paraffin oil	N/A	59 % WTW	[116]
Ag (15 nm)	Dodecanethiol	1.0 wt%	PAO4	37 %	95 % W_{Vol}	[117]
Cu (5 nm)	Dialkyldithiophosphate	0.5 wt%	Paraffin oil	N/A	58 % WTW	[116]
Pd (2-4 nm)	Dodecanethiol	1.0 wt%	PAO4	~40 %	98 % W_{Vol}	[117]
Ni (7 nm)	OM and OA	0.05 wt%	PAO6	COF increases	30 % WTW	[119]

Functionalized metal oxide NPs (Table 1.9): Wright et al. [120] studied the lubricating performances of PLMA brush-grafted titania NPs, as additives of PAO4 for different molecular mass of the coating (8-21 kDa of PLMA). The modified TiO_2 NPs were not regular in shape with plate and rod-like nanostructures. For all the studied nanodispersions, the COF decreased, obtaining with the lowest molecular mass NPs the highest friction reduction (40 %) with respect to that obtained with PAO4. Meanwhile, wear was also significantly reduced (91 %) in terms of worn volume of iron plates.

Liñeira del Río et al. [56] characterized the tribological performance of two nanolubricants composed by TMPTO base oil with superparamagnetic NPs: Fe_3O_4 (6.3 nm) and Fe_3O_4 (10 nm), all of them coated with OA, being the NP concentration 0.015 wt%. For the tribological tests performed under pure sliding conditions, COFs for the two nanolubricants are lower than that achieved with the base oil, with the best friction performance achieved for the Fe_3O_4-OA (10 nm) nanolubricant with a friction decrease of 18 % in comparison to TMPTO base oil. NPs of both sizes also improved wear, with the Fe_3O_4-OA (10 nm) nanolubricant also achieving the highest wear reduction 76 % in terms of W_{Vol}.

Table 1.9 Friction and wear reduction of nanolubricants based on modified metal oxide NPs

Nanoparticle	Functionalization	Best concentration	Base oil	Friction reduction	Wear reduction	Ref.
Al_2O_3 (78 nm)	GOPS	0.1 wt%	Machine oil	18 %	42 % WTW	[122]
TiO_2 (15 nm)	PLMA	1.0 wt%	PAO4	~40 %	91 % W_{Vol}	[120]
Fe_3O_4 (6.3, 10 nm)	OA	0.015 wt%	TMPTO	18 %	76 % W_{Vol}	[56]

In general, tribological results with nanolubricants based on modified metal oxide NPs are meaningful, highlighting those related to nanolubricants containing oil-soluble polymer brush-grafted TiO_2 NPs, improving the results when the brush molecular mass reduces. Reductions up to 40 % in friction and 91 % in W_{Vol} were found. Regarding the lubrication mechanisms, protective tribofilms formed on the friction surfaces were suggested in all the cases. Furthermore, rolling mechanism was identified for nanolubricants including spherical Al_2O_3 NPs [122]. Finally, the mechanisms due to the presence of superparamagnetic NPs also include mending and polishing effects. It must be noted that NPs with different shapes lead to excellent tribological properties: in the case of the brush-grafted TiO_2 NPs they are irregularly shaped with rod-like nanostructures and those superparamagnetic NPs showed spherical and cubical shapes.

Functionalized metal sulfide NPs (Table 1.10): Jiang et al. [125] prepared dispersions of OM-modified ultrathin tungsten disulfide nanosheets in PAO6 base oil and evaluated their tribological performance with a four-ball machine. The best antiwear and friction-reducing ability was obtained at 75 ºC with the 2.0 % mass fraction nanodispersion, resulting in 96 % and 44 % reductions, respectively. Moreover, the tribological behavior of modified WS_2 nanosheets as additives of PAO6 is better than that of OM as additive. These authors [125] also evaluated the effect of temperature and load on the tribological behavior of the later nanolubricant, obtaining that WTW and COF increased with increasing temperature (or load), remaining better than those of PAO6 base oil. These reductions are because stable suspensions can effectively transfer the NPs onto the contact zone of rubbing steel surfaces, forming a surface protective layer. In a later work, Jiang et al. [126] also studied the tribological behavior of OM and MADE capped WS_2 NPs in an ester oil (DIOS) at different temperatures and loads, finding wear and friction reductions in all the conditions. The best tribological results were at 75 ºC with reductions of 56 % and 83 % for COF and W_{Vol}, respectively. The tribological behavior with NP concentration followed the same trend as in their previous work [125].

Considering the aforementioned results, it is clear that modified WS_2 nanoplatelets exhibit significant tribological performance over a broad range of temperatures, because of the nanoadditives are capable to form on the worn surfaces both adsorbed films with a low shear force and tribochemical reaction films [125,126].

Table 1.10 Friction and wear reduction of nanolubricants based on modified metal sulfide NPs

Nanoparticle	Functionalization	Best concentration	Base oil	Friction reduction	Wear reduction	Ref.
WS_2 (6-8 nm)	OM	2.0 wt%	PAO6	Load 392N: r.t.: 0 % 75 ºC: 44 % 150 ºC: 37 % 200 ºC: 39 %	W_{Vol}: r.t.: 77 %, 75 ºC: 96 %, 150 ºC: 97 %, 200 ºC: 96 %	[125]
WS_2 (6-8 nm)	OM and MADE	2.0 wt%	DIOS	Load 392 N: 20 ˚C 50 %, 75 ˚C 56 %, 150 ˚C 15 %	W_{Vol}: 20 ˚C 68 %, 75 ˚C 83 %, 150 ˚C 52 %	[126]

Other functionalized NPs (Table 1.11): Li et al. [116] examined the enhancement of the antiwear properties of a paraffin oil by the addition of dialkyldithiophosphate coated LaF_3. WTW is highly reduced with the addition of NPs compared to that of neat paraffin oil, especially at higher loads.

As regards to SiO_2 NPs, Li et al. [127] studied the tribological behavior of ST5W/30 gas mobile oil with three different silane modified silica NPs (APTES, GOPS or 3-MPS) as separately additives with a reciprocating tribotester and a four-ball tester. In both cases 3-MPS modified SiO_2 NPs lead to the best friction and wear reductions.

Sui et al. [55] used HSNs tethering separately three different amino functionalized silanes (APTES, AEAPS or DETAS) onto silica NPs with different sizes. The tribological properties of these HSNs dispersed in PAO100 were measured on a four-ball tester. Among the three HSNs of 20 nm size, the NPs coated with AEAPS leads to the best tribological behavior. Regarding the 50 and 100 nm HSNs, DETAS HSNs showed the best friction reduction and antiwear properties, being in both cases the COF lower than that of 20 nm AEAPS HSNs. For 100 nm DETAS HSNs the maximum reductions in WTW and COF were found, being 60 % and 40 %, respectively, comparing to neat PAO100. In a later article, Sui et al. [29] studied the effect of different functional groups (amino, carboxyl, phenyl, and alkyl groups) tethered on DETAS HSNs on their tribological performance. The best antiwear and friction reductions (40 %) correspond to the NH_2 terminated HSNs at the optimum concentration of 1 wt%, but showed concentration sensitive behavior, due to the hydrogen bonding between the primary NH_2 groups leads to aggregation. The CH_3 and C_6H_5 terminated HSNs improved the tribological performance and the stability of the HSNs. Sui et al. [54] also modified silica NPs with DETAS and OTES in different ratios to obtain bifunctional hairy silica NPs (BHSN). The optimal DETAS:OTES ratio in BHSNs was investigated, obtaining the best tribological properties with the 2:1 ratio, specifically, reductions of 40 % in COF and 60 % in WTW compared to those of the neat PAO100.

Wright et al. [120] studied the lubricating performances of PLMA brush-grafted silica NPs with different average molecular weights as additives for PAO4 using a tribotester in a ball-on-plate reciprocating configuration. Modified SiO_2 with the lower molecular weights (4.1 kDa) as PAO additives (at 1 wt%) showed a noticeable reduction in COF (30 %) and important reductions in W_{Vol} (up to ~90 % for both plate and ball). Free polymer PLMA (38 kDa) dispersed in PAO4 was evaluated for comparison with modified SiO_2 and performed similarly to neat PAO4. To investigate the concentration effect, three additional dispersions of PLMA brush-grafted silica (21.7 kDa) were dispersed in PAO4, decreasing the COF when the NP concentration increases, until achieving a concentration of 4.0 wt% in the lubricant. Moreover, Seymour et al. [73] studied the effect of alkyl pendant chain length (6, 8, 12, 13, 16 and 18 C atoms) of a series of PLMA brush-grafted HSNs, using a ball-on-plate reciprocating tribotester. All the dispersions led to lower COFs than those of ZDDP in PAO and of neat PAO, being the maximum friction reduction 38 % with the HSNs with alkyl pendant chain length of 16 C atoms. Nevertheless, the antifriction behavior showed by the HSNs with different alkyl pendant chains is similar, which indicates the relevance of the core silica NPs in the efficacy as lubricant additives. Likewise, W_{Vol} values of the iron plates evaluated with HSN dispersions were found to be similar, reducing up to 90 % compared to that of neat PAO, but are slightly higher than that of ZDDP in PAO.

Regarding the tribological mechanisms that take place when using other modified NPs (Table 1.11), which are all nearly spherical, most authors describe that these NPs are embedded

in the nanogrooves on the wear surface and can form protective films that reduce friction and wear.

Liñeira del Río et al. [56] characterized the tribological performance of TMPTO dispersions of OA modified Nd alloy NPs ($Nd_2Fe_{14}B$) with a diameter of 19 nm, being the NP concentration 0.015 wt%. At under pure sliding conditions, in comparison to TMPTO a COF decrease of 29 % base oil was found as well as a 99 % wear reduction in terms of W_{Vol}. A smoother surface was found when the pins are lubricated with the nanolubricant instead of with the base oil, being the roughness reduction 54 %. Boundary tribofilm, polishing and mending effects happen owing to the presence of NPs.

Table 1.11 Friction and wear reduction of nanolubricants based on other modified NPs

Nanoparticle	Functionalization	Best concentration	Base oil	Friction reduction	Wear reduction	Ref
LaF_3 (8 nm)	Dialkyldithiophosphate	0.5 wt%	Paraffin oil	N/A	WTW: 48 %	[116]
SiO_2 (15-20 nm)	APTES	0.3 wt%	Gas mobile oil	42.8 %	31 % WTW	[127]
	GOPS	0.3 wt%		25.3 %	22 % WTW	
	3-MPS	0.3 wt%		40.6 %	23 % WTW	
SiO_2 (20, 50, 100 nm)	DETAS	1.0 wt%	PAO100	40 %	60% WTW	[55]
SiO_2 (100 nm)	DETAS	1.0 wt%	PAO100	43 %	N/A	[29]
SiO_2 (100 nm)	DETAS and OTES	1.0 wt%	PAO100	40 %	60% WTW	[54]
SiO_2 (24 nm)	PLMA	1.0 wt%	PAO4	30 %	W_{Vol}: 92 % plate 95 % ball	[120]
SiO_2 (23 nm)	PLMA	1.0 wt%	PAO4	38 %	90 % W_{Vol}	[73]
SiO_2 (54 nm)	OA	0.05 wt%	Paraffin oil	28 %	34 % WTW	[128]
Nd alloy (19 nm)	OA	0.015 wt%	TMPTO	29 %	99 % W_{Vol}	[56]

Functionalized nanocomposites (Table 1.12): Jiao et al. [132] tested Al_2O_3/SiO_2 nanocomposites modified with GOPS coupling agent as additives of a lubricating oil with a four-ball tribometer, obtaining the best tribological performance at 0.5 wt%, reducing COF by 20 % and WTW by 22 %. In addition, thrust-ring tests led to a 50 % COF reduction, which was better than those obtained with single Al_2O_3 or SiO_2 dispersions. Li et al. [135] dispersed functionalized graphene/montmorillonite (FG/MTT) nanosheets, in a 15W40 engine oil, evaluating the tribological properties in a four-ball tribometer. At the optimal concentration, COF and WTW were improved by 50 % and 13 %, respectively, compared with those obtained with the neat oil, being the friction reduction notably higher than those obtained using as additives FGO or MTT separately. Regarding the tribological mechanisms, two situations must be distinguished, considering the shape of the NPs: one that involves nanocomposites with the two types of NPs almost spherical and other in which at least one type of NPs is laminar. The first is the case of Al_2O_3/SiO_2 nanocomposite, which can form a thin lubricating layer between the contact surfaces and act as bearings changing the sliding friction to rolling friction The latter is the case of functionalized Graphene/MTT, where the lamellar structure of graphene is combined with smaller nanoplatelets of MTT, filling the asperities on the contact surface with sheets of different sizes and also reacting with this surface to form a repairing tribolayer.

Table 1.12 Friction and wear reduction of nanolubricants based on modified nanocomposites

Nanoparticle	Functionalization	Best concentration	Base oil	Friction reduction	Wear reduction	Ref.
Al_2O_3/SiO_2 (70 nm)	GOPS	0.5 wt%	Machine oil	20 %	22 % WTW	[132]
MoS_2 (50 nm)/ rGO-T	Triazole	0.8 wt%	Group II oil	16 %	29 % WTW	[133]
Graphene/MTT	APTES	0.4 g L^{-1}	15W40	50 %	13 % WTW	[135]

The effect of the size of the NPs and their modifying agents on reductions of the COF and wear has been analyzed (Figure 1.11), in a similar way to the analysis carried out with the stability time of the nanodispersions (Figure 1.7). The same five categories of the modifying agents were considered. Only the tribological behavior of those nanodispersions with more than 4 weeks of stability were analyzed. Most of the NPs (83 %) that appear in Figure 1.8 have sizes smaller than 40 nm, being all the NPs with sizes greater than 60 nm silanized. For most nanodispersions, the wear reductions are higher than the COF reductions. In fact, the COF can increase while the wear decreases due to the NPs [109,119]. The highest friction reduction in Figure 1.11 is 72 % for N-doped CDs (8 nm) dispersed in PEG [108], followed by WS_2-(OM+MADE) (6-8 nm) dispersed in a ester, CNP-OM (25-35 nm) dispersed in PAO10 with reductions of 56 % and 47%, respectively. These last nanoadditives are spherical. Nevertheless, the highest friction reduction (75 %) was obtained with rGO-PEI-PSS (unknown size) dispersed in a paraffin oil. On the other hand, the highest wear reduction reaches a 99 % for an OA modified Nd alloy NP (19 nm) in an ester [56], followed by Pd-Dodecanethiol (2-4 nm) in PAO4, WS_2-OM (6-8 nm) in PAO6, Ag-Dodecanethiol (15 nm) in PAO4 and SiO_2-PLMA (24 nm) in PAO4 with 98 %, 97 %, 95 % and 95 %, respectively. All these nanoadditives are spherical except the coated Nd alloy NPs which are cubic. Notably, there are ten nanodispersions with wear reductions higher than 75 %, none of them contains silanized NPs, for which the highest wear reduction is 60 % for a DETAS silanized SiO_2 NPs (100 nm) dispersed in PAO100 [55].

Apart from the size, modifying agent and chemical structure of the NPs, as well as the polarity of the base oil, the viscosity of the oil should be considered. In general, the NPs led to higher friction and wear reductions dispersed in low viscosity oils (as PAO4, PAO6, DIOS) [117,125,126] than in high viscosity oils [29,135].
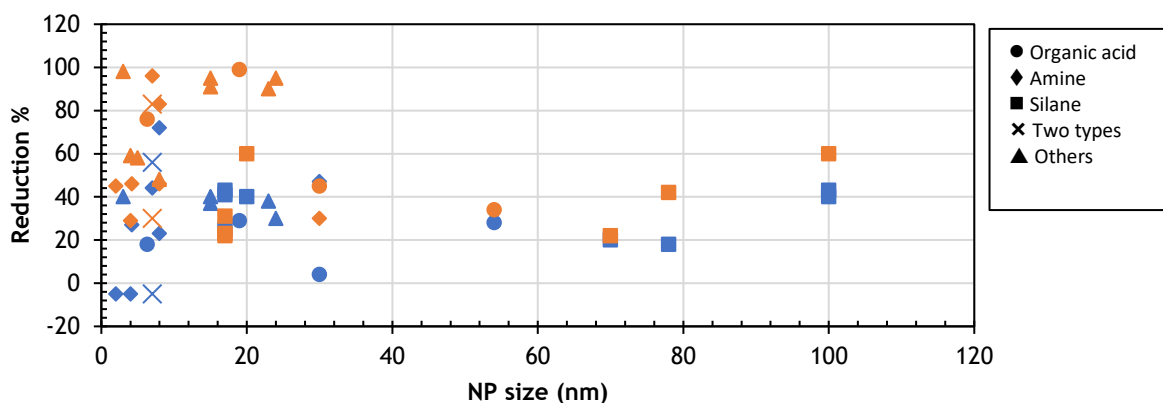
Figure 1.11 Effect of the size of the nanoparticle and its modifying agent on the reduction of friction (blue) and wear (orange)

1.3.3. Overview

To sum up this state of art, some conclusions can be inferred. As regards to the preparation of the nanodispersions, although the two-step method is the most widely used to prepare nanolubricants, the dispersion methods involving evaporation of a volatile solvent led to greater stability results compared to the former. To determine the stability time of the nanolubricants, the sediment photograph capturing is the most common method. This technique should be accompanied by a more quantitative method; however, some of them, like DLS or UV-Vis, show important limitations when the nanodispersions are dark, opaque, or highly concentrated.

As regards to the dispersibility of the nanoadditives in the base oil, several parameters affect the stability of the nanodispersions, such as the morphology, size and concentration of the NPs, or the viscosity of the base oil and the type of coating. Another factor that affects stability is the grafting density of the modifying agent bonded to the NP [28], however, this factor could not be evaluated due to the lack of information available in the abovementioned literature. Analyzing the results with longer stabilities (several months), the most common morphology was spherical with a NP size lower than 20 nm (CQDs, Ag, Cu, Pd, Fe_3O_4, SiO_2, WS_2). These nanodispersions have concentrations between 0.015 wt% and 1 wt% in most cases, being the longer stability (longer than 11 months) for the lowest NP concentration. Regarding the type of chemical modifier, the most important factors for a good stabilizing performance in nonpolar base oils is the length of the alkyl chain, which should be of at least 12 carbon atoms, such as stearic acid (C18), oleic acid (C18), oleylamine (C18), dodecanethiol (C12), and the presence of a nonpolar CH_3 termination, whereas the type of polar functional group linked to the bare NPs hardly has influence. Nevertheless, for spherical NPs (SiO_2, Al_2O_3) with diameters higher than 70 nm, silane modifiers seem to be more appropriate (Table 1.3 and 1.5). Polymer functionalization gives rise to nanodispersions with stabilities of two months with excellent tribological properties. Studies on the effect of the length of the polymer coatings of the NPs on the stabilities of the nanodispersions are scarce. With respect to the effect of the functionalized NPs on the tribological performance, in most cases the nanolubricants reduce more effectively the wear than the friction.

Regarding the viscosity of the base oils, higher values lead to better stabilities, although, some of the more stable nanodispersions are based on low viscosity oils such as PAO4 or PAO6 proving that the chemical modification and other parameters (such as the NP size) play an important role in stabilizing the nanolubricants. Low viscosity oils (viscosity at 100 ºC lower than 10 cSt) should be developed as transmission fluids for electrical vehicles, among other applications. In this regard, Tables 1-12 allow to identify the following candidates for low viscosity nanolubricants: a) Nd alloy NPs (19 nm) functionalized with OA dispersed in TMPTO (viscosity at 100 ºC 8.45 cSt) which are stable more than 11 months and provide reductions up to 29 % for friction and 99 % for W_{Vol}, b) WS_2 NPs functionalized with OM or OM and MADE (6-8 nm) dispersed in PAO6 or DIOS: six months stability, friction and W_{Vol} reductions of up to 50 % and 97 % and c) Ag (15 nm) or Pd (2-4 nm) NPs functionalized with dodecanethiol, dispersed in PAO4: several months stability, friction and W_{Vol} reductions around 40 % and 95 % respectively. Tribofilm, mending, polishing, and rolling effects can explain this tribological behavior.

1.4 PhD Thesis framework

This PhD Thesis was carried out in the Laboratory of Thermophysical and Tribological Properties (LTTP) at the Applied Physics Department of the *Universidade de Santiago de Compostela*. This Laboratory is part of the Nanomaterials, Photonics and Soft Matter, NaFoMat, research group (GI-1488) of the *Universidade de Santiago de Compostela*. The NaFoMat group has received funding from the *Consellería de Cultura, Educación e Ordenación Universitaria* (*Xunta de Galicia*) as competitive reference group (GRC ED431C 2016/001 and GRC ED431C 2020/10). Since January 2019 NaFoMat participated in the Galician Strategic Grouping of Materials, AeMAT (AGRUP2018708), collaborating through the project "Development of nanolubricants based on functionalized 1D and 2D nanoparticles and nanomaterials (nanoLUBs)" with the NANOMAG laboratory. As a result of the achievements of AeMAT, in December 2020 the Institute of Materials of the University of Santiago de Compostela (iMATUS) was created. Among the topics of the iMATUS, the LTTP group works in the research line "Efficient energy systems: nanolubricants and advanced electrochemical storage devices".

This PhD Thesis was developed in the framework of two national research projects. The first one, titled "Development of hybrid nanofluids, nanolubricants and nano-enhanced Phase Change Materials for the transfer, storage and production of energy" (AdLuTer, 2018-30/9/2021, call "RETOS 2017") coordinated together with the University of Vigo. The LTTP group specifically developed the subproject 2 "Advanced nanoadditive based lubricants for gears and motors" (ENE2017-86425-C2-2-R). This project was supported by the Spanish Ministry of Science, Innovation and Universities and the European Regional Development Fund (ERDF, FEDER in Spanish). The main objective of the AdLuTer project is the proposal of new advanced materials focused on the field of lubrication, storage, and transfer of thermal energy guide to renewable energies (solar, wind, hydraulic and geothermal) and for automotive applications. The main objective of the subproject 2 is to propose advanced lubricants based on nanodispersions for gears and motors in the field of wind, hydraulic and automotive transmissions, with attention on the aggregation of nanoadditives and on the control of the stability. The second is "Nanomaterials for Electric Vehicles: Transmission Fluids and coatings", subproject 2 of the coordinated project "Innovative applications for nanofluids and nanomaterials in renewable energies and electric vehicles (NanoGeoVe)" awarded in the call *RETOS 2020* (PID2020-112846RB-C22). One of the main goals of this subproject is the development of new nanolubricants formulated for the transmission systems of electric and hybrid vehicles. An important factor in the development of these new nanolubricants is the improvement of their stability through the chemical modification of the surface of the NPs using various modifying agents.

Part of the work presented in this PhD Thesis (synthesis and functionalization of some nanoparticles) was performed in collaboration with two research groups from iMATUS, specifically, NANOMAG and R+D Pharma. Moreover, a part of this PhD Thesis was conducted during a stay of three months in the *Instituto de Ciência e Inovação em Engenharia Mecânica e Engenharia Industrial* (INEGI) of the *Faculdade de Engenharia da Universidade do Porto* (FEUP) under the supervision of Prof. Seabra. This stay has been financed by the IACOBUS 2021 Program, which focuses on promoting cooperation between higher education institutions of the Galicia - North Portugal Euroregion.

In the framework of the above projects, this PhD Thesis focuses in two applications: gearboxes for wind turbines and automatic transmissions for electric and hybrid vehicles. In

both cases, in the selection of the optimal lubricant, many factors must be considered, such as working temperature range, load, speed, materials [141].

The use of renewable energy sources, like wind or solar power, has gained relevance in the development of more efficient and environmentally friendly energy production systems [142]. Net power generation from wind power worldwide rose by more than 437 % over the 2010-2021 period [143]. New designs of larger and more powerful wind turbines have been developed, which need multi-stage gearboxes to multiply the speed until it is suitable for the generator [144]. Wind turbine gearboxes are mechanical components that rarely reach their design life (20 years) [145,146] because they are prone to pitting and fatigue failure [35]. According to the analytical study from 2008 to 2016 of the National Renewable Energy Laboratory, 76 % of the wind turbine failures occurred in the gearbox [147]. Due to the remote location of wind turbines and their large size, repair and maintenance costs for the gearbox are high [148], and during those procedures, wind turbines remain inactive for several days [149]. Selecting the right lubricants can increase the power output of wind turbines while reducing capital costs. Wind companies are demanding lubricants with longer life. Offshore wind farms require lubricants that are resistant to water contamination and perform well over a wide range of temperatures [150]. Approximately 30 % of the energy losses in wind turbine gearboxes occur in the rolling bearings. At high torque conditions, the friction between the meshing teeth causes higher energy losses. One of the aims of the selection of the gear oil is to prevent these losses as well as help dissipate heat, which further enhances the efficiency of the wind turbines. Excellent resistance to aging and oxidation for extended service intervals. All types of oils degrade with use, so it is important to maintain the lubrication conditions optimal for their operation; excellent resistance to aging and oxidation is required for extended service intervals. For this reason, it is important to improve the time of use of the lubricants to have a positive impact on maintenance costs. This is an important factor affecting the oil change interval, which is three times higher for PAOs than for mineral oils. Additionally, a reduction in wear also leads to an extension of oil service life; the presence of metal particles from the gearbox in the oil can act as catalysts in the oxidation reaction [151]. Nowadays, PAOs are the most widely used lubricants in wind turbine gearboxes [152-154]. PAO oils are considered to be the best option for gearboxes due to their great low-temperature properties, wide operating temperature range, high-load performance, and high oxidation resistance, withstanding temperatures as high as 250-300 ℃ [35,151]. Another important factor in choosing the appropriate lubricant is its viscosity and anti-scuffing properties at temperatures above 80 ℃ [155,156]. To effectively maintain the lubricant film when the working temperature is above 80 ℃, the use of synthetic oils is preferable [157]. In summary, the selected gearbox lubricant must offer a) excellent scuffing resistance at high loads; b) great micropitting resistance against fatigue damage; c) good compatibility with other materials (paints, elastomers, seals…); d) oxidative resistance for increased service life; e) appropriate viscosity to ensure sufficient lubricant film at elevated temperatures; f) good pumpability; g) wide operating temperature range [150]. It is a major challenge to reduce the wind energy losses by improving the tribological behavior of the gear oils, for this aim, new high-performance nanolubricants for gearboxes are being studied [10,51,60,150,152].

The electric vehicle (EV) has become an alternative transportation to reduce related emissions, which are 14 % of the total emitted greenhouse gasses, as stated by the Intergovernmental Panel on Climate Change [158]. The average energy efficiency of EVs generated from the electrical grid is significantly higher (77 %) than that from the total fuel

energy provided from internal combustion engine (ICE) vehicles (21 %) [2]. The increased performance of EVs results in a substantial reduction in CO_2 emissions [159], particularly when using electricity produced from renewable sources [160].

Comparing to traditional ICE vehicles, mechanical parts of EVs work at higher speeds, loads, and temperatures, as well as, under electromagnetic fields [81,161]. One of the challenges of electric vehicles (EVs) is to extend their driving range, which could be done by improving the performances of the battery and lubricant [162]. The electric motor (EM) can be located in different positions depending on the type of EV [163,164]. If the EM is located within the transmission of the EV (that is, electric drivetrain), the electric transmission fluids (ETFs) interact with the EM, which requires that they meet several requirements: a) ability to limit corrosion of copper and compatibility with polymers of the housing and of the electronic components; b) low viscosity; c) suitable electric and thermal properties [164-166]. An adequate gear lubrication is key for transmission operation. Firstly, the right viscosity must be selected depending on the specific application [167]. The reason behind using low viscosity lubricants is the high torque and operational speeds of tribological elements in EVs. Electric motors used in EVs operate at high speeds, from 3000 to 16000 rpm, and high-performance motors reach over 20000 rpm [167]. In addition, by reducing the viscosity of the oil, viscous heating decrease and heat transfer is increased [81]. Reducing the lubricant viscosity leads to a shift from full film to boundary lubrication, which can lead to severe surface wear and affects the fatigue life of mechanical parts such as gears and bearings, decreasing the component durability [168]. Thus, improved anti-wear and anti-friction properties are needed. One of the most successful methods to reduce friction and wear is the use of nanoadditives in lubricants [22,169].

As far as we know, fluids for automatic transmissions (ATF), for automatic continuously variable transmissions (CVT), for automatic dual-clutch transmissions (DCT), and for automatic direct-shift gearboxes (DSG) are based on similar low-viscosity oils with different additive packages and could be used as starting point to develop transmission oils for electrified drivetrains. According to McCoy [170], the current standard for lubricating electrified vehicle drivetrains is automatic transmission fluids (ATFs), which is not optimized for EVs. Some properties of these ETFs would be common to those of ATFs, such as efficiency, durability, seal compatibility, or wide operating range, among others. However, other properties gain significance in ETFs, like oxidation stability, copper compatibility and electrical conductivity. Others, like traction properties (critical for wet clutches) lose importance in ETFs [167]. Nanoadditives used in conventional ICE lubricants reduce friction and wear [80,171,172]. However, studies on their performance under the tribological conditions of the ETFs in EVs are limited. Hence, Mustafa et al. [81] reviewed articles on low-viscosity nanolubricants for EVs, among them those based on PAOs (20-100 cSt at 40 ℃). These PAOs can withstand high temperatures, making them desirable for EV application not only as base lubricants but also as oil-coolants, which support temperatures up to 150 ℃ in the transmission and EM housing [173]. In addition, the thermal conductivity and heat capacity of PAOs are 10 % higher than the corresponding mineral oils [35].

1.5 OBJECTIVES

The main goal of this PhD Thesis is to contribute to the design and characterize efficient nanolubricants based on three PAOs and functionalized NPs for wind turbine gearboxes and EV transmissions. To achieve this aim, the following specific objectives are considered:

1. Selection, synthesis, and characterization of functionalized nanoadditives to design new potential nanolubricants.
2. Obtaining long-term stable nanolubricants of coated nanoadditives in PAOs.
3. Evaluation of thermophysical properties of the potential nanolubricants.
4. Evaluation of the tribological behavior under pure sliding conditions of nanolubricants and influence of concentration, type of functionalized nanoadditive, dispersant and comparison with commercial additives.
5. Study of the tribochemical processes occurring in the interface between the nanolubricant and the worn lubricated surfaces.
6. Evaluation of the tribological behavior of EV nanolubricants under rolling-sliding conditions.

Suitable base oils have been chosen for these two applications and the temperature of the tribological tests has been adapted to each application, but many studies would be needed to propose specific formulations for EVs and gearboxes, since other properties would have to be measured, new tribological experiments would have to be carried out with more suitable speed and SRR ranges and other additives would have to be used. This is far from the objectives of this thesis, among other reasons because we do not have the necessary apparatus.

1.6 PhD THESIS STRUCTURE

To describe the steps needed to achieve its goals this PhD Thesis is structured as follows. Once the motivation and background of this research is explained, the chapter 2 describes the procedure used to select the base oil, NPs, and functionalization agent, as well as the methodology used in this work. The results are presented in two sections depending on the application of the designed nanolubricant. The first section, Chapter 3, is focused on lubricants for wind turbine gearboxes. The second section, Chapters 4 and 5, is centered on transmission fluids for electric or hybrid vehicle transmissions. Finally, Chapter 6 presents the general conclusions of this doctoral thesis and future work related to it. Additional information is provided at the end of this dissertation in four appendices. Appendix A shows the list of publications and authorizations of the publishers for the use of the articles in this PhD Thesis, as well as the conference contributions; Appendix B summarized the preliminary work carried out in this PhD Thesis; Appendix C shows the lists of tables and figures that appear through the chapters; and the Appendix D summarizes in Galician language all the sections of this PhD Thesis.

1.7 REFERENCES

[1]   K. Holmberg, A. Erdemir, Influence of tribology on global energy consumption, costs and emissions, Friction 5 (2017) 263-284, https://doi.org/10.1007/s40544-017-0183-5.

[2]   K. Holmberg, A. Erdemir, The impact of tribology on energy use and CO_2 emission globally and in combustion engine and electric cars, Tribology International 135 (2019) 389-396, https://doi.org/10.1016/j.triboint.2019.03.024.

[3]   M.K. Ahmed Ali, H. Xianjun, F. Essa, M.A. Abdelkareem, A. Elagouz, S. Sharshir, Friction and wear reduction mechanisms of the reciprocating contact interfaces using nanolubricant under different loads and speeds, Journal of Tribology 140 (2018), https://doi.org/10.1115/1.4039720.

[4]   W. Dai, B. Kheireddin, H. Gao, H. Liang, Roles of nanoparticles in oil lubrication, Tribology International 102 (2016) 88-98, https://doi.org/10.1016/j.triboint.2016.05.020.

[5]   F. Dassenoy, Nanoparticles as additives for the development of high performance and environmentally friendly engine lubricants, Tribology Online 14 (2019) 237-253, https://doi.org/10.2474/trol.14.237.

[6]   S. Sabarinath, S. Prabha Rajeev, P. Rajendra Kumar, K. Prabhakaran Nair, Development of fully formulated eco-friendly nanolubricant from sesame oil, Applied Nanoscience 10 (2020) 577-586, https://doi.org/10.1177/1350650119837831.

[7]   H. Wu, S. Yin, L. Wang, Y. Du, Y. Yang, J. Shi, H. Wang, Investigation on the robust adsorption mechanism of alkyl-functional boric acid nanoparticles as high performance green lubricant additives, Tribology International 157 (2021) 106909, https://doi.org/10.1016/j.triboint.2021.106909.

[8]   E. Larsson, P. Olander, S. Jacobson, Boric acid as a lubricating fuel additive – Simplified lab experiments to understand fuel consumption reduction in field test, Wear 376-377 (2017) 822-830, https://doi.org/10.1016/j.wear.2017.01.105.

[9]   R. Xia, D. Lou, H. Younes, J. Haiston, H. Chen, H. Hong, Synergistic effect of hexagonal boron nitride and carbon nanofibers on tribological behavior of nanolubricant, Tribology International 177 (2023) 107957, https://doi.org/10.1016/j.triboint.2022.107957.

[10]   K.I. Nasser, J.M. Liñeira del Río, F. Mariño, E.R. López, J. Fernández, Double hybrid lubricant additives consisting of a phosphonium ionic liquid and graphene nanoplatelets/hexagonal boron nitride nanoparticles, Tribology International 163 (2021) 107189, https://doi.org/10.1016/j.triboint.2021.107189.

[11]   M.K.A. Ali, H. Xianjun, M.A. Abdelkareem, M. Gulzar, A. Elsheikh, Novel approach of the graphene nanolubricant for energy saving via anti-friction/wear in automobile engines, Tribology International 124 (2018) 209-229, https://doi.org/10.1016/j.triboint.2018.04.004.

[12]   J. Kałużny, M. Waligorski, G.M. Szymański, J. Merkisz, J. Różański, M. Nowicki, M. Al Karawi, K. Kempa, Reducing friction and engine vibrations with trace amounts of carbon nanotubes in the lubricating oil, Tribology International 151 (2020) 106484, https://doi.org/10.1016/j.triboint.2020.106484.

[13]   S.C. Tung, M.L. McMillan, Automotive tribology overview of current advances and challenges for the future, Tribology International 37 (2004) 517-536, https://doi.org/10.1016/j.triboint.2004.01.013.

[14]   A. Rasheed, M. Khalid, A. Javeed, W. Rashmi, T. Gupta, A. Chan, Heat transfer and tribological performance of graphene nanolubricant in an internal combustion engine, Tribology International 103 (2016) 504-515, https://doi.org/10.1016/j.triboint.2016.08.007.

[15]   N.G. Demas, E.V. Timofeeva, J.L. Routbort, G.R. Fenske, Tribological effects of BN and MoS_2 nanoparticles added to polyalphaolefin oil in piston skirt/cylinder liner tests, Tribology Letters 47 (2012) 91-102, https://doi.org/10.1007/s11249-012-9965-0.

[16]   W.A.A. Mustafa, F. Dassenoy, M. Sarno, A. Senatore, A review on potentials and challenges of nanolubricants as promising lubricants for electric vehicles, Lubrication Science 34 (2022) 1-29, https://doi.org/10.1002/ls.1568.

[17]   Y. Chen, S. Jha, A. Raut, W. Zhang, H. Liang, Performance characteristics of lubricants in electric and hybrid vehicles: a review of current and future needs, Frontiers in Mechanical Engineering 6 (2020) 571464, https://doi.org/10.3389/fmech.2020.571464.

[18]   M.A.M. Ali, A.I. Azmi, M.N. Murad, M.Z.M. Zain, A.N.M. Khalil, N.A. Shuaib, Roles of new bio-based nanolubricants towards eco-friendly and improved machinability of Inconel 718 alloys, Tribology International 144 (2020) 106106, https://doi.org/10.1016/j.triboint.2019.106106.

[19]   H. Spikes, Friction modifier additives, Tribology Letters 60 (2015) 5, https://doi.org/10.1007/s11249-015-0589-z.

[20]   M.Z. Saidi, C. El Moujahid, A. Pasc, N. Canilho, C. Delgado-Sanchez, A. Celzard, V. Fierro, R. Kouitat-Njiwa, T. Chafik, Enhanced tribological properties of wind turbine engine oil formulated with flower-shaped MoS_2 nano-additives, Colloids and Surfaces A: Physicochemical and Engineering Aspects 620 (2021) 126509, https://doi.org/10.1016/j.colsurfa.2021.126509.

[21]   S.C. Tung, M. Woydt, R. Shah, Global insights on future trends of Hybrid/EV driveline lubrication and thermal management, Frontiers in Mechanical Engineering 6 (2020) 74, https://doi.org/10.3389/fmech.2020.571786.

[22]   N. Nyholm, N. Espallargas, Functionalized carbon nanostructures as lubricant additives – A review, Carbon 201 (2023) 1200-1228, https://doi.org/10.1016/j.carbon.2022.10.035.

[23]   N.F. Azman, S. Samion, Dispersion stability and lubrication mechanism of nanolubricants: A review, International Journal of Precision Engineering and Manufacturing-Green Technology 6 (2019) 393-414, https://doi.org/10.1007/s40684-019-00080-x.

[24]   V. Zin, F. Agresti, S. Barison, L. Colla, E. Mercadelli, M. Fabrizio, C. Pagura, Tribological properties of engine oil with carbon nano-horns as nano-additives, Tribology Letters 55 (2014) 45-53, https://doi.org/10.1007/s11249-014-0330-3.

[25]   V.N. Bakunin, G.N. Kuzmina, M. Kasrai, O.P. Parenago, G.M. Bancroft, Tribological behavior and tribofilm composition in lubricated systems containing surface-capped molybdenum sulfide nanoparticles, Tribology Letters 22 (2006) 289-296, https://doi.org/10.1007/s11249-006-9095-7.

[26]   N. Nunn, Z. Mahbooba, M.G. Ivanov, D.M. Ivanov, D.W. Brenner, O. Shenderova, Tribological properties of polyalphaolefin oil modified with nanocarbon additives, Diamond and Related Materials 54 (2015) 97-102, https://doi.org/10.1016/j.diamond.2014.09.003.

[27]   P. Rabaso, F. Dassenoy, F. Ville, M. Diaby, B. Vacher, T. Le Mogne, M. Belin, J. Cavoret, An Investigation on the Reduced Ability of IF-MoS_2 Nanoparticles to Reduce Friction and Wear in the Presence of Dispersants, Tribology Letters 55 (2014) 503-516, https://doi.org/10.1007/s11249-014-0381-5.

[28]   Y. Chen, P. Renner, H. Liang, Dispersion of nanoparticles in lubricating oil: A critical review, Lubricants 7 (2019) 7, https://doi.org/10.3390/lubricants7010007.

[29]   T. Sui, B. Song, F. Zhang, Q. Yang, Effects of functional groups on the tribological properties of hairy silica nanoparticles as an additive to polyalphaolefin, RSC Advances 6 (2016) 393-402, https://doi.org/10.1039/C5RA22932D.

[30]   C. Kumara, H. Luo, D.N. Leonard, H.M. Meyer, J. Qu, Organic-modified silver nanoparticles as lubricant additives, ACS Applied Materials & Interfaces 9 (2017) 37227-37237, https://doi.org/10.1021/acsami.7b13683.

[31]   X. Wu, K. Gong, G. Zhao, W. Lou, X. Wang, W. Liu, Surface Modification of MoS$_2$ Nanosheets as Effective Lubricant Additives for Reducing Friction and Wear in Poly-α-olefin, Industrial & Engineering Chemistry Research 57 (2018) 8105-8114, https://doi.org/10.1021/acs.iecr.8b00454.

[32]   E. Burello, A.P. Worth, QSAR modeling of nanomaterials, Wiley Interdisciplinary Reviews: Nanomedicine and Nanobiotechnology 3 (2011) 298-306, https://doi.org/10.1002/wnan.137.

[33]   C.S. Torres Castillo, C. Bruel, J.R. Tavares, Chemical affinity and dispersibility of boron nitride nanotubes, Nanoscale Advances 2 (2020) 2497-2506, https://doi.org/10.1039/D0NA00136H.

[34]   H.E. Henderson, Chapter 19. Chemically Modified Mineral Oils. in: L.R. Rudnick, (Ed.), Synthetics, mineral oils, and bio-based lubricants: chemistry and technology, CRC Press, 2020.

[35]   L.R. Rudnick, Chapter 1. Polyalphaolefins. in: L.R. Rudnick, (Ed.), Synthetics, mineral oils, and bio-based lubricants: chemistry and technology, CRC Press, 2020.

[36]   J.F. Carpenter, Biodegradability and toxicity of polyalphaolefin base stocks, Journal of Synthetic Lubrication 12 (1995) 13-20, https://doi.org/10.1002/jsl.3000120103.

[37]   C.S.C. Davison, Wear prevention in early history, Wear 1 (1957) 155-159, https://doi.org/10.1016/0043-1648(57)90007-8.

[38]   W. McTurk, Synthetic lubricants WADC Technical Report 53–88, Contract AF 33(038)-14593, RDO No. 613–15, Standard Oil Development CO Elizabeth NJ (1953).

[39]   C. Murphy, W. Zisman, Structural guides for synthetic lubricant development, Industrial Engineering Chemistry 42 (1950) 2415-2420.

[40]   M.R. Greaves, Chapter 7. Oil Soluble Polyalkylene Glycols. in: L.R. Rudnick, (Ed.), Synthetics, mineral oils, and bio-based lubricants: chemistry and technology, CRC Press, 2020.

[41]   G. Karmakar, P. Ghosh, B.K. Sharma, Chemically modifying vegetable oils to prepare green lubricants, Lubricants 5 (2017) 44, https://doi.org/10.3390/lubricants5040044.

[42]   B.K. Sharma, G. Karmakar, S.Z. Erhan, Chapter 24. Modified Vegetable Oils for Enviromentally Friendly Lubricant Applications. in: L.R. Rudnick, (Ed.), Synthetics, mineral oils, and bio-based lubricants: chemistry and technology, CRC Press, 2020.

[43]   L. Kong, J. Sun, Y. Bao, Preparation, characterization and tribological mechanism of nanofluids, RSC Advances 7 (2017) 12599-12609, https://doi.org/10.1039/C6RA28243A.

[44]   S.U. Ilyas, R. Pendyala, N. Marneni, Preparation, sedimentation, and agglomeration of nanofluids, Chemical Engineering & Technology 37 (2014) 2011-2021, https://doi.org/10.1002/ceat.201400268.

[45]   W. Yu, H. Xie, A review on nanofluids: preparation, stability mechanisms, and applications, Nanomaterials 2012 (2012) 1-17, https://doi.org/10.1155/2012/435873.

[46]   J.A. Eastman, S. Choi, S. Li, W. Yu, L. Thompson, Anomalously increased effective thermal conductivities of ethylene glycol-based nanofluids containing copper nanoparticles, Applied Physics Letters 78 (2001) 718-720, https://doi.org/10.1063/1.1341218.

[47]   H.-T. Zhu, Y.-S. Lin, Y.-S. Yin, A novel one-step chemical method for preparation of copper nanofluids, Journal of Colloid and Interface Science 277 (2004) 100-103, https://doi.org/10.1016/j.jcis.2004.04.026.

[48]   H. Bönnemann, S.S. Botha, B. Bladergroen, V.M. Linkov, Monodisperse copper- and silver-nanocolloids suitable for heat-conductive fluids, Applied Organometallic Chemistry 19 (2005) 768-773, https://doi.org/10.1002/aoc.889.

[49]   D. Wu, H. Zhu, L. Wang, L. Liu, Critical issues in nanofluids preparation, characterization and thermal conductivity, Current Nanoscience 5 (2009) 103-112, http://doi.org/10.2174/157341309787314548.

[50]   J. Sanes, M.-D. Avilés, N. Saurín, T. Espinosa, F.-J. Carrión, M.-D. Bermúdez, Synergy between graphene and ionic liquid lubricant additives, Tribology International 116 (2017) 371-382, https://doi.org/10.1016/j.triboint.2017.07.030.

[51]   K.I. Nasser, J.M. Liñeira del Río, E.R. López, J. Fernández, Hybrid combinations of graphene nanoplatelets and phosphonium ionic liquids as lubricant additives for a polyalphaolefin, Journal of Molecular Liquids 336 (2021) 116266, https://doi.org/10.1016/j.molliq.2021.116266.

[52]   M.K.A. Ali, H. Xianjun, Colloidal stability mechanism of copper nanomaterials modified by bis(2-ethylhexyl) phosphate dispersed in polyalphaolefin oil as green nanolubricants, Journal of Colloid and Interface Science 578 (2020) 24-36, https://doi.org/10.1016/j.jcis.2020.05.092.

[53]   T. Sui, M. Ding, C. Ji, S. Yan, J. Wei, A. Wang, F. Zhao, J. Fei, Dispersibility and rheological behavior of functionalized silica nanoparticles as lubricant additives, Ceramics International 44 (2018) 18438-18443, https://doi.org/10.1016/j.ceramint.2018.07.061.

[54]   T. Sui, B. Song, Y.-H. Wen, F. Zhang, Bifunctional hairy silica nanoparticles as high-performance additives for lubricant, Scientific Reports 6 (2016) 22696, https://doi.org/10.1038/srep22696.

[55]   T. Sui, B. Song, F. Zhang, Q. Yang, Effect of particle size and ligand on the tribological properties of amino functionalized hairy silica nanoparticles as an additive to polyalphaolefin, Journal of Nanomaterials 2015 (2015) 492401, https://doi.org/10.1155/2015/492401.

[56]   J.M. Liñeira del Rio, E.R. López, M. González Gómez, S. Yáñez Vilar, Y. Piñeiro, J. Rivas, D.E.P. Gonçalves, J.H.O. Seabra, J. Fernández, Tribological behavior of nanolubricants based on coated magnetic nanoparticles and trimethylolpropane trioleate base oil, Nanomaterials 10 (2020) 683, https://doi.org/10.3390/nano10040683.

[57]   M.K.A. Ali, H. Xianjun, Role of bis (2-ethylhexyl) phosphate and Al_2O_3/TiO_2 hybrid nanomaterials in improving the dispersion stability of nanolubricants, Tribology International 155 (2021) 106767, https://doi.org/10.1016/j.triboint.2020.106767.

[58]   V.S. Mello, E.A. Faria, S.M. Alves, C. Scandian, Enhancing CuO nanolubricant performance using dispersing agents, Tribology International 150 (2020) 106338, https://doi.org/10.1016/j.triboint.2020.106338.

[59]   S.M. Alves, V.S. Mello, E.A. Faria, A.P.P. Camargo, Nanolubricants developed from tiny CuO nanoparticles, Tribology International 100 (2016) 263-271, https://doi.org/10.1016/j.triboint.2016.01.050.

[60]   K.I. Nasser, J.M. Liñeira del Río, E.R. López, J. Fernández, Synergistic effects of hexagonal boron nitride nanoparticles and phosphonium ionic liquids as hybrid lubricant additives, Journal of Molecular Liquids 311 (2020) 113343, https://doi.org/10.1016/j.molliq.2020.113343.

[61]   J.M. Liñeira del Río, E.R. López, J. Fernández, Synergy between boron nitride or graphene nanoplatelets and tri(butyl)ethylphosphonium diethylphosphate ionic liquid as

lubricant additives of triisotridecyltrimellitate oil, Journal of Molecular Liquids 301 (2020) 112442, https://doi.org/10.1016/j.molliq.2020.112442.

[62]   V. Khare, M.-Q. Pham, N. Kumari, H.-S. Yoon, C.-S. Kim, J.-I.L. Park, S.-H. Ahn, Graphene–ionic liquid based hybrid nanomaterials as novel lubricant for low friction and wear, ACS Applied Materials & Interfaces 5 (2013) 4063-4075, https://doi.org/10.1021/am302761c.

[63]   J.M. Liñeira del Río, M.J.G. Guimarey, M.J.P. Comuñas, E.R. López, A. Amigo, J. Fernández, Thermophysical and tribological properties of dispersions based on graphene and a trimethylolpropane trioleate oil, Journal of Molecular Liquids 268 (2018) 854-866, https://doi.org/10.1016/j.molliq.2018.07.107.

[64]   B.T. Seymour, W. Fu, R.A.E. Wright, H. Luo, J. Qu, S. Dai, B. Zhao, Improved lubricating performance by combining oil-soluble hairy silica nanoparticles and an ionic liquid as an additive for a synthetic base oil, ACS Applied Materials & Interfaces 10 (2018) 15129-15139, https://doi.org/10.1021/acsami.8b01579.

[65]   H.P. Mungse, O.P. Khatri, Chemically functionalized reduced graphene oxide as a novel material for reduction of friction and wear, The Journal of Physical Chemistry C 118 (2014) 14394-14402, https://doi.org/10.1021/jp5033614.

[66]   J.C. Sánchez-López, M.D. Abad, L. Kolodziejczyk, E. Guerrero, A. Fernández, Surface-modified Pd and Au nanoparticles for anti-wear applications, Tribology International 44 (2011) 720-726, https://doi.org/10.1016/j.triboint.2009.12.013.

[67]   J.M. Liñeira del Río, E.R. López, J. Fernández, F. García, Tribological properties of dispersions based on reduced graphene oxide sheets and trimethylolpropane trioleate or PAO 40 oils, Journal of Molecular Liquids 274 (2019) 568-576, https://doi.org/10.1016/j.molliq.2018.10.107.

[68]   Y. Li, J. Zhao, C. Tang, Y. He, Y. Wang, J. Chen, J. Mao, Q. Zhou, B. Wang, F. Wei, J. Luo, G. Shi, Highly exfoliated reduced graphite oxide powders as efficient lubricant oil additives, Advanced Materials Interfaces 3 (2016) 1600700, https://doi.org/10.1002/admi.201600700.

[69]   D. Zheng, Z.-B. Cai, M.-X. Shen, Z.-Y. Li, M.-H. Zhu, Investigation of the tribology behaviour of the graphene nanosheets as oil additives on textured alloy cast iron surface, Applied Surface Science 387 (2016) 66-75, https://doi.org/10.1016/j.apsusc.2016.06.080.

[70]   J.M. Liñeira del Río, M.J.G. Guimarey, M.J.P. Comuñas, E.R. López, J.I. Prado, L. Lugo, J. Fernández, Tribological and thermophysical properties of environmentally-friendly lubricants based on trimethylolpropane trioleate with hexagonal boron nitride nanoparticles as an additive, Coatings 9 (2019) 509, https://doi.org/10.3390/coatings9080509.

[71]   J. Lee, Y.-j. Yoon, J. Eaton, K. Goodson, S. Bai, Analysis of Oxide (Al_2O_3, CuO, and ZnO) and CNT Nanoparticles Disaggregation Effect on the Thermal Conductivity and the Viscosity of Nanofluids, International Journal of Precision Engineering and Manufacturing 15 (2014) 703-710, https://doi.org/10.1007/s12541-014-0390-1.

[72]   V. Saini, J. Bijwe, S. Seth, S.S.V. Ramakumar, Interfacial interaction of PTFE sub-micron particles in oil with steel surfaces as excellent extreme-pressure additive, Journal of Molecular Liquids 325 (2021) 115238, https://doi.org/10.1016/j.molliq.2020.115238.

[73]   B.T. Seymour, R.A.E. Wright, A.C. Parrott, H. Gao, A. Martini, J. Qu, S. Dai, B. Zhao, Poly(alkyl methacrylate) brush-grafted silica nanoparticles as oil lubricant additives: Effects of alkyl pendant groups on oil dispersibility, stability, and lubrication property, ACS Applied Materials & Interfaces 9 (2017) 25038-25048, https://doi.org/10.1021/acsami.7b06714.

[74]   J.-F. Lou, H. Zhang, R. Wang, Experimental investigation of graphite nanolubricant used in a domestic refrigerator, Advances in Mechanical Engineering 7 (2015) 1687814015571011, https://doi.org/10.1177/1687814015571011.

[75]   N. Rivera, D. Blanco, J.L. Viesca, A. Fernández-González, R. González, A.H. Battez, Tribological performance of three fatty acid anion-based ionic liquids (FAILs) used as lubricant additive, Journal of Molecular Liquids 296 (2019) 111881, https://doi.org/10.1016/j.molliq.2019.111881.

[76]   M.Z. Saidi, A. Pasc, C. El Moujahid, N. Canilho, M. Badawi, C. Delgado-Sanchez, A. Celzard, V. Fierro, R. Peignier, R. Kouitat-Njiwa, H. Akram, T. Chafik, Improved tribological properties, thermal and colloidal stability of poly-α-olefins based lubricants with hydrophobic MoS_2 submicron additives, Journal of Colloid and Interface Science 562 (2020) 91-101, https://doi.org/10.1016/j.jcis.2019.12.007.

[77]   M.J.G. Guimarey, M.J.P. Comuñas, E.R. López, A. Amigo, J. Fernández, Thermophysical properties of polyalphaolefin oil modified with nanoadditives, The Journal of Chemical Thermodynamics 131 (2019) 192-205, https://doi.org/10.1016/j.jct.2018.10.035.

[78]   M.J.G. Guimarey, M.R. Salgado, M.J.P. Comuñas, E.R. López, A. Amigo, D. Cabaleiro, L. Lugo, J. Fernández, Effect of ZrO_2 nanoparticles on thermophysical and rheological properties of three synthetic oils, Journal of Molecular Liquids 262 (2018) 126-138, https://doi.org/10.1016/j.molliq.2018.04.027.

[79]   M.J.G. Guimarey, J.M. Liñeira del Río, J. Fernández, Improvement of the lubrication performance of an ester base oil with coated ferrite additives for different material pairs, Journal of Molecular Liquids (2022) 118550, https://doi.org/10.1016/j.molliq.2022.118550.

[80]   G. Paul, S. Shit, H. Hirani, T. Kuila, N. Murmu, Tribological behavior of dodecylamine functionalized graphene nanosheets dispersed engine oil nanolubricants, Tribology International 131 (2019) 605-619, https://doi.org/10.1016/j.triboint.2018.11.012.

[81]   W. Ahmed Abdalglil Mustafa, F. Dassenoy, M. Sarno, A. Senatore, A review on potentials and challenges of nanolubricants as promising lubricants for electric vehicles, Lubrication Science 34 (2022) 1-29, https://doi.org/10.1002/ls.1568.

[82]   N.F. Azman, S. Samion, M.N.H.M. Sot, Investigation of tribological properties of CuO/palm oil nanolubricant using pin-on-disc tribotester, Green materials 6 (2018) 30-37, https://doi.org/10.1680/jgrma.17.00026.

[83]   M. Gulzar, H.H. Masjuki, M.A. Kalam, M. Varman, N.W.M. Zulkifli, R.A. Mufti, R. Zahid, Tribological performance of nanoparticles as lubricating oil additives, Journal of Nanoparticle Research 18 (2016) 223, https://doi.org/10.1007/s11051-016-3537-4.

[84]   W.K. Shafi, A. Raina, M.I. Ul Haq, Tribological performance of avocado oil containing copper nanoparticles in mixed and boundary lubrication regime, Industrial Lubrication and Tribology 70 (2018) 865-871, https://doi.org/10.1108/ILT-06-2017-0166.

[85]   J. Taha-Tijerina, L. Peña-Paras, T.N. Narayanan, L. Garza, C. Lapray, J. Gonzalez, E. Palacios, D. Molina, A. García, D. Maldonado, P.M. Ajayan, Multifunctional nanofluids with 2D nanosheets for thermal and tribological management, Wear 302 (2013) 1241-1248, https://doi.org/10.1016/j.wear.2012.12.010.

[86]   J. Viesca, A.H. Battez, R. González, R. Chou, J. Cabello, Antiwear properties of carbon-coated copper nanoparticles used as an additive to a polyalphaolefin, Tribology international 44 (2011) 829-833, https://doi.org/10.1016/j.triboint.2011.02.006.

[87]   L. Peña-Parás, J. Taha-Tijerina, L. Garza, D. Maldonado-Cortés, R. Michalczewski, C. Lapray, Effect of CuO and Al_2O_3 nanoparticle additives on the tribological behavior of fully formulated oils, Wear 332-333 (2015) 1256-1261, https://doi.org/10.1016/j.wear.2015.02.038.

[88]   Á.I. Szabó, Á.D. Tóth, M.Z. Leskó, H. Hargitai, Investigation of the Applicability of Y_2O_3–ZrO_2 Spherical Nanoparticles as Tribological Lubricant Additives, Lubricants 10 (2022) 152, https://doi.org/10.3390/lubricants10070152.

[89]   I.E. Uflyand, V.A. Zhinzhilo, V.E. Burlakova, Metal-containing nanomaterials as lubricant additives: State-of-the-art and future development, Friction 7 (2019) 93-116, https://doi.org/10.1007/s40544-019-0261-y.

[90]   S. Samanta, S. Singh, R.R. Sahoo, Simultaneous chemical reduction and surface functionalization of graphene oxide for efficient lubrication of steel–steel contact, RSC Advances 5 (2015) 61888-61899, https://doi.org/10.1039/C5RA10696F.

[91]   V. Srinivas, K.R.R. Chebattina, N. Mohan Rao, Lubricating and physico-chemical properties of CI- 4 plus engine oil dispersed with surface modified multi-walled carbon nanotubes, Tribology - Materials, Surfaces & Interfaces 12 (2018) 107-114, https://doi.org/10.1080/17515831.2018.1452847.

[92]   C. Yegin, W. Lu, B. Kheireddin, M. Zhang, P. Li, Y. Min, H.-J. Sue, M. Sari, M. Akbulut, The effect of nanoparticle functionalization on lubrication performance of nanofluids dispersing silica nanoparticles in an ionic liquid, Journal of Tribology 139 (2016) 041802, https://doi.org/10.1115/1.4035342.

[93]   H. Sade, A. Moshkovich, J.-P. Lellouche, L. Rapoport, Testing of WS_2 nanoparticles functionalized by a humin-like shell as lubricant additives, Lubricants 6 (2018) 3, https://doi.org/10.3390/lubricants6010003.

[94]   J.L. Viesca, A. Hernández Battez, R. González, R. Chou, J.J. Cabello, Antiwear properties of carbon-coated copper nanoparticles used as an additive to a polyalphaolefin, Tribology International 44 (2011) 829-833, https://doi.org/10.1016/j.triboint.2011.02.006.

[95]   J. Patel, A. Kiani, Effects of reduced graphene oxide (rGO) at different concentrations on tribological properties of liquid base lubricants, Lubricants 7 (2019) 11, https://doi.org/10.3390/lubricants7020011.

[96]   J. Zhao, Y. Huang, Y. He, Y. Shi, Nanolubricant additives: A review, Friction 9 (2021) 891-917, https://doi.org/10.1007/s40544-020-0450-8.

[97]   H. Tamura, K. Mita, A. Tanaka, M. Ito, Mechanism of hydroxylation of metal oxide surfaces, Journal of colloid interface science 243 (2001) 202-207, https://doi.org/10.1006/jcis.2001.7864.

[98]   X. Phung, J. Groza, E.A. Stach, L.N. Williams, S.B. Ritchey, Surface characterization of metal nanoparticles, Materials Science Engineering: A 359 (2003) 261-268, https://doi.org/10.1016/S0921-5093(03)00348-4.

[99]   G. Wang, J. Yang, J. Park, X. Gou, B. Wang, H. Liu, J. Yao, Facile synthesis and characterization of graphene nanosheets, The Journal of Physical Chemistry C 112 (2008) 8192-8195, https://doi.org/10.1021/jp710931h.

[100]   L. Liu, M. Qing, Y. Wang, S. Chen, Defects in graphene: generation, healing, and their effects on the properties of graphene: a review, Journal of Materials Science Technology 31 (2015) 599-606, https://doi.org/10.1016/j.jmst.2014.11.019.

[101]   L. Stobinski, B. Lesiak, A. Malolepszy, M. Mazurkiewicz, B. Mierzwa, J. Zemek, P. Jiricek, I. Bieloshapka, Graphene oxide and reduced graphene oxide studied by the XRD, TEM

and electron spectroscopy methods, Journal of Electron Spectroscopy Related Phenomena 195 (2014) 145-154, https://doi.org/10.1016/j.elspec.2014.07.003.

[102]   H.P. Mungse, K. Gupta, R. Singh, O.P. Sharma, H. Sugimura, O.P. Khatri, Alkylated graphene oxide and reduced graphene oxide: Grafting density, dispersion stability to enhancement of lubrication properties, Journal of Colloid and Interface Science 541 (2019) 150-162, https://doi.org/10.1016/j.jcis.2019.01.064.

[103]   C.S. Chen, X.H. Chen, L.S. Xu, Z. Yang, W.H. Li, Modification of multi-walled carbon nanotubes with fatty acid and their tribological properties as lubricant additive, Carbon 43 (2005) 1660-1666, https://doi.org/10.1016/j.carbon.2005.01.044.

[104]   H.P. Mungse, N. Kumar, O.P. Khatri, Synthesis, dispersion and lubrication potential of basal plane functionalized alkylated graphene nanosheets, RSC Advances 5 (2015) 25565-25571, https://doi.org/10.1039/C4RA16975A.

[105]   S. Samanta, R.R. Sahoo, Layer by layer assembled functionalized graphene oxide-based polymer brushes for superlubricity on steel–steel tribocontact, Journal of Soft Matter 17 (2021) 7014-7031, https://doi.org/10.1039/D1SM00690H.

[106]   C. Zhu, Y. Yan, F. Wang, J. Cui, S. Zhao, A. Gao, G. Zhang, Facile fabrication of long-chain alkyl functionalized ultrafine reduced graphene oxide nanocomposites for enhanced tribological performance, RSC Advances 9 (2019) 7324-7333, https://doi.org/10.1039/C9RA00433E.

[107]   Z. Liang, B. Wang, M. Luo, H. Lu, Synthesis of hexadecylamine modified carbon dots and their friction-reducing and anti-wear performance in polyalphaolefin, Diamond and Related Materials 112 (2021) 108238, https://doi.org/10.1016/j.diamond.2021.108238.

[108]   W. Shang, M. Ye, T. Cai, L. Zhao, Y. Zhang, D. Liu, S. Liu, Tuning of the hydrophilicity and hydrophobicity of nitrogen doped carbon dots: A facile approach towards high efficient lubricant nanoadditives, Journal of Molecular Liquids 266 (2018) 65-74, https://doi.org/10.1016/j.molliq.2018.06.042.

[109]   M. Ye, T. Cai, L. Zhao, D. Liu, S. Liu, Covalently attached strategy to modulate surface of carbon quantum dots: Towards effectively multifunctional lubricant additives in polar and apolar base fluids, Tribology International 136 (2019) 349-359, https://doi.org/10.1016/j.triboint.2019.03.045.

[110]   X. Ci, W. Zhao, J. Luo, Y. Wu, T. Ge, L. Shen, X. Gao, Z. Fang, Revealing the lubrication mechanism of fluorographene nanosheets enhanced GTL-8 based nanolubricant oil, Tribology International 138 (2019) 174-183, https://doi.org/10.1016/j.triboint.2019.05.044.

[111]   L. Zhang, Y. He, L. Zhu, Z. Jiao, W. Deng, C. Pu, C. Han, S. Tang, Alkyl phosphate modified graphene oxide as friction and wear reduction additives in oil, Journal of Materials Science 54 (2019) 4626-4636, https://doi.org/10.1007/s10853-018-03216-7.

[112]   T. Chen, Y. Xia, Z. Jia, Z. Liu, H. Zhang, Synthesis, characterization, and tribological behavior of oleic acid capped graphene oxide, Journal of Nanomaterials 2014 (2014) 654145, https://doi.org/10.1155/2014/654145.

[113]   J.M. Liñeira del Río, E.R. López, F. García, J. Fernández, Tribological synergies among chemical-modified graphene oxide nanomaterials and a phosphonium ionic liquid as additives of a biolubricant, Journal of Molecular Liquids 336 (2021) 116885, https://doi.org/10.1016/j.molliq.2021.116885.

[114]   N.A. Ismail, S. Bagheri, Highly oil-dispersed functionalized reduced graphene oxide nanosheets as lube oil friction modifier, Materials Science and Engineering: B 222 (2017) 34-42, https://doi.org/10.1016/j.mseb.2017.04.010.

[115]   H. Lu, W. Tang, X. Liu, B. Wang, Z. Huang, Oleylamine-modified carbon nanoparticles as a kind of efficient lubricating additive of polyalphaolefin, Journal of Materials Science 52 (2017) 4483-4492, https://doi.org/10.1007/s10853-016-0694-x.

[116]   B. Li, X. Wang, W. Liu, Q. Xue, Tribochemistry and antiwear mechanism of organic–inorganic nanoparticles as lubricant additives, Tribology Letters 22 (2006) 79-84, https://doi.org/10.1007/s11249-005-9002-7.

[117]   C. Kumara, D.N. Leonard, H.M. Meyer, H. Luo, B.L. Armstrong, J. Qu, Palladium nanoparticle-enabled ultrathick tribofilm with unique composition, ACS Applied Materials & Interfaces 10 (2018) 31804-31812, https://doi.org/10.1021/acsami.8b11213.

[118]   L. Sun, Z.J. Zhang, Z.S. Wu, H.X. Dang, Synthesis and characterization of DDP coated Ag nanoparticles, Materials Science and Engineering: A 379 (2004) 378-383, https://doi.org/10.1016/j.msea.2004.03.002.

[119]   Y. Chen, Y. Zhang, S. Zhang, L. Yu, P. Zhang, Z. Zhang, Preparation of nickel-based nanolubricants via a facile in situ one-step route and investigation of their tribological properties, Tribology Letters 51 (2013) 73-83, https://doi.org/10.1007/s11249-013-0148-4.

[120]   R.A. Wright, K. Wang, J. Qu, B. Zhao, Oil-soluble polymer brush grafted nanoparticles as effective lubricant additives for friction and wear reduction, Angewandte Chemie 128 (2016) 8798-8802, https://doi.org/10.1002/ange.201603663.

[121]   F.T. Hong, A. Schneider, S.M. Sarathy, Enhanced lubrication by core-shell TiO_2 nanoparticles modified with gallic acid ester, Tribology International 146 (2020) 106263, https://doi.org/10.1016/j.triboint.2020.106263.

[122]   T. Luo, X. Wei, X. Huang, L. Huang, F. Yang, Tribological properties of Al_2O_3 nanoparticles as lubricating oil additives, Ceramics International 40 (2014) 7143-7149, https://doi.org/10.1016/j.ceramint.2013.12.050.

[123]   X. Ran, X. Yu, Q. Zou, Effect of particle concentration on tribological properties of ZnO nanofluids, Tribology Transactions 60 (2017) 154-158, https://doi.org/10.1080/10402004.2016.1154233.

[124]   C. Shahar, D. Zbaida, L. Rapoport, H. Cohen, T. Bendikov, J. Tannous, F. Dassenoy, R. Tenne, Surface functionalization of WS_2 fullerene-like nanoparticles, Langmuir 26 (2010) 4409-4414, https://doi.org/10.1021/la903459t.

[125]   Z. Jiang, Y. Zhang, G. Yang, K. Yang, S. Zhang, L. Yu, P. Zhang, Tribological properties of oleylamine-modified ultrathin WS_2 nanosheets as the additive in polyalpha olefin over a wide temperature range, Tribology Letters 61 (2016) 24, https://doi.org/10.1007/s11249-016-0643-5.

[126]   Z. Jiang, Y. Zhang, G. Yang, J. Ma, S. Zhang, L. Yu, P. Zhang, Tribological properties of tungsten disulfide nanoparticles surface-capped by oleylamine and maleic anhydride dodecyl ester as additive in diisooctylsebacate, Industrial & Engineering Chemistry Research 56 (2017) 1365-1375, https://doi.org/10.1021/acs.iecr.6b04074.

[127]   X. Li, Z. Cao, Z. Zhang, H. Dang, Surface-modification in situ of nano-SiO_2 and its structure and tribological properties, Applied Surface Science 252 (2006) 7856-7861, https://doi.org/10.1016/j.apsusc.2005.09.068.

[128]   D.X. Peng, C.H. Chen, Y. Kang, Y.P. Chang, S.Y. Chang, Size effects of SiO_2 nanoparticles as oil additives on tribology of lubricant, Industrial Lubrication and Tribology 62 (2010) 111-120, https://doi.org/10.1108/00368791011025656.

[129] G. Wen, X. Wen, P. Bai, Y. Meng, L. Ma, Y. Tian, Effect of mixing procedure of oleic acid and BN nanoparticles as additives on lubricant performance of PAO8, Tribology International 175 (2022) 107842, https://doi.org/10.1016/j.triboint.2022.107842.

[130] S. Kumari, O.P. Sharma, O.P. Khatri, Alkylamine-functionalized hexagonal boron nitride nanoplatelets as a novel material for the reduction of friction and wear, Physical Chemistry Chemical Physics 18 (2016) 22879-22888, https://doi.org/10.1039/C6CP04741F

[131] X. Song, S. Zheng, J. Zhang, W. Li, Q. Chen, B. Cao, Synthesis of monodispersed $ZnAl_2O_4$ nanoparticles and their tribology properties as lubricant additives, Materials Research Bulletin 47 (2012) 4305-4310, https://doi.org/10.1016/j.materresbull.2012.09.013.

[132] D. Jiao, S. Zheng, Y. Wang, R. Guan, B. Cao, The tribology properties of alumina/silica composite nanoparticles as lubricant additives, Applied Surface Science 257 (2011) 5720-5725, https://doi.org/10.1016/j.apsusc.2011.01.084.

[133] M. Farsadi, S. Bagheri, N.A. Ismail, Nanocomposite of functionalized graphene and molybdenum disulfide as friction modifier additive for lubricant, Journal of Molecular Liquids 244 (2017) 304-308, https://doi.org/10.1016/j.molliq.2017.09.008.

[134] Q. Chen, S. Zheng, S. Yang, W. Li, X. Song, B. Cao, Enhanced tribology properties of ZnO/Al_2O_3 composite nanoparticles as liquid lubricating additives, Journal of Sol-Gel Science and Technology 61 (2012) 501-508, https://doi.org/10.1007/s10971-011-2651-0.

[135] Y. Li, R. Yang, Q. Hao, W. Lei, Tribological properties of the functionalized graphene/montmorillonite nanosheets as a lubricant additive, Tribology Letters 69 (2021) 1-13, https://doi.org/10.1007/s11249-021-01495-x.

[136] Y. Meng, F. Su, Y. Chen, Synthesis of nano-Cu/graphene oxide composites by supercritical CO_2-assisted deposition as a novel material for reducing friction and wear, Chemical Engineering Journal 281 (2015) 11-19, https://doi.org/10.1016/j.cej.2015.06.073.

[137] Z. Jia, T. Chen, J. Wang, J. Ni, H. Li, X. Shao, Synthesis, characterization and tribological properties of Cu/reduced graphene oxide composites, Tribology International 88 (2015) 17-24, https://doi.org/10.1016/j.triboint.2015.02.028.

[138] W.K. Shafi, M.S. Charoo, An overall review on the tribological, thermal and rheological properties of nanolubricants, Tribology - Materials, Surfaces & Interfaces 15 (2021) 20-54, https://doi.org/10.1080/17515831.2020.1785233.

[139] J. Sun, S. Du, Application of graphene derivatives and their nanocomposites in tribology and lubrication: A review, RSC Advances 9 (2019) 40642-40661, https://doi.org/10.1039/C9RA05679C.

[140] J. Zhao, T. Gao, Y. Li, Y. He, Y. Shi, Two-dimensional (2D) graphene nanosheets as advanced lubricant additives: A critical review and prospect, Materials Today Communications 29 (2021) 102755, https://doi.org/10.1016/j.mtcomm.2021.102755.

[141] B. Hamrock, S. Schmid, B. Jacobson, Fundamentals of fluid film lubrication, 2004, CRC press 114 741-756, https://doi.org/10.1201/9780203021187.

[142] A.Y. Al-Hasan, Electricity generation cost between proposed photovoltaic station and conventional units in Kuwait, Renewable energy 12 (1997) 291-301, https://doi.org/10.1016/S0960-1481(97)00045-1.

[143] Renewable Energy Generation, Our World in data (2023), https://ourworldindata.org/grapher/renewable-energy-gen?time=2010..latest.

[144] P.M. Marques, C.M. Fernandes, R.C. Martins, J.H. Seabra, Efficiency of a gearbox lubricated with wind turbine gear oils, Tribology International 71 (2014) 7-16, https://doi.org/10.1016/j.triboint.2013.10.017.

[145] M. Evans, White structure flaking (WSF) in wind turbine gearbox bearings: effects of 'butterflies' and white etching cracks (WECs), Materials Science Technology 28 (2012) 3-22, https://doi.org/10.1179/026708311X13135950699254.

[146] G. Nicholas, B. Clarke, R. Dwyer-Joyce, Detection of lubrication state in a field operational wind turbine gearbox bearing using ultrasonic reflectometry, Lubricants 9 (2021) 6, https://doi.org/10.3390/lubricants9010006.

[147] D.K. Singh, J. Kurien, A. Villayamore, Study and analysis of wind turbine gearbox lubrication failure and its mitigation process, Materials Today: Proceedings 44 (2021) 3976-3983, https://doi.org/10.1016/j.matpr.2020.10.047.

[148] C.M. Fernandes, A.H. Battez, R. González, R. Monge, J. Viesca, A. García, R.C. Martins, J.H. Seabra, Torque loss and wear of FZG gears lubricated with wind turbine gear oils using an ionic liquid as additive, Tribology International 90 (2015) 306-314, https://doi.org/10.1016/j.triboint.2015.04.037.

[149] S. Sheng, Wind turbine gearbox reliability database, condition monitoring, and operation and maintenance research update, National Renewable Energy Lab.(NREL), Golden, CO (United States) (2016).

[150] J.B. A. Igartua, G. Mendoza, E. Aranzabe, M. Hernaiz, A. Malaga, I. Bayon, A. Arnaiz, J. Terradillos, A. Aranzabe, Environmentally friendly & durable windmill lubrication,, Proceedings of the eighth European Conference and Exhibition on "Lubrication, Maintenance and Tribotechnology", LUBMAT, Preston, UK (17th - 19th July 2023).

[151] D.A. Lauer, Chapter 36. Industrial Gear Lubricants. in: L.R. Rudnick, (Ed.), Synthetics, mineral oils, and bio-based lubricants: chemistry and technology, CRC Press, 2020.

[152] M.A. Gutierrez, M. Haselkorn, P. Iglesias, The lubrication ability of ionic liquids as additives for wind turbine gearboxes oils, Lubricants 4 (2016) 14, https://doi.org/10.3390/lubricants4020014.

[153] K. Michaelis, B.R. Höhn, M. Hinterstoißer, Influence factors on gearbox power loss, Industrial Lubrication Tribology - Materials, Surfaces & Interfaces (2011), http://doi.org/10.1108/00368791111101830.

[154] R. Monge, R. González, A.H. Battez, A. Fernández-González, J. Viesca, A. García, M. Hadfield, Ionic liquids as an additive in fully formulated wind turbine gearbox oils, Wear 328 (2015) 50-63, https://doi.org/10.1016/j.wear.2015.01.041.

[155] C. Sequeira, A. Pacheco, P. Galego, E. Gorbeña, Analysis of the efficiency of wind turbine gearboxes using the temperature variable, Renewable Energy 135 (2019) 465-472, https://doi.org/10.1016/j.renene.2018.12.040.

[156] D. Coronado, J. Wenske, Monitoring the oil of wind-turbine gearboxes: Main degradation indicators and detection methods, Machines 6 (2018) 25, https://doi.org/10.3390/machines6020025.

[157] J. Zellmann, Main types of damage to wind turbine gearboxes, Wind Kraft J (2009) 2-5.

[158] C. Intergovernmental Panel on Climate, Climate Change 2014: Mitigation of Climate Change: Working Group III Contribution to the IPCC Fifth Assessment Report (2015).

[159] M. Woydt, The importance of tribology for reducing CO_2 emissions and for sustainability, Wear 474-475 (2021) 203768, https://doi.org/10.1016/j.wear.2021.203768.

[160] S. Bellekom, R. Benders, S. Pelgröm, H. Moll, Electric cars and wind energy: Two problems, one solution? A study to combine wind energy and electric cars in 2020 in The Netherlands, Energy 45 (2012) 859-866, https://doi.org/10.1016/j.energy.2012.07.003.

[161] Y. Kwak, C. Cleveland, A. Adhvaryu, X. Fang, S. Hurley, T. Adachi, Understanding base oils and lubricants for electric drivetrain applications, SAE Technical Paper (2019), https://doi.org/10.4271/2019-01-2337.

[162] R. Shah, B. Gashi, A. Rosenkranz, Latest developments in designing advanced lubricants and greases for electric vehicles—An overview, Lubrication Science 34 (2022) 515-526, https://doi.org/10.1002/ls.1605.

[163] Q. Xue, X. Zhang, T. Teng, J. Zhang, Z. Feng, Q. Lv, A comprehensive review on classification, energy management strategy, and control algorithm for hybrid electric vehicles, Energies 13 (2020) 5355, https://doi.org/10.3390/en13205355.

[164] A. García, G.D. Valbuena, A. García-Tuero, A. Fernández-González, J.L. Viesca, A. Hernández Battez, Compatibility of Automatic Transmission Fluids with Structural Polymers Used in Electrified Transmissions, Applied Sciences 12 (2022) 3608, https://doi.org/10.3390/app12073608.

[165] L.I. Farfan-Cabrera, Tribology of electric vehicles: A review of critical components, current state and future improvement trends, Tribology International 138 (2019) 473-486, https://doi.org/10.1016/j.triboint.2019.06.029.

[166] N. Rivera, J.L. Viesca, A. García, J.I. Prado, L. Lugo, A.H. Battez, Cooling Performance of Fresh and Aged Automatic Transmission Fluids for Hybrid Electric Vehicles, Applied Sciences 12 (2022) 8911, https://doi.org/10.3390/app12178911.

[167] M.N. B. Zhmud, L. Everlid, Gear Design and Tribology of EV Transmissions, Proceedings of the eighth European Conference and Exhibition on "Lubrication, Maintenance and Tribotechnology", LUBMAT, Preston, UK (17th - 19th July 2023).

[168] M. Iino, A. Tada, K. Masuda, S. Matsuki, Drivetrain Lubricants with High Cooling and Efficiency-Boosting Properties for Electric Vehicles, SAE Technical Paper (2021) Paper No. 2021-2001-1215.

[169] B. Wang, F. Qiu, G.C. Barber, Q. Zou, J. Wang, S. Guo, Y. Yuan, Q. Jiang, Role of nano-sized materials as lubricant additives in friction and wear reduction: A review, Wear 490-491 (2022) 204206, https://doi.org/10.1016/j.wear.2021.204206.

[170] B. McCoy, Next generation driveline lubricants for electrified vehicles, Tribology Lubrication Technology 77 (2021) 38-40.

[171] M.K.A. Ali, X. Hou, M.A.A. Abdelkareem, Anti-wear properties evaluation of frictional sliding interfaces in automobile engines lubricated by copper/graphene nanolubricants, Friction 8 (2020) 905-916, https://doi.org/10.1007/s40544-019-0308-0.

[172] M. Goodarzi, D. Toghraie, M. Reiszadeh, M. Afrand, Experimental evaluation of dynamic viscosity of ZnO–MWCNTs/engine oil hybrid nanolubricant based on changes in temperature and concentration, Journal of Thermal Analysis and Calorimetry 136 (2019) 513-525, https://doi.org/10.1007/s10973-018-7707-8.

[173] Y. Alexandrova, R.S. Semken, J. Pyrhönen, Permanent magnet synchronous generator design solution for large direct-drive wind turbines: Thermal behavior of the LC DD-PMSG, Applied Thermal Engineering 65 (2014) 554-563, https://doi.org/10.1016/j.applthermaleng.2014.01.054.

2 MATERIALS AND METHODS

The purpose of this section of the PhD Thesis is to summarize the materials and methods used during the research process. The main materials selected are base oils, NPs, and modifying agents. Regarding the methods can be summarized as techniques used to characterize the selected materials, the nanodispersions and the worn surfaces, as well as those used to the preparation of nanodispersions, the device used to thermophysical characterization and the tribometers. The techniques used and the procedure followed in this PhD Thesis are summarized in the flowchart in Figure 2.1.

Some of the information presented in this chapter is related to the following publications (the publisher authorizations for the use of these publications are in the Appendix A):

F. Mariño[a], E. R. López[a], A. Arnosa[b], M. A. González Gómez [b], Y. Piñeiro[b], J. Rivas[b], C. Alvarez-Lorenzo[c], J. Fernández[a]. ZnO nanoparticles coated with oleic acid as additives for a polyalphaolefin lubricant. *Journal of Molecular Liquids*, 348, (2022) 118401. (Open access) https://doi.org/10.1016/j.molliq.2021.118401

[a] Laboratory of Thermophysical and Tribological Properties, Nafomat Group, Department of Applied Physics, Faculty of Physics, and Institute of Materials (iMATUS), Universidade de Santiago de Compostela, 15782 Santiago de Compostela, Spain
[b] NANOMAG Laboratory, Department of Applied Physics, Faculty of Physics, and Institute of Materials (iMATUS), Universidade de Santiago de Compostela, 15782 Santiago de Compostela, Spain
[c] Departamento de Farmacología, Farmacia y Tecnología Farmacéutica, R+D Pharma Group (GI-1645), Facultad de Farmacia, Instituto de Materiales (iMATUS) and Health Research Institute of Santiago de Compostela (IDIS), Universidade de Santiago de Compostela, 15782 Santiago de Compostela, Spain

The main contributions of the PhD student to this study are explicitly indicated below:

Experimental: Investigation, Formal analysis.

Manuscript: Writing – original draft.

J. M. Liñeira del Río[a,b], F. Mariño[a], E. R. López[a], D. E. P. Gonçalves[b], J. H. O. Seabra[c], J. Fernández[a]. Tribological enhancement of potential electric vehicle lubricants using coated TiO_2 nanoparticles as additives. *Journal of Molecular Liquids*, 371, (2022) 121097. (Open access) https://doi.org/10.1016/j.molliq.2022.121097

[a] Laboratory of Thermophysical and Tribological Properties, Nafomat Group, Department of Applied Physics, Faculty of Physics, and Institute of Materials (iMATUS), Universidade de Santiago de Compostela, 15782 Santiago de Compostela, Spain
[b] Unidade de tribologia, vibraçoes e manutençao industrial, INEGI, Universidade do Porto, Porto, Portugal
[c] FEUP, Faculdade de Engenharia da Universidade do Porto, Rua Dr. Roberto Frias s/n, 4200-465 Porto, Portugal

The main contributions of the PhD student to this study are explicitly indicated below:

Experimental: Investigation, Methodology, Conceptualization

Manuscript: Writing – review & editing
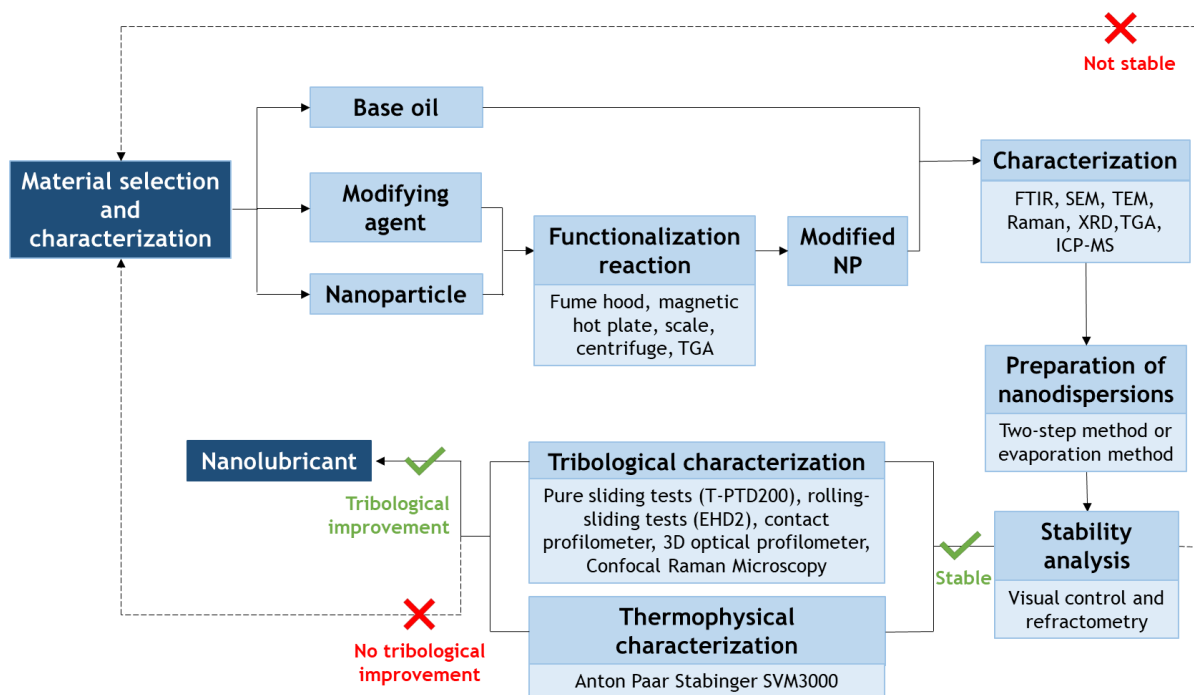
Figure 2.1 Flowchart of the techniques and procedures used in this PhD Thesis

2.1 MATERIALS

2.1.1 Selection of materials

The selection of base oils, NPs, and modifying agents was the first task of this work (Figure 2.1). As it was thoroughly discussed in Chapter 1, overall, polyalphaolefins (PAOs) have better physical and chemical properties, such as enhanced thermal and oxidative stabilities, compared to base oils belonging to groups I-III and V, being then more durable [1]. Thus, three PAOs were chosen as base fluids of the nanolubricants for the referred applications because are the most convenient base oils due to the working conditions required [2], as it was explained in Section 1.4. So, the specific polyalphaolefins shown in Table 2.1 were selected considering their application and availability:

- Wind turbine gearboxes: a high viscosity PAO, PAO40.
- Electric Drivetrains: two low viscosity PAOs, PAO8 and PAO6 [3].

Table 2.1 Thermophysical properties of the selected base oils

Base oil	Supplier	Density (g/cm^3) at 40 °C	Viscosity (mPa·s) at 40 °C	VI
PAO40		0.8345	332.53	150
PAO8	Repsol	0.8163	39.47	138
PAO6		0.8114	24.84	138

The selection of the NPs was carried out taking into account all the literature reviewed in the previous chapter, as well as the preliminary work described in Appendix B. From Figure 1.7, and Tables 1.1-1.6 it was concluded that the best stability results are obtained when spherical NPs, smaller than 20 nm, are chemically modified with organic acids or amines with alkyl chains longer than 12C. Figure 1.8 and table 1.3 show that some coated metal oxides NPs smaller than 20 nm, lead to nanolubricants with long stabilities in PAO, ester and mineral oils. Furthermore, Figure 1.9 shows the stability results from the literature for PAOs for NP sizes up

to 200 nm, with the largest NPs being silane-coated and used for a high viscosity base oil (PAO100). Moreover, from our previous results reported in Appendix B, we concluded that silanization via sCO_2 was quite unsuccessful, so the use of silanized NPs was discarded. Additionally, we also discarded carbon nanomaterials (graphene nanoplatelets and GO) due to poorer stability results (specially GO) even after their functionalization. From a tribological point of view, the effect of the nanoparticle and the modifying agent was also presented in Figure 1.11. Again, the best results for friction and wear reduction are obtained when the nanoparticle size is smaller than 20 nm. In addition, from the preliminary results (Appendix B) we also discarded other carbon nanomaterials such as modified GnPs due to their poorer tribological capabilities compared to the functionalized metal oxides NPs tested.

Regarding the nature of the nanoparticle, metal or ceramic oxides are advantageous due to the ease with which they can react with organic acids or other functional groups such as amines or silanes. In presence of water, the oxidized surface of the NPs provides highly reactive hydroxyl groups that can react with the modifying agents.

From Table 1.3 and 1.9, we chose two metal oxide NPs. One of them, TiO_2 NPs, was selected because of the promising stability and tribology results shown in the Wright et al. article [4] but using a different low-viscosity PAO and a different coating agent. The other one, ZnO NPs, was selected to test whether similar ZnO-OA NPs could be dispersed for a longer period in PAO instead of a mineral oil [5]. From Table 1.5 and 1.11, we selected SiO_2 NPs as a ceramic oxide due to the promising stability and tribology results obtained by other authors with polymer grafted SiO_2 NPs in low-viscosity PAOs [4,6].

Thus, in this PhD Thesis, three types of spherical NPs, metal, or ceramic oxides, with sizes between 5 and 10 nm were selected as bare nanoadditives as indicated in Table 2.2. TiO_2 and SiO_2 NPs were purchased from US Research Nanomaterials, Inc. (Houston, TX, USA), whereas ZnO NPs were synthesized during this PhD Thesis.

Table 2.2 Technical information about the selected NPs

Nanoparticle	Supplier	CAS Number	Purity	Average size	Morphology
ZnO	None*	1314-13-2	-	10 nm	
TiO_2	US Research	1317-70-0	99.9 %	5 nm	Spherical
SiO_2	Nanomaterials, Inc.	7631-86-9	99 %	8 nm	

* Synthesized in the laboratory (Section 3.1.1)

All the previously mentioned nanoadditives were functionalized before their addition to the PAO base oil to improve their dispersibility in the oil and the time stability of the nanodispersions. According with the literature reviewed in Chapter 1, the most common modifying agents are organic acids, amines, and silanes (Figure 1.2). For all these cases, the modifying agent is formed by a polar group and a non-polar aliphatic chain with at least ten carbon atoms. Organic acids, also known as fatty acids [7], are organic molecules formed by a carboxylic acid and an aliphatic chain which can be saturated or unsaturated. Taking into account the conclusions described in the previous chapter, in this PhD Thesis we used a saturated fatty acid, stearic acid (SA), an unsaturated fatty acid, oleic acid (OA). The molecular structure and technical information of the two modifying agents are indicated in Figure 2. and in Table 2.3. The chemically modified NPs that we have analyzed in this PhD Thesis are summarized in Table 2.4.

Table 2.3 Technical information about the selected modifying agents

Modifying agents	Supplier	CAS Number	Purity
Oleic acid (OA)	Sigma-Aldrich	112-80-1	90 %
Stearic acid (SA)		57-11-4	95 %

Oleic acid (OA)

$C_{18}H_{34}O_2$

Stearic acid (SA)

$C_{18}H_{36}O_2$
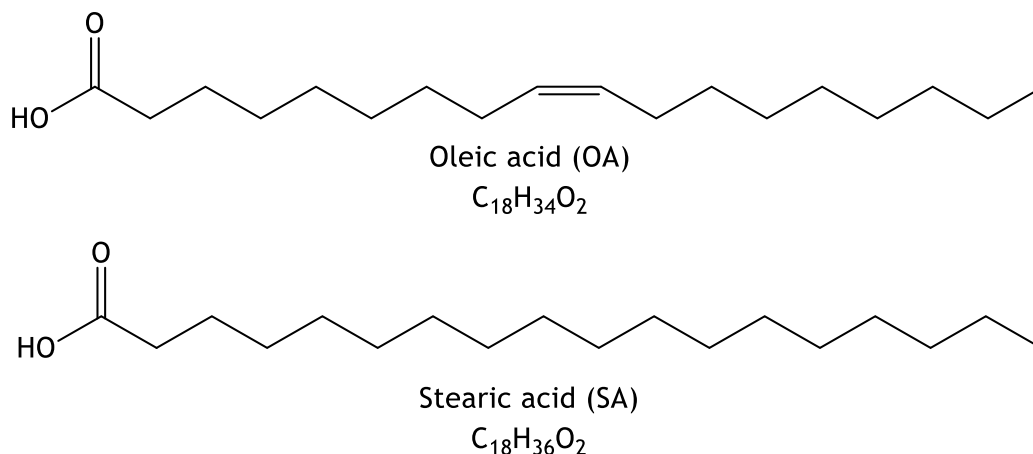
Figure 2.2 Chemical structure of the modifying agents

Table 2.4 Summary of the functionalized nanoparticles

Bare nanoparticles	Modifying agent	Average size	Coated nanoparticles
ZnO	OA	10 nm	ZnO-OA
TiO$_2$	OA	5 nm	TiO$_2$-OA
SiO$_2$	SA	8 nm	SiO$_2$-SA

2.1.2 Synthesis and functionalization of nanoparticles

Once the nanoparticle and the modifying agent have been selected, the next step was the synthesis and functionalization of those NPs to obtain the chemically modified NPs (Figure 2.1). All synthesis carried out follow some general guidelines for the synthesis of bare ZnO NPs and for the functionalization of the three NPs of Table 2.2: a fume hood (Figure 2.a) was used to carry out the reactions safely, an assembly for refluxing reactions (Figure 2.b), a round bottom flask coupled to a condenser that contains the reaction stirred with a magnetic bar in a silicone bath and a heating plate with magnetic stirring (Figure 2.3c,d). The solid reagents were weighted with a high precision Sartorius MC 210P Microbalance (Figure 2.4a) and the reaction products were separated and washed with the aid of a MPW M-Universal centrifuge (Figure 2.4b). In the case of ZnO NPs synthesis and functionalization, a Perkin Elmer Pirys 7 TGA of NANOMAG research group from the USC (Figure 2.4c) was used to know the concentration of NPs dispersed in a solvent. To know the amount of modifying agent on the surfaces of SiO$_2$ (Figure 2.4d), a TGA/DSC 1 (Mettler Toledo) was used. In all the other cases, due to the unavailability of the TGA, a stove Memmert BM400 (Figure 2.4e) was used with a similar strategy, 1 mL of nanodispersion was weighted before and after evaporating the solvent.
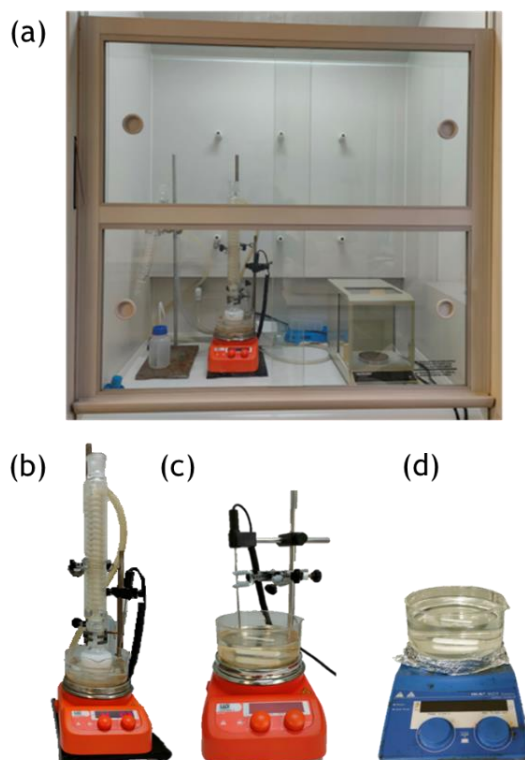
Figure 2.3 Material used for the synthesis: (a) Fume hood; (b) Reaction set-up; (c) Magnetic hot plate LBX H03D; (d) Magnetic hot plate IKA RCT basic (NANOMAG)
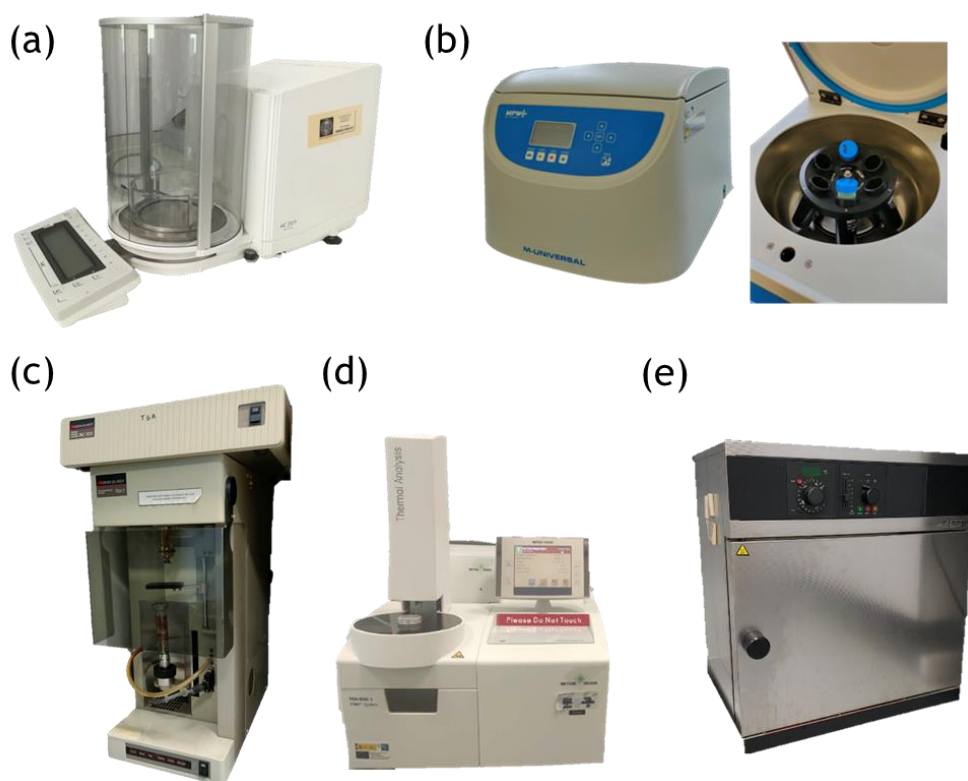
Figure 2.4 Used equipment during the synthesis and functionalization of the NPs: (a) High precision Sartorius MC 210P Microbalance; (b) Centrifuge MPW M-Universal; (c) Perkin Elmer Piryis THA (NANOMAG); (d) TGA/DSC 1 Mettler Toledo (RIAIDT of the USC); (e) Stove Memmert BM400

2.2 Characterization techniques

In this section, a description of several techniques used for the characterization of base oils, modifying agents and NPs, as well as worn steel pins used in the tribological measurements are presented. Most of these techniques belong to the Network of Infrastructures to Support Research and Technological Development (RIAIDT) of the University of Santiago de Compostela.

2.2.1 Fourier transform infrared spectroscopy

Infrared Spectroscopy is a non-destructive technique based on the absorption of infrared radiation and the conversion of this energy in characteristic molecular vibrations for each chemical bond present on the tested compound [8]. A Fourier transform infrared (FTIR) spectrum can be displayed as a graph of absorbance (or transmittance) of infrared light on the vertical axis versus frequency, wavenumber, or wavelength on the horizontal axis. Thus, a FTIR spectrometer VARIAN 670-IR (Figure 2.5), coupled to an attenuated total reflectance accessory (ATR) was used to record the absorbance spectra of base oils, modifying agents and NPs. The most relevant application of FTIR in this PhD Thesis is to verify the efficiency of the surface functionalization of the NPs through the appearance of new chemical bonds between the nanoparticle and the functionalization molecules, as well as the disappearance of the hydroxyl peak of the carboxylic group of the fatty acids.

Figure 2.5 Fourier transform infrared spectrometer: FTIR VARIAN 670-IR (RIAIDT of the USC)

2.2.2 Electron microscopy

A scanning electron microscope (SEM) scans the analyzed surface with a focus beam of electrons. Due to the interaction of this beam with the sample secondary electrons are emitted and reflected from the surface, which are detected by a secondary electron detector producing signals of different intensities depending on the surface geometry, chemical characteristics, and bulk chemical composition [9]. The obtained image is therefore a distribution map of the intensity of the emitted signals from the scanned area [10]. The spatial resolution of a conventional SEM is 50-100 nm [9]. The instrument used to observe the morphology of the commercial TiO_2 and SiO_2 NPs, as well as the worn pin surface of those pins lubricated with PAO6 and its formulated lubricants, was a field emission scanning electron microscope (FESEM) which differs from a traditional SEM in the electron generation system, and provides images with a spatial resolution three to six times better [9]. The used Zeiss FESEM Ultraplus (Figure 2.6a) has an acceleration voltage range from 0.02 to 30 kV and resolutions of 1.0 nm/15 kV, 1.7 nm/1 kV and 4.0 nm/0.1 kV.

A transmission electron microscope (TEM) is another electron microscope in which a beam of electrons is transmitted through the sample to form an image using a detector [11]. The image

formation is due to the interaction of the electrons with the sample during the scan and can reach atomic resolution [12]. To further analyze the morphology and size of the NPs a high-resolution TEM JEOL JEM-1011 was used (Figure 2.6b) due to its enhanced capability to magnify the samples compared to SEM. To perform these analyses dry NPs were dispersed in a volatile solvent and placed in copper grids with carbon films. Subsequently, the TEM was configured with a high brightness lanthanum hexaboride (LaB_6) source and an accelerating voltage between 40 and 100 kV.
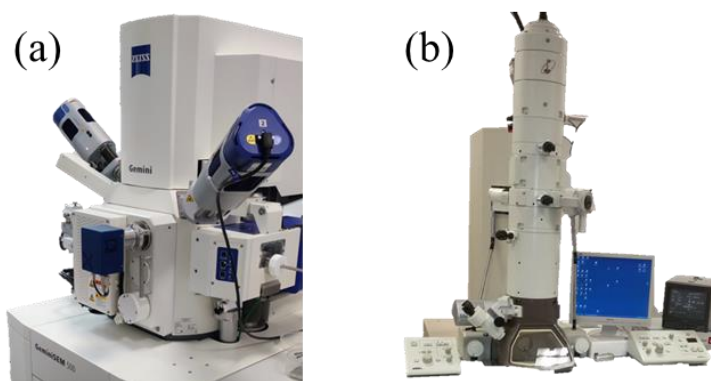
Figure 2.6 Electron microscopes (RIAIDT of USC): (a) Zeiss FESEM Ultra Plus SEM; (b) JEOL JEM-1011 TEM

2.2.3 Confocal Raman microscopy

Raman spectroscopy is a commonly used technique in chemical characterization that provides a fingerprint of the analyzed samples from the vibrational modes of molecules [13]. A confocal Raman microscope combines the Raman spectral information with the spatial filtering of a confocal microscope, eliminating out of-focus signals [14], for high resolution chemical mappings of samples [15]. This device was used to characterize the PAOs and coated NPs through Raman spectroscopy, as well as to perform elemental mappings of the worn surfaces to identify the tribological mechanisms during the rubbing process, i.e., analyze the role the NPs have in the wear reduction by detecting the components present on the worn surface after a cleaning step with hexane solvent to remove the excess nanodispersion. A Witec alpha300R+ confocal Raman microscope (Figure 2.7) operating at 532 nm was used with two scanning systems: a coarse motorized stage for large areas and a piezo stage for subnanometer adjustments. This device gives chemical information and a mapping of the components of the scanned area.
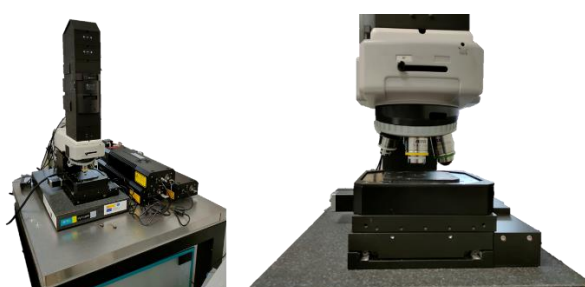
Figure 2.7 Confocal Raman Microscope: WITec alpha300R+ (RIAIDT of the USC)

2.2.4 X-ray diffractometer

X-ray diffraction is an analytical technique that determines the three-dimensional geometry of crystalline materials using electromagnetic radiation (X-rays) [16]. The atomic structures of crystals are regular and repetitive through the whole structure. When the X-rays travel through

this type of structure, diffraction occurs through the atomic or molecular layers conforming the crystal. These diffracted rays interfere with each other through constructive and destructive interferences. The patterns formed after the diffraction of those X-rays can be evaluated and areas specific for each material.

A Philips PW1710 diffractometer (Figure 2.8) with a graphite diffracted beam monochromator and a copper radiation source (λ (Cu Kα) = 1.5406 Å), at 40 kV and 30 mA was used to determine the crystal structure of the synthesized NPs. Measurements were carried out for a 2θ angle from 10° to 80° every 0.02° and 10 s/step on the powder sample.

Figure 2.8 X-ray diffractometer: Philips PW1710 (RIAIDT of the USC)

2.2.5 Elemental analysis

Inductively coupled plasma mass spectrometry (ICP-MS) is an inorganic elemental and isotopic analysis technique able to determine and quantify most of the elements of the periodic table [17]. The procedure consists in the transformation of a liquid sample into ions that differ by their mass. For this PhD Thesis, the ICP-MS was used to quantitatively determine the concentration of Zn in the nanodispersion containing ZnO NPs modified with OA before and after a tribological test to identify the role of these NPs in the reduction of wear. A reduction in the NP concentration means that part of the nanoadditive remains on the worn surface by physical or chemical adsorption in the tribological process, while no changes in the NP concentration would indicate that there was no NP adsorption. An Agilent 7900x ICP-MS (Figure 2.9a) was used after a microwave-assisted acid digestion (Figure 2.9b) which was necessary due to the viscous nature of the sample.

Figure 2.9 Equipment for elemental analysis (RIAIDT of the USC): (a) Inductively coupled plasma mass spectrometer Agilent 7900x; (b) Milestone ultraWAVE3 microwave digestion system

2.3 PREPARATION AND CHARACTERIZATION OF THE NANODISPERSIONS

After the characterization of the base oils, NPs and modifying agents, as well as the chemically modified NPs, the next step is the preparation and characterization of the nanodispersions (Figure 2.1). For this purpose, several procedures were selected taking into account the conclusions of Chapter 1. The preparation method of Liñeira del Rio et al. [18] (Figure 1.5) was adapted for the preparation of most of the nanodispersions. The stability of the nanodispersions with time was evaluated using two methods: visual control and refractometry. Moreover, density, viscosity, and viscosity index at atmospheric pressure of the base oils and nanodispersions were measured at several temperatures.

2.3.1 Preparation method

Most of the nanodispersions were prepared with similar procedures (Figure 2.10) with some differences according with the availability of some of the devices (Figures 2.11), such as the rotary evaporator or the TGA.

In the case of OA modified ZnO NPs (ZnO-OA NPs), homogeneous dispersions in PAO40 were prepared following the procedure indicated in Figure 2.10a. At the end of the synthesis procedure, ZnO-OA NPs were dispersed in chloroform (Section 3.1.1) to avoid agglomeration being the concentration determined by TGA (2.12 wt%). Known amounts of this ZnO-OA/chloroform dispersion and PAO40 were mixed. Subsequently, this blend was homogenized with both an OVAN ultrasonic bath (Figure 2.11a) for 15 min and a Branson ultrasonic Sonifier S-250A probe sonicator (Figure 2.11b) for 5 min at 200 W of effective power and 60 Hz sonication frequency with a 20 % amplitude. The next step was to evaporate the chloroform with a rotary evaporator (Figure 2.11e) at 60 ℃ for 30 min. The obtained PAO40 + 1.00 wt% ZnO-OA dispersion was then further sonicated for 240 min using a Fisherbrand ultrasonic bath FB11203 (Figure 2.11c), in a continuous shaking mode at 180 W effective power and 37 kHz sonication frequency. Two replicates were prepared, one for the stability study, and the other for thermophysical and tribological characterizations. Diluted nanodispersions (0.10, 0.25, 0.50, 0.75 wt%) were obtained from the PAO + 1.00 wt% ZnO-OA nanodispersion adding PAO40. All the nanodispersions were further sonicated in the Fisherbrand ultrasonic bath (Figure 2.14 c) under the same conditions.

To determine the optimal conditions for the rotary evaporator step, several tests were previously carried out to find the time and temperature necessary to remove completely the chloroform. For this task, chloroform was mixed with PAO40 and afterwards evaporated using the rotary evaporator at different temperatures during several times. After each temperature–time test, the viscosity of the sample was measured with an Anton Paar Stabinger SVM3000 rotational viscosimeter (Figure 2.13). The viscosity values, from 5 to 100 °C, were compared with those of neat PAO40, considering as optimal temperature–time conditions those for which viscosity values of neat PAO40 and of the sample were closest, being these conditions: 60 °C and 30 min.

For other nanodispersions (OA modified TiO_2 NPs, TiO_2-OA, and SA modified SiO_2, SiO_2-SA) the rotary evaporator was substituted by a magnetic hot plate LBX H03D (Figure 2.2c), being the procedure summarized in Figure 2.10b. The optimal time and temperature conditions for the complete evaporation of hexane (the volatile solvent for the nanodispersions based on PAO6 or PAO8) was determined similarly using the same viscosimeter. To carry out this task, previously a known concentration of NP/hexane dispersion (known using the stove, Figure 2.4e) was mixed with an appropriate amount of PAO6 or PAO8 using the Fisherbrand ultrasonic bath for 15 min, followed by the evaporation of hexane in the hot plate with magnetic agitation

for 60 min at 90 °C, obtaining a concentrated nanodispersion in PAO. Dilutions of this dispersion were carried out. To improve the dispersibility of NPs in the PAO6 or PAO8, OA or SA was added to each nanodispersion of TiO_2-OA and SiO_2-SA, respectively.
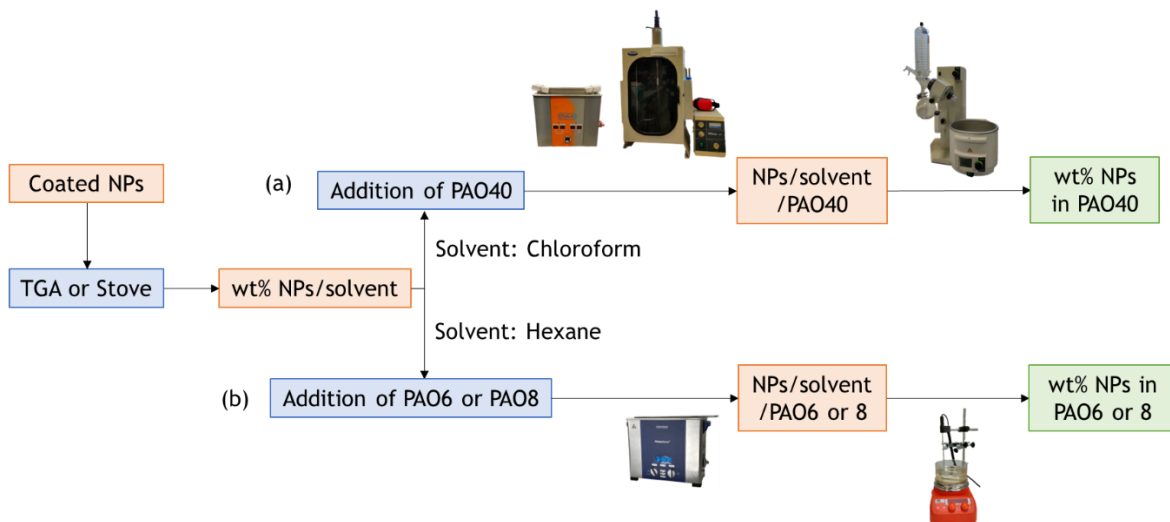
Figure 2.10 Schematic procedure for preparing nanodispersions: (a) using a rotary evaporator; (b) using a magnetic hot plate
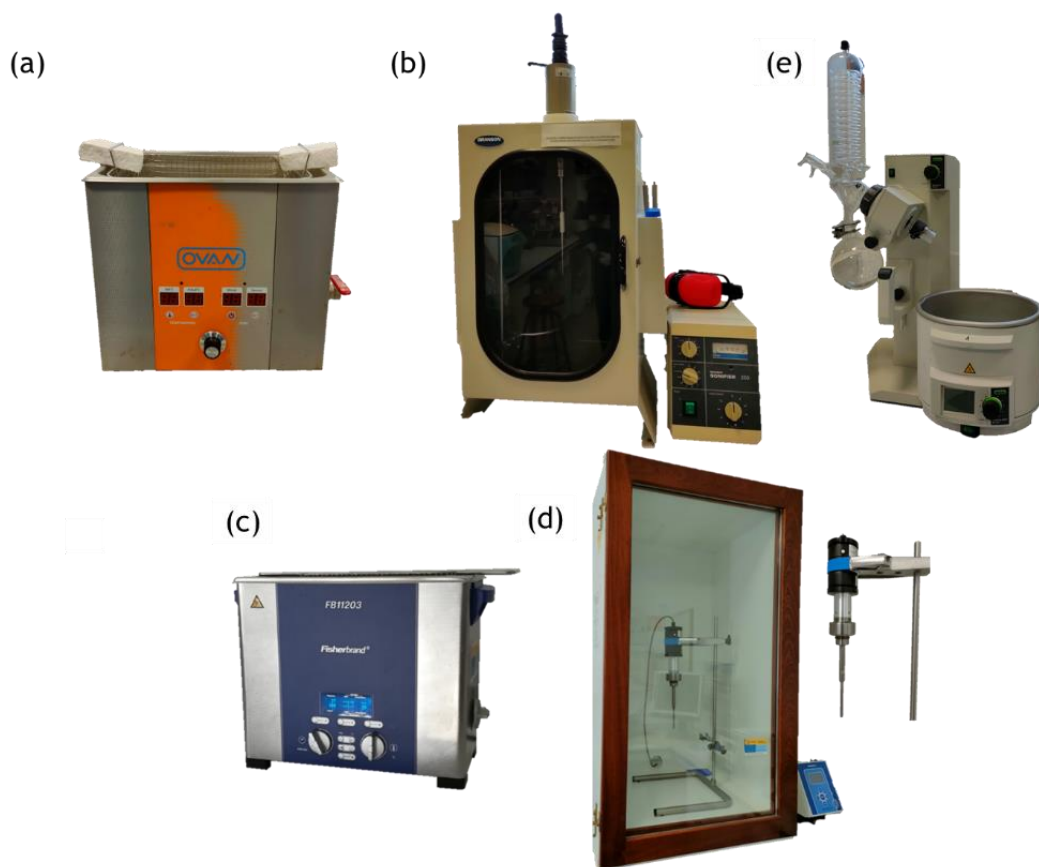
Figure 2.11 Ultrasonication devices: (a) OVAN ultrasonic bath (NANOMAG); (b) Branson ultrasonic Sonifier S-250A probe sonicator (NANOMAG); (c) Fisherbrand ultrasonic bath FB11203; (d) ultrasonic HD 2200 Sonopuls disruptor; (e) Büchi Rotavapor R-210 (NANOMAG)

Table 2.5 summarizes the designed nanodispersions with coated NPs, prepared and tribologically characterized during this PhD Thesis, as well as the other evaluated lubricants such as those with uncoated NPs or other lubricants tested in Chapter 5. Other prepared nanodispersions, analyzed in the preliminary work, are summarized in Appendix B.

Table 2.5 Summary of the tribologically characterized lubricants

Additive	Base oil	Concentrations (wt%)	Dispersants (wt%)
ZnO-OA	PAO40	0.10, 0.25, 0.50, 0.75, 1.00	None
TiO$_2$-OA	PAO8	0.10, 0.25. 0.35, 0.50	OA (0.20)
SiO$_2$-SA		0.05, 0.10, 0.20, 0.30	SA (0.05, 0.10, 0.20, 0.30)
SiO$_2$-SA		0.20	None
SiO$_2$	PAO6	0.20	None
SA		0.20	None
ZDDP		0.20	None

2.3.2 Stability of the nanodispersions

One of the main objectives of this PhD Thesis is to improve the stability time of nanodispersions by chemically modifying the surface of the nanoadditives. For this aim, two complementary methods were used to evaluate this stability.

Firstly, the stability was roughly determined by taking photographs of the nanodispersions over time using the setup of Figure 2.12a. For this, the newly prepared nanodispersions are placed inside the cardboard platform, without external disturbances, being periodically photographed until sedimentation is observed.

Secondly, the time evolution of the refractive index, n, of the nanodispersions is evaluated using a Mettler Toledo RA-510 M refractometer (Figure 2.12b) operating at the wavelength of the sodium D-line (589.3 nm). The refractometer works within the range of n from 1.32 to 1.56 with a resolution of 0.00001 and an uncertainty of $2 \cdot 10^{-5}$ [19]. Measurements were performed at 25 ºC, for regular intervals of time. Base oils and stable nanodispersions show a refractive index with a slope close to zero, while unstable nanodispersions show an increase in refractive index with time.
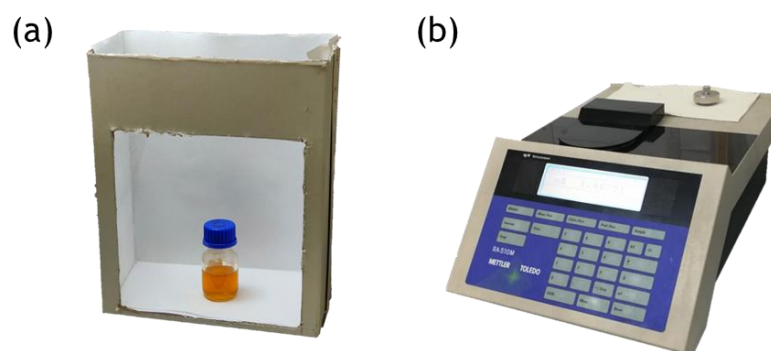
Figure 2.12 Techniques used to evaluate the stability of the nanodispersions: (a) Set-up for visual control; (b) Refractometer Mettler Toledo RA-510 M

2.3.3 Thermophysical characterization

Once the stability of the nanodispersions was characterized, it is important to evaluate their thermophysical properties and compare them with the base oil (Figure 2.1). In the framework of this PhD Thesis, density and viscosity of the base oils and the nanodispersions were measured using an Anton Paar Stabinger SVM3000 viscosimeter (Figure 2.13), which is a rotational

viscosimeter with cylindrical geometry equipped with a density measurement cell. Thus, this instrument allows to simultaneously measure density (ρ) and dynamic viscosity (η), and automatically calculates viscosity index (VI). This last property for an oil is related to its viscosity change when temperature varies, the higher the VI, the lower the viscosity-temperature dependence.

The Anton Paar Stabinger SVM3000 viscosimeter operates from -40 to 105 ℃ at 0.1 MPa in a viscosity range from 0.2 mPa s to 20 Pa s. A thermostat with cascaded Peltier elements controls the temperature inside the cells, being measured with an expanded uncertainty, k = 2, of 0.02 K through a Pt100 thermoresistor. The density cell uses the "U" tube oscillation principle, which allows the density of the sample to be determined from the measurement of the oscillation frequency of the U-tube cell according to the standard DIN 51757 with an expanded uncertainty of 0.0005 g cm^{-3}. Meanwhile, the viscosity measuring cell is built according to the modified Couette principle. It contains a tube that rotates at a constant speed and is filled with the sample fluid, while a measuring rotor with a built-in magnet float freely in the sample. Shear forces from the sample drive the rotor while magnetic forces retard its rotation. Shortly after the start of the measurement, the rotor reaches equilibrium speed, which is related to the viscosity of the fluid. The expanded uncertainty of dynamic viscosity, k = 2, is 1 % [20]. Viscosity index is determined using ASTM D2270 standard [21] with an estimated uncertainty of 2.7.
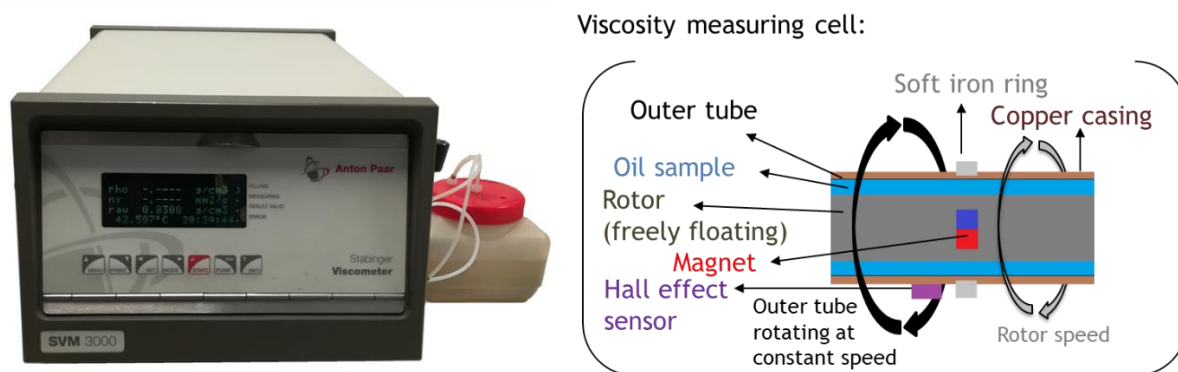
Figure 2.13 Rotational viscosimeter: Anton Paar Stabinger SVM3000

2.4 TRIBOLOGICAL CHARACTERIZATION

The tribological characterization of the base oil and the nanodispersion is performed at the same time as the thermophysical characterization, (Figure 2.1).

2.4.1 Anton Paar T-PTD200 tribological cell

An Anton Paar modular rheometer MCR 302 equipped with a T-PTD 200 tribological module was used to measure the friction coefficient of steel/steel contacts lubricated with the base oils and the nanodispersions (Figure 2.14). This module is based on the ball-on-three-plates principle [22,23]. The temperature of these contacts was controlled using a Peltier hood HPTD 200, being the operating temperature range -40 to 300 ℃. The configuration, characteristics, and experimental conditions of the tribological tests are shown in Table 2.6. The ball-on-three-pins configuration consists of a rotating ball attached to an axial shaft fixed to the rotary motor. The ball is in contact with the three pins partially inserted in a sample holder

(Figure 2.14c). The shaft and the pins form an angle of 45º (Figure 2.14d). The axial force (F) is equally transferred to the pins through normal forces (F_N) and is calculated by eq. 2.1.

$$F_N = \frac{F}{3 \cdot \cos 45°}$$

(2.1)

During the tribological tests, the rotational movement of the shaft and ball produces a sliding speed of the ball with respect to the pin surface at their contact point, which can vary from 0 to 1.4 m/s. When the device is turned-on an automatic calibration is carried out, then the experiments can be performed with no need of recalibration between tests. The device also ensures that the ball contacts the pins with zero contact force before the test starts. Finally, the lubricant is placed in the sample holder, completely submerging the pins (around 1.3 mL), and the experiment can begin. All the experiments were performed using an axial force F of 20 N, which corresponds to three normal forces F_N of 9.43 N (eq. 2.1), and a constant sliding speed of 0.1 m/s (angular speed of 213 rpm). The sliding distance and temperature varied depending on the application:

- For the wind turbine gearboxes (nanolubricants with PAO40) the chosen temperature was 80 ℃ and the sliding distance was 180 m. According to some authors [24,25], the oil temperatures of wind turbines reach peaks up to 80 ℃, for this reason it was chosen as the testing temperature.
- For the electric drivetrains of EVs (nanolubricants with PAO6 or PAO8) the chosen temperature was 120 ℃ and the sliding distance was 340 m. The temperature was chosen considering the temperatures that gears and main parts of the electric motor can reach inside the transmission [26]. Thus, according to the literature the temperature should be kept under 110 or 150 ℃ to prevent demagnetization [27,28].

The friction coefficient was recorded as a function of time or as a function of the sliding distance. For each lubricant, the tests were repeated at least three times. Thus, the average COF value for each lubricant was determined from the mean COF values of the repetitions and its standard deviation was calculated. The expanded uncertainty was determined using the standard deviation of the average and a coverage factor, k, of 2. The uncertainty contribution of type B has not been calculated due to the lack of information about the uncertainties of the properties affecting the COF measurement [29]. At the end of each test, the pins and ball were cleaned with hexane and hot air.

Table 2.6 Pure sliding tests: Tribometer configuration, characteristics, and experimental conditions

Tribology Cell T-PTD200 (Anton Paar)		
Ball-on-three pins configuration		Peltier hood HPTD200
Tribo-pair	Experimental conditions	
100Cr6 steel ball: 12.7 mm diameter and 0.15 μm Ra	Sample: 1.3 mL (3 replicates)	80 ℃
		or
	Axial force (F): 20 N	120 ℃
100Cr6 pins: 6 mm diameter and a 0.3 μm Ra		
	Tribological normal force (F_N): 9.43 N	
Both:	Maximum Hertzian contact pressure: 1.1 GPa	
Hardness: 58–65 HRC		
Young modulus: 190–210 GPa		
Poisson ratio: 0.29	Sliding distance: 180 m or 340 m	
	Rotational speed: 213 rpm	
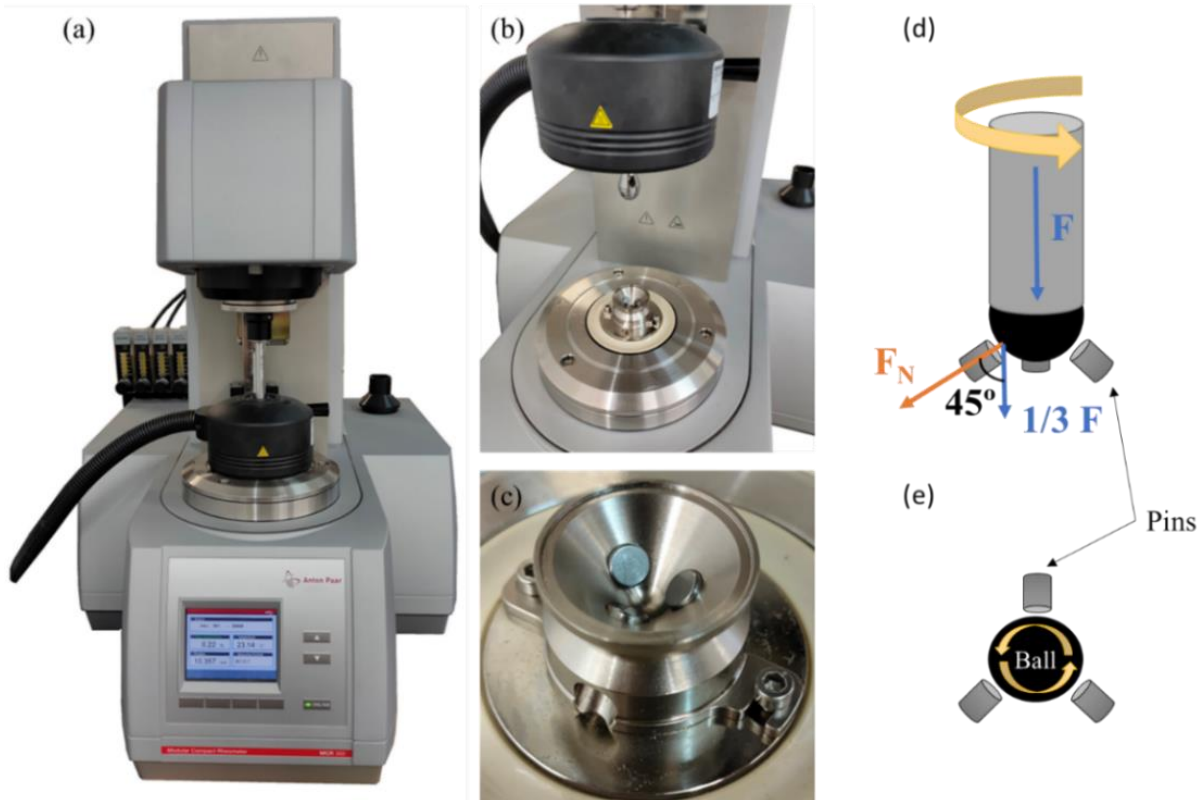
Figure 2.14 (a-b) Anton Paar modular rheometer MCR 302 equipped with a Peltier heated T-PTD200 tribological module; (c-e) rotating ball-on-three-pins configuration for pure sliding tests

2.4.2 EHD2 tribometer

A ball-on-disc tribometer model EHD2 from PCS Instruments was used to determine the friction behavior of a contact pair consisting of a ball and a rotating disc (Figure 2.15). Disc and ball are run with two electric motors to perform the tests in rolling-sliding motion. The selected normal load is automatically applied to the disc with a load cell. The friction force is determined on the ball by means of a torque cell installed on the ball shaft, firstly when the disc is rotating quicker than the ball, and then, for the identical entrainment speed (U_s) when the ball turning faster than the disc. Subsequently, coefficient of friction is determined from normal and friction forces.

It should be noted that these friction tests were performed for the base oils and the nanolubricants under fully flooded lubrication (around 130 mL of lubricant) at the operating temperature of 120 °C, under a constant 50 N load that generates a maximum Hertz pressure of 0.7 GPa, and a 5 % slide-to-roll ratio (SRR), which can be calculated by eq.2.2:

$$SRR \ (\%) = 2 \cdot \frac{(U_{disc} - U_{ball})}{(U_{disc} + U_{ball})} \cdot 100 \qquad (2.2)$$

U_{disc} and U_{ball} are the speeds of the contact points of the disc and the ball, respectively, whereas the entrainment speed is calculated by eq. 2.3:

$$U_s = \frac{(U_{disc} + U_{ball})}{2} \qquad (2.3)$$

For all the discs (Figure 2.16) friction coefficients of nanolubricants and base oil were analyzed by means of Stribeck curves for a 5 % SRR value. For this task, test with three discs

with different roughness were performed. For each test, the same ramp of entrainment speeds was used: 0.05 m/s to 2 m/s. Specifically, the lowest speed of ball is 0.047 m/s and the highest is 1.997 m/s for all the tests whereas, the lowest speed of the disc is 0.052 m/s and the highest is 2.101 m/s. During tests, the EHD2 tribometer automatically regulates disc and ball speeds. The friction coefficient is obtained as the average of those achieved from two different friction tests, one ramp raising speed and the other one reducing speed. Ball and disc properties, as well as experimental conditions, are detailed in Table 2.7 and the surface roughness of the ball and the three discs were measured with a Profiler Hommelwerke (Figure 2.18).

5 % SRR value have been chosen because it was used in previous works by our group [18,30-32] and the University of Porto's group. To make comparisons, this value was kept. 5% SRR is the value used when you want to reproduce similar conditions to the bearings. For conditions at 5 % SRR, the tribosystems are rather in "linear" or "isothermal" region. At higher SRRs, when the sliding component increases (higher shear rate) the lubricant may have a non-Newtonian behavior.

Table 2.7 Rolling-sliding tests: EHD2 tribometer configuration, characteristics, and experimental conditions

EHD2 apparatus (PCS Instruments)	
Specimens	**Experimental conditions**

Material: 100Cr6 steel
    Young modulus: 210 GPa
    Poisson ratio: 0.29
Disc diameter: 100 mm
Ball diameter: 19.05 mm
Surface roughness:
    smooth disc, Ra = 0.02 μm
    rough disc 1, Ra = 0.10 μm
    rough disc 2, Ra = 0.34 μm
    ball, σ = 0.02 μm
	Temperature: 120 ºC
	Load: 50 N
	SRR: 5 %
	Speed: Ramp from 0.05 to 2 m s^{-1}
	Sample: 130 mL
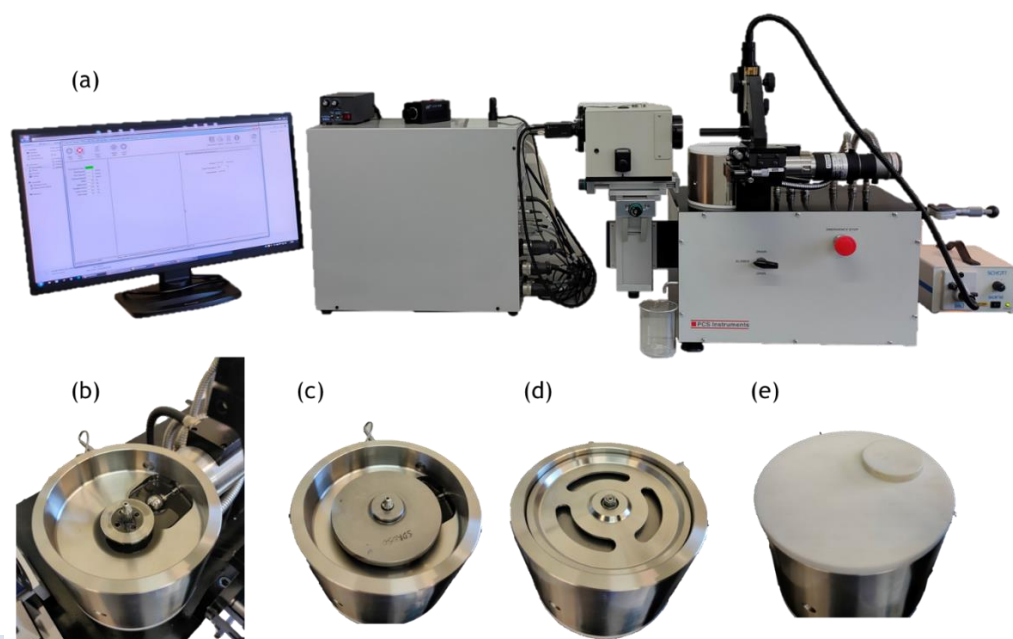
Figure 2.15 (a) EHD2 tribometer set-up; (b) Ball placement; (c, d) Disc placement; (e) Set-up for Stribeck curve measurements

Figure 2.16 Steel discs with different roughness for Stribeck Curve measurements

In this PhD Thesis, the Stribeck curves are obtained plotting the coefficient of friction versus specific film thickness, which is defined by the following expression:

$$\Lambda = \frac{h_t}{R_a} \qquad (2.4)$$

where h_t is the theoretical central film thickness and R_a is the composite average roughness of the surfaces given by $R_a = \sqrt{(R_{a,disc})^2 + (R_{a,ball})^2}$. The theoretical central film thickness (h_t) at the temperature of 120 °C was calculated by means of the Hamrock and Downson equation [33], considering the geometry and material properties of ball and discs (roughness, Young's modulus and Poisson's ratio reported in Table 2.6), the lubricant properties (viscosity and pressure-viscosity coefficient) and the operating conditions (entrainment speed, load and SRR). As regards the lubricant properties, the experimental values of pressure-viscosity coefficient of PAO6 of Gonçalves et al. [34] were used.

Generally, a typical full Stribeck curve (Figure 2.17) shows three lubrication regimes: boundary film, mixed film, and full film lubrication. In general, boundary film lubrication appears if $\Lambda < \Lambda_0$, mixed film lubrication if $\Lambda_0 \leq \Lambda \leq \Lambda_1$, and EHD lubrication if $\Lambda > \Lambda_1$ [18,35]. The values of Λ_0 and Λ_1, depend on several parameters, in particular the composite surface roughness, lubricant additives, lubricant temperature (120 °C) and the application (e.g., ball-on-disc geometry, rolling bearings, gears).
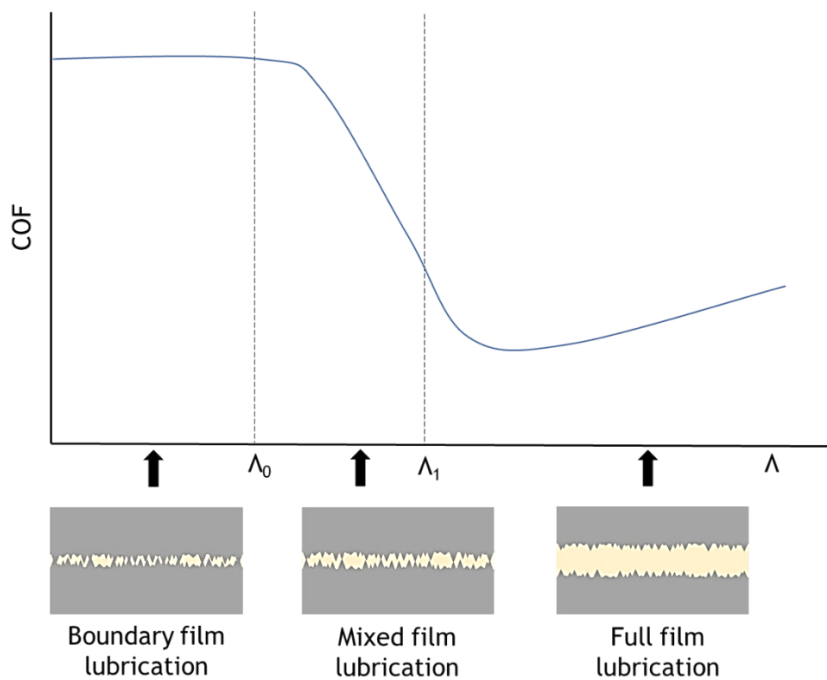
Figure 2.17 Full Stribeck curve scheme

2.4.3 Hommelwerke contact profilometer

The surface roughness for each steel disc used in the EHD2 tribometer was previously measured using a Hommelwerke LV50 profilometer equipped with a TKL300/17 probe (Figure 2.18), which has an amplitude of 300 μm, a diamond cone of 90º and a radius tip of 5 μm. The average roughness (Ra) is obtained by calculating the arithmetic mean value of all measured heights (valleys and peaks) in the analyzed surface area. The Hommelwerke contact profilometer allows to measure in an area around 7x1.5 mm every 1 μm [36].
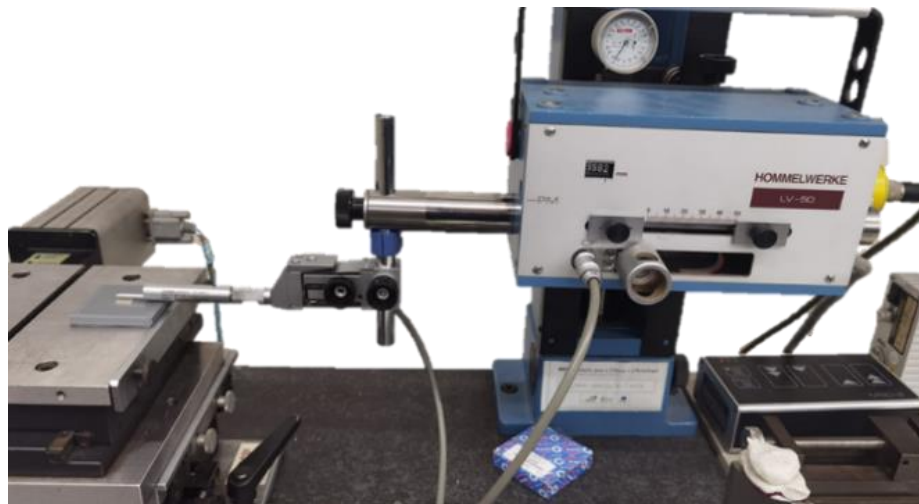
Figure 2.18 Contact profilometer Hommelwerke LV50

2.4.4 3D optical profilometer Sensofar S Neox

The worn pins from the tribological tests from the Anton Paar tribological module were analyzed using a 3D Sensofar S Neox optical profilometer (Figure 2.19a). Table 2.8 summarized its technical specifications and measured parameters.

The profilometer has three optical lenses, 10x, 20x and 50x and can operate in three different modes: confocal, interferometry and focus variation mode; the vertical and lateral resolutions are 0.01 nm and 0.1 μm, respectively. In this PhD Thesis the measurements were performed using the confocal mode, which allows the measurement of surface heights, with the 10x optical lens being optimal for the sample size. The observed worn track produced by the ball on the pins has a concave shape and its generated 3D image is obtained with the SensoScan Software (Figure 2.19b). These images are then transferred to SensoMap Software which is based on Mountains technology from Digital Surf for a precise analysis of the surface topology (Figure 2.19c). Several wear parameters (Figure 2.19d-f) can be determined using the SensoMap Software, such as: wear track width (WTW), wear track depth (WTD), maximum transversal worn area (area) and worn volume (W_{Vol}). In this PhD Thesis the W_{Vol} was not determined due to its higher expanded uncertainty compared to the other parameters. The values of these parameters are automatically calculated by the software after the manual selection of the limits in the profile. In Figure 2.19d, for the determination of WTW and WTD, the limits are indicated by the user through the vertical lines marked with 0 and 1 inside squares. The same selection is used for the maximum transversal area (Figure 2.19e) that is indicated by the solid black lines. In the case of WTD, the user should also indicate the deepest point of the maximum transversal area. For the worn volume (W_{Vol}), the limits (contour) are indicated by the user as shown by the dots surrounding its highest horizontal surface in Figure 2.19f. The average values of the parameters (WTW, WTD and area) and their standard deviations were obtained from the worn

track profiles of the nine pins tested with each lubricant. Finally, the expanded uncertainties were determined from the standard deviations of the average and k = 2. The uncertainty contribution of type B has not been calculated due to the lack of information about the uncertainties of the properties affecting the measurement of the wear parameters [29].

Table 2.8 Profilometer specifications and measured wear parameters

S Neox (Sensofar)	
Specifications	**Measured parameters**
Mode: confocal	Wear Track Width (WTW)
	Wear Track Depth (WTD)
Magnification objective: 10×	Worn area (Area)
	Wear volume (W_{Vol})
Software:	Surface roughness (R_a, R_q):
• SensoScan	• ISO 4287 standard
• SensoMap	• Gaussian filter wavelength cut-off: 0.025 or 0.08 mm
	Skewness (R_{sk}) and Kurtosis (R_{ku})
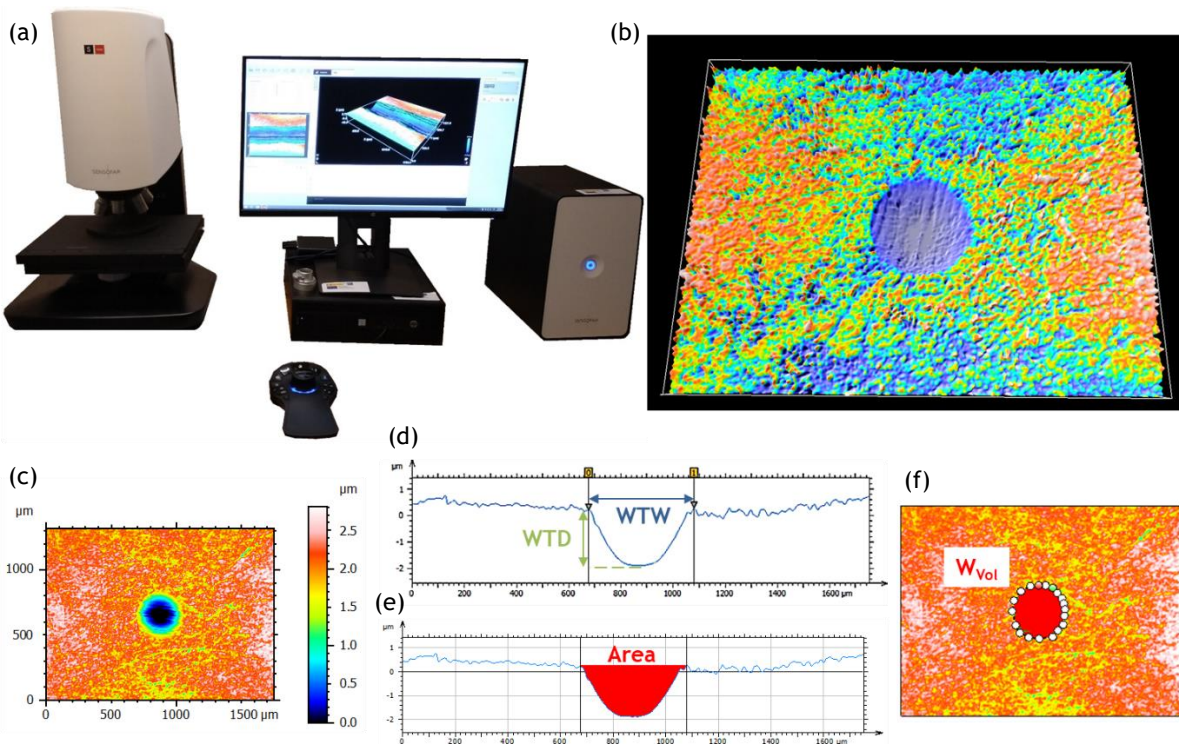
Figure 2.19 Non-contact 3D optical profilometer: (a) Sensofar S Neox, (b) 3D image of the worn surface in SensoScan Software (c) topographic layer of the worn surface in SensoMap Software, (c) WTW and WTD of the worn profile, (d) area of the worn profile, (e) W_{Vol}.

There are several roughness parameters to characterize the surface topography, and the most used is the arithmetic average height (R_a) which is defined as the average absolute deviation of the roughness anomalies from the mean line over the sampled surface [37]. However, R_a is not sensitive to small changes in the profile. Another parameter with better sensitivity than R_a is the root mean square roughness (R_q) and represents the standard deviation of the distribution of surface heights [37]. Other interesting parameters to characterize a surface are the skewness

(R_{sk}) and the kurtosis (R_{ku}). The R_{sk} is used to measure the symmetry of the profile about the mean line [37], and it sensitive to deep valleys or high peaks. A positive R_{sk} means that the profile has more valleys than peaks, meanwhile a negative R_{sk} would have more peaks than valleys. A R_{sk} value of zero would mean that the surface has as many peaks as valleys. The R_{ku} describes the sharpness of the probability density of the profile [37]. If the R_{ku} value is lower than three, then its considered platykurtoic and has few high peaks and low valleys. If the R_{ku} value is higher than 3, then it is leptokurtoic and has many high peaks and low valleys. In this PhD Thesis, using this profilometer, these four roughness parameters were obtained from selected areas on the pins.

2.5 REFERENCES

[1]   L.I. Farfan-Cabrera, Tribology of electric vehicles: A review of critical components, current state and future improvement trends, Tribology International 138 (2019) 473-486, https://doi.org/10.1016/j.triboint.2019.06.029.

[2]   L.R. Rudnick, Polyalphaolefins. in: L.R. Rudnick, (Ed.), 1, Synthetics, mineral oils, and bio-based lubricants: chemistry and technology, CRC press, 2020.

[3]   Y. Kwak, C. Cleveland, A. Adhvaryu, X. Fang, S. Hurley, T. Adachi, Understanding base oils and lubricants for electric drivetrain applications, SAE Technical Paper (2019), https://doi.org/10.4271/2019-01-2337.

[4]   R.A. Wright, K. Wang, J. Qu, B. Zhao, Oil-soluble polymer brush grafted nanoparticles as effective lubricant additives for friction and wear reduction, Angewandte Chemie 128 (2016) 8798-8802, https://doi.org/10.1002/ange.201603663.

[5]   X. Ran, X. Yu, Q. Zou, Effect of particle concentration on tribological properties of ZnO nanofluids, Tribology Transactions 60 (2017) 154-158, https://doi.org/10.1080/10402004.2016.1154233.

[6]   B.T. Seymour, R.A. Wright, A.C. Parrott, H. Gao, A. Martini, J. Qu, S. Dai, B. Zhao, Poly (alkyl methacrylate) brush-grafted silica nanoparticles as oil lubricant additives: effects of alkyl pendant groups on oil dispersibility, stability, and lubrication property, ACS Applied Materials Interfaces 9 (2017) 25038-25048, https://doi.org/10.1021/acsami.7b06714.

[7]   Y. Chen, P. Renner, H. Liang, Dispersion of nanoparticles in lubricating oil: A critical review, Lubricants 7 (2019) 7, https://doi.org/10.3390/lubricants7010007.

[8]   A. Dutta, Fourier transform infrared spectroscopy, Spectroscopic methods for nanomaterials characterization (2017) 73-93, https://doi.org/10.1016/B978-0-323-46140-5.00004-2.

[9]   A. Mayeen, L.K. Shaji, A.K. Nair, N. Kalarikkal, Chapter 12 - Morphological Characterization of Nanomaterials. in: S. Mohan Bhagyaraj, O.S. Oluwafemi, N. Kalarikkal, S. Thomas, (Eds.), Characterization of Nanomaterials, Woodhead Publishing, 2018, pp. 335-364.

[10]   A. Mohammed, A. Abdullah, Scanning electron microscopy (SEM): A review, Proceedings of the 2018 International Conference on Hydraulics and Pneumatics—HERVEX, Băile Govora, Romania, 2018, pp. 7-9.

[11]   Z.L. Wang, New developments in transmission electron microscopy for nanotechnology, Advanced Materials 15 (2003) 1497-1514, https://doi.org/10.1002/adma.200300384.

[12]   W. Sigle, Analytical transmission electron microscopy, Annual Review of Materials Research 35 (2005) 239-314, https://doi.org/10.1146/annurev.matsci.35.102303.091623.

[13]   P. Rostron, S. Gaber, D. Gaber, Raman spectroscopy, review, Laser 21 (2016) 24.

[14]   A. Nwaneshiudu, C. Kuschal, F.H. Sakamoto, R.R. Anderson, K. Schwarzenberger, R.C. Young, Introduction to confocal microscopy, Journal of Investigative Dermatology 132 (2012) 1-5, https://doi.org/10.1038/jid.2012.429.

[15]   G. Giridhar, R.R.K.N. Manepalli, G. Apparao, Chapter 7 - Confocal Raman Spectroscopy. in: S. Thomas, R. Thomas, A.K. Zachariah, R.K. Mishra, (Eds.), Spectroscopic Methods for Nanomaterials Characterization, Elsevier, 2017, pp. 141-161.

[16]   J. Epp, X-ray diffraction (XRD) techniques for materials characterization. in: G. Hübschen, I. Altpeter, R. Tschuncky, H.-G. Herrmann, (Eds.), Materials Characterization Using Nondestructive Evaluation (NDE) Methods, Woodhead Publishing, 2016, pp. 81-124.

[17]   S.C. Wilschefski, M.R. Baxter, Inductively coupled plasma mass spectrometry: introduction to analytical aspects, The Clinical Biochemist Reviews 40 (2019) 115, https://doi.org/10.33176/AACB-19-00024.

[18]   J.M. Liñeira del Rio, E.R. López, M. Gonzalez Gomez, S. Yañez Vilar, Y. Piñeiro, J. Rivas, D.E. Gonçalves, J.H. Seabra, J. Fernández, Tribological behavior of nanolubricants based on coated magnetic nanoparticles and trimethylolpropane trioleate base oil, Nanomaterials 10 (2020) 683, https://doi.org/10.3390/nano10040683.

[19]   K. Granados, J. Gracia-Fadrique, A. Amigo, R. Bravo, Refractive index, surface tension, and density of aqueous mixtures of carboxylic acids at 298.15 K, Journal of Chemical Engineering Data 51 (2006) 1356-1360, https://doi.org/10.1021/je060084c.

[20]   F.M. Gaciño, T. Regueira, L. Lugo, M.J. Comuñas, J. Fernández, Influence of molecular structure on densities and viscosities of several ionic liquids, Journal of Chemical Engineering Data 56 (2011) 4984-4999, https://doi.org/10.1021/je200883w.

[21]   ASTM D2270 2016 Standard practice for calculating viscosity index from kinematic viscosity at 40 and 100 °C.

[22]   P. Heyer, J. Läuger, Correlation between friction and flow of lubricating greases in a new tribometer device, Lubrication Science 21 (2009) 253-268, https://doi.org/10.1002/ls.88.

[23]   R. Gilardi, Tribology of graphite-filled polystyrene, Lubricants 4 (2016) 20, https://doi.org/10.3390/lubricants4020020.

[24]   D. Coronado, J. Wenske, Monitoring the oil of wind-turbine gearboxes: Main degradation indicators and detection methods, Machines 6 (2018) 25, https://doi.org/10.3390/machines6020025.

[25]   R.J. Andrade Vieira, M.Á. Sanz Bobi, Evaluación de Indicadores de la Condición de Aerogeneradores, Anales de mecánica y electricidad 90 (2013) 17-26, http://hdl.handle.net/11531/5003.

[26]   E. Rodríguez, N. Rivera, A. Fernández-González, T. Pérez, R. González, A.H. Battez, Electrical compatibility of transmission fluids in electric vehicles, Tribology International 171 (2022) 107544, https://doi.org/10.1016/j.triboint.2022.107544.

[27]   K.-H. Lee, H.-R. Cha, Y.-B. Kim, Development of an interior permanent magnet motor through rotor cooling for electric vehicles, Applied Thermal Engineering 95 (2016) 348-356, https://doi.org/10.1016/j.applthermaleng.2015.11.022.

[28]   P. Ponomarev, M. Polikarpova, J. Pyrhönen, Thermal modeling of directly-oil-cooled permanent magnet synchronous machine, 2012 XXth International Conference on Electrical Machines, IEEE, 2012, pp. 1882-1887.

[29]   Evaluation of measurement data—Guide to the expression of uncertainty in measurement. GUM 1995 with minor corrections, JCGM 100 (2008) 1-116.

[30]   X. Paredes, J.M. Liñeira del Río, D.E. Gonçalves, M.J. Guimarey, M.a.J. Comuñas, J.H. Seabra, J. Fernández, Thermophysical and Tribological Properties of Highly Viscous Biolubricants, Industrial & Engineering Chemistry Research 61 (2022) 8346-8356, https://doi.org/10.1021/acs.iecr.2c00915.

[31]   M.J. Guimarey, D.E. Goncalves, J.M. Liñeira del Río, M.J. Comunas, J. Fernandez, J.H. Seabra, Lubricant properties of trimethylolpropane trioleate biodegradable oil: High pressure

density and viscosity, film thickness, Stribeck curves and influence of nanoadditives, Journal of Molecular Liquids 335 (2021) 116410, https://doi.org/10.1016/j.molliq.2021.116410.

[32]	J.M. Lineira del Rio, E.R. López, D.E. Gonçalves, J.H. Seabra, J.J.L.S. Fernández, Tribological properties of hexagonal boron nitride nanoparticles or graphene nanoplatelets blended with an ionic liquid as additives of an ester base oil, 33 (2021) 269-278.

[33]	B.J. Hamrock, D. Dowson, Minimum film thickness in elliptical contacts for different regimes of fluid-film lubrication, (1978), Organization Source: NASA Lewis Research Center: Cleveland, OH, USA, 1978, NASA-TP-1342.

[34]	D.E. Gonçalves, J.M. Liñeira del Rio, M.J.P. Comuñas, J. Fernández, J.H. Seabra, High Pressure Characterization of the Viscous and Volumetric Behavior of Three Transmission Oils, Industrial Engineering Chemistry Research 58 (2019) 1732-1742, https://doi.org/10.1021/acs.iecr.8b05090.

[35]	H. Spikes, Mixed lubrication—an overview, Lubrication Science 9 (1997) 221-253, https://doi.org/10.1002/ls.3010090302.

[36]	J.A. Brandão, J.H.O. Seabra, M.J.D. Castro, Surface fitting of an involute spur gear tooth flank roughness measurement to its nominal shape, Measurement 91 (2016) 479-487, https://doi.org/10.1016/j.measurement.2016.05.076.

[37]	E. Gadelmawla, M.M. Koura, T.M. Maksoud, I.M. Elewa, H. Soliman, Roughness parameters, Journal of Materials Processing Technology 123 (2002) 133-145, https://doi.org/10.1016/S0924-0136(02)00060-2.

SECTION I. NANOLUBRICANTS FOR GEARBOXES

3 ZINC OXIDE NANOPARTICLES COATED WITH OLEIC ACID AS ADDITIVES FOR A POLYALPHAOLEFIN LUBRICANT

The results presented in this section are related to the following publication (the editorial authorization for the use of this publication is in the Appendix A):

[a] Laboratory of Thermophysical and Tribological Properties, Nafomat Group, Department of Applied Physics, Faculty of Physics and Institute of Materials (iMATUS), Universidade de Santiago de Compostela, 15782 Santiago de Compostela, Spain

[b] NANOMAG Laboratory, Department of Applied Physics, Faculty of Physics and Institute of Materials (iMATUS), Universidade de Santiago de Compostela, 15782 Santiago de Compostela, Spain

[c] Departamento de Farmacología, Farmacia y Tecnología Farmacéutica, I+D Farma Group (GI-1645), Facultad de Farmacia, Instituto de Materiales (iMATUS) and Health Research Institute of Santiago de Compostela (IDIS), Universidade de Santiago de Compostela, 15782 Santiago de Compostela, Spain

The main contributions of the PhD student to this study are explicitly indicated below:

Experimental: Investigation, Formal analysis.

Manuscript: Writing – original draft.

Among the most critical challenges in science, technology and economy is planning long-term resource consumption and societal trend and trying to balance them in the best possible way [1]. Nanoadditives have proven to be an effective way to improve antifriction and antiwear capabilities of lubricants, which is of great significance for diminishing energy consumption and emission reduction [2]. Among the possible nanoadditives, in this work ZnO NPs were selected, because they are currently used in commercial applications due to their photolytic properties [3], as a photocatalyst [4] and as an additive in wastewater treatment and cosmetics [5]. Comparative studies have shown that metal oxide NPs, among them ZnO NPs (ZnO NPs), when used as additives, improve the lubricating properties of the base oils [6]. Xue et al. [7] analyzed the effect of bare ZnO NPs (50 nm) in a mineral oil (Yubase-6) and compared the effect of these NPs with zinc dialkyl dithiophosphate (ZDDP), and obtained similar antioxidant, antifriction and antiwear behaviors, with reductions up to 45 % (1.0 wt% ZnO) for COF and 40 % (0.5 wt% ZnO) for WSD. Nevertheless, there was no information about the stability of these nanodispersions.

Regarding the use of dispersants to enhance the stability (section 1.2.1) of ZnO NPs, Hernández Battez et al. [8] analyzed the tribological behavior of uncoated ZnO NPs (20 nm) as additives of a polyalphaolefin (PAO6) with two non-ionic commercial dispersants (OL100 and a poly-12-hydroxy stearic acid) using four-ball test, showing good results in extreme pressure conditions. Nevertheless, the stability of NP dispersions containing the dispersants was still poor, especially for OL100. Gara and Zou [9] used oleic acid (OA) to disperse ZnO NPs (diameter 40–100 nm) into a paraffinic mineral oil, claiming improvements in the stability of the dispersions in comparison with those without OA. In addition, these authors show that oleic acid as a dispersant reduces COF to some extent. Regarding the chemical modification of ZnO to enhance the stability of their nanodispersions, Ran et al. [10] dispersed OA surface-modified ZnO NPs (core diameter 10–30 nm) in a mineral oil (60SN base oil) obtaining a stability of 12 h for concentrations up to 0.5 wt% and reductions around 29 % and 15 % for COF and WTW, respectively, in comparison to the base oil. Wu et al. [11] modified ZnO NPs with OA and tested them as lubricant additives in a PAO, likely a mixture of PAO2, PAO3 and PAO4, and in diisooctyl sebacate, claiming that the coating of the ZnO NPs with OA significantly improved their dispersibility in both oils. In addition, tribological performance of OA-modified ZnO (4.04 nm) as additives in PAO (optimal concentration in NPs 1.2 wt%) was better than in sebacate, with reductions of up to 9.9 % for the COF and up to 31.2 % for the WTW compared to those of neat PAO.

The aim of this chapter is to obtain homogeneous and efficient nanolubricants of ZnO NPs coated with oleic acid, ZnO-OA, in PAO40, which is an appropriate base oil for wind turbine gearboxes that has been previously studied for this purpose by Gutierrez et al. [12]. For this purpose, it is necessary to know a) the optimum concentration of the ZnO-OA NPs synthesized by us for friction and wear reduction b) the stability of the nanodispersion at the optimum concentration c) the variations of viscosity, density and viscosity index of the nanodispersions with respect to PAO 40 d) the empirical equations that predict well the density and viscosity of the nanodispersions e) the mechanisms of the nanoadditives for friction and wear reduction. Thus, tribological tests were performed at 80 °C using the Anton Paar MCR 302 rheometer equipped with the ball-on-three-pin tribological module. This temperature was chosen because in wind turbine gearboxes the oil can reach temperature peaks around 80 °C [13,14]. The tribological mechanisms of the dispersions were analyzed by 3D profilometry and confocal Raman microscopy on the worn tracks of the tested pins.

3.1 Nanoparticle synthesis and characterization
3.1.1 Synthesis and functionalization of nanoparticles

The reagents used in the synthesis of ZnO NPs were: zinc acetate dihydrate (≥ 98 %), potassium hydroxide (≥ 85 %) and oleic acid (90 %) from Sigma-Aldrich (Saint Louis, MO, USA); acetone (reagent grade) and ammonium hydroxide (25 %) from Fisher (Madrid, Spain); hydrochloric acid (37 %) used to neutralize the ZnO dispersion (Acros Organics, Geel, Belgium) and absolute ethanol used as the reaction solvent (Scharlau, Barcelona, Spain). All these products were used without further purification.

ZnO NPs were prepared using Shamhari et al. [15] method through the following reaction:

$$Zn(CH_3COO)_2 \cdot 2\,H_2O + 2KOH \xrightarrow{60\,°C,\ EtOH} ZnO + 2CH_3COOK + 2H_2O \qquad \text{(3.1)}$$
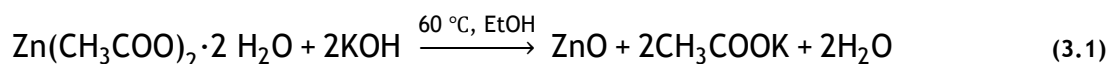
Briefly, $Zn(CH_3COO)_2 \cdot 2H_2O$ (1.49 g) was dissolved in absolute ethanol (64 mL) in a Schott bottle provided with a magnetic stirrer, the blend being heated to 60 °C. KOH (0.79 g) was dissolved separately in absolute ethanol (30 mL) under the same conditions, the solution being slowly added dropwise to the $Zn(CH_3COO)_2 \cdot 2H_2O$ solution at 60 °C. After 3 hours of

vigorous stirring (500 rpm), ZnO precipitated and it was collected by centrifugation (4000 rpm) for 10 minutes, washed twice with acetone and once with ultrapure water. Finally, ZnO was dispersed in ultrapure water for storage, the dispersion concentration being determined by TGA using the Perkin Elmer Pirys 7 TGA. The measurements were made from 50 to 850 ℃ at a heating rate of 10 ℃/min under a nitrogen flow of 20 mL/min.

The ZnO NPs were coated with OA summarized in the reaction:

$$\text{ZnO} \xrightarrow[\substack{\text{2) 95 ℃, reflux, 2 h}}]{\substack{\text{NH}_4\text{OH, OA} \\ \text{1) 60 ℃, 30 min}}} \text{ZnO-OA} \tag{3.2}$$

The as prepared ZnO water dispersion was sonicated for 15 minutes in an ultrasonic bath. Then, 100 mg (12.9 mL) of this dispersion were introduced in a round-bottom flask, provided with a magnetic stir bar, and heated to 60 ℃. Once the setting temperature was reached, NH$_4$OH (2.4 mL) was added, and 1 minute later OA (300 mg, 0.27 mL) was also added. The mixture was kept at 60 ℃ for 30 minutes and then the temperature was raised to 95 ℃ with reflux for 2 hours. The excess of NH$_4$OH was neutralized with HCl (9 vol%) and the precipitate (ZnO-OA) was collected by centrifugation under the same conditions as ZnO NPs and washed with ultrapure water and hexane. The ZnO-OA NPs were dispersed in chloroform for storage and to avoid agglomeration. The concentration of this dispersion was determined also by TGA (2.12 wt%).

3.1.2 Characterization of nanoparticles

One of the techniques used to confirm the effectiveness of the chemical modification of the NPs is the thermogravimetric analysis of the modified NPs dispersed in a solvent. Thus, the thermogram (Figure 3.1) gives information about the degradation temperature of the OA coating on the ZnO NPs, and the mass of each constituent (OA coatings and ZnO NPs). From these experimental data, it is possible to obtain the coupling density of OA molecules per surface unit of a ZnO nanoparticle. The first mass loss (until 90 ℃) is due to the evaporation of the organic solvent (chloroform) used to disperse the NPs after reaction 3.2. The thermal degradation of the OA takes place from around 250 ℃ to 550 ℃, the remaining mass is uncoated ZnO NPs. The TGA determined that the content of OA on the NPs was 65 wt% for the ZnO-OA NPs determined and the number of OA molecules per NP surface area unit in nm^2 was 91. The experimental diffraction pattern of the ZnO-OA NPs, obtained with XRD, together with the theoretical pattern of a hexagonal phase of zincite [16] (JCPDS card No. 36-1451) is shown in Figure 3.2. The main diffraction peaks, (1 0 0), (0 0 2), (1 0 1), (1 0 2), (1 1 0), (1 0 3), (2 0 0), (1 1 2), (2 0 1), (0 0 4) and (2 0 2), perfectly matched each other.
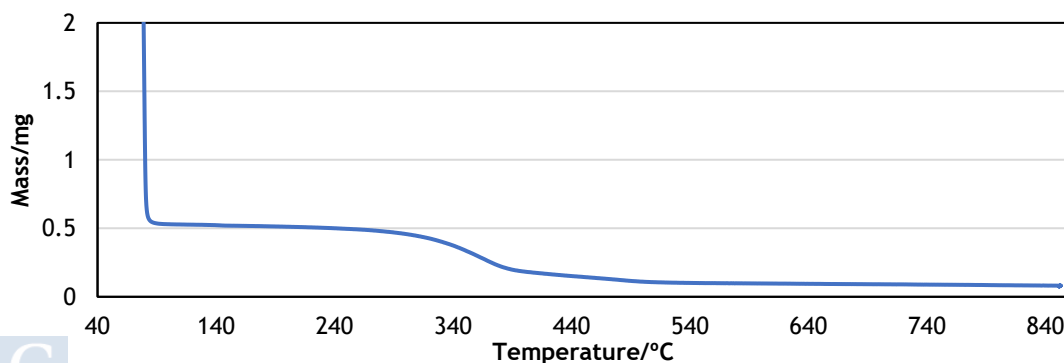
Figure 3.1 Thermogram of ZnO-OA NPs dispersed in chloroform
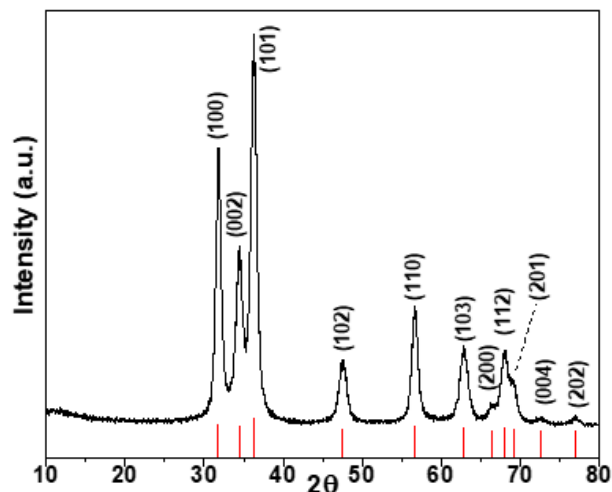
Figure 3.2 Experimental XRD pattern of ZnO-OA NPs (black line) with the main peaks labelled with their corresponding Miller indices, and theoretical reflections (red bars) for zincite phase (JCPDS card No. 36-1451)

TEM micrograph (Figure 3.3a) of the oleic acid coated ZnO NPs, dispersed after synthesis in chloroform, revealed spherical NPs with relatively inhomogeneous size distribution (medium size distribution of around 10 nm, Figure 3.3b). Size distribution was performed using the ImageJ software for a sample of 200 NPs.
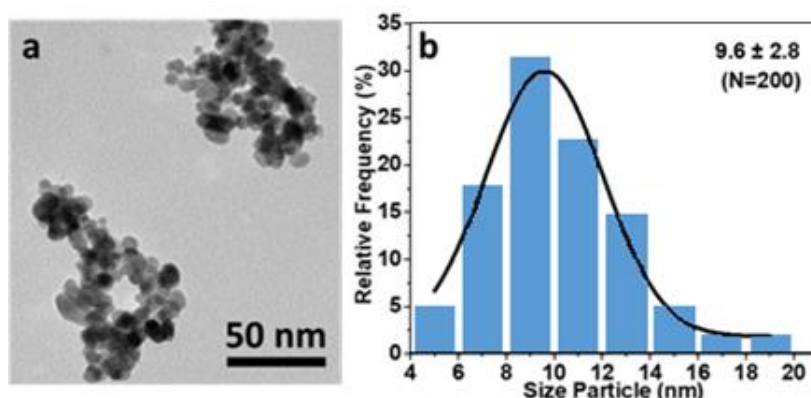
Figure 3.3 TEM micrograph (a) and the size distribution (b) of the ZnO-OA NPs

As aforementioned, the ZnO NPs were coated with OA to facilitate their dispersibility in the base oil. The effective surface functionalization of these NPs was also analyzed by FTIR and Raman spectroscopies. The FTIR spectrum (Figure 3.4) presents an absorption band at 3410 cm^{-1}, corresponding to the stretching vibrations of the O-H group attributed to the presence of hydroxyl residue, probably due to atmospheric moisture. In addition, the peaks appearing at 2923, 2853, and 722 cm^{-1} correspond to the C–H stretching vibration bands of –CH$_3$ and –CH$_2$, and the -CH$_2$ bending vibration, respectively. The peaks that appear at 1543 and 1435 cm^{-1} were assigned to the asymmetric and symmetric stretching vibrations of –COO–, respectively. The peaks at 1543 and 1435 cm^{-1} were assigned to the asymmetric and symmetric stretch vibrations of –COO–, respectively. Finally, the vibration band observed at 468 cm^{-1} corresponds to the stretching vibration of the zincite structure (Zn-O) [17]. These findings confirmed that ZnO NPs were successfully coated with oleic acid. It is worth mentioning that the FTIR spectrum of Figure 3.4 is very similar to that reported by Wu et al. [11] for other ZnO-OA NPs.
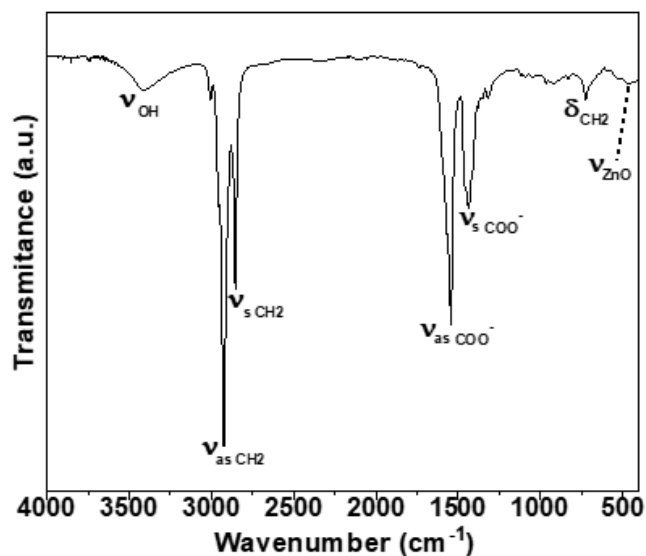
Figure 3.4 FTIR spectrum of ZnO-OA with the characteristic bands as evidence

The ZnO-OA NPs Raman spectrum is shown in Figure 3.5. As expected, the signals corresponding to oleic acid were identified: a Raman band around 2800-3000 cm^{-1} corresponding to symmetric and asymmetric stretching of CH_2, other CH_2 peaks at 1447 and 1306 cm^{-1} corresponding to scissoring and twisting, respectively, a CH_3 rocking peak at 879 cm^{-1}, several peaks at 1068, 1090 and 1117 cm^{-1} corresponding to C-C vibration, as well as peaks related with the C=C double bond, at 3008 cm-1 from =C-H vibration peak, 1663 cm^{-1} C=C vibration, and 1268 and 971 cm^{-1} assignable to C=C-H bending peaks. Nevertheless, the peaks corresponding to ZnO were not clearly detected, likely due to the high oleic acid content [18,19].
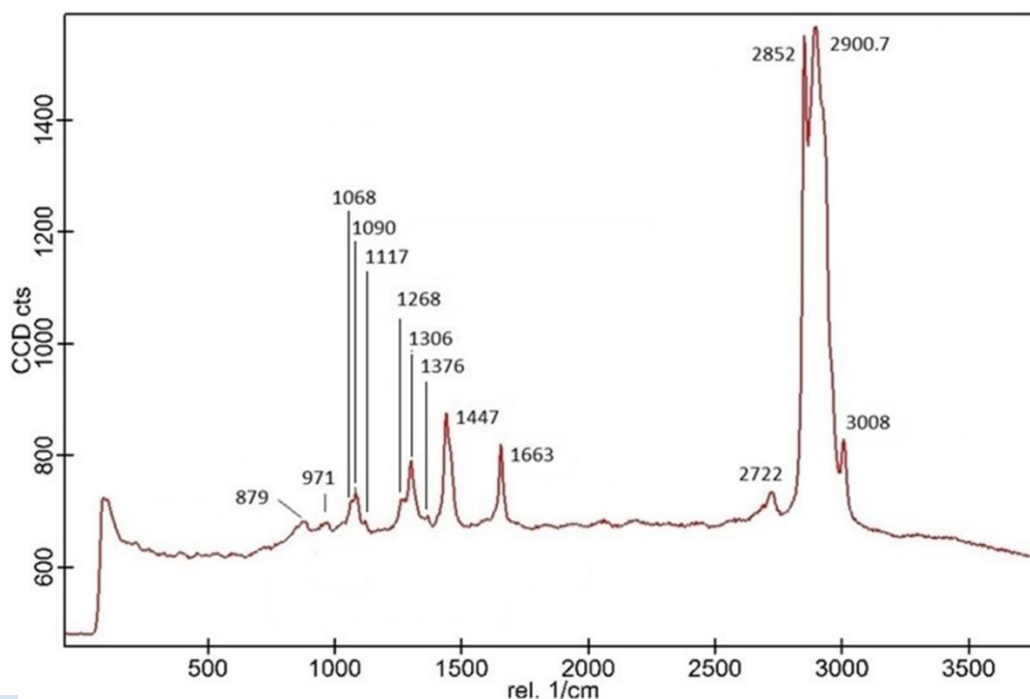
Figure 3.5 Raman spectrum of ZnO-OA nanoparticles

3.2 STABILITY RESULTS

Nanodispersions based on PAO40 with ZnO-OA NPs as additive (0.10, 0.25, 0.50, 0.75 and 1.00 wt%) were prepared as it was described in Section 2.3.1. A PAO40 aliquot was previously characterized by MALDI-TOF mass, FTIR and Raman spectroscopy [11,12].

The PAO40 + 0.25 wt% ZnO-OA dispersion had good stability features (Figure 3.6 and 3.7). The appearance of the dispersion was monitored by recording photographs since immediately after the dispersion sonication (time 0 h). The dispersion started to be less transparent 29 days after sonication. Refractive index of PAO40 and the nanolubricant are shown in Figure 3.6 at 20 ºC. The evolution of the refractive index followed a near-to-zero slope close to that of the neat PAO40. After 45 hours, the relative increase of the refractive index was 0.013 %, which was 10 times lower to that of the PAO40 + 0.05 wt% h-BN dispersion reported in a previous work [20]. From all the above results it can be concluded that the ZnO-OA NPs have around one-month stability in PAO40 at 0.25 wt% concentration. To analyze the effect of the OA coating on the stability results, a 0.25 wt% ZnO dispersion in PAO40 was prepared. Although the preparation method explained in Figure 2.10a was attempted, it did not work because of the poor dispersibility of the uncoated ZnO NPs in CHCl$_3$, forming a bulky agglomerate that did not disappear even after bath or tip ultrasonication, as shown in Figure 3.7b. To solve this problem, it was necessary to dry the NPs and to prepare the dispersion using a two-step method [21], consisting of adding the dried ZnO nanopowder to the PAO40 followed by a homogenization step in an ultrasonic bath for 4 hours. The attempt to prepare a homogeneous dispersion of PAO40 + 0.25 wt% ZnO was also unsuccessful as the uncoated ZnO NPs did not disperse in the base oil. After 4 hours in the ultrasonic bath, these NPs were still aggregated at the bottom of the glass flask, due to their strong oleophobicity, as shown in Figure 3.7c. Thus, when the container was turned over, it was seen how aggregates fall.
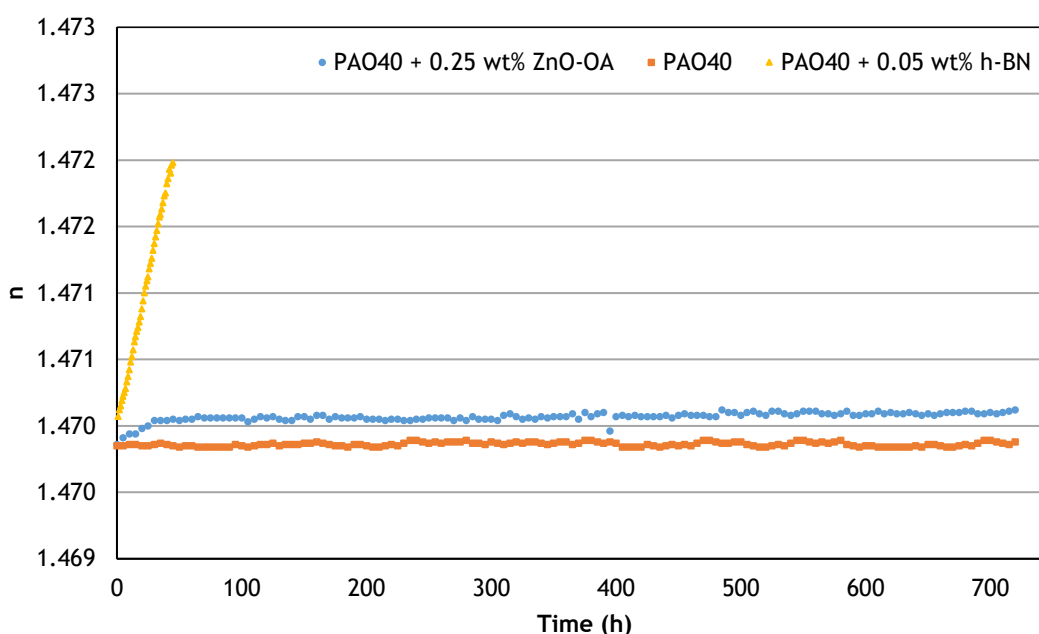
Figure 3.6 Evolution with time of refractive index, n, of PAO40 (orange), PAO40 + 0.25 wt% ZnO-OA (blue) and PAO40 + 0.05 wt% h-BN (yellow, [20]) at 25 ºC

(a) PAO40 + 0.25 wt% ZnO-OA

| 0 h (0 days) | 168 h (7 days) | 336 h (14 days) | 504 h (21 days) | 696 h (29 days) |

(b) CHCl₃ + ZnO

(c) PAO40 + 0.25 wt% ZnO

0 h   0 h (upside down)
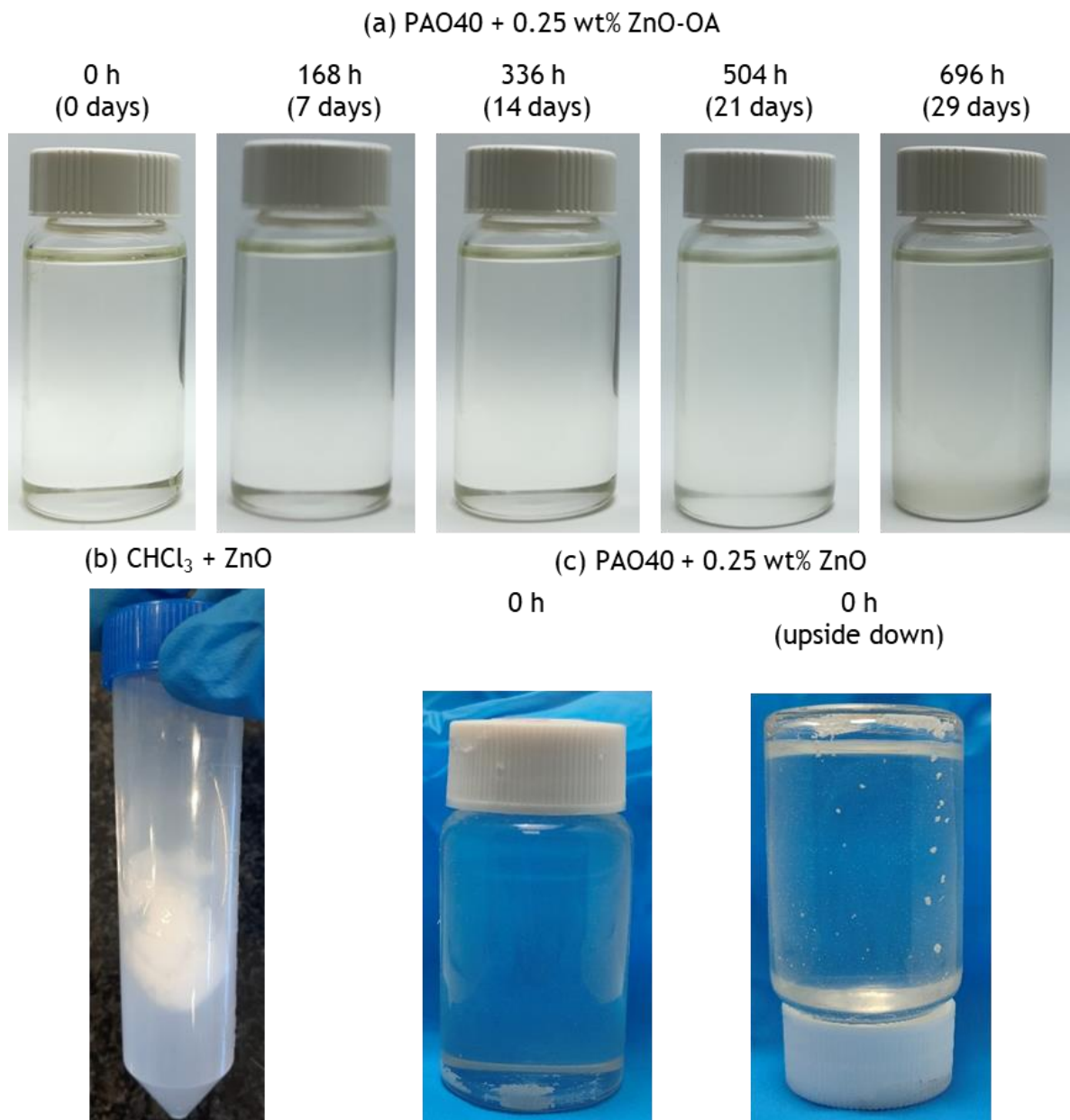
Figure 3.7 Photographs of PAO40 + 0.25 wt% ZnO-OA (a), CHCl₃ + ZnO (b) and PAO40 + 0.25 wt% ZnO (c) showing visual stability up to 696 h

3.3 THERMOPHYSICAL PROPERTIES

Nanodispersions density, ρ, measured with the SVM3000 Stabinger equipment, showed an increment with the mass concentration of NPs, as summarized in Figure 3.8 and Table 3.1. Thus, the ZnO-OA nanodispersions at 0.10, 0.25, 0.50, 0.75 and 1.00 wt% caused relative increases with respect to the PAO40 density of about 0.1 %, 0.2 %, 0.3 %, 0.4 % and 0.5 %, respectively. Some authors [22] attributed the increase in the nanofluid density with the concentration of NPs to their agglomeration, however the density increase may be simply because the density of the ZnO-OA NPs is greater than that of PAO40.
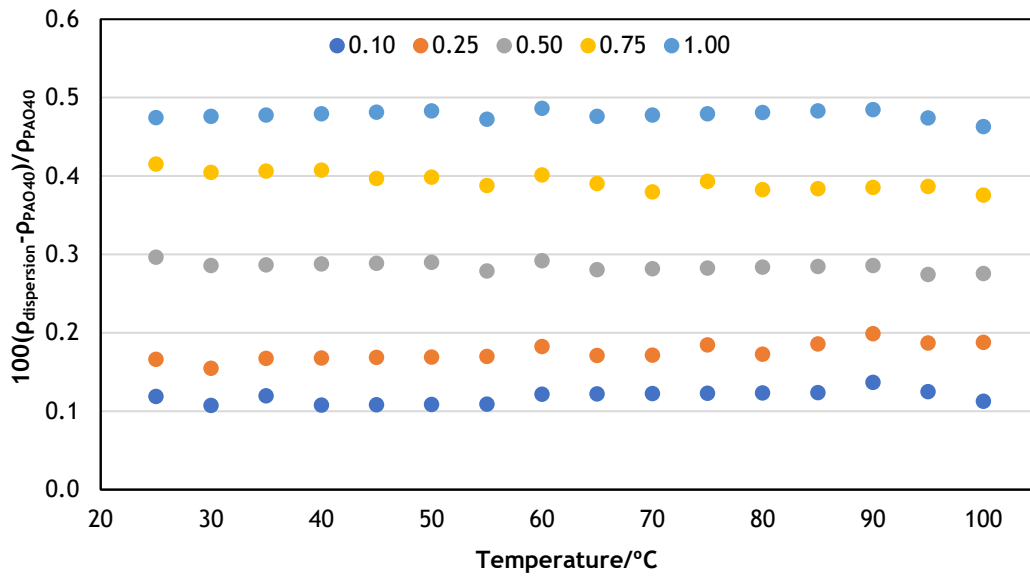
Figure 3.8 Percentage variation of density between ρ values of the dispersions at different concentrations of ZnO-OA (ρ$_{dispersion}$) with respect to neat PAO40 (ρ$_{PAO40}$) from 25 to 100 °C

Table 3.1 Density (ρ, g cm^{-3}) of PAO40 and its ZnO-OA nanodispersions as a function of temperature, T, at 0.1 MPa

PAO40 + wt% ZnO-OA	0 wt%	0.10 wt%	0.25 wt%	0.50 wt%	0.75 wt%	1.00 wt%
T/°C	ρ/g cm^{-3}	ρ/g cm^{-3}	ρ/g cm^{-3}	ρ/g cm^{-3}	ρ/g cm^{-3}	ρ/g cm^{-3}
25	0.8430	0.8440	0.8444	0.8455	0.8465	0.8470
30	0.8401	0.8410	0.8414	0.8425	0.8435	0.8441
35	0.8371	0.8381	0.8385	0.8395	0.8405	0.8411
40	0.8342	0.8351	0.8356	0.8366	0.8376	0.8382
45	0.8313	0.8322	0.8327	0.8337	0.8346	0.8353
50	0.8284	0.8293	0.8298	0.8308	0.8317	0.8324
55	0.8255	0.8264	0.8269	0.8278	0.8287	0.8294
60	0.8225	0.8235	0.8240	0.8249	0.8258	0.8265
65	0.8196	0.8206	0.8210	0.8219	0.8228	0.8235
70	0.8167	0.8177	0.8181	0.8190	0.8198	0.8206
75	0.8137	0.8147	0.8152	0.8160	0.8169	0.8176
80	0.8108	0.8118	0.8122	0.8131	0.8139	0.8147
85	0.8078	0.8088	0.8093	0.8101	0.8109	0.8117
90	0.8048	0.8059	0.8064	0.8071	0.8079	0.8087
95	0.8019	0.8029	0.8034	0.8041	0.8050	0.8057
100	0.7990	0.7999	0.8005	0.8012	0.8020	0.8027

The densities of the nanodispersions have been estimated with the Pak and Cho [23] and Wasp et al. [24] empirical equations (eq. 3.1 and 3.2, respectively). For this aim, it was necessary to determine the volume fraction of each ZnO-OA nanodispersion, which was estimated considering:

- spherical shape of ZnO and ZnO-OA NPs, based on TEM results;
- the average radius of the ZnO core of the ZnO-OA NPs, R$_{ZnO}$, is 4.8 nm based on the TEM histogram and the width of the OA spherical coating is 1.5 nm [25]. Hence, R$_{ZnO-OA}$ is assumed to be 6.3 nm;

- the density of ZnO NPs is equal to the ZnO bulk density and the density of the OA coating is the same as that of the liquid oleic acid.

Thus, the volume fraction of ZnO-OA NPs in each nanodispersion can be computed by:

$$\varphi = \frac{V_{NPs}}{V} = \frac{m_{NPs}}{V} \cdot \frac{R_{ZnO\text{-}OA}^3}{R_{ZnO}^3 \cdot \rho_{ZnO} + \left(R_{ZnO\text{-}OA}^3 - R_{ZnO}^3\right) \cdot \rho_{OA}} \qquad (3.1)$$

being m_{NPs} the mass of ZnO-OA NPs contained in a volume V of the nanodispersion, and ρ_{ZnO} and ρ_{OA} the densities of bulk ZnO and of the OA, respectively. The density of OA in the temperature range was calculated from Sagdeev et al. [26] experimental correlation and that of ZnO from Lin et al. [27]. Using this procedure, the density of ZnO-OA NPs was estimated to be 2.992 g/cm^3 at 25 ºC.

Using the volume fraction of the ZnO-OA NPs in the nanodispersions determined with eq. 3.1, different predictive models have been applied to estimate the densities and viscosities of the nanodispersions from those of the PAO40.

Then, densities of the nanodispersions, ρ_{nd}, can be predicted with the Pak and Cho equation [23]:

$$\rho_{nd} = (1-\varphi) \cdot \rho_{PAO40} + \varphi \cdot \rho_{ZnO\text{-}OA} \qquad (3.2)$$

As it was commented previously, the experimental densities of the nanodispersions have also been compared with those provided by Wasp et al. [24] predictive equation:

$$\rho_{nd} = \frac{1}{\frac{(1-\varphi)}{\rho_{PAO40}} + \frac{\varphi}{\rho_{ZnO-OA}}} \qquad (3.3)$$

being ϕ the mass fraction of the NPs in the solution.

For each composition, the absolute average deviation (AAD%) obtained with the Pak and Cho model between experimental and predicted densities in the whole temperature range is lower than 0.25 % being the maximum deviation 0.28%. Worse results have been obtained with the equation due to Wasp et al. [24] (eq. 3.3), being 0.42 % the maximum AAD%, corresponding to the nanodispersion with 1.00 wt% ZnO-OA mass fraction. In Figure 3.9, the predicted densities have been plotted together with the experimental ones.
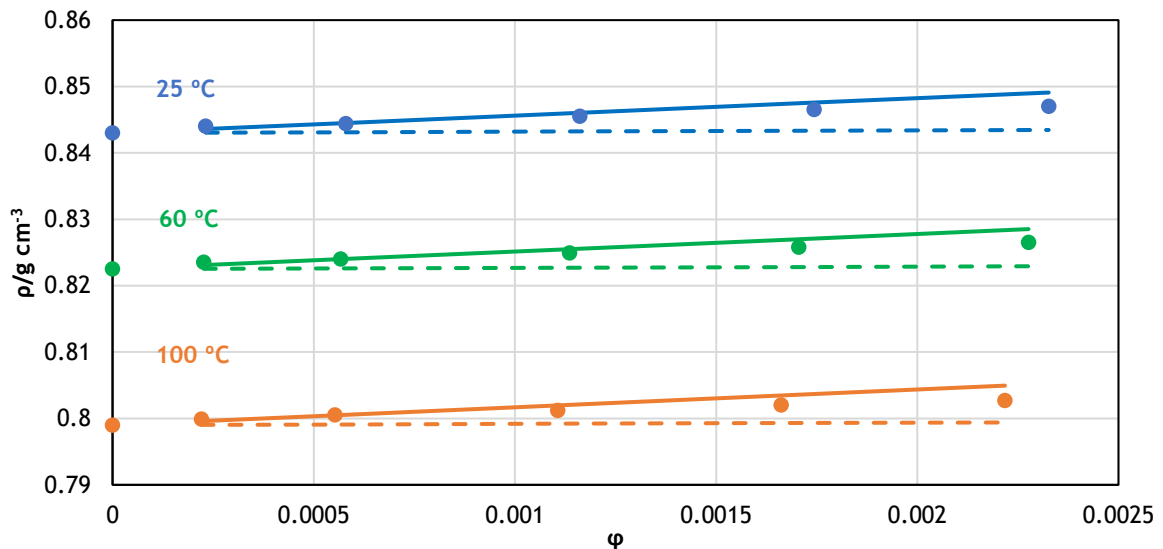
Figure 3.9 Densities of neat PAO40 and its ZnO-OA nanodispersions at 25, 60 and 100 ºC against ZnO-OA volume fraction. Symbols: experimental data. Solid lines: predictions of the Pak and Cho empirical equation [23]. Dashed lines: predictions of the Wasp et al. equation [24].

75

Regarding dynamic viscosity, its relative changes caused by the addition of the ZnO-OA NPs to the PAO40 are shown in Figure 3.10 and Table 3.2 gathers the experimental dynamic viscosity values of PAO40 and the nanolubricants. Viscosities increased up to 4 % with the addition of ZnO-OA NPs due to the enhancement of the internal shear stress of the nanolubricants, i.e., the increase of internal friction [18].
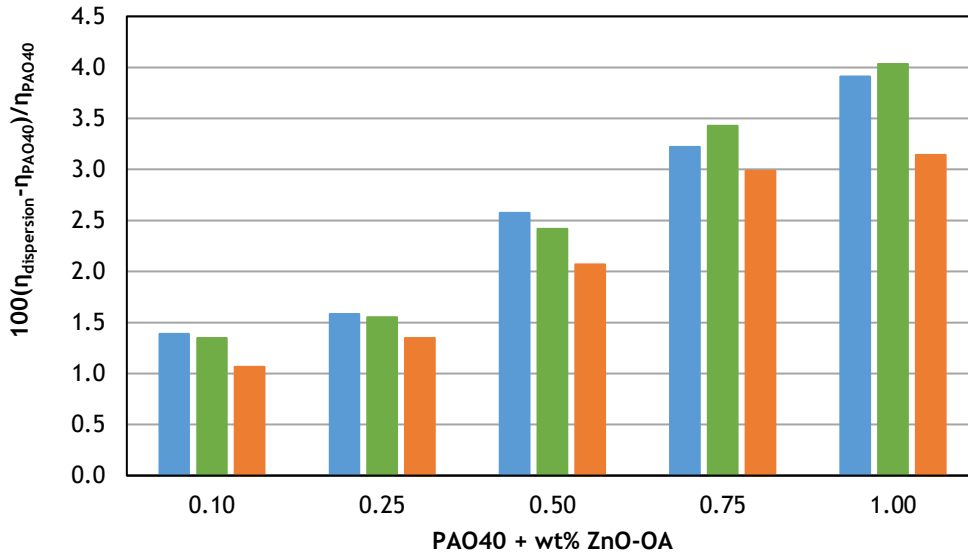
Figure 3.10 Percentage variation of the dynamic viscosity (η) corresponding to the different PAO40 + ZnO-OA dispersions (η_dispersion) with respect to that of neat PAO40 (η_PAO40), at 25, 40 and 100 °C

Table 3.2 Dynamic Viscosity (η, mPa s) of PAO40 and its ZnO-OA nanodispersions as a function of temperature, T, at 0.1 MPa

PAO40 + wt% ZnO-OA	0 wt%	0.10 wt%	0.25 wt%	0.50 wt%	0.75 wt%	1.00 wt%
T/°C	η/mPa s	η/mPa s	η/mPa s	η/mPa s	η/mPa s	η/mPa s
25	801.5	812.6	814.2	822.1	827.3	832.9
30	587.9	594.9	598.3	602.0	607.9	610.9
35	439.4	444.5	446.9	450.0	454.5	456.8
40	333.8	338.3	339.0	341.9	345.3	347.3
45	257.7	261.1	262.1	263.7	266.3	268.1
50	201.8	204.4	205.1	206.4	208.4	209.8
55	160.1	162.1	162.7	163.7	165.3	166.4
60	128.5	130.2	120.7	131.5	132.7	133.6
65	104.5	105.8	106.2	106.8	107.8	108.5
70	85.86	86.91	87.21	87.72	88.56	89.12
75	71.40	72.11	72.35	72.79	73.46	73.91
80	59.83	60.40	60.60	60.97	61.51	61.87
85	50.55	51.05	51.20	51.56	51.96	52.25
90	43.06	43.47	43.61	43.90	44.25	44.47
95	36.94	37.32	37.43	37.68	37.99	38.15
100	31.92	32.26	32.35	32.58	32.87	32.92

As in the case of densities, the nanodispersion viscosities have been predicted by three empirical models: the Einstein equation [28] (eq. 3.4), the Pak and Cho equation [23] (eq. 3.5) and the Chen et al. equation [29] (eq. 3.6):

$$\eta_{nd}=\eta_{PAO40}\cdot(1+2.5\varphi) \tag{3.4}$$

$$\eta_{nd}=\eta_{PAO40}\cdot(1+39.11\varphi+533.9\varphi^2) \tag{3.5}$$

$$\eta_{nd}=\left[1+10.6\varphi+(10.6\varphi)^2\right]\cdot\eta_{PAO40} \tag{3.6}$$

Despite its simplicity, the equation due to Einstein predicts experimental viscosities with AAD% lower than 2.9 %. The worse results are those provided by Pak and Cho model [23] (AAD% lower than 7.3 %). The best results are those provided by Chen et al. equation [29], with AADs lower than 0.87 %. In Figure 3.11 the predicted viscosities are plotted together with the experimental ones.
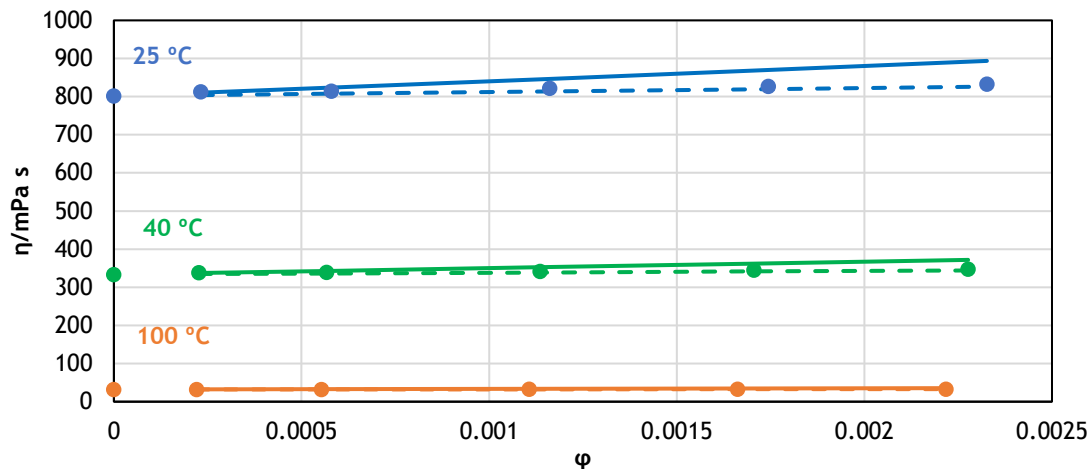
Figure 3.11 Viscosities of neat PAO40 and its ZnO-OA nanodispersions at 25, 40 and 100 ºC against ZnO-OA volume fraction. Symbols: experimental data. Solid lines: predictions of the Pak and Cho empirical equation [23]. Dashed lines: predictions of the Chen et al. equation [29].

According with the Carreau parameters reported for PAO40 [30], up to very high shear rates at 0.1 MPa (from $2\cdot10^6$ s^{-1} at 20 ºC to $3\cdot10^7$ s^{-1} at 100 ºC), its behavior is Newtonian. These shear rates are much higher than those applied when using SVM3000 apparatus, which remain between 10 and 10^3 s^{-1}, being dependent on the fluid viscosity [31]. So, taking these facts into account and the small influence of the addition of NPs on the viscosity (lower than 4 %) in the range of concentrations analyzed, it is expected that the nanodispersions do not display any shear thinning in the shear conditions of the viscosity measurements. Finally, the measured viscosity indices (VI) of the nanodispersions were slightly lower than that of PAO40 (VI 151) and remained approximately constant regardless of the composition (VI 149).

3.4 TRIBOLOGICAL RESULTS
3.4.1 Pure sliding tests

The friction results of the ball-on-three-pins tests for PAO40 and all the ZnO-OA nanodispersions are summarized in Table 3.3 and presented in Figure 3.12. The five studied dispersions decreased the coefficient of friction compared to the neat PAO40, ranging from 14 % to 25 %. The lowest friction value was achieved when 0.25 wt% ZnO-OA was added to PAO40; a further increase on nanoparticle concentration resulted in worse friction reduction. Therefore, based on these results, the optimal ZnO-OA concentration for COF reduction was

0.25 wt%. Minima in the friction-concentration curves for several nanolubricants were previously reported by different authors [10,11,32-35].

Table 3.3 Average friction coefficient values, COF, at 80 °C and the expanded uncertainties, U, for PAO40 base oil and PAO40+ wt% ZnO-OA lubricants at different NP weight percentages, wt%

Lubricant	COF	U	Reduction %
PAO40	0.0938	0.0027	-
+ 0.10 wt% ZnO-OA	0.0721	0.0028	23
+ 0.25 wt% ZnO-OA	0.0701	0.0022	25
+ 0.50 wt% ZnO-OA	0.0757	0.0032	19
+ 0.75 wt% ZnO-OA	0.0765	0.0012	18
+ 1.00 wt% ZnO-OA	0.0802	0.0023	14
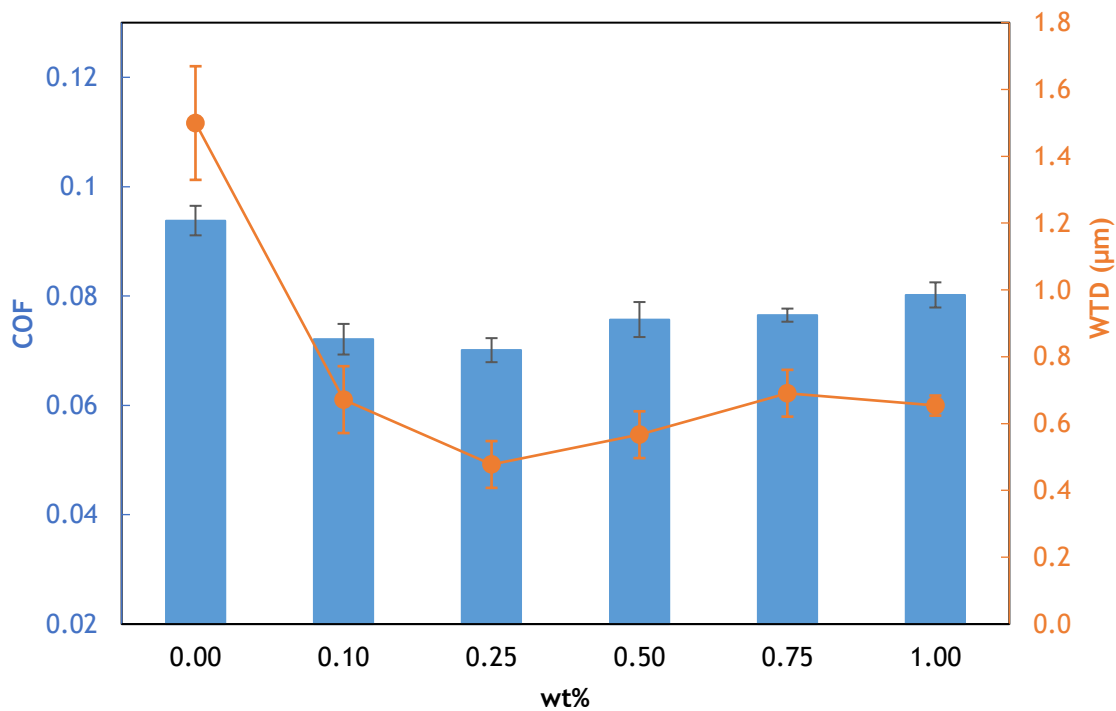
Figure 3.12 Average friction coefficient, COF, (blue) and wear track depth, WTD, (orange) with the expanded uncertainty bars for PAO40 and PAO40 + wt% ZnO-OA nanodispersions for different NP weight percentages, wt% (the orange line is a guide for the eye)

3.4.2 Wear surface characterization

Regarding the WTD at the surface of the pins (Figure 3.13), the best antiwear performance was also obtained for the nanolubricant prepared with 0.25 wt% ZnO-OA NPs. Dispersions with lower concentrations did not have enough NPs to minimize friction and wear. On the other hand, for higher NP concentrations, ZnO-OA NPs or aggregates could act as debris particles, increasing friction and wear [36]. Average values of various wear parameters and the respective expanded uncertainties, such as wear track width (WTW), depth (WTD), and cross-sectional area of the worn pins are summarized in Table 3.4. The greatest reductions for these wear

parameters were also found with the PAO40 + 0.25 wt% ZnO-OA nanodispersion, being 38 %, 68 % and 82 %, in WTW, WTD and cross-sectional area, respectively.

Table 3.4 Average values of the width, WTW, depth, WTD, and cross-sectional area of the wear track and the expanded uncertainties, U, for PAO40 + wt% ZnO-OA lubricants for different NP weight percentages, wt%

Lubricant	WTW/μm	U/μm	WTD/μm	U/μm	Area/μm²	U/μm²
PAO40	370	7	1.50	0.17	411	54
+ 0.10 wt% ZnO-OA	269	15	0.67	0.10	119	36
+ 0.25 wt% ZnO-OA	230	14	0.48	0.07	75	18
+ 0.50 wt% ZnO-OA	241	15	0.57	0.07	78	14
+ 0.75 wt% ZnO-OA	289	29	0.69	0.07	96	22
+ 1.00 wt% ZnO-OA	259	25	0.65	0.03	119	31

2D images and 3D profiles of the worn pins are shown in Figure 3.13. Wear was strongly reduced as evidenced when comparing a pin tested with PAO40 (Figure 3.13a and 3.13b) with a pin tested with PAO40 + 0.25 wt% ZnO-OA (Figure 3.13c and 3.13d). Furthermore, the wear reductions were also evident in the cross-sectional profiles of those same worn pins in Figure 3.14.
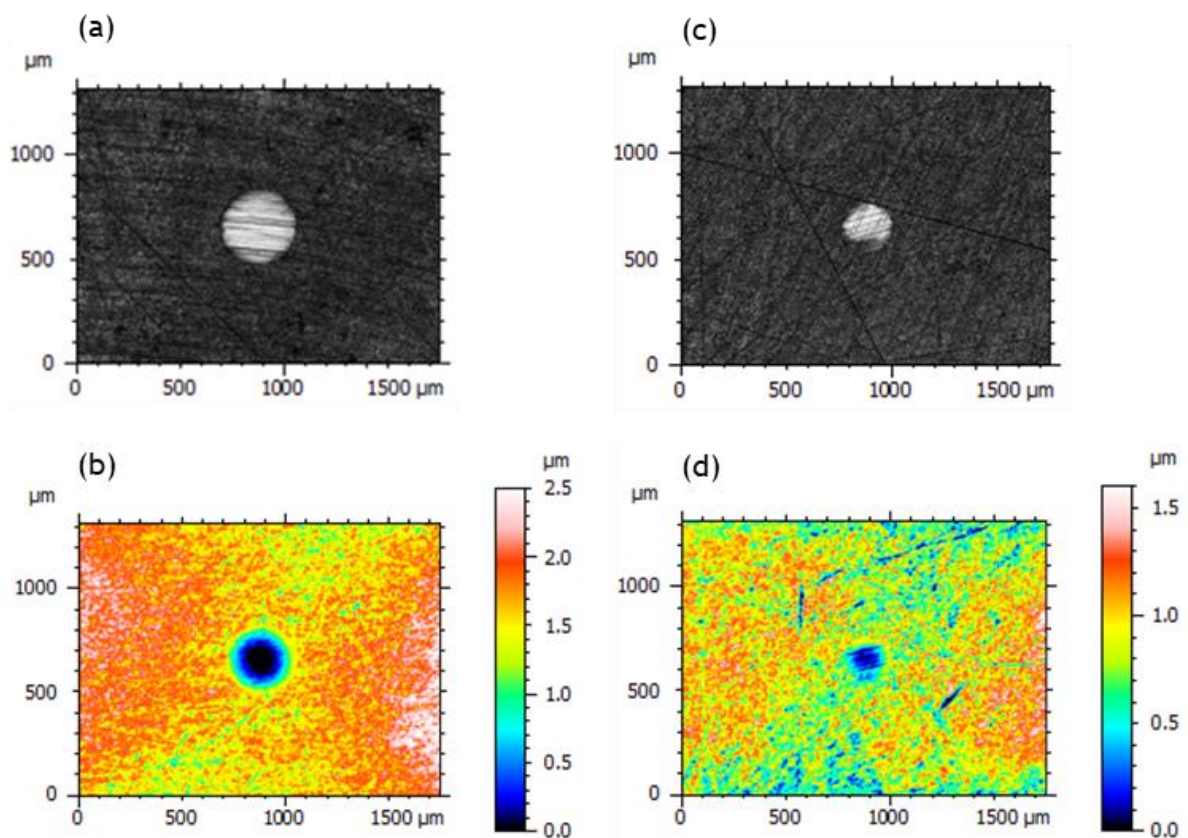
Figure 3.13 2D Images and 3D profiles of the wear tracks in the pins tested with neat PAO40 (a, b) and with its nanolubricant containing 0.25 wt% ZnO-OA (c, d)
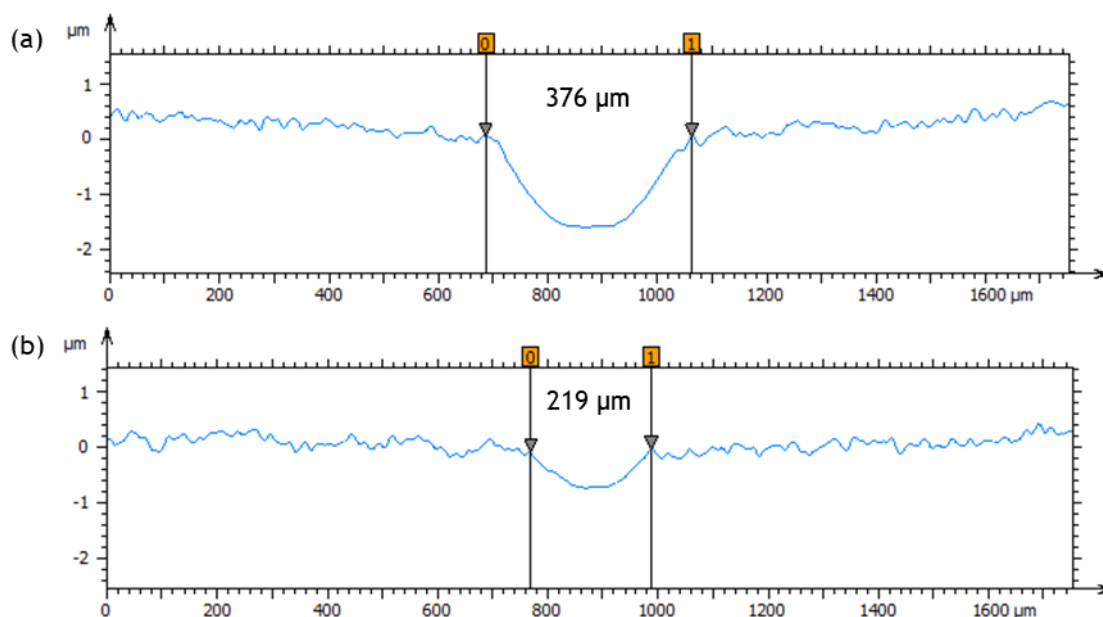
Figure 3.14 Cross-sectional profiles of the wear tracks on the pins lubricated with neat PAO40 (a) PAO40 + 0.25 wt% ZnO-OA (b)

The roughness (R_a) of wear tracks was another parameter measured by 3D profilometry to analyze the anti-wear capability of the nanolubricants. The surface roughness of the untested pins was also characterized. The average values of the roughness are shown in Figure 3.15 for worn and untested pins. All nanodispersions, except for 1.00 wt% ZnO-OA in PAO40, provided worn surfaces with lower R_a values than those of the untested pins, however, only the dispersions with the two lowest NP concentrations (0.1 and 0.25 wt%) led to lower Ra values than neat PAO40, obtaining the optimal Ra value for 0.25 wt% ZnO-OA dispersion, which reduced the R_a value by 67 % compared to that of the untested pin surface and 43 % compared to that lubricated with PAO40.
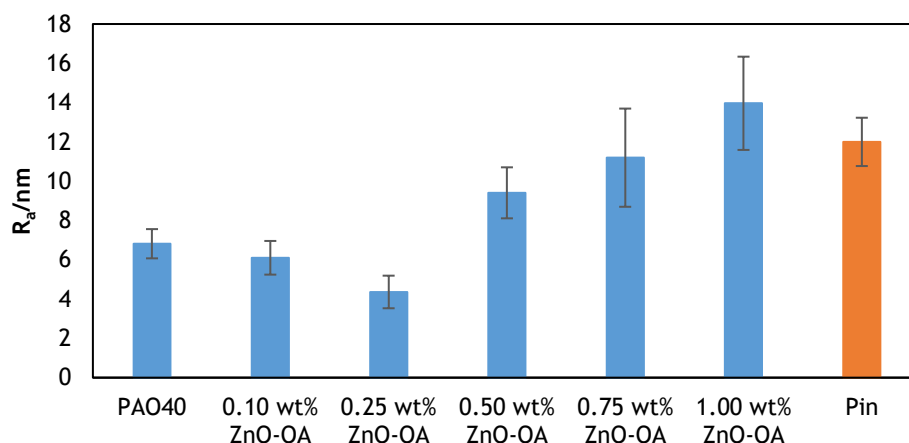
Figure 3.15 Roughness (R_a) of the untested pin surface (orange) and of the worn pin surfaces (blue) with the expanded uncertainty bars tested with PAO40 and PAO40 + wt% ZnO-OA nanodispersions with different NP weight percentages, wt%

Raman spectra of ZnO-OA (Figure 3.16) and of PAO40 (Figure 3.17) are very similar due to the structural similarity of both compounds containing C-C bonds and -CH$_2$ groups. Nevertheless, there were two clear differences in the case of oleic acid (Figure 3.16): there was

a C = C signal at 1663 cm^{-1} due to the vibration of the double bond and another signal at 3008 cm^{-1} corresponding to vibration = C-H, which did not appear in the PAO40 spectrum. Raman maps of the worn pin surfaces were also recorded. To distinguish between PAO40 and ZnO-OA in the Raman maps of these surfaces, the dissimilar peak at 1663 cm^{-1} of the ZnO-OA spectrum was used to identify the presence of these NPs. Similar procedure has been used previously by Nasser at al. [37-39] to discriminate between the PAO32 Raman spectrum and those of three ionic liquids.
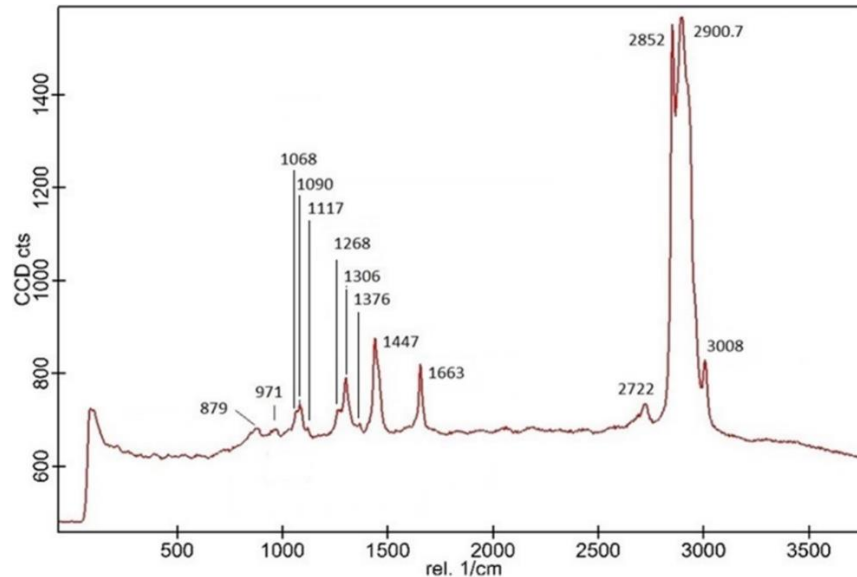
Figure 3.16 Raman spectrum of ZnO-OA NPs
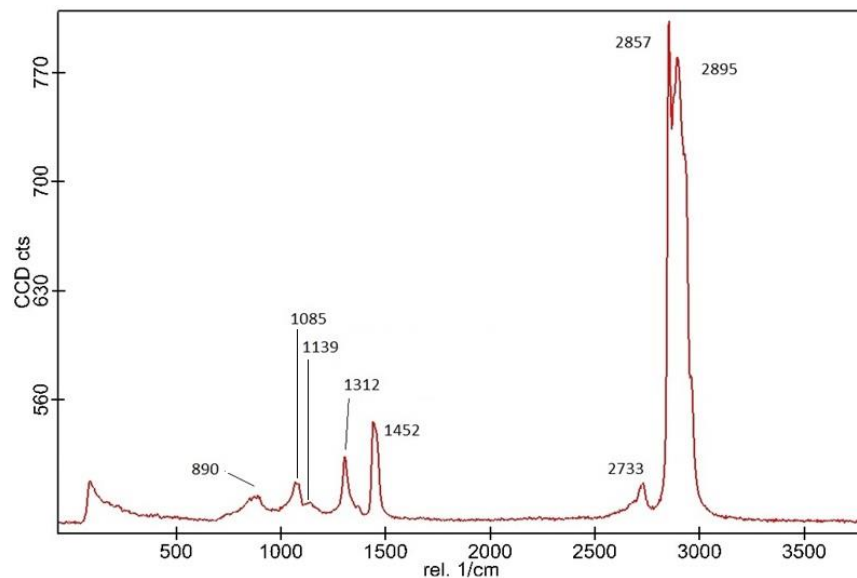
Figure 3.17 Raman spectrum of PAO40

From the Raman map corresponding to the worn pin surface lubricated with neat PAO40 (Figure 3.18), the presence of PAO40 (red area), iron oxides (blue area) as well as small and scarce carbon areas (yellow) were evidenced. These results agree with those found by Ratoi et al. [40] from XPS measurements on a disk wear track obtained with PAO6 from ball-on-disk tribological tests at 120 ºC, using a similar tribo-pair. These authors concluded that the tribofilm built up on the wear track was mainly formed by carbon, iron, and oxygen, and thus the smooth

wear could be due to oxide formation and lubricant degradation on the wear track among other effects. In addition, recently, from confocal Raman microscopy, Nasser et al. [37] also found for a similar pin worn surface tested with PAO32 at 80 ℃; namely, the boundary tribofilms were composed of iron oxides, carbon, and the oil itself.
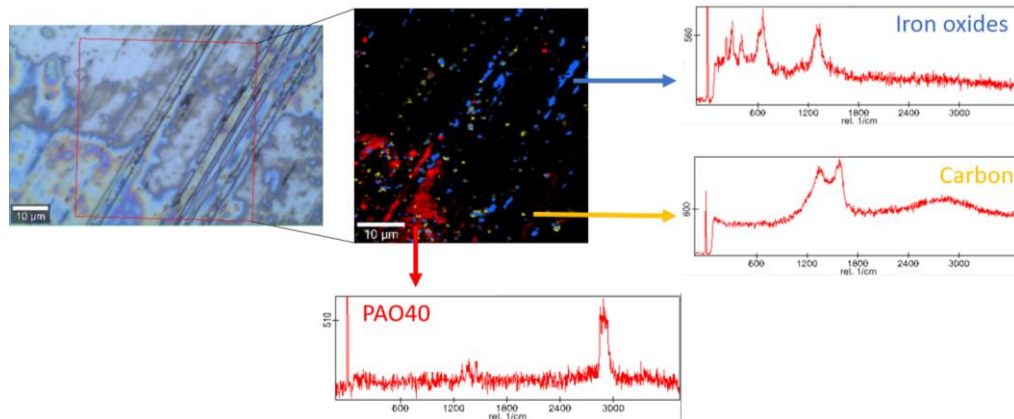
Figure 3.18 Raman map of the worn pin surface tested with PAO40 and spectra of the components present on this surface: PAO40 (red), carbon (yellow) and iron oxides (blue)

Raman map on the worn surface tested with PAO40 + 0.25 wt% ZnO-OA (Figure 3.19) shows the presence of PAO40 (red color), oleic acid, i.e., ZnO-OA NPs, (green color) and iron oxides (blue color). The obtained signals of the ZnO-OA NPs in the worn scar overlapped with those of another component, probably carbon, which appeared also in the worn surfaces of neat PAO40 (Figure 3.18, yellow color). The presence of the ZnO-OA NPs in the worn scar tribofilm was also shown in the ICP-MS analysis of the nanolubricant collected after the tribotest. This nanolubricant contains 0.21 wt% of ZnO-OA NPs, i.e., a 16 % reduction.
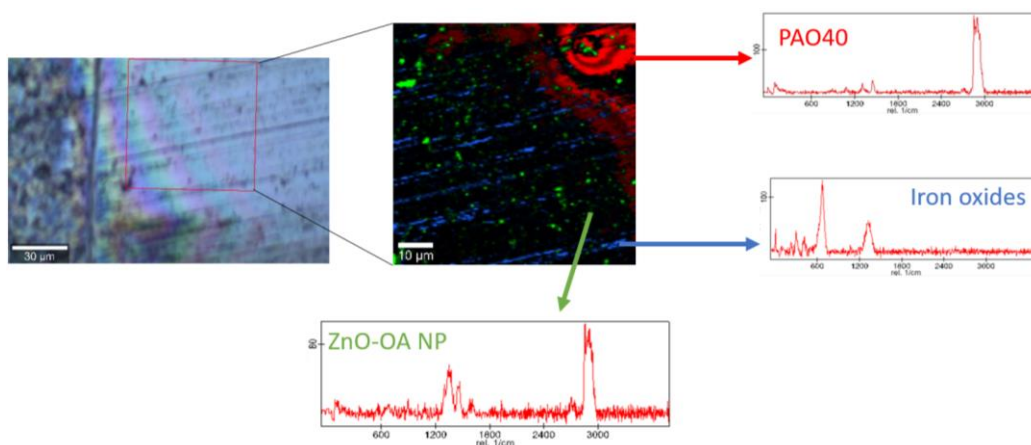
Figure 3.19 Raman map of the worn pin surface tested with PAO40 + 0.25 wt% ZnO-OA and spectra of the components present on that surface: PAO40 (red), ZnO-OA (green) and iron oxides (blue)

Regarding the tribological mechanisms, both rolling and mending effects could be behind the better tribological performance of nanolubricants with respect to that of neat PAO40. Rolling may transform sliding friction into rolling friction [41,42] as a result of the spherical shape of ZnO-OA NPs (Figure 3.3). The mending effect was evidenced by the presence of small

areas of ZnO-OA NPs in the Raman maps of the contact surfaces and by the decrease of their roughness. Raman mapping also evidenced the presence of large PAO40 tribofilms.

3.5 CONCLUSIONS

The features achieved in this chapter can be summarized as:

- The synthesis and coating with oleic acid of ZnO NPs were carried out successfully. The oleic acid coated ZnO (ZnO-OA) NPs, with an average diameter around 10 nm, were characterized by XRD (the nanoparticle core) and FTIR (the coating).
- The OA coating of the ZnO NPs enable their dispersion in the PAO40, reaching stability times up to 29 days for the 0.25 wt% nanodispersion.
- Using as neat base oil PAO40, five nanolubricants with ZnO-OA concentrations ranging from 0.10 to 1.00 wt% were designed as well as thermophysically and tribologically characterized.
- Density increases roughly linearly with the mass concentration of NPs, reaching 0.5 % for nanodispersion with 1.00 wt% ZnO-OA. Dynamic viscosities also increase with the concentration of NPs, with relative increases of up to 4.0 % for the base oil additivated with 1 wt% of ZnO-OA. On the contrary, viscosity indices vary hardly with the nanoparticle concentration, being slightly lower than that of PAO40.
- At 80 ℃, all the nanolubricants improve the tribological behavior of PAO40, being the optimal concentration 0.25 wt% of ZnO-OA (25 % of reduction in the COF and wear reductions up to 82 %, for cross-sectional area, with respect to those obtained with the neat base oil).
- The better tribological performance of the nanolubricants with respect to that of neat PAO40 could be due to the occurrence of rolling and mending mechanisms owing to the spherical shape of the NPs and to the lower roughness values on the rubbed steel surfaces, respectively.
- From confocal Raman microscopy on the worn surfaces obtained from tribological test with PAO40 + 0.25 wt% ZnO-OA dispersion, it is illustrated the built up of tribofilms composed by PAO40, as well as smaller areas of ZnO-OA NPs.

3.6 REFERENCES

[1]   M. Kandeva, V. Majstorović, E. Assenova, Tribology enhancement of lubricant quality and safety, Advanced Quality 42 (2014) 1-5.
[2]   J. Zhao, Y. Huang, Y. He, Y. Shi, Nanolubricant additives: A review, Friction 9 (2021) 891-917, https://doi.org/10.1007/s40544-020-0450-8.
[3]   S.J. Klaine, P.J. Alvarez, G.E. Batley, T.F. Fernandes, R.D. Handy, D.Y. Lyon, S. Mahendra, M.J. McLaughlin, J.R. Lead, Nanomaterials in the environment: behavior, fate, bioavailability, and effects, Environmental Toxicology Chemistry: An International Journal 27 (2008) 1825-1851, https://doi.org/10.1897/08-090.1.
[4]   C.B. Ong, L.Y. Ng, A.W. Mohammad, A review of ZnO nanoparticles as solar photocatalysts: Synthesis, mechanisms and applications, Renewable and Sustainable Energy Reviews 81 (2018) 536-551, https://doi.org/10.1016/j.rser.2017.08.020.
[5]   E.Y. Shaba, J.O. Jacob, J.O. Tijani, M.A.T. Suleiman, A critical review of synthesis parameters affecting the properties of zinc oxide nanoparticle and its application in wastewater treatment, Applied Water Science 11 (2021) 48, https://doi.org/10.1007/s13201-021-01370-z.

[6]   S.B. Mousavi, S.Z. Heris, P. Estellé, Viscosity, tribological and physicochemical features of ZnO and MoS₂ diesel oil-based nanofluids: An experimental study, Fuel 293 (2021) 120481, https://doi.org/10.1016/j.fuel.2021.120481.

[7]   W.G. Xue, Z.H. Zhao, P. Wang, Z.L. Jin, X.H. Xu, X.G. Zhou, Performance study of zinc oxide nanoparticles for lubricant oil, Advanced Materials Research 1118 (2015) 195-204, https://doi.org/10.4028/www.scientific.net/AMR.1118.195.

[8]   A. Hernandez Battez, J. Fernandez Rico, A. Navas Arias, J. Viesca Rodriguez, R. Chou Rodriguez, J. Diaz Fernandez, The tribological behaviour of ZnO nanoparticles as an additive to PAO6, Wear 261 (2006) 256-263, https://doi.org/10.1016/j.wear.2005.10.001.

[9]   L. Gara, Q. Zou, Friction and wear characteristics of oil-based ZnO nanofluids, Tribology Transactions 56 (2013) 236-244, https://doi.org/10.1080/10402004.2012.740148.

[10]   X. Ran, X. Yu, Q. Zou, Effect of particle concentration on tribological properties of ZnO nanofluids, Tribology Transactions 60 (2017) 154-158, https://doi.org/10.1080/10402004.2016.1154233.

[11]   L. Wu, Y. Zhang, G. Yang, S. Zhang, L. Yu, P. Zhang, Tribological properties of oleic acid-modified zinc oxide nanoparticles as the lubricant additive in poly-alpha olefin and diisooctyl sebacate base oils, RSC Advances 6 (2016) 69836-69844, https://doi.org/10.1039/C6RA10042B.

[12]   M.A. Gutierrez, M. Haselkorn, P. Iglesias, The lubrication ability of ionic liquids as additives for wind turbine gearboxes oils, Lubricants 4 (2016) 14, https://doi.org/10.3390/lubricants4020014.

[13]   R.J. Andrade Vieira, M.Á. Sanz Bobi, Evaluación de Indicadores de la Condición de Aerogeneradores, (2013), www.iit.comillas.edu/docs/IIT-13-030A.pdf.

[14]   D. Coronado, J. Wenske, Monitoring the oil of wind-turbine gearboxes: Main degradation indicators and detection methods, Machines 6 (2018) 25, https://doi.org/10.3390/machines6020025.

[15]   N.M. Shamhari, B.S. Wee, S.F. Chin, K.Y. Kok, Synthesis and characterization of zinc oxide nanoparticles with small particle size distribution, Acta Chimica Slovenica 65 (2018) 578-585, http://dx.doi.org/10.17344/acsi.2018.4213.

[16]   Y.T. Prabhu, K.V. Rao, V.S.S. Kumar, B.S. Kumari, Synthesis of ZnO nanoparticles by a novel surfactant assisted amine combustion method, Advances in Nanoparticles 2 (2013) 45, https://doi.org/10.4236/anp.2013.21009.

[17]   R. Hong, T. Pan, J. Qian, H. Li, Synthesis and surface modification of ZnO nanoparticles, Chemical Engineering Journal 119 (2006) 71-81, https://doi.org/10.1016/j.cej.2006.03.003.

[18]   M. Šćepanović, M. Grujić-Brojčin, K. Vojisavljević, S. Bernik, T. Srećković, Raman study of structural disorder in ZnO nanopowders, Journal of Raman Spectroscopy 41 (2010) 914-921, https://doi.org/10.1002/jrs.2546.

[19]   M. Yoshikawa, K. Inoue, T. Nakagawa, H. Ishida, N. Hasuike, H. Harima, Characterization of ZnO nanoparticles by resonant Raman scattering and cathodoluminescence spectroscopies, Applied Physics Letters 92 (2008) 113115, https://doi.org/10.1063/1.2901159.

[20]   J.M. Liñeira del Río, E.R. López, J. Fernández, Tribological properties of graphene nanoplatelets or boron nitride nanoparticles as additives of a polyalphaolefin base oil, Journal of Molecular Liquids 333 (2021) 115911, https://doi.org/10.1016/j.molliq.2021.115911.

[21]   N.F. Azman, S. Samion, Dispersion stability and lubrication mechanism of nanolubricants: a review, International journal of precision engineering manufacturing-green technology 6 (2019) 393-414, https://doi.org/10.1007/s40684-019-00080-x.

[22]   S. Kannaiyan, C. Boobalan, A. Umasankaran, A. Ravirajan, S. Sathyan, T. Thomas, Comparison of experimental and calculated thermophysical properties of alumina/cupric oxide hybrid nanofluids, Journal of Molecular Liquids 244 (2017) 469-477, https://doi.org/10.1016/j.molliq.2017.09.035.

[23]   B.C. Pak, Y.I. Cho, Hydrodynamic and heat transfer study of dispersed fluids with submicron metallic oxide particles, Experimental Heat Transfer an International Journal 11 (1998) 151-170, https://doi.org/10.1080/08916159808946559.

[24]   E.J. Wasp, J.P. Kenny, R.L. Gandhi, Solid-liquid flow: slurry pipeline transportation, Ser. Bulk Mater. Handl. 1 (1977).

[25]   K. Yang, H. Peng, Y. Wen, N. Li, Re-examination of characteristic FTIR spectrum of secondary layer in bilayer oleic acid-coated Fe_3O_4 nanoparticles, Applied Surface Science 256 (2010) 3093-3097, https://doi.org/10.1016/j.apsusc.2009.11.079.

[26]   D. Sagdeev, I.g. Gabitov, C. Isyanov, V. Khairutdinov, M. Farakhov, Z. Zaripov, I. Abdulagatov, Densities and viscosities of oleic acid at atmospheric pressure, Journal of the American Oil Chemists' Society 96 (2019) 647-662, https://doi.org/10.1002/aocs.12217.

[27]   S.-S. Lin, J.-L. Huang, D.-F. Lii, The effects of rf power and substrate temperature on the properties of ZnO films, Surface Coatings Technology 176 (2004) 173-181, https://doi.org/10.1016/S0257-8972(03)00665-0.

[28]   A. Einstein, Eine neue bestimmung der moleküldimensionen, ETH Zurich (1905)

[29]   H. Chen, Y. Ding, C. Tan, Rheological behaviour of nanofluids, New journal of physics 9 (2007) 367, https://doi.org/10.1088/1367-2630/9/10/367.

[30]   S.S. Bair, High pressure rheology for quantitative elastohydrodynamics (2019).

[31]   N. Marx, L. Fernández, F. Barceló, H. Spikes, Shear thinning and hydrodynamic friction of viscosity modifier-containing oils. Part I: shear thinning behaviour, Tribology Letters 66 (2018) 1-14, https://doi.org/10.1007/s11249-018-1039-5.

[32]   B. Gupta, N. Kumar, K. Panda, S. Dash, A. Tyagi, Energy efficient reduced graphene oxide additives: Mechanism of effective lubrication and antiwear properties, Scientific Reports 6 (2016) 1-10, https://doi.org/10.1038/srep18372.

[33]   J.M. Liñeira del Río, M.J. Guimarey, M.J. Comuñas, E.R. Lopez, A. Amigo, J. Fernandez, Thermophysical and tribological properties of dispersions based on graphene and a trimethylolpropane trioleate oil, Journal of Molecular Liquids 268 (2018) 854-866, https://doi.org/10.1016/j.molliq.2018.07.107.

[34]   L. Liu, Z. Fang, A. Gu, Z. Guo, Lubrication effect of the paraffin oil filled with functionalized multiwalled carbon nanotubes for bismaleimide resin, Tribology Letters 42 (2011) 59-65, https://doi.org/10.1007/s11249-011-9749-y.

[35]   V. Zin, S. Barison, F. Agresti, L. Colla, C. Pagura, M. Fabrizio, Improved tribological and thermal properties of lubricants by graphene based nano-additives, RSC Advances 6 (2016) 59477-59486, http://doi.org/10.1039/C6RA12029F.

[36]   N.A. Ismail, S. Bagheri, Highly oil-dispersed functionalized reduced graphene oxide nanosheets as lube oil friction modifier, Materials Science Engineering: B 222 (2017) 34-42, https://doi.org/10.1016/j.mseb.2017.04.010.

[37]   K.I. Nasser, J.M. Liñeira del Río, E.R. López, J. Fernández, Synergistic effects of hexagonal boron nitride nanoparticles and phosphonium ionic liquids as hybrid lubricant additives, Journal of Molecular Liquids 311 (2020) 113343, https://doi.org/10.1016/j.molliq.2020.113343.

[38]   K.I. Nasser, J.M. Liñeira del Río, E.R. López, J. Fernández, Hybrid combinations of graphene nanoplatelets and phosphonium ionic liquids as lubricant additives for a

polyalphaolefin, Journal of Molecular Liquids 336 (2021) 116266, https://doi.org/10.1016/j.molliq.2021.116266.

[39]   K.I. Nasser, J.M. Liñeira del Río, F. Mariño, E.R. López, J. Fernández, Double hybrid lubricant additives consisting of a phosphonium ionic liquid and graphene nanoplatelets/hexagonal boron nitride nanoparticles, Tribology International 163 (2021) 107189, https://doi.org/10.1016/j.triboint.2021.107189.

[40]   M. Ratoi, H. Tanaka, B.G. Mellor, J. Sugimura, Hydrocarbon lubricants can control hydrogen embrittlement, Scientific reports 10 (2020) 1-14, https://doi.org/10.1038/s41598-020-58294-y.

[41]   M.K.A. Ali, X. Hou, M.A. Abdelkareem, Anti-wear properties evaluation of frictional sliding interfaces in automobile engines lubricated by copper/graphene nanolubricants, Friction 8 (2020) 905-916, https://doi.org/10.1007/s40544-019-0308-0.

[42]   D. Singh, U. Bhan, P.K. Painuly, Effect of ZnO nanoparticles concentration on the friction and wear behaviour of Mahua oil, Materials Today: Proceedings 46 (2021) 10117-10120, https://doi.org/10.1016/j.matpr.2020.09.379.

SECTION II. NANOLUBRICANTS FOR ELECTRIC DRIVETRAINS IN ELECTRIC VEHICLES

4 TITANIUM OXIDE NANOPARTICLES COATED WITH OLEIC ACID FOR TRIBOLOGICAL ENHANCEMENT FOR ELECTRIC VEHICLE LUBRICANTS

The results presented in this chapter are related to the following publication (the editorial authorization for the use of this publication is in the Appendix A):

[a] Laboratory of Thermophysical and Tribological Properties, Nafomat Group, Department of Applied Physics, Faculty of Physics and Institute of Materials (iMATUS), Universidade de Santiago de Compostela, 15782 Santiago de Compostela, Spain

[b] Unidade de tribologia, vibraçoes e manutençao industrial, INEGI, Universidade do Porto, Porto, Portugal

[c] FEUP, Faculdade de Engenharia da Universidade do Porto, Rua Dr. Roberto Frias s/n, 4200-465 Porto, Portugal

The main contributions of the PhD student to this study are explicitly indicated below:

Experimental: Investigation, Methodology, Conceptualization

Manuscript: Writing – review & editing

Globally, transportation is one of the main contributors to CO$_2$ emissions, producing 28 % of total emissions [1]. In this regard, it is estimated that the CO$_2$ global emissions produced by vehicles with internal combustion engines (ICE) are between 4 and 5 times higher than by electric vehicles (EVs) when the electrical energy is provided through renewable sources [2]. In comparison to traditional ICE vehicles, mechanical elements of EVs work at higher loads, speeds, temperatures, and under electromagnetic fields [2,3]. Key areas of focus in the design of new transmission fluids suitable for use in EVs are obtaining low-viscosity oils with optimal tribological properties, and improving their electrical and thermal properties, among others. Here the additives play a fundamental role. Currently, among the most successful approaches in the study of new additives for lubricants that can provide both optimal anti-wear and anti-friction properties, as well as high thermal conductivity, those based on nanotechnology stand out [4]. Nevertheless, as it was pointed out in Chapter 1, in spite of the several developments that have been reached with nanopowders in the area of lubricants, there is yet an important difficulty with the nanodispersions stability due to sedimentation, because nanopowders have

a tendency to agglomerate each other [5]. This drawback is even more accentuated in low-viscosity lubricants. In this chapter, the key objective is to analyze the stability times and tribological properties of TiO_2 NPs with an oleic acid coating, TiO_2-OA, as additives of a low-viscosity base oil (PAO8). Nowadays, nanomaterials such as ZnO or TiO_2 NPs are used in commercial applications, such as sunscreens, solar panels, or paints, due to their photolytic properties [6,7]. Non-coated TiO_2 NPs have shown good tribological properties as additives of an engine lubricant and a vegetable oil [8,9]. Thus, Birleauno et al. [8] recently examined the addition of TiO_2 NPs and a surfactant to 10W30 engine oil, observing that the NPs can improve the friction reduction and the antiwear properties of the neat lubricant. Moreover, Cortes et al. [9] researched the lubrication behavior of a sunflower oil containing non-coated SiO_2 and TiO_2 nanopowders. These authors observed that the friction coefficient was reduced thanks to adding SiO_2 or TiO_2 NPs, around 80 % and 95 %, respectively, comparing to the sunflower oil and that the loss of volume was dropped by around 75 % and 70 %, respectively. Regarding TiO_2 NPs toxicity, Cerrillo et al. [6] tested the nanoecotoxicity of TiO_2 NPs in microalgae, finding that the toxicity of these NPs is reduced with the presence of natural organic matter (NOM), even at low NOM concentration. Interestingly, the organic material used in this study [6] is predominantly humic acid which is composed by organic acids and conjugated bases.

The main aim of this chapter is to design new low-viscosity nanolubricants based on commercial TiO_2 NPs (5 nm), which were chemically modified by oleic acid (OA) to improve their stability in PAO8. For this purpose, it is necessary to know as in the previous chapter: a) the optimal concentration of the NPs for friction and wear reduction; b) the stability of the nanodispersion at the optimal concentration; c) the variations of viscosity, density and viscosity index of the optimal nanodispersion with respect to PAO8; d) the mechanisms of the nanoadditives for friction and wear reduction for sliding conditions; in addition, in this chapter we would like also to know: e) how the TiO_2-OA + OA nanolubricants perform under rolling-sliding conditions. The worn surface in pure sliding condition tests was examined using a 3D optical profilometer and confocal Raman microscopy to understand the NPs tribological performance. Several nanodispersions were tribologically tested using pure sliding conditions and rolling-sliding conditions (5 % slide-to-roll ratio) at high temperature (120 °C). In addition, in this chapter we would also like to know e) how TiO_2-OA + OA nanolubricants behave under mixed and EHL conditions. The worn surface under pure sliding conditions was examined using a 3D optical profilometer and confocal Raman microscopy to understand the tribological performance of the nanoparticles. Various nanodispersions were tribologically tested under pure sliding conditions and under rolling-sliding conditions (5 % rolling to sliding ratio) at high temperature (120 °C).

4.1 NANOPARTICLE SYNTHESIS AND CHARACTERIZATION

4.1.1 Functionalization of nanoparticles

Regarding the nanoadditives, TiO_2 NPs coated with oleic acid (TiO_2-OA) were synthesized using commercial TiO_2, purity: 99.9 % and diameter of 5 nm, which were provided by US Research Nanomaterials, Inc. The TiO_2 nanopowders have been coated with OA following the reaction:

$$TiO_2 + OA \xrightarrow[\text{2) 95 °C, reflux, 2h}]{\substack{\text{NaOH} \\ \text{1) 60 °C, 30 min}}} TiO_2\text{-OA} \tag{4.1}$$
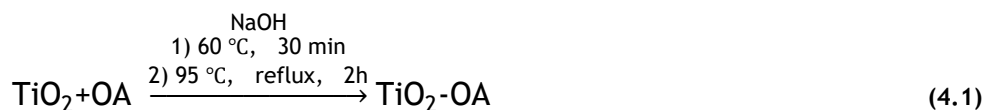
Briefly, 200 mg of commercial TiO_2 nanopowder were dispersed in distilled H_2O (20 mL) in a round bottom flask that contains a magnetic stir bar. This blend was heated to 60 °C under stirring (400 rpm) until this temperature was reached. After that, 5 mL of NaOH (0.05 M) were added and after one-minute, oleic acid, OA (0.6 mL), was also added. This blend remained at 60 °C for 30 min and then the temperature was increased to 95 °C and the sample was refluxed for 1 h 30 min, observing aggregation. The excess of NaOH was neutralized using HCl and the formed precipitate (TiO_2-OA) was isolated by centrifugation under 4000 rpm for 10 min and washed two times with ultrapure water and hexane. Subsequently, the obtained nanodispersion (hexane with 4.9 wt% TiO_2 NPs coated with OA) was added to PAO8 using an ultrasonic bath to homogenize the new dispersion. Finally, a hot plate was used to evaporate the hexane (low boiling point) thus obtaining the desired PAO8 + TiO_2-OA nanolubricant (3 wt% in TiO_2-OA). Figure 4.1 presents the preparation scheme of the nanodispersions of TiO_2-OA NPs in PAO8.
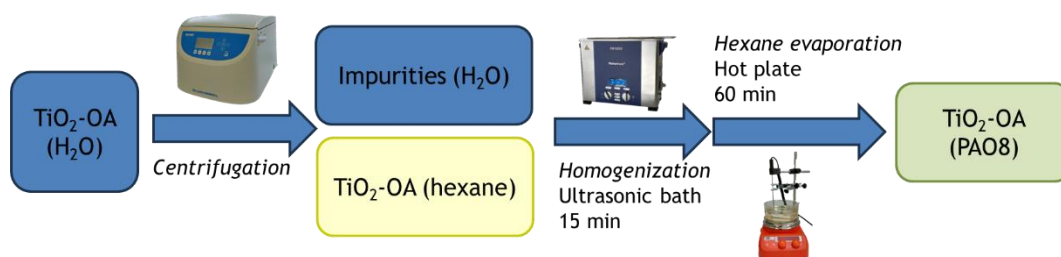
Figure 4.1 Preparation scheme of the nanodispersions of TiO_2-OA nanoparticles in PAO8

4.1.2 Characterization of nanoparticles

Bare TiO_2 NPs were also characterized by means of scanning electron microscopy (SEM) to obtain information about its shape. Figure 4.2 shows the TiO_2 NPs with two magnifications observing that these NPs have roughly spherical spongy shape. To confirm that the OA coating is properly linked to the TiO_2 nanopowders, FTIR analyses of synthetized TiO_2-OA nanopowders were carried out with the spectrometer VARIAN 670-IR. Figure 4.3 provides the FTIR spectrum of OA, TiO_2 and coated TiO_2-OA NPs. The peaks at 2910 and 2846 cm^{-1} for the TiO_2-OA NPs evidence that CH_3 and CH_2 of OA are present in the coated TiO_2 molecular structure [10]. Furthermore, peaks at 1490 and 1452 cm^{-1} prove that the –COO− functional group of OA is present [10]. In this regard, the disappearance of the intense peak at 1708 cm^{-1} implies that the –COOH of OA has totally reacted with TiO_2 NPs to form the coated TiO_2-OA nanopowders [10]. Furthermore, an absorption band for the nano-TiO_2 core is identified at low frequencies, because of the peak around 540 cm^{-1} is associated to the Ti-O-O bond vibration [11]. Considering these FTIR results, it is confirmed that the OA coating was carried out successfully.
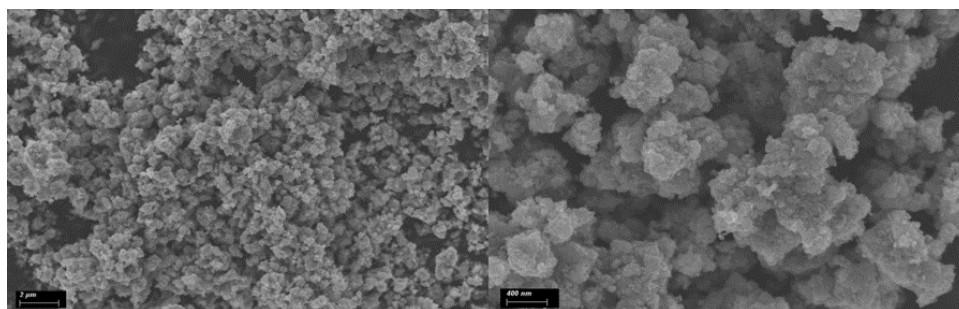
Figure 4.2 SEM images of TiO_2 nanopowders
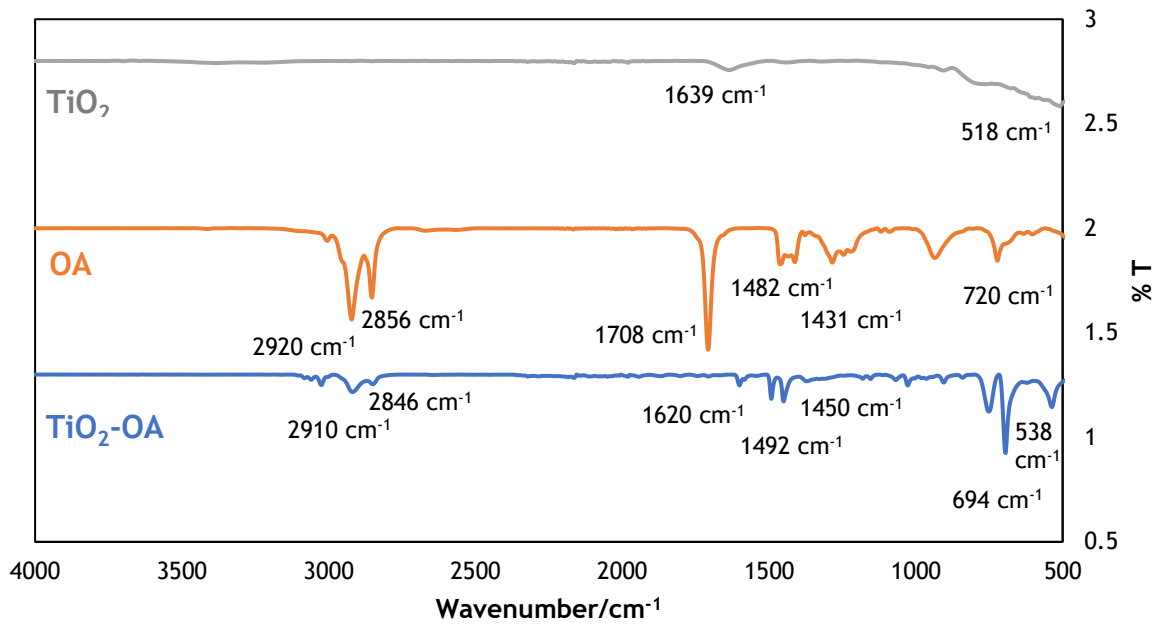
Figure 4.3 FTIR spectrum of TiO₂ nanoparticles, OA, and coated TiO₂-OA nanoparticles with their characteristic vibrational bands

4.2 STABILITY RESULTS

Nanolubricants were prepared with various weight percentages of TiO$_2$-OA (0.10, 0.25, 0.35 and 0.50 wt%) in PAO8. The PAO8 sample was characterized by FTIR and the results are presented in Figure 4.4, which reveals a weak peak at 721 cm^{-1} associated to -CH$_2$ alkyl chains, a peak at 1460 cm^{-1} owing to the C-H bending, two robust peaks around 2850 and 2920 cm^{-1} which correspond to the C-H stretching [12,13]. It can be noted that there is no presence of signals attributed for C=C bonds.
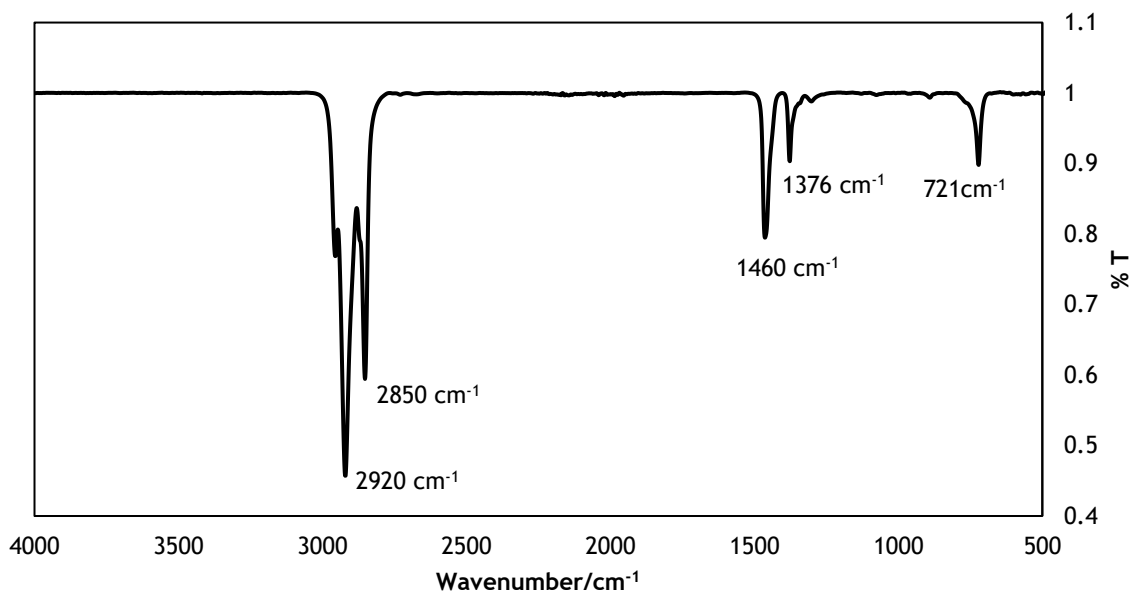
Figure 4.4 FTIR spectrum of PAO8 base oil

To prepare these nanodispersions, dilutions of the previously obtained 3 wt% TiO_2-OA nanolubricant were carried out adding PAO8. Furthermore, to improve the dispersibility of NPs in the PAO8 oil, oleic acid was added for each TiO_2-OA nanodispersion to obtain an OA mass concentration of 0.2 wt%. Finally, the nanodispersions were homogenized by means of an ultrasonic bath (Fisherbrand FB11203), operating in continuous sonication mode (4 h, 180 W and 37 kHz). It should be noted that during the sonication procedure the temperature was under control to prevent overheating of samples. Furthermore, nanodispersions stability was examined by sediment photo capturing of lubricants and by measuring the evolution of the refractive index during time by means of the Mettler Toledo refractometer.

Figure 4.5 shows that for the four designed TiO_2-OA nanolubricants no signs of sedimentation have appeared for at least three weeks just after homogenization. Nevertheless, for the most concentrated (and less stable) TiO_2-OA nanolubricant (0.50 wt%), it seems that sedimentation starts at four weeks after sonication. It should be noted that the visual stability times of uncoated TiO_2 nanolubricants were lower than 48 h (Figure 4.6), therefore an important stability improvement was achieved with the OA coating. Thus, the stability time of prepared TiO_2-OA nanolubricants is much greater than that required to carried out pure sliding and rolling-sliding tribological tests, around 8 h.
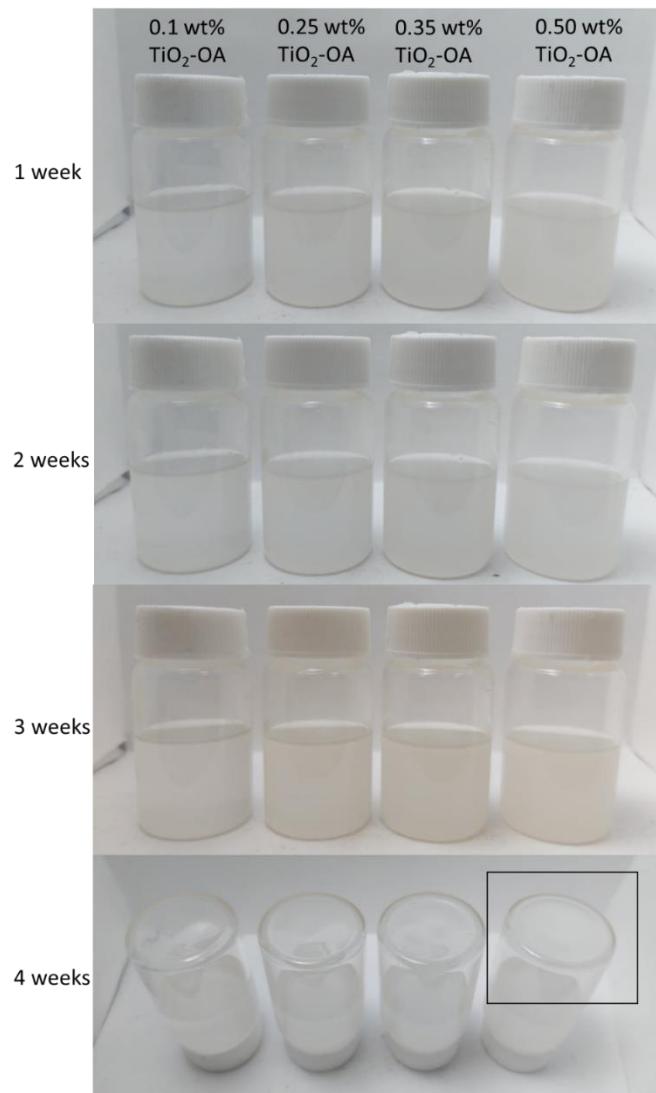
Figure 4.5 Visual stability of TiO₂-OA nanolubricants
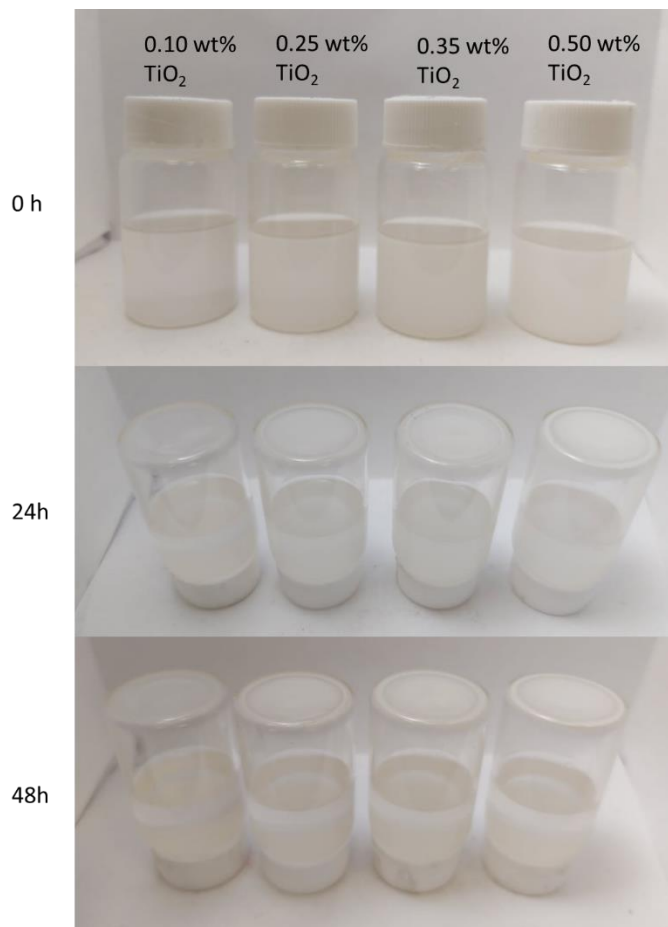
Figure 4.6 Visual stability of uncoated TiO$_2$ nanolubricants

The other method used to test the temporal stability of TiO$_2$-OA nanolubricants against sedimentation is refractometry. Figure 4.7 presents the time evolution of the refractive index for the TiO$_2$-OA nanolubricant and for the bare TiO$_2$ nanolubricant, both with a NP concentration of 0.10 wt%. It can be clearly observed that for the 0.10 wt% TiO$_2$ nanolubricant after the first ten hours the NPs are full sedimented, whereas in the case of the 0.10 wt% TiO$_2$-OA nanolubricant the sedimentation is slower. Specifically, for the former nanolubricant the refractive index increased 0.27 % after 10 h while for the TiO$_2$-OA nanolubricant it raised just 0.06 %, which indicates that the oleic acid coating of TiO$_2$ NPs clearly enhances the stability of nanolubricants. Moreover, the TiO$_2$-OA refractive index evolution shows a significant enhancement in the stability compared to other previously measured nanolubricants [13]. In particular, with trimethylolpropane trioleate based nanolubricants (higher viscosity oil) containing graphene oxide nanoadditives, refractive index raises 0.44 % after 50 h [13], whereas for the same time (50 h) and with a very low viscosity oil (PAO8), the refractive index shows increases of 0.32 % for 0.10 wt% TiO$_2$-OA nanolubricant. It should be noted that for low viscosity oils is more difficult to find good stabilities, since the NPs have less resistance to drop in oil. Considering this fact, in this research a high stability was achieved owing to the oleic acid coating of the TiO$_2$ NPs.
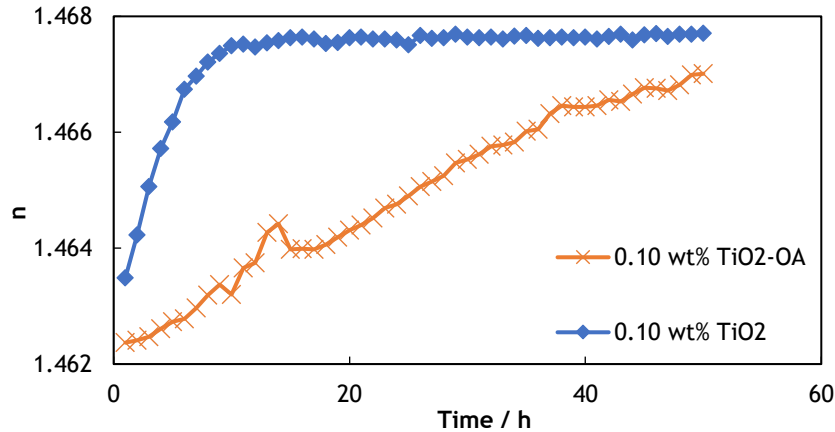
Figure 4.7 Refractive index evolution for 0.10 wt% TiO$_2$ and TiO$_2$-OA nanolubricants

4.3 THERMOPHYSICAL PROPERTIES

PAO8 base oil and the PAO8 + 0.35 wt% TiO$_2$-OA nanodispersion were thermophysically characterized with the SVM3000 Stabinger. These results are presented in Table 4.1. Comparing with the corresponding PAO8 property, the nanolubricant density showed a maximum variation of 0.06%, close to the measurement uncertainty, and the dynamic viscosity shows an increment up to 15 %. Finally, the VI value of this nanodispersion (VI 149) is 7 % higher than that of PAO8 base oil (VI 138).

Table 4.1 Densities (ρ) and dynamic viscosities (η) of PAO8 and 0.35 wt% TiO$_2$-OA nanolubricant measured at atmospheric pressure

Lubricant	PAO8	0.35 wt% TiO$_2$-OA	PAO8	0.35 wt% TiO$_2$-OA
T/°C	ρ/g cm^{-3}	ρ/g cm^{-3}	η/mPa.s	η/mPa.s
5	0.8375	0.8378	253.1	289.2
10	0.8345	0.8347	184.3	210.1
15	0.8315	0.8317	137.1	156.1
20	0.8285	0.8287	103.6	117.9
25	0.8255	0.8257	79.77	90.78
30	0.8224	0.8227	62.13	70.77
35	0.8194	0.8197	49.18	56.04
40	0.8163	0.8167	39.47	44.99
45	0.8133	0.8136	32.09	36.60
50	0.8102	0.8106	26.41	30.13
55	0.8072	0.8076	21.98	25.10
60	0.8041	0.8045	18.50	21.12
65	0.8010	0.8014	15.71	17.94
70	0.7979	0.7984	13.46	15.38
75	0.7948	0.7953	11.63	13.30
80	0.7918	0.7922	10.13	11.60
85	0.7887	0.7891	8.893	10.18
90	0.7856	0.7860	7.860	9.006
95	0.7825	0.7829	6.992	8.017
100	0.7794	0.7798	6.262	7.184

The viscosities measured in the Stabinger SVM3000 were correlated with the Vogel-Fulcher-Tammann (VFT) equation [14]. This equation was chosen because of its capability to extrapolate at temperatures out of the measurement range [dx.doi.org/10.1021/je200883w]. The VFT correlation was used to obtain the dynamic viscosity of each nanolubricant and the base oil (PAO8) at 120 °C, since the viscosimeter does not allow to measure above 100 °C. This viscosity value is required for the film thickness estimation needed to plot the Stribeck curve of the rolling-sliding tribological tests performed at 120 ºC.

4.4 TRIBOLOGICAL RESULTS
4.4.1 Pure sliding tests

Average friction coefficients obtained under pure sliding conditions for PAO8 and the four nanolubricants composed by TiO_2-OA NPs and PAO8 base oil are presented in Figure 4.8 and Table 4.2 It can be obviously seen that for all the TiO_2-OA nanolubricants the achieved coefficients of friction are lower than that of PAO8 without additives, being the greatest friction decrease achieved for the nanolubricant containing 0.35 wt% TiO_2-OA NPs. Specifically, the lowest average coefficient of friction is 0.098, obtained with this last nanolubricant, whereas the one obtained for the base oil is 0.139. Thus, a maximum 30 % friction reduction owing to the TiO_2-OA nanoadditives is achieved. Regarding the other nanolubricants, friction reductions of 16 %, 24 % and 23 % were obtained for 0.10 wt% TiO_2-OA, 0.25 wt% TiO_2-OA and 0.50 wt% TiO_2-OA nanolubricants, respectively.
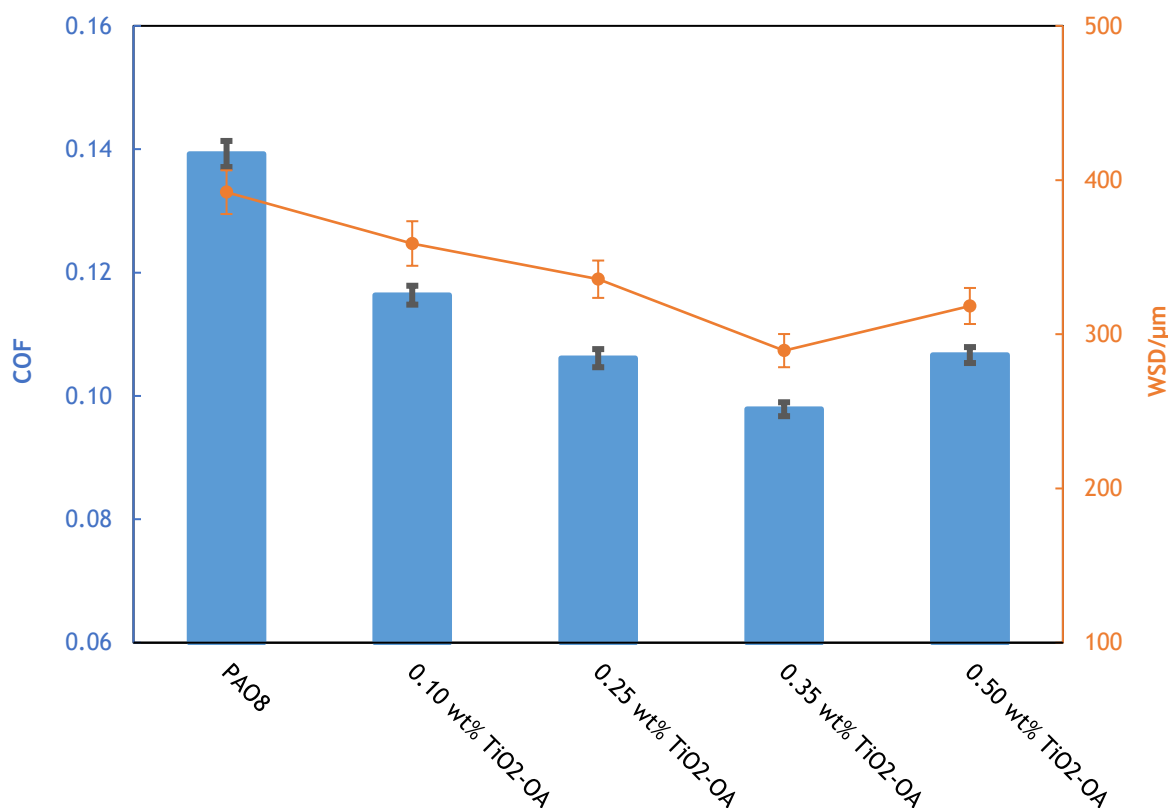
Figure 4.8 Average friction coefficient, COF, and WTW with the expanded uncertainty bars of PAO8 and its nanolubricants containing TiO_2 nanoparticles coated with oleic acid (the orange line is a guide for the eye)

Table 4.2 Average coefficients of friction, COF, and mean wear parameters, including the expanded uncertainty, U, for the tested PAO8 lubricants

Lubricant	COF	U	WTW/μm	U/μm	WTD/μm	σ/μm	Area/ μm²	U/ μm²
PAO8	0.1392	0.0021	392	14	2.35	0.17	605	52
+ 0.10 wt% TiO₂-OA	0.1163	0.0015	359	14	2.11	0.18	527	41
+ 0.25 wt% TiO₂-OA	0.1061	0.0015	336	12	1.85	0.12	459	39
+ 0.35 wt% TiO₂-OA	0.0978	0.0011	289	11	0.82	0.11	163	18
+ 0.50 wt% TiO₂-OA	0.1066	0.0013	318	12	1.04	0.14	245	17

4.4.2 Wear surface characterization

To compare qualitatively 3D Profiles, worn areas and cross section profiles of the pins tested in pure sliding conditions with the PAO8 base oil and with the optimal TiO₂-OA nanolubricant are shown in Figures 4.9 and 4.10. Average wear produced in pins after tribological tests was quantified by means of different parameters: WTW, WTD and worn area, which results are reported in Table 4.2 for each lubricant tested. As it can be observed, for all the tested TiO₂-OA nanolubricants, the three wear parameters were smaller than those found with PAO8 oil. The maximum wear reductions were found for 0.35 wt% TiO₂-OA nanolubricant with reductions of 26 %, 65 % and 73 % for WTW, WTD and worn area, respectively. These impressive wear reductions can be clearly observed in Figures 3.2.9 and 3.2.10 for the nanolubricant with the optimal concentration (0.35 wt% TiO₂-OA). Wear results show a good correlation with friction, as it can be observed in Figure 4.8.
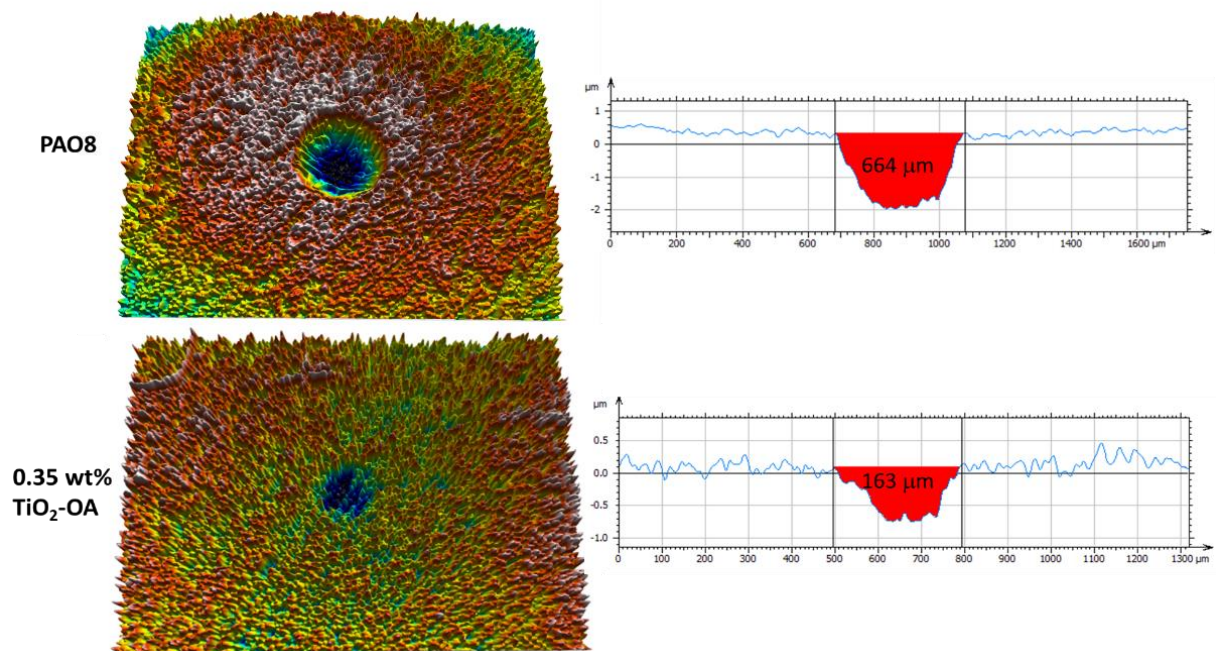
Figure 4.9 3D images and worn areas of worn tracks lubricated with PAO8 oil and with the optimum TiO₂-OA nanolubricant (0.35 wt%)
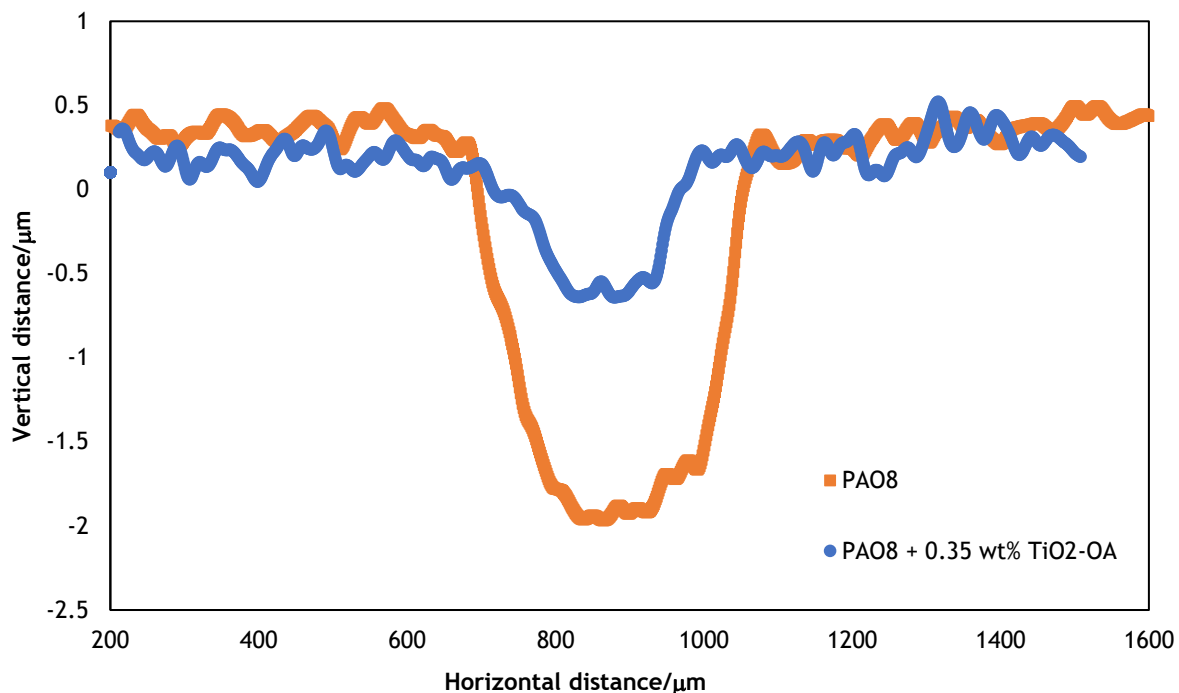
Figure 4.10 Profiles comparison of worn tracks lubricated with PAO8 oil and with the 0.35 wt% TiO$_2$-OA nanolubricant

Furthermore, roughness (R$_a$) of worn tracks of pins was investigated to obtain more information about the antiwear properties of TiO$_2$-OA NPs. Worn tracks lubricated with TiO$_2$-OA nanolubricants are less rough than those lubricated with PAO8 without additives (Table 4.3). In particular, a R$_a$ value of 18.8 nm was found for the worn track lubricated with PAO8 while for the surface lubricated with the 0.35 wt% TiO$_2$-OA nanolubricant a smaller R$_a$ was reached (12.8 nm), which leads to a 32 % roughness reduction. Therefore, it can be suggested that polishing and/or mending effects occur owing to the presence of TiO$_2$-OA NPs. Due to the mending effect, NPs can fill the grooves and scars of the rubbing surface developing an improved surface finish [15,16]. To quantify better the effect of the TiO$_2$-OA NPs in the roughness, other two parameters were analyzed: skewness, R$_{sk}$, and kurtosis, R$_{ku}$. The untested surface has a R$_{sk}$ higher than 0 (1.51), which means that the surface contains more peaks and asperities than valleys [17]. The decrease in the R$_{sk}$ parameter due to the friction process to a negative value closer to zero (-0.76 − -0.35) confirms that the worn surfaces lubricated with base oil and nanolubricants are very flat, most of the material being concentrated around the valleys. As regards R$_{ku}$, the value before tribological tests is higher than 3 (5.54), which indicates the presence of very high peaks and/or deep valleys (this parameter does not distinguish between peaks and valleys) [17]. After friction tests this value decreases (2.98– 2.41), which implies low both peaks and valleys. Comparing the average R$_a$, R$_{sk}$ and R$_{ku}$ values of the worn pins lubricated with PAO8 with those of worn pins lubricated with PAO8 + 0.35 wt% TiO$_2$-OA, it can be concluded that the last pins have flatter worn surfaces. These facts confirm that polishing and/or mending effects takes place. Table 4.3 also shows that the worn surfaces lubricated with PAO8 + 0.5 wt% TiO$_2$-OA are flatter than those tested with the optimal nanolubricant (PAO8 + 0.35 wt% TiO$_2$-OA).

Table 4.3 Average roughness parameters, R_a, R_{sk} and R_{ku} and the expanded uncertainties, U, in worn pins tested with PAO8 lubricants (Gaussian filter: 0.08 mm cut-off)

Lubricant	R_a/nm	U	R_{sk}	U	R_{ku}	U
PAO8	18.8	1.7	-0.562	0.048	2.98	0.21
+ 0.15 wt% TiO_2-OA	15.7	1.5	-0.434	0.055	2.44	0.18
+ 0.25 wt% TiO_2-OA	14.4	1.7	-0.512	0.045	2.41	0.17
+ 0.35 wt% TiO_2-OA	12.8	1.2	-0.356	0.052	2.46	0.18
+ 0.50 wt% TiO_2-OA	13.3	1.1	-0.762	0.062	2.52	0.15

Finally, with the aim of obtaining information about the nanoparticle distribution in worn tracks after pure sliding tests, Raman mappings of the worn surfaces were recorded. First, Raman spectra of the PAO8 base oil (Figure 4.11), oleic acid (Figure 4.12) and the TiO_2 nanopowders (Figure 4.13) were obtained to identify the components in mapping. Therefore, mapping of the worn pin lubricated with the optimal TiO_2-OA nanolubricant (Figure 4.14) was performed to identify the role that NPs play in the wear decrease. Figure 4.14 shows the relevant areas in green and blue color, that coincide with the spectra obtained for TiO_2 and OA (Figures 4.12 and 4.13), respectively. This fact indicates that tribofilms containing OA and TiO_2 were produced on the worn surface during the friction test. Considering the Raman and roughness results, it seems that the main tribological mechanisms that occur are tribofilm formation and mending and polishing effects.
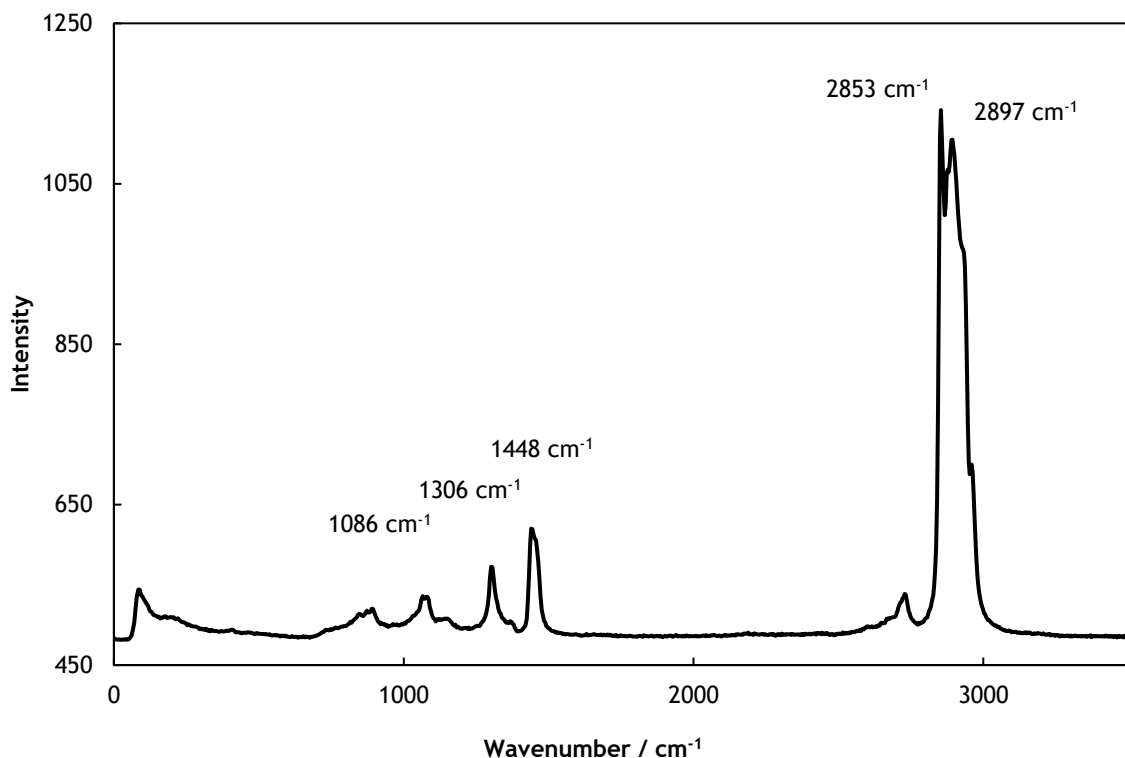
Figure 4.11 Raman Spectrum of PAO8 base oil
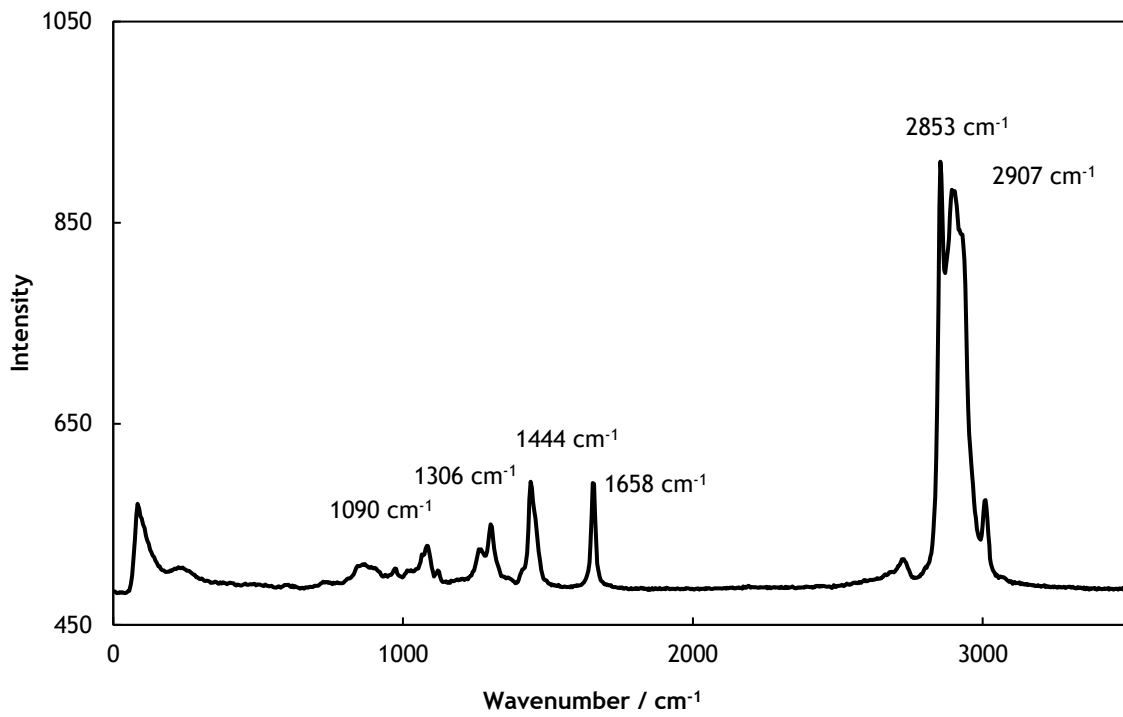
Figure 4.12 Raman spectrum of oleic acid
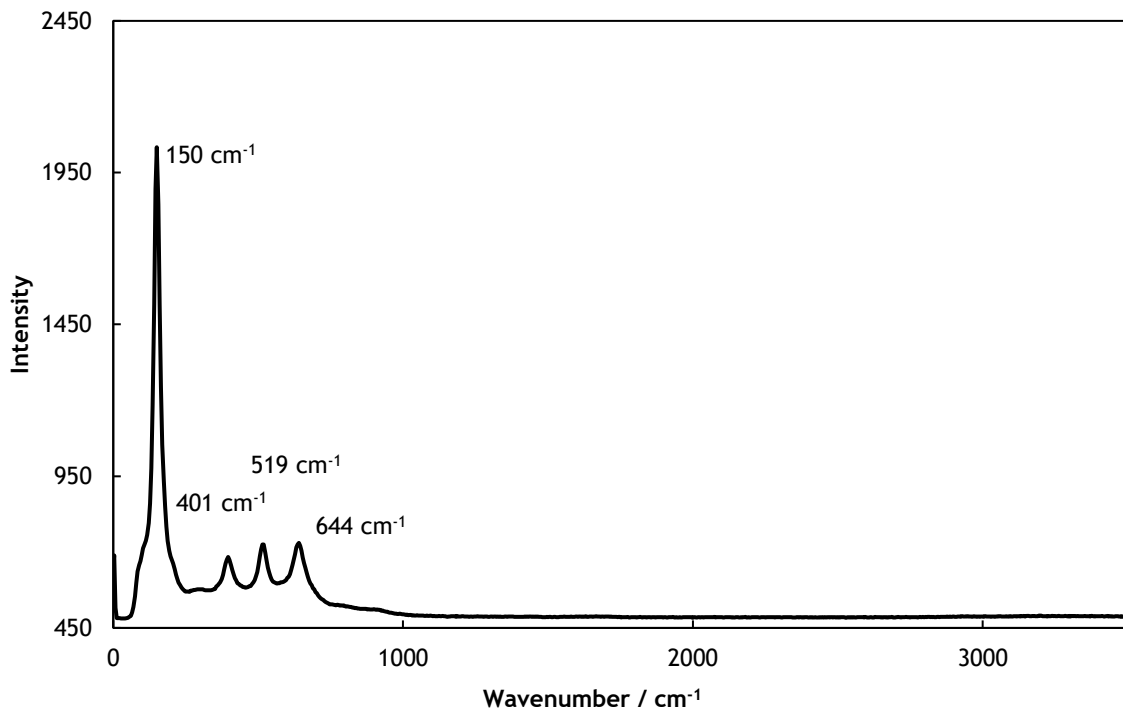
Figure 4.13 Raman Spectrum of TiO$_2$ nanoparticles
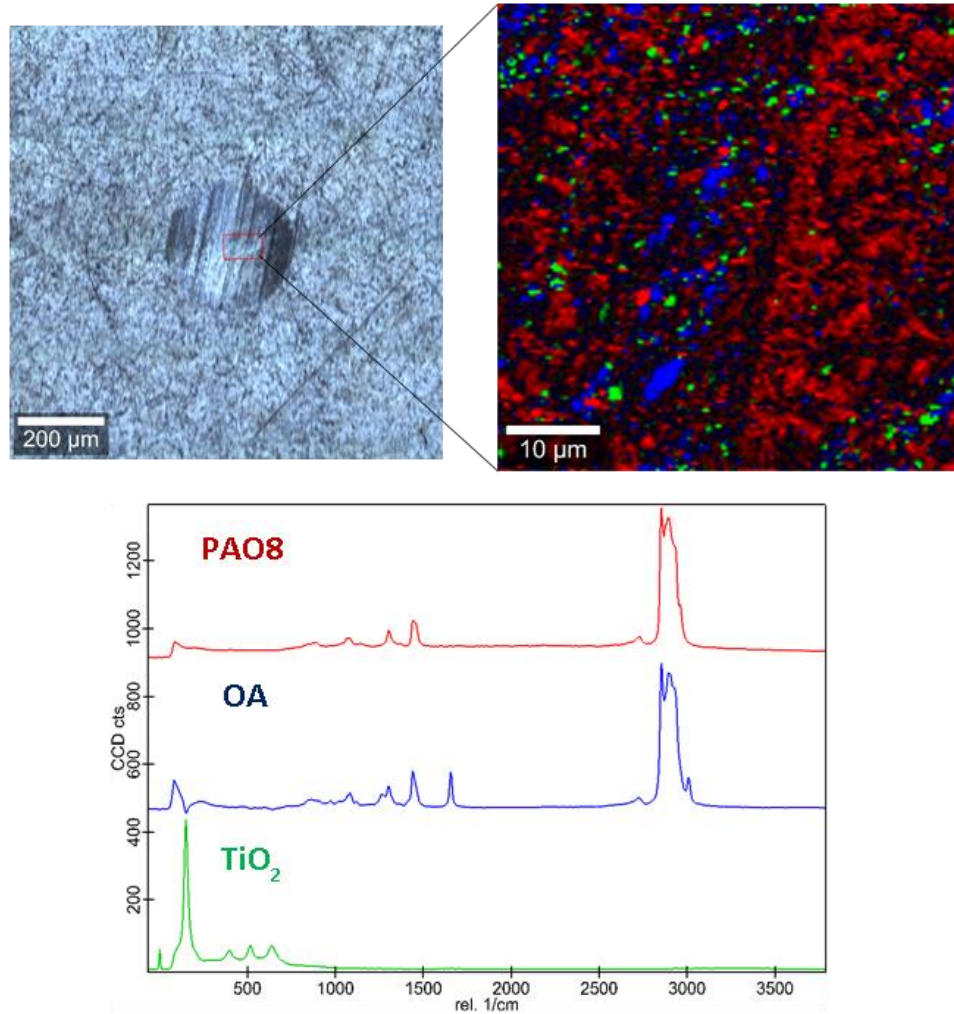
Figure 4.14 Elemental mapping and Raman characterization of worn surface obtained with the PAO8 + 0.35 wt% TiO$_2$-OA nanolubricant

4.4.3 Rolling-sliding tests

Rolling-sliding tribological measurements for PAO8 base oil and the designed TiO$_2$-OA nanolubricants were carried out at the same temperature than pure sliding tests (120 °C) and with a SRR of 5 %. Results are reported as Stribeck Curves (Figures 4.15 and 4.16) obtained by plotting the coefficient of friction versus specific film thickness Λ. To cover the different lubrication regimes, three discs with different roughness were tested (Table 2.6).

The Stribeck curves are presented in Figures 4.15 and 4.16 for PAO8 base oil and TiO$_2$-OA nanolubricants. As usual, friction tests carried out with the rough discs showed higher friction values than those made with the smooth disc. Figure 4.15 clearly shows that, for each tested disc, the friction coefficients are quite lower for all the TiO$_2$-OA nanolubricants than for the PAO8 base oil. Once again, the best friction behavior was found for the 0.35 wt% TiO$_2$-OA nanolubricant and that is why only the full Stribeck curves of PAO8 base oil and 0.35 wt% TiO$_2$-OA nanolubricant are presented in Figure 4.16. The results presented in Figure 4.15 for each disc are very interesting since it can be observed that for high entrainment speeds (right part of the curves) and consequently higher specific film thickness, the friction coefficient is quite similar for all nanolubricants and base oil. However, at low entrainment speeds the effect of TiO$_2$-OA NPs is crucial, contributing to greatly reduce the friction when the hydrodynamic effect is poor (low speeds).
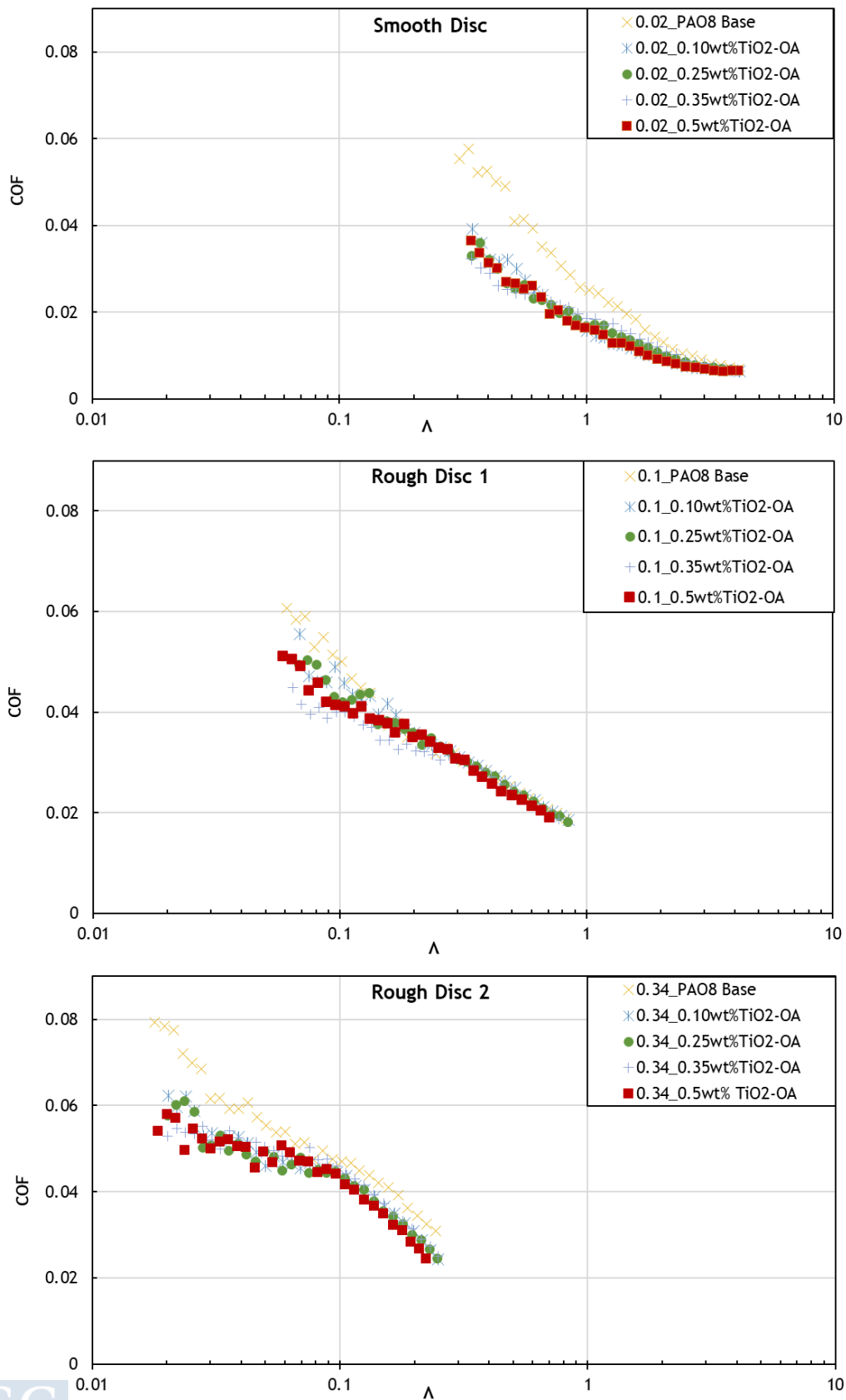
Figure 4.15 Stribeck curves of PAO8 and PAO8 + TiO$_2$-OA nanolubricants tested with each disc at 120 ˚C and 5 % SRR

Regarding the effect of NPs concentration in friction behavior, the friction coefficient decreases as the concentration of NPs increases, until the optimal value of 0.35 wt% is reached. This result is in perfect agreement with the friction results obtained for the pure sliding tests, where the 0.35 wt% TiO$_2$-OA concentration was also the optimal ones. A higher nanoparticle content leads to higher friction values, which means that there should be a saturation point (optimal concentration) above which the nanoparticle content cannot provide further friction reduction. In Figure 4.16 the COF values of PAO8 and its 0.35 wt% TiO$_2$-OA nanodispersion are plotted against Λ, defined by eq. 2.4. In the case of the nanodispersion, it can be observed that for $\Lambda <$ 0.07 (approximately) the COF is almost constant (around 0.05) which is typical of the boundary film lubrication regime of lubricants containing additives. For $0.07 < \Lambda < 1$ (approximately) the COF decreases as the Λ values increase, which is typical of the mixed film lubrication regime. The smooth disc shows a different behavior to the rough 1 and rough 2 discs for the PAO8 base oil: the difference between COF values of the PAO8 and the nanolubricant (observed at $\Lambda >$ 0.3) for the smooth disc is higher than that observed for the two rougher discs. After reaching $\Lambda > 2$, the COF decreases with Λ more smoothly for PAO8 and its nanolubricant, and there are no significant differences between both Stribeck curves, meaning that the influence of the NPs and of the surface roughness are no longer significant, which is typical of full film lubrication regime.

The values of $\Lambda_0 \approx 0.07$ and $\Lambda_1 \approx 1$ observed for this nanolubricant in this case are not general (Section 2.4.2), they fit the contact geometry considered (ball-on-disc), the roughness parameter (Ra) considered to define Λ and the test temperature (120 °C in the present case).
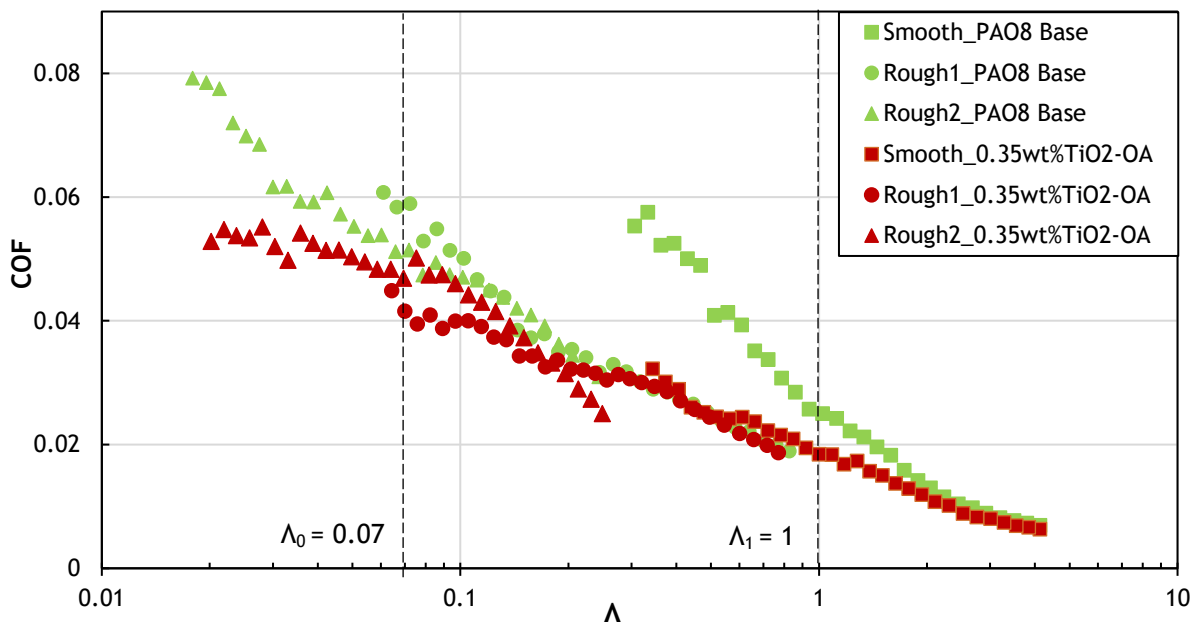
Figure 4.16 Full Stribeck curves of PAO8 (green) and PAO8 + 0.35 wt% TiO$_2$-OA nanolubricant (red) tested with each disc (squares smooth, circles rough 1, triangles rough 2) at 120 °C and 5 % SRR

4.5 CONCLUSIONS

Four nanolubricants based on a low-viscosity oil, PAO8, TiO$_2$-OA NPs as antifriction and antiwear additives, and oleic acid as dispersant were tribologically characterized. The conclusions of this chapter can be briefly expressed as:

- The OA coating of the commercial TiO_2 NPs was proven successful by FTIR analysis.
- Both the OA coating and dispersant improved the time stability from 48 h, for the nanolubricant with uncoated TiO_2 NPs, to at least 1 month for nanodispersions up to 0.35 wt% of TiO_2-OA, higher concentrations (0.5 wt%) sedimented after 4 weeks.
- Friction coefficients attained with TiO_2-OA nanolubricants are smaller than those observed for the neat PAO8 oil for all tribological tests (pure sliding or rolling/sliding contacts).
- In pure sliding conditions, for all the TiO_2-OA nanolubricants the wear observed in pins is much lower than the wear found with the PAO8 base oil, the highest reductions reaching 26 %, 65 % and 73 % in width, depth, and area, respectively, for PAO8 + 0.35 wt% TiO_2-OA nanolubricant.
- From roughness measurements and Raman mappings of worn pins tested in pure sliding conditions, it is concluded that the lubrication mechanism can be described by adsorbed tribofilms as well as the polishing and mending effects.
- In the rolling/sliding tests (small slide to roll-ratio SRR), the antifriction capability of TiO_2-OA NPs is more important at low speeds, which shows that the use of NPs is particularly important when operating in the boundary lubrication regime.

4.6 REFERENCES

[1]   R. Shah, B. Gashi, A. Rosenkranz, Latest developments in designing advanced lubricants and greases for electric vehicles—An overview, Lubrication Science 34 (2022) 515-526 https://doi.org/10.1002/ls.1605.

[2]   W. Ahmed Abdalglil Mustafa, F. Dassenoy, M. Sarno, A. Senatore, A review on potentials and challenges of nanolubricants as promising lubricants for electric vehicles, Lubrication Science 34 (2022) 1-29 https://doi.org/10.1002/ls.1568.

[3]   Understanding Base Oils and Lubricants for Electric Drivetrain Applications.

[4]   Y. Chen, S. Jha, A. Raut, W. Zhang, H. Liang, Performance characteristics of lubricants in electric and hybrid vehicles: a review of current and future needs, Frontiers in Mechanical Engineering 6 (2020) 571464 https://doi.org/10.3389/fmech.2020.571464.

[5]   Y. Chen, P. Renner, H. Liang, Dispersion of nanoparticles in lubricating oil: A critical review, Lubricants 7 (2019) 7 https://doi.org/10.3390/lubricants7010007.

[6]   C. Cerrillo, G. Barandika, A. Igartua, O. Areitioaurtena, G. Mendoza, Towards the standardization of nanoecotoxicity testing: Natural organic matter 'camouflages' the adverse effects of TiO_2 and CeO_2 nanoparticles on green microalgae, Science of The Total Environment 543 (2016) 95-104 https://doi.org/10.1016/j.scitotenv.2015.10.137.

[7]   S.J. Klaine, P.J. Alvarez, G.E. Batley, T.F. Fernandes, R.D. Handy, D.Y. Lyon, S. Mahendra, M.J. McLaughlin, J.R. Lead, Nanomaterials in the environment: behavior, fate, bioavailability, and effects, Environmental Toxicology Chemistry: An International Journal 27 (2008) 1825-1851 https://doi.org/10.1897/08-090.1.

[8]   C. Birleanu, M. Pustan, M. Cioaza, A. Molea, F. Popa, G. Contiu, Effect of TiO_2 nanoparticles on the tribological properties of lubricating oil: an experimental investigation, Scientific Reports 12 (2022) 5201 https://doi.org/10.1038/s41598-022-09245-2.

[9]   V. Cortes, K. Sanchez, R. Gonzalez, M. Alcoutlabi, J.A. Ortega, The performance of SiO_2 and TiO_2 nanoparticles as lubricant additives in sunflower oil, Lubricants 8 (2020) 10 https://doi.org/10.3390/lubricants8010010.

[10]   Y. Gao, G. Chen, Y. Oli, Z. Zhang, Q. Xue, Study on tribological properties of oleic acid-modified TiO_2 nanoparticle in water, Wear 252 (2002) 454-458 https://doi.org/10.1016/S0043-1648(01)00891-2.

[11]   G. Rajakumar, A.A. Rahuman, S.M. Roopan, V.G. Khanna, G. Elango, C. Kamaraj, A.A. Zahir, K. Velayutham, Fungus-mediated biosynthesis and characterization of TiO_2 nanoparticles and their activity against pathogenic bacteria, Spectrochimica Acta Part A: Molecular Biomolecular Spectroscopy 91 (2012) 23-29 https://doi.org/10.1016/j.saa.2012.01.011.

[12]   R. González, A.H. Battez, J. Viesca, A. Higuera-Garrido, A. Fernández-González, Lubrication of DLC coatings with two tris (pentafluoroethyl) trifluorophosphate anion-based ionic liquids, Tribology Transactions 56 (2013) 887-895 https://doi.org/10.1080/10402004.2013.810319.

[13]   J.M. Liñeira del Río, E.R. López, J. Fernández, F. García, Tribological properties of dispersions based on reduced graphene oxide sheets and trimethylolpropane trioleate or PAO 40 oils, Journal of Molecular Liquids 274 (2019) 568-576 https://doi.org/10.1016/j.molliq.2018.10.107.

[14]   D.E. Gonçalves, J.M. Liñeira del Rio, M.J.P. Comuñas, J. Fernández, J.H. Seabra, High Pressure Characterization of the Viscous and Volumetric Behavior of Three Transmission Oils, Industrial Engineering Chemistry Research 58 (2019) 1732-1742 https://doi.org/10.1021/acs.iecr.8b05090.

[15]   U. Maurya, V. Vasu, D. Kashinath, Three-way compatibility study among Nanoparticles, Ionic Liquid, and Dispersant for potential in lubricant formulation, Materials Today: Proceedings 59 (2022) 1651-1658 https://doi.org/10.1016/j.matpr.2022.03.329.

[16]   V. Saini, J. Bijwe, S. Seth, S. Ramakumar, Interfacial interaction of PTFE sub-micron particles in oil with steel surfaces as excellent extreme-pressure additive, Journal of Molecular Liquids 325 (2021) 115238 https://doi.org/10.1016/j.molliq.2020.115238.

[17]   J. Kałużny, A. Świetlicka, Ł. Wojciechowski, S. Boncel, G. Kinal, T. Runka, M. Nowicki, O. Stepanenko, B. Gapiński, J. Leśniewicz, Machine Learning Approach for Application-Tailored Nanolubricants' Design, Nanomaterials 12 (2022) 1765 https://doi.org/10.3390/nano12101765.

5 STEARIC ACID COATED SILICON OXIDE NANOPARTICLES AS ADDITIVE FOR A LOW VISCOSITY PAO LUBRICANT

[a] Laboratory of Thermophysical and Tribological Properties, Nafomat Group, Department of Applied Physics, Faculty of Physics and Institute of Materials (iMATUS), Universidade de Santiago de Compostela, 15782 Santiago de Compostela, Spain

[b] Unidade de tribologia, vibraçoes e manutençao industrial, INEGI, Universidade do Porto, Porto, Portugal

[c] FEUP, Faculdade de Engenharia da Universidade do Porto, Rua Dr. Roberto Frias s/n, 4200-465 Porto, Portugal

The main contributions of the PhD student to this study are explicitly indicated below:

Experimental: Investigation, Methodology, Conceptualization

Manuscript: Writing - original draft, Writing - review & editing

As regards the nanoadditives chosen in this chapter, silicon oxide NPs (SiO$_2$ NPs) have many advantages, including controllable size, flexible structure, good thermal stability, low toxicity, high porosity and hydroxyl groups on their surface enabling easy for surface modification and superior adsorption capacity [1,2]. In addition, the production cost of these NPs is low. Remzova et al. [3] evaluated the toxicity of bare and organic coated SiO$_2$ NPs in human lung cells, concluding that bare SiO$_2$ NPs were not cytotoxic but reduced cell viability, which could be improved by the organic coating of the NPs. SiO$_2$ NPs are used in various applications, including biomedicine, cosmetics, adsorbents, food, and printing [4]. These NPs were also analyzed as lubricant additives, showing great capability as friction and wear modifiers [5-9]. Cortés et al. [5] analyzed the effectiveness of uncoated spherical SiO$_2$ NPs (diameter 20-30 nm) as additives for a vegetable oil, obtaining reductions up to 77 % for friction and 74 % for wear volume. Zawawi et al. [10] used both SiO$_2$ NPs (30 nm) and Al$_2$O$_3$ NPs (13 nm) to prepare nanolubricants based on a PAG finding an optimum composite volume concentration of 0.02 % at which the friction and wear rate reductions are 4.8 % and 13%, respectively. Several authors [6-9,11] modified the surface of SiO$_2$ NPs to improve the stability of their nanodispersions, being a common modification their functionalization with oleic acid as was done by Peng et al. [6] achieving a stability time of around 30 days for a paraffin oil (43 cSt at 40 ºC) with concentrations varying from 0.05 to 1.0 wt% of oleic acid modified SiO$_2$ NPs (92-110 nm). Peng et al. [7] also studied the influence of the size of SiO$_2$ NPs on tribological properties

concluding that nanodispersions of the smallest oleic acid modified SiO_2 NPs (58 nm) in a paraffin oil showed the best tribological results and a stability of at least 30 days. Singh et al. [11] modified the surface of SiO_2 NPs (35 nm) with isopropyl alcohol and prepared nanodispersions of the modified NPs in epoxidized Madhuca indica oil (45.1 cSt at 40 °C) achieving strong friction and wear reductions with the nanodispersions of 0.8 wt% modified SiO_2 NPs. Silanization of SiO_2 NPs is another common surface-modification. Sui et al. [8] prepared hairy silica NPs (HSNs) with different ratios of two tethered silanes one polar and the other nonpolar, the more nonpolar tethered silane leads to the best stability time (2 months) due to the lower polarity of the resulting modified surface, which is more compatible with PAO100. Sui et al. [9] further confirmed the improvement of stability of HSNs with a nonpolar modification by comparing the effect of different tethered functionalities on amino silane modified SiO_2 NPs, the best stability results (2 months) in PAO100 were obtained for CH_3 terminated HSNs.

In this chapter we intended to use commercial SiO_2 NPs (8 nm), which were chemically modified through stearic acid (SA) to improve their stability in PAO6, to design low-viscosity nanolubricants. In addition to the same specific objectives of the previous chapter, in this chapter we would like also to know 1) if there is synergy between the SiO_2-SA NPs and the SA dispersant and 2) if the friction and wear reductions in sliding conditions with these nanolubricants are better than with PAO6 + a zinc dithiophosphate (ZDDP). This latter compound, ZDDP, is one of the most widely used friction and wear modifying additives in engine, industrial and transmission oils but for environmental restrictions and operational problems this additive should be replaced [12-14]. For this task, several mixtures and nanodispersions were tribologically tested using pure sliding conditions and rolling-sliding conditions (5 % slide-to-roll ratio) at high temperature (120 °C).

5.1 NANOPARTICLE SYNTHESIS AND CHARACTERIZATION
5.1.1 Functionalization of the nanoparticles

SiO_2 NPs (8 nm, 99 %) were acquired from US Research Nanomaterials, Inc. (Houston, TX, USA). The reagents used in the esterification reaction were sodium hydroxide (0.05 M) from Honeywell (Charlotte, NC, USA), stearic acid (95 %) from Sigma-Aldrich (Saint Louis, MO, USA) and hydrochloric acid (37 %) from Merck (Darmstadt, Germany). The solvent used to transfer the NPs to PAO6 is n-hexane (95 %) from Labkem (Barcelona, Spain). All these products were used with no additional purification. ZDDP was provided by REPSOL.

An esterification reaction was used to functionalize the SiO_2 NPs with SA (Figure 5.1), following a procedure similar to that presented in Chapter 3. Thus, commercial SiO_2 NPs (200 mg) were dispersed in distilled water (20 mL) in a round-bottom flask, containing a magnetic stir bar, and heated to 60 °C with 350 rpm agitation, using a magnetic hot-plate (Figure 5.1a). Meanwhile, SA (415 mg) was dissolved in distilled water (10 mL) with the aid of ultrasonication (Fisherbrand Ultrasonic Bath, 180 W, 37 kHz). Once the SiO_2 aqueous dispersion reached the set temperature (60 °C), 5 mL of NaOH (0.05 M) were added (Figure 5.1b). A minute later, the SA aqueous solution was added dropwise. The obtained mixture was kept for 30 minutes at 60 °C, and then refluxed at 95 °C for 90 minutes, finally obtaining the SA coated SiO_2 NPs (SiO_2-SA) dispersed in water (Figure 5.1c).
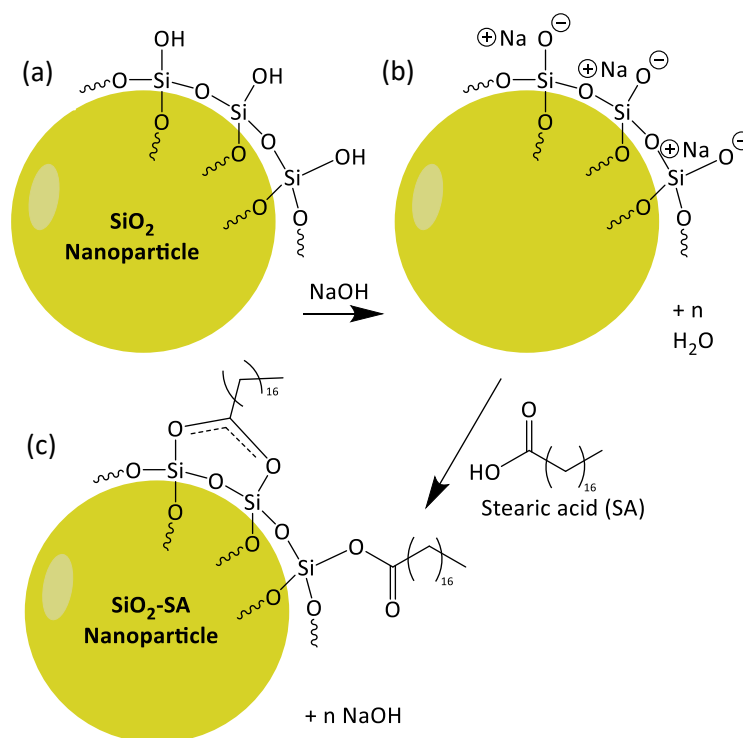
Figure 5.1 Schematic drawing of the esterification reaction: (a) SiO$_2$ NPs in water, (b) after the addition of NaOH and (c) after the SA addition

5.1.2 Characterization of the nanoparticles

The JEOL JEM-1011 TEM was used to observe the morphology of the uncoated SiO$_2$ nanopowders. TEM images (Figure 5.2) of the nanopowders, dispersed previously in water, show small agglomerates of roughly spherical NPs.
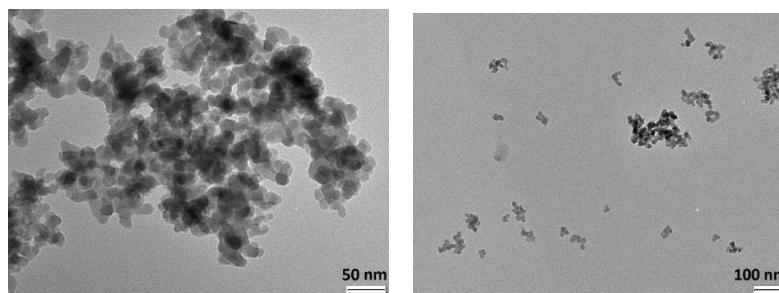
Figure 5.2 TEM micrographs of the uncoated SiO$_2$ NPs

The infrared spectra of pure SA, commercial SiO$_2$ NPs and dried SiO$_2$-SA NPs are displayed in Figure 5.3. Table 5.1 shows details of the characteristic peaks of these spectra. The FTIR spectrum of SiO$_2$-SA NPs shows signals from both SiO$_2$ NPs and SA, which are: two symmetrical stretching bands at 2917 and 2848 cm^{-1} corresponding to C—H bond in —CH$_3$ and —CH$_2$ from SA, as well as two wagging vibration bands at 1458 and 1450 cm^{-1} of C—C in —CH$_2$ [15]; some important weaker peaks appear at 1683 and 1064 cm^{-1}, the former due to the C=O stretching of SA and the later from the Si—O—Si anti-symmetric stretching of the SiO$_2$ NPs [16]. All these signals present a slight shift compared to those of SA and SiO$_2$ counterparts, most likely due to the strong interactions between both core and shell. An important evidence of the existence of covalent bonds between them is the absence of FTIR signals corresponding to in-plane and out-of-plane bending O—H vibrations [17] at 1429 and

939 cm^{-1}, respectively, which appear in the FTIR spectrum of SA. Furthermore, the drop in the intensity of the C=O stretching band shows that some of the SA molecules have reacted with both groups containing oxygen, —OH and C=O, as it has been plotted in Figure 5.1. In addition, Raman spectra of SA, SiO$_2$ NPs and SiO$_2$-SA NPs were performed (Figure 5.4). These spectra were also used in Subsection 5.4.1 for the Raman analysis of the worn surface.

Table 5.1 FTIR spectra: wavenumber and vibration mode assigned to each chemical bond

Substance	Peak (cm^{-1})	Vibration mode		Chemical bond
SiO$_2$	1064	ν_{as}	Anti-symmetric stretching	Si—O—Si
	950	ν	Stretching	Si—O
	782	δ	Bending	Si—O—Si
	451	ρ	Rocking	Si—O
SA	2913	ν_s	Symmetrical stretching	C—H bond in —CH$_3$
	2846	ν_s	Symmetrical stretching	C—H bond in —CH$_2$
	1700	ν	Stretching	C=O
	1429	δ_{ip}	In-plane bending	O—H
	1400-1180	ω	Wagging	C—C in —CH$_2$
	939	δ_{oop}	Out-of-plane bending	O—H
SiO$_2$-SA	2917	ν_s	Symmetrical stretching	C—H bond in —CH$_3$
	2848	ν_s	Symmetrical stretching	C—H bond in —CH$_2$
	1683	ν	Stretching	C=O
	1454	ω	Wagging	C—C in —CH$_2$
	1450	ω	Wagging	C—C in —CH$_2$
	1064	ν_{as}	Anti-symmetric stretching	Si—O—Si
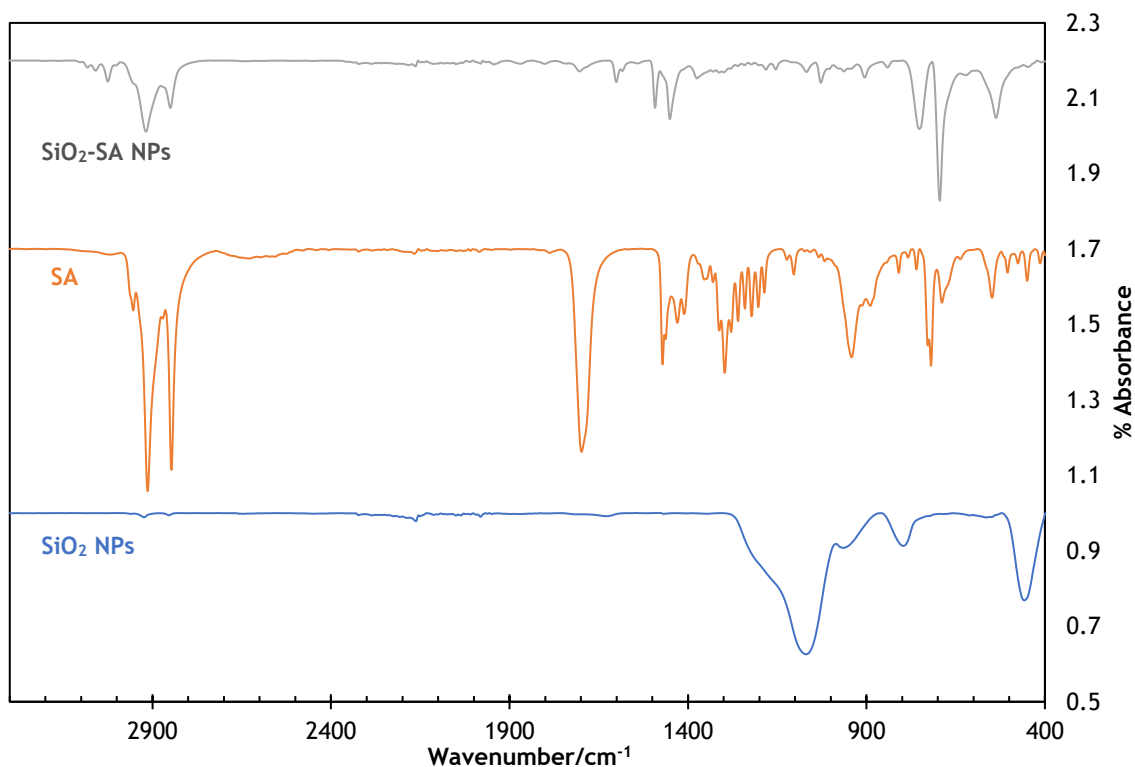
Figure 5.3 FTIR spectra of uncoated SiO$_2$ NPs (blue), SA (orange) and SiO$_2$-SA NPs (grey)
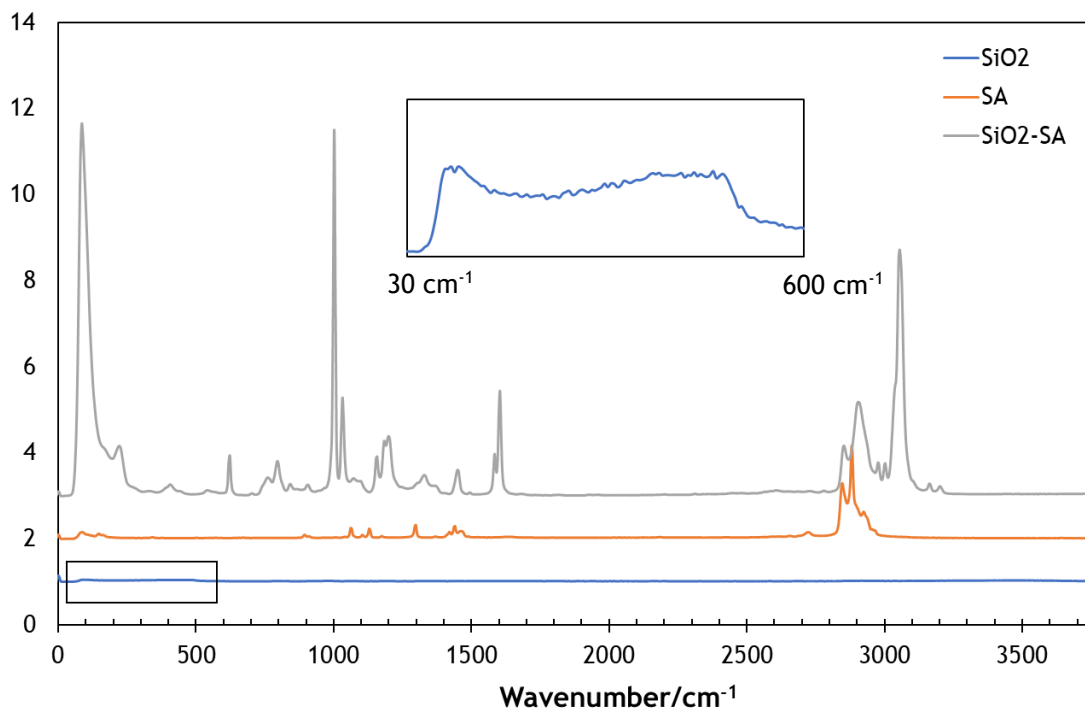
Figure 5.4 Raman spectra of uncoated SiO$_2$ NPs (blue), SA (orange) and SiO$_2$-SA NPs (grey). Inset detail of Raman spectra for SiO$_2$ at low wavenumbers

5.2 STABILITY RESULTS

PAO6 oil was characterized by means of FTIR (Figure 5.5) and by Raman spectroscopy (Figure 5.13). Regarding the FTIR results, the observed peaks are the same than those present in PAO8 from Chapter 5 (Figure 4.4). This is to be expected because all PAOs have the same basic chemical structure, saturated hydrocarbon chains. Thus, the only observed peaks are from C–H and –CH$_2$ bond vibrations.
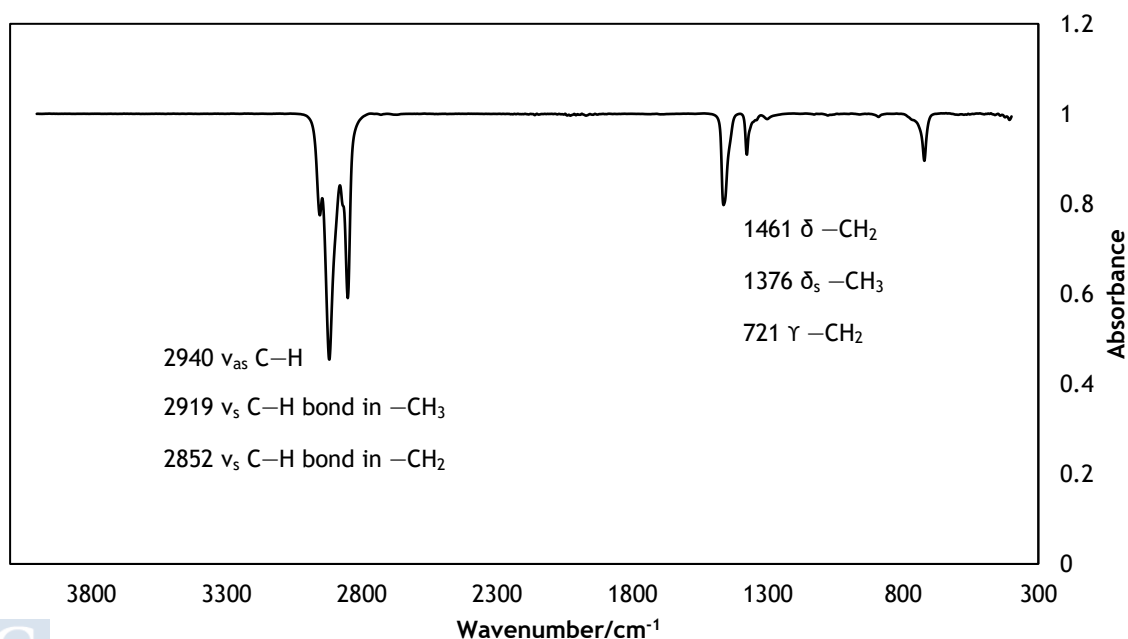
Figure 5.5 FTIR spectrum of PAO6

The dispersion method of the SiO_2-SA NPs in PAO6, summarized in Figure 5.6, is the same as the used for TiO_2-OA NPs (Figure 4.1) and has been further described in Subsection 2.3.1 from Chapter 2 (Figure 2.10b). After the esterification reaction, the SiO2 NPs were washed with the aid of a centrifuge. The collected NPs were redispersed in n-hexane for storage and subsequent handling. After this purification process, the concentration of SiO_2-SA NPs was obtained by difference in weight of 1 mL of the nanodispersion before and after the evaporation of n-hexane. Then, a known amount of n-hexane nanodispersion was added to a given amount of PAO6. This new dispersion was homogenized and then heated up to 95 ºC, remaining at this temperature for 60 min to remove the n-hexane, obtaining a 4.7 wt% SiO_2-SA + PAO6 nanodispersion. Finally, this dispersion was diluted to obtain nanodispersions with concentrations of 0.3, 0.2, 0.1 and 0.05 wt% in SiO_2-SA. In order to further enhance the stability time of these last nanodispersions, the same wt% of SA as of SiO_2-SA was added as surfactant.
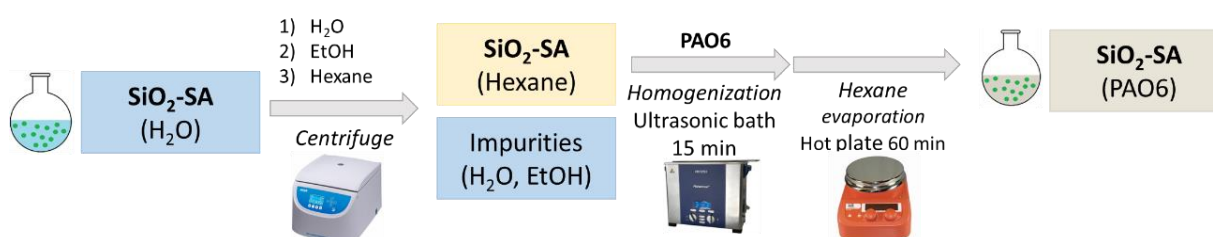
Figure 5.6 Scheme of the dispersion method

The stability of the nanodispersions was assessed by visual observation over time until sedimentation was detected. The images are shown in Figure 5.7. Just after their preparation, the SiO_2 and SiO_2-SA + SA nanodispersions presented a high transparency (Figures 5.7a and 5.7d). The nanodispersion with uncoated SiO_2 NPs sedimented after 24 h. Thus, a yellow-white turbidity appeared in the bottom of the flask (Figure 5.7b), turning more yellow and compact over time (Figure 5.7c). In contrast, the SiO_2-SA nanodispersion kept the same slightly white and transparent appearance even after 100 days (Figure 5.7f). Therefore, the nanodispersion containing the modified SiO_2 NPs showed an important enhancement of the stability compared to that containing unmodified SiO_2 NPs.
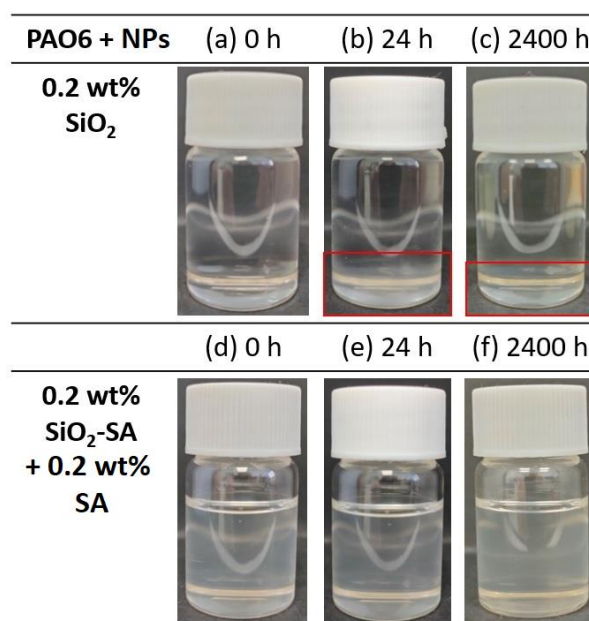
Figure 5.7 Photographs of PAO6 + 0.2 wt% SiO_2 and PAO6 + 0.2 wt% SiO_2-SA + 0.2 wt% SA dispersions at 0 h (a,d), 24 h (b,e) and 2400 h (c,f) after their preparation

5.3 THERMOPHYSICAL PROPERTIES

Density and dynamic viscosity of the base oil and the nanolubricant PAO6 + 0.20 wt% SiO$_2$-SA + 0.20 wt% SA were measured at 0.1 MPa from 5 to 100 ºC using a rotational viscosimeter Stabinger SVM3000 (Anton Paar, Graz, Austria). The experimental results are presented in Table 5.2. The density of this nanodispersion had an average absolute variation of 0.012 %, with respect to PAO6 (Table 5.2), which is lower than the density uncertainty (0.06 %) meaning that the addition of SiO$_2$-SA and SA additives does not affect the density value of PAO6 at the studied temperature range and 0.1 MPa. Regarding the dynamic viscosity (Table 5.2), the effect of both additives (SA and SiO$_2$-SA) is greater, leading to increments around 9 % and up to a 13 % at higher temperatures. Furthermore, viscosity index was also measured, which is for the nanodispersion (VI 154) 12 % higher to that of PAO6 (VI 0.138).

Table 5.2 Density (ρ) and dynamic viscosity (η) of PAO6 and PAO6 + 0.20 wt% SiO$_2$-SA + 0.20 wt% SA nanodispersion as a function of temperature, T, at 0.1 MPa

T/°C	PAO6 ρ/g cm^{-3}	0.20 wt% SiO$_2$-SA + 0.20 wt% SA ρ/g cm^{-3}	PAO6 η/mPa·s	0.20 wt% SiO$_2$-SA + 0.20 wt% SA η/mPa·s
5	0.8329	0.8328	137.9	151.3
10	0.8298	0.8297	102.8	113.1
15	0.8268	0.8267	78.15	86.19
20	0.8238	0.8237	60.36	66.73
25	0.8207	0.8206	47.55	52.67
30	0.8176	0.8175	37.70	41.86
35	0.8145	0.8144	30.40	33.84
40	0.8114	0.8114	24.84	27.71
45	0.8084	0.8083	20.54	22.95
50	0.8053	0.8052	17.17	19.22
55	0.8021	0.8021	14.50	16.26
60	0.7990	0.7989	12.36	13.89
65	0.7959	0.7958	10.63	11.96
70	0.7928	0.7927	9.207	10.39
75	0.7897	0.7896	8.040	9.102
80	0.7866	0.7864	7.070	8.041
85	0.7834	0.7833	6.262	7.063
90	0.7803	0.7802	5.582	6.300
95	0.7772	0.7770	5.008	5.659
100	0.7740	0.7739	4.521	5.111

Similarly to Chapter 4, to obtain the Stribeck curves of the rolling-sliding tribological tests at 120 °C, the dynamic viscosity of each nanolubricant and the base oil (PAO6) at this temperature is needed. For this reason, the experimental viscosities were correlated with the VFT equation [18].

5.4 Tribological results
5.4.1 Pure sliding conditions

Table 5.3 and Figure 5.9 summarize the average values of the COF for PAO6 and for the studied lubricants. All the nanodispersions (PAO6 + SiO_2-SA + SA) lead to coefficients of friction lower than that measured for the PAO6 base oil, the reductions varying from 15 to 56 %, depending on the concentration. The mass concentrations of the dispersions leading to the most significant COF reductions are (0.2 and 0.3) wt% SiO_2-SA + (0.2 or 0.3) wt% SA in PAO6. Comparing the coefficients of friction of the PAO6 + 0.2 wt% SiO_2-SA + 0.2 wt% SA nanodispersions with the PAO6 + 0.2 wt% SA mixture, the former showed a 17 % COF reduction compared to the latter. SA and SiO_2-SA NPs seem to have a synergistic effect: the reduction of COF of the combined additives (53 %) is higher than the reductions of friction obtained when only one of the additives is present, the PAO6 + SA mixture shows a 44 % reduction and the PAO6 + SiO_2-SA nanodispersion a 15 % reduction, both compared to the base oil. In addition, the SA coating on the SiO_2 NPs surfaces leads to a higher COF reduction than uncoated SiO_2 NPs, which did not have any COF reduction effect on the PAO6 base oil. Besides, the PAO6 + 0.2 wt% SiO_2-SA + 0.2 wt% SA nanodispersion has shown higher COF reduction than that of PAO6 + 0.2 wt% ZDDP mixture, which led to 33 % reduction compared to PAO6.

Table 5.3 Average coefficients of friction, COF, at 120 ºC and the expanded uncertainty, U, for PAO6 base oil and all studied lubricants

Lubricants	COF	U	Reduction % compared to PAO6
PAO6	0.1542	0.0026	
+ 0.05 wt% SiO_2-SA + 0.05% SA	0.1316	0.0021	15
+ 0.10 wt% SiO_2-SA + 0.10 % SA	0.1264	0.0014	18
+ 0.20 wt% SiO_2-SA + 0.20 % SA	0.0719	0.0015	53
+ 0.30 wt% SiO_2-SA + 0.30 % SA	0.0680	0.0003	56
+ 0.2 wt% SA	0.0864	0.0048	44
+ 0.2 wt% SiO_2	0.1554	0.0039	0
+ 0.2 wt% SiO_2-SA	0.1303	0.0063	15
+ 0.2 wt% ZDDP	0.1034	0.0022	33

5.4.2 Wear Surface characterization

The topology of the worn surfaces of the pins tested in the friction tests was analyzed using a 3D profilometer. Table 5.4 summarizes the average values of WTW, WTD and worn area and the expanded uncertainties. The WTD values are plotted in Figure 5.8 for the studied lubricants. All the nanodispersions (SiO_2-SA + SA) lead to lower WTD values than PAO6. In what regards to wear, the optimum nanolubricant leading to the highest reductions for all the parameters (55 %, WTW; 86 %, WTD; and 92 %, worn area) is the PAO6 + 0.20 wt% SiO_2-SA + 0.20 wt% SA nanodispersion.

USC
UNIVERSIDADE
DE SANTIAGO
DE COMPOSTELA

Table 5.4 Average values of the width, WTW, depth, WTD, and area of worn tracks and the expanded uncertainties, U, for PAO6 and all studied lubricants

Lubricants	WTW/ μm	U/ μm	WTD/ μm	U/ μm	Area/ μm^2	U/ μm^2
PAO6	435	10	2.60	0.19	806	65
+ 0.05 wt% SiO$_2$-SA + 0.05 wt% SA	256	14	0.99	0.12	200	32
+ 0.10 wt% SiO$_2$-SA + 0.10 wt% SA	268	19	0.55	0.05	104	18
+ 0.20 wt% SiO$_2$-SA + 0.20 wt% SA	195	17	0.35	0.06	40	9
+ 0.30 wt% SiO$_2$-SA + 0.30 wt% SA	240	18	0.51	0.07	61	12
+ 0.20 wt% SA	422	19	2.54	0.25	723	76
+ 0.20 wt% SiO$_2$	471	21	3.01	0.22	967	69
+ 0.20 wt% SiO$_2$-SA	342	14	1.82	0.21	353	44
+ 0.20 wt% ZDDP	232	12	0.64	0.11	81.2	13

In Figure 5.9 the profiles of the worn surface obtained with PAO6 and each nanodispersion (PAO6 + SiO$_2$-SA + SA) are shown. The largest groove is obtained using the base oil, and the smallest one using PAO6 + 0.20 wt% SiO$_2$-SA + 0.20 wt% SA nanodispersion. Comparing the PAO6 + 0.20 wt% SiO$_2$-SA + 0.20 wt% SA nanodispersion with the PAO6 + 0.20 wt% SA mixture, the former showed an 86 % reduction in WTD compared to the latter, which only led to a wear reduction of 3 % in WTD compared to PAO6. The reductions in WTD obtained with PAO6 + 0.20 wt% SiO$_2$-SA was also lower (30 %) than using combination of both additives (86 %), which indicates a great synergy among both additives. This trend is similar to that obtained for the COF results. Hence, the nanodispersion containing both SiO$_2$-SA and SA showed an enhanced tribological behavior. Regarding the SA coating effect on the SiO$_2$ antiwear results, the commercial SiO$_2$ NP was the only studied nanodispersion that worsen the PAO6 wear results, increasing a 15 % the WTD compared with PAO6. Furthermore, the optimal nanodispersion of PAO6 + 0.20 wt% SiO$_2$-SA + 0.20 wt% SA also has a better wear reduction capability compared to the PAO6 + 0.20 wt% ZDDP, which had a 75 % WTD reduction compared to PAO6 base oil. In view of these results, from now on only PAO6 + SiO$_2$-SA + SA nanodispersions will be considered.
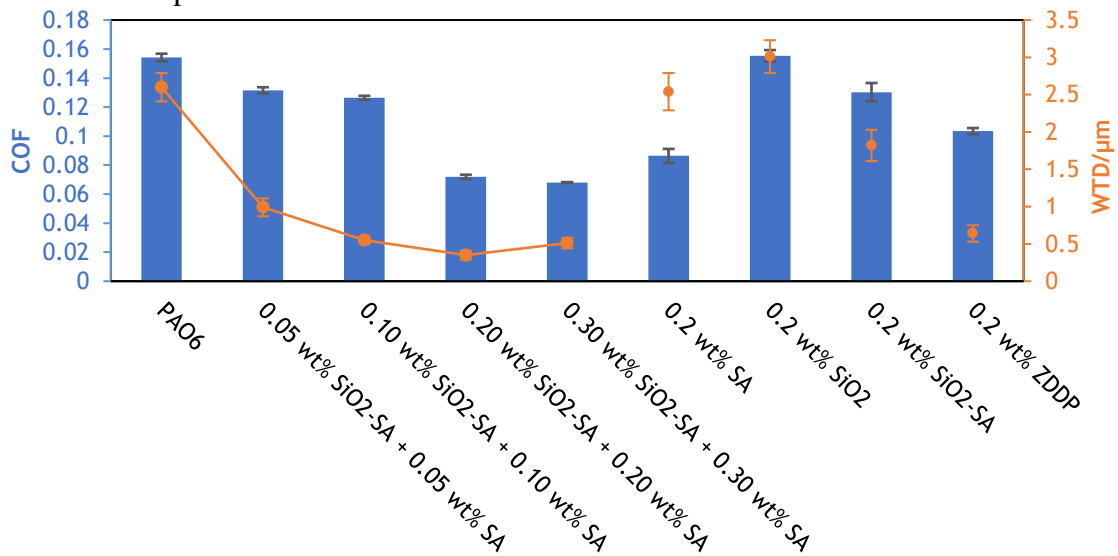
Figure 5.8 Average coefficients of friction, COF, (blue) and wear track depth, WTD, (orange) with the expanded uncertainty bars for PAO6 and the studied lubricants based on PAO6 (the orange line is a guide for the eye)
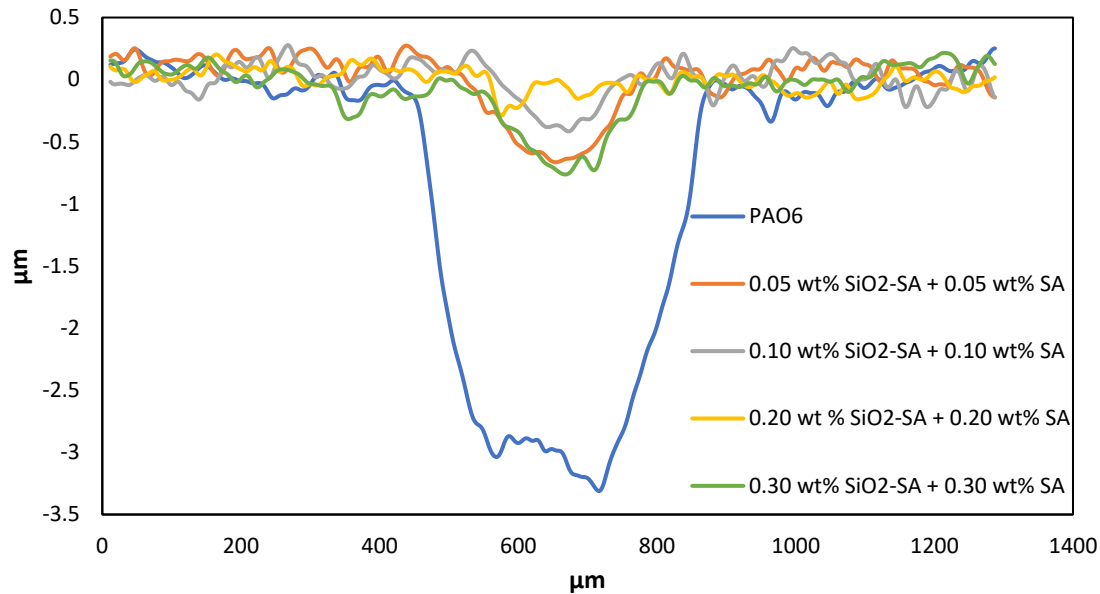
Figure 5.9 Profile images of worn tracks lubricated with PAO6 (blue) and PAO6 + wt% SiO₂-SA + wt% SA nanodispersions (0.05 wt%, orange; 0.10 wt% grey; 0.20 wt%, yellow; 0.30 wt%, green)

The arithmetic average roughness, R_a, was also measured through 3D profilometry, considering a gaussian filter 0.25 mm. In Table 5.5 the average values of R_a are plotted for all the worn surfaces lubricated with PAO6 and PAO6 + SiO₂-SA + SA nanodispersions, as well as for the unworn surface of a pin. All the nanodispersions led to worn tracks with smaller R_a than those of the unworn surface and of the worn pins lubricated with PAO6. The lowest R_a is that of the worn surface lubricated with PAO6 + 0.3 wt% SiO₂-SA being 41 % lower than that of the unworn surface, and 53 % of the worn surface lubricated with PAO6. However, 0.10 and 0.20 wt% nanodispersions exhibit very similar results with more than a 30 % reduction compared to the unworn surface and a 45 % compared to the worn surface from PAO6. Another parameter used to characterize the topology of the surfaces is the root mean square roughness (R_q), which is more sensitive to large deviations from the mean line than R_a [19]. The same trend with lubricants and pins, for R_a and R_q, have been found, as can be seen in Table 5.5.

Table 5.5 Average values of the R_a and R_q of untested pin surface, worn tracks and the expanded uncertainties, U, for PAO6 and PAO6 + wt% SiO₂-SA + wt% SA nanodispersions

	R_a/nm	U/nm	R_q/nm	U/nm
PAO6	11.2	1.4	15.3	2.4
+ 0.05 wt% SiO₂-SA + 0.05 wt% SA	8.5	0.6	10.4	0.7
+ 0.10 wt% SiO₂-SA + 0.10 wt% SA	6.1	1.0	8.8	2.5
+ 0.20 wt% SiO₂-SA + 0.20 wt% SA	6.2	1.3	7.3	1.5
+ 0.30 wt% SiO₂-SA + 0.30 wt% SA	5.2	0.7	6.2	0.9
Untested Pin	8.9	0.6	10.4	0.6

3D images of the worn tracks of the steel balls used in the friction tests are shown in Figure 5.11. The nanolubricant containing SiO₂-SA and SA as dispersant showed the lowest wear on the ball, 172.6 µm for WTW. Interestingly, the absence of SA dispersant (PAO6 + 0.20 wt% SiO₂ and PAO6 + 0.20 wt% SiO₂-SA) leads to WTW values similar or higher than that obtained with neat PAO6 base oil. However, the use of only SA as additive generated a slightly higher WTW value (201 µm) compared to the optimal nanodispersion, which is coherent with the wear results from the pins, thus a synergistic effect of both additives is observed. The ball lubricated

with PAO6 containing ZDDP as additive showed good wear reduction, although the WTW value was higher (198 µm) than that obtained for the optimal nanodispersion.
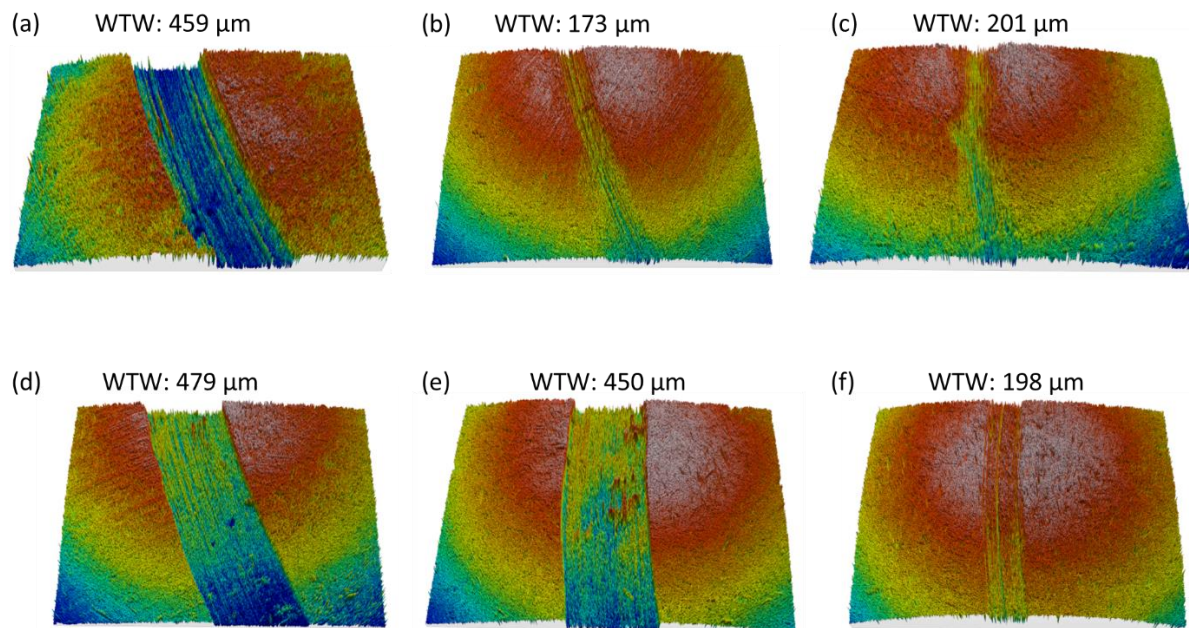
Figure 5.10 3D images of the worn ball surfaces for (a) PAO6, (b) PAO6 + 0.20 wt% SiO₂-SA + 0.20 wt% SA, (c) PAO6 + 0.20 wt% SA, (d) PAO6 + 0.20 wt% SiO₂, (e) PAO6 + 0.20 wt% SiO₂-SA, (f) PAO6 + 0.20 wt% ZDDP, and their WTW values

As regards to Raman microscopy, for the assignation of the components in the worn surface, the signals were separated using the software Project FIVE. Figures 5.12 and 5.13 show the Raman mappings of the worn tracks of pins with distinctive areas indicated with several colors corresponding to different compounds. Regarding the worn pins tested with the base oil (Figure 5.11), the presence of PAO6 (blue), as well as of iron oxides (yellow) and of carbon (green) coming from the lubricant degradation were observed (Figure 3.18). On the other hand, the Raman mapping from the 0.20 wt% SiO_2-SA + 0.20 wt% SA nanodispersion in PAO6 (Figure 5.12) indicates the presence of SiO_2 NPs (red), as well as of PAO6 or SA (blue) and of carbon (green). Regarding the blue areas in the Raman mapping in Figure 5.13, the corresponding intense peaks around 3000 cm^{-1} are characteristic C-H signals. Both PAO6 and SA have saturated alkyl chains which present very similar Raman spectra (Figure 5.13) with the most intense peaks being the 3000 cm^{-1} ones. Thus, it is not possible to differentiate those compounds in the Raman mapping of the pin lubricated with the nanodispersion. The presence of SiO_2 NPs is confirmed by the appearance of an intense and sharp peak close to 500 cm^{-1} [20]. This peak does not appear in the Raman spectrum of iron oxide, which instead presents peaks of similar intensity in the lower region of the spectrum (Figure 5.11) [21], i.e., with the addition of SiO_2-SA NPs, iron oxides were not observed. On the other hand, in the Raman spectra of the mapping of Figure 5.12, the lack of SA signal in the SiO_2 spectrum (red areas in the mapping) reveals that, during the tribo-tests, some tribo-chemical reactions occur promoted by the high both temperatures and pressures due to the friction process. Thus, these conditions cause the breaking of the bonds between SA and the SiO_2 NPs, similarly to what was found by Zhang et al. [22] for SA modified TiO_2 NPs through XPS. Assuming the same hypothesis as these authors [22], the uncoated SiO_2 NPs are easily adsorbed on the worn surface, generating a boundary lubricating film. Moreover, SA could be physically adsorbed on the steel surface during the

tribotests [23-25] and be partially removed with the hexane solvent in the cleaning process of the worn pins before the confocal Raman analysis.

Figures 5.11 and 5.12 show that the chemical components are located in the grooves formed during the tribological experiments. When adding the SiO_2-SA NPs and SA to the PAO6 lubricant the tribofilm created in the worn track is mainly composed by SiO_2 NPs and carbon, being the tribological mechanisms governed by the NPs rather than the base oil or the SA dispersant. Considering the roughness values and these Raman mappings it can be assumed that on the worn surface tribofilm formation, polishing and/or mending effects occur.
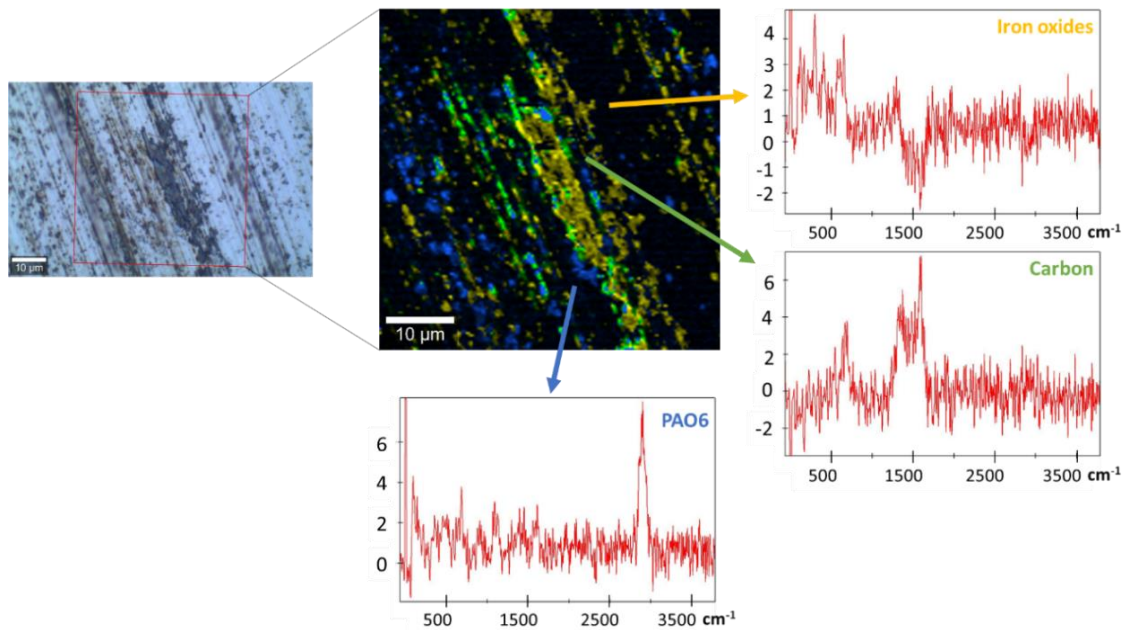
Figure 5.11 Elemental mapping and Raman spectra of worn pins tested with PAO6 base oil
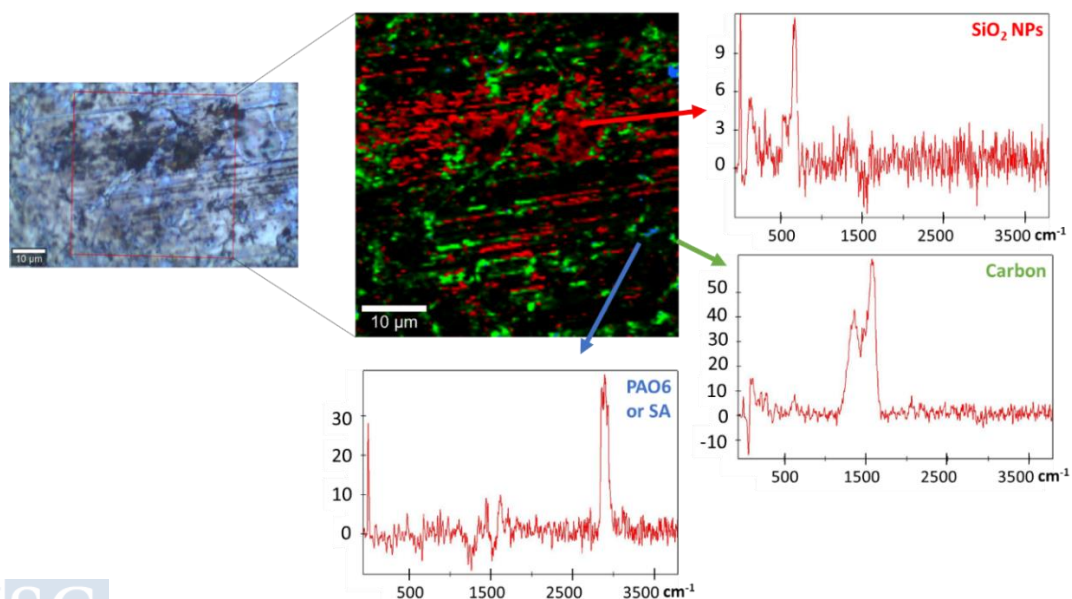
Figure 5.12 Elemental mapping and Raman spectra of worn pins tested with 0.20 wt% SiO_2-SA + 0.20 wt% SA nanolubricant
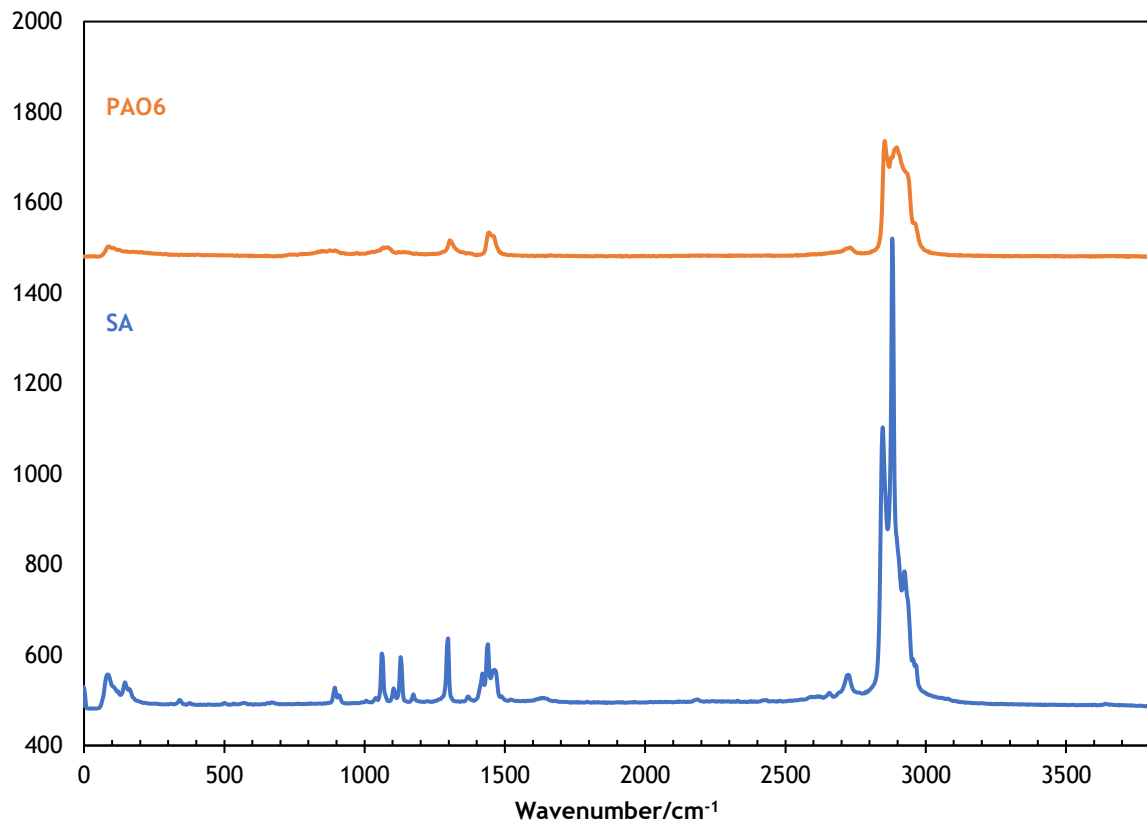
Figure 5.13 Raman spectra of PAO6 (orange) and SA (blue)

Regarding the SEM micrographs of the worn pins (Figure 5.14), an inspection of these images reveals that abrasive wear in the sliding direction is the main wear mechanism in the case of the worn surface lubricated by PAO6, with evident ploughing even at the lowest magnification (500x). This type of wear is slightly reduced when using SA as the only additive. The addition of SiO_2 or SiO_2-SA NPs reduce the grooves in the worn surface but micro-cracks on the surfaces appears. In addition, when ZDDP is used as additive to PAO6, although the wear track is considerably reduced, the surface presents similar damage. The least damaged surface is the one obtained with PAO6 + 0.20 wt% SiO_2-SA + 0.20 wt% SA, which again highlights the positive synergies between both additives, that increase scuffing resistance and reduce wear. These results agree with those obtained with profilometry for the pins.
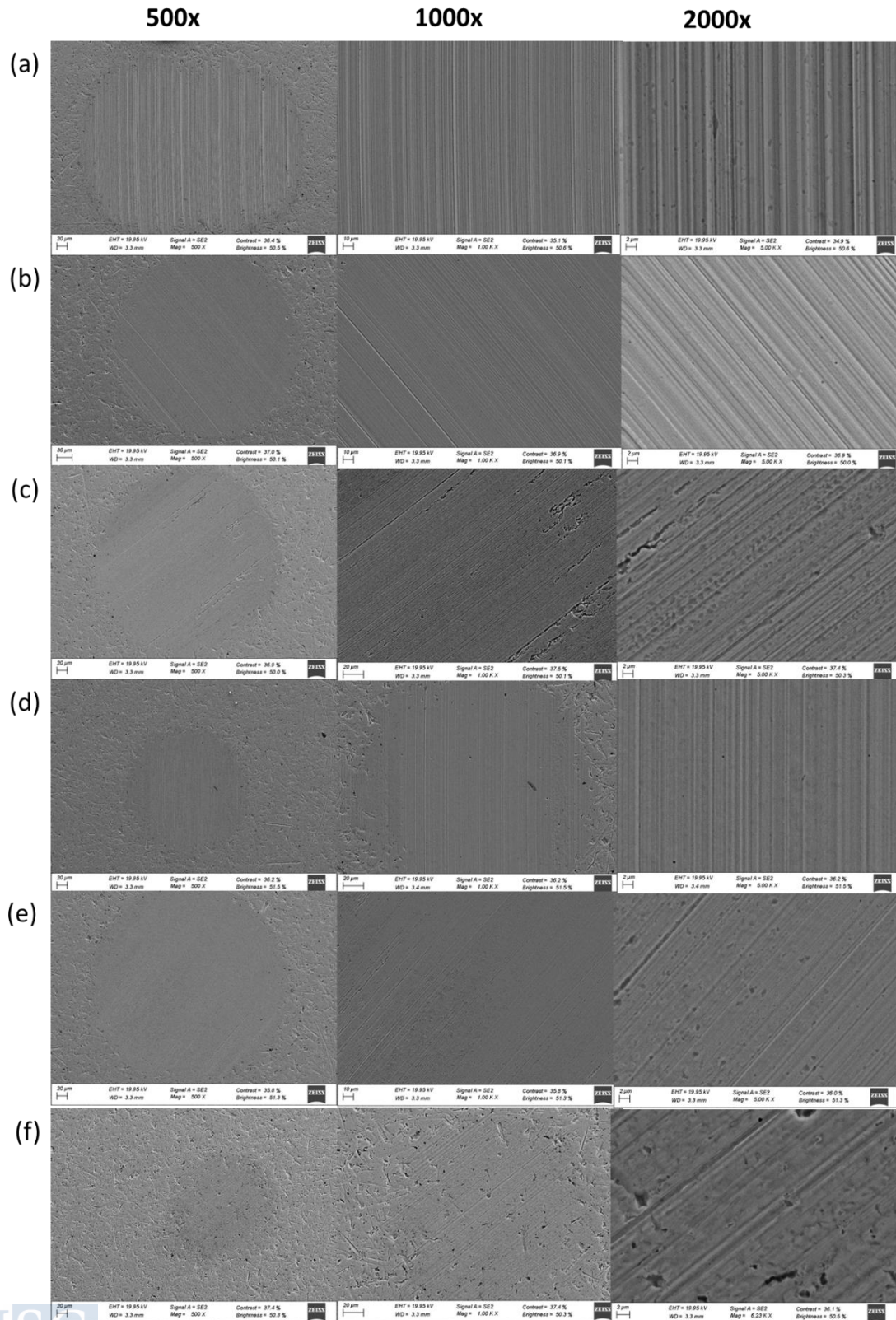
Figure 5.14 SEM micrographs at three magnifications of the worn pin surfaces lubricated by PAO6 and lubricants based on PAO6

5.4.3 Rolling-sliding conditions

Rolling-sliding tribological results obtained with PAO6 base oil and the SiO_2-SA + SA nanodispersions are presented as Stribeck curves (Figures 5.15 and 5.16).

Figure 5.15 shows the Stribeck curves for PAO6 neat oil as well as for SiO_2-SA nanolubricants using three different discs: smooth, rough 1 and rough 2 discs (see Table 2.6). As expected, ball-on-disc tests using the rough discs generate lower Λ values and consequently show higher coefficients of friction than those performed with the smooth disc. At the lowest specific lubricant film thickness, i.e., lowest entrainment speeds, the COF values are much lower with any nanolubricants (SiO_2-SA + SA) than with the PAO6 neat oil, for all discs. Therefore, the key effect of SiO_2-SA NPs is to significantly reduce the friction under boundary film when the lubricant film build-up is poor (low speeds and low Λ values).

Regarding the effect of mass concentration of nanoadditives in the tribological performance, the COF decreases as the concentration of nanoadditives rises. For this reason, the Stribeck curve of PAO6 neat oil together with that of 0.30 wt% SiO_2-SA + 0.30 wt% SA nanolubricant was plotted in Figure 5.16. This result agrees with the COF measurements achieved for the pure sliding tests, where the 0.30 wt% SiO_2-SA + 0.30 wt% SA was one of the optimal concentrations as anti-friction nanolubricant. At high entrainment speeds (right section of the Stribeck curves) and therefore large specific lubricant film thickness, the COF is quite similar for all nanolubricants and base oil.

In Figure 5.16 the coefficients of friction of PAO6 and of the nanodispersion (PAO6 + 0.30 wt% SiO_2-SA + 0.30 wt% SA) are plotted against Λ defined by eq. 2.4. In the case of the nanodispersion, it can be observed that for $\Lambda < 0.08$ (approximately) the coefficient of friction is almost constant (COF ≈ 0.04) which is typical of the boundary film lubrication regime of lubricants containing additives.

It is also clear that for $\Lambda < 0.6$ (within the boundary and mixed film regimes) there is a significant different behavior between the nanodispersion and the PAO6 base oil. In fact, in the case of the PAO6 base oil the COF increases continuously as the Λ decreases, which is typical of base oils without additives. For $\Lambda > 0.6$ the COF decreases as Λ increases, but there are no significant differences between the nanodispersion and the PAO6 base oil, meaning that the influence of the nanoadditives and of the surface roughness are no longer significant, which is typical of full film lubrication regime.

As indicated in subsection 4.4.2, the values of Λ_0 and Λ_1 depend on the contact geometry (ball-on-disc), the composite roughness parameter (σ) considered to define Λ (eq. 2.4) and the test temperature (120 °C). For PAO6 +0.30 wt% SiO_2-SA + 0.30 wt% SA nanolubricant the obtained values are $\Lambda_0 \approx 0.08$ and $\Lambda_1 \approx 0.6$.

Figure 5.16 also shows that at boundary and mixed film regimes up to $\Lambda=0.4$ the COF values using PAO6 + 0.30 wt% SiO_2-SA NPs + 0.30 wt% SA are strongly lower than those using PAO6. These COF reductions are greater than those obtained using PAO8 + 0.35 wt% TiO_2-OA NPs nanolubricant (Figure 4.16) compared to PAO8, obtained at the same conditions of load, temperature, speed and SRR. For the same conditions except temperature, Liñeira et al. [26] have also found at 30 °C, 50 °C and 80 °C lower COF reductions using TMPTO + 0.015 wt% (Fe_3O_4-OA or Nd-Alloy-OA) NPs than those obtained using 0.30 wt% SiO_2-SA NPs + 0.30 wt% SA as additive of PAO6). The strong COF reductions obtained for the latter nanolubricant in the rolling-sliding conditions (boundary and mixed film regimes) are

consistent with the high COF reductions obtained at sliding conditions (56%), due to the combined effect of the SiO2-SA NPs and the SA dispersant. Thus, the positive synergy also takes place in the rolling-sliding conditions. It can be seen in figure 1.11 that there is only a case with a higher COF reduction value (72% COF reduction in pure sliding conditions, [27]).
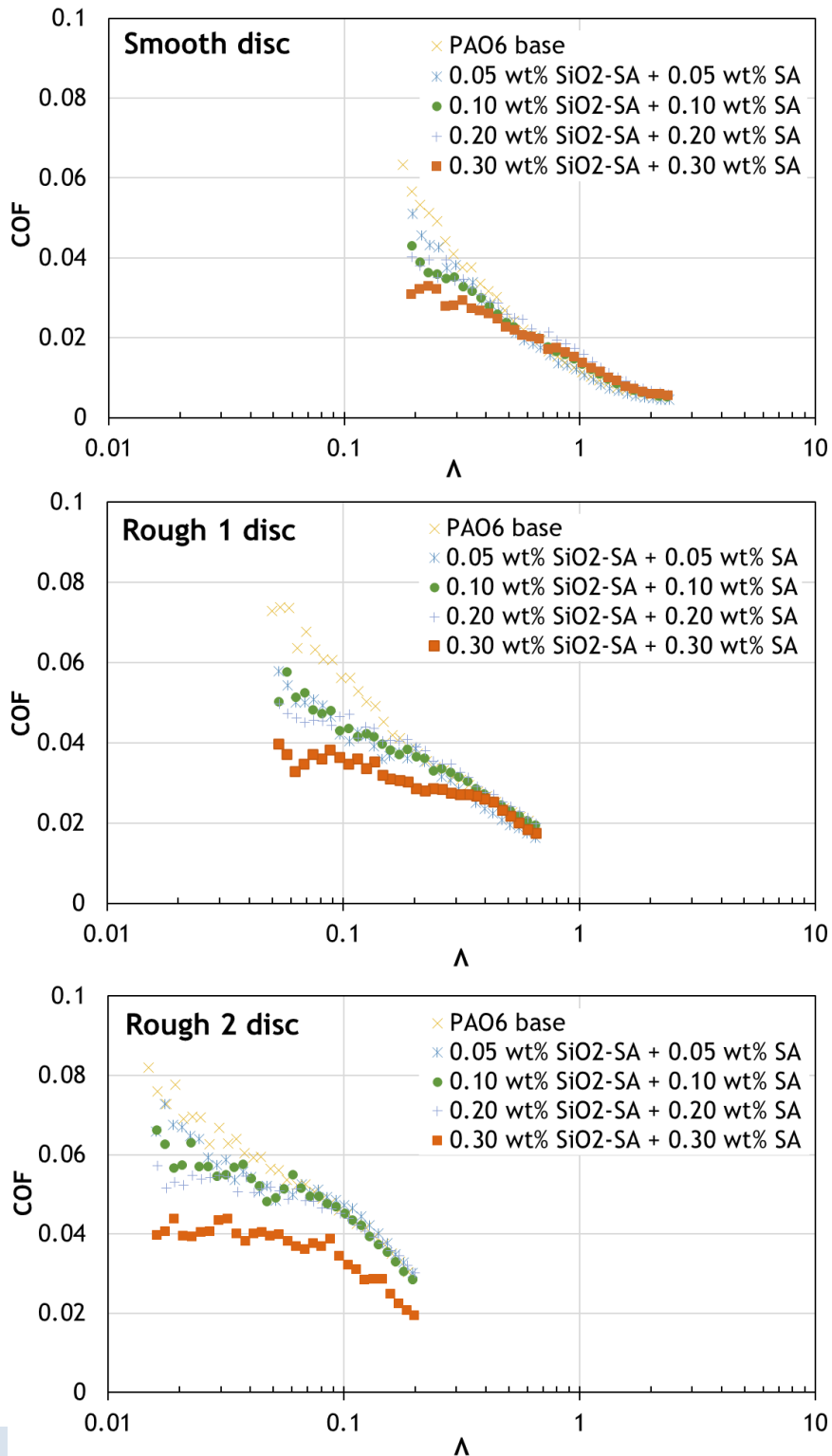
Figure 5.15 Partial Stribeck curves of PAO6 and SiO$_2$-SA + SA nanodispersions tested for three different discs at 120 °C and 5 % SRR
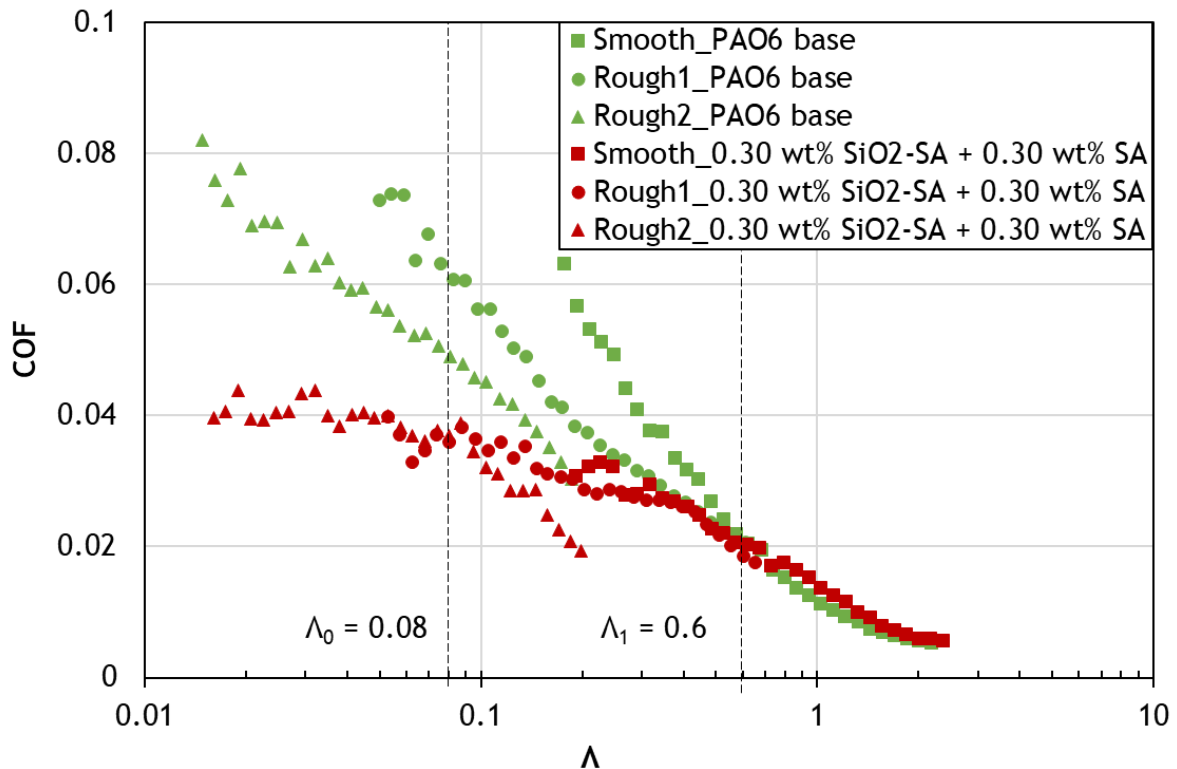
Figure 5.16 Stribeck curves of PAO6 and 0.30 wt% SiO$_2$-SA + 0.30 wt% SA nanodispersions tested for the three discs at 120 °C and 5 % SRR

5.5 CONCLUSIONS

SiO$_2$ NPs were successfully coated with SA, greatly improving the stability of their PAO6 based nanodispersions compared with that of the nanodispersions containing uncoated SiO$_2$:

- The SiO$_2$ NPs were effectively functionalized with SA via esterification reaction as was verified by FTIR analysis.
- The addition of SA as dispersant and as coating of those NPs with the same modifying agent led to an enhanced stability, reaching up to 100 days, in contrast with the commercial SiO$_2$ NPs dispersed in PAO6 that show a 24 h stability.
- Improvements in friction and wear results have been obtained at 120 °C at pure sliding conditions, with reductions up to 56 % for COF and up to 92 % for worn area, with respect to those obtained with PAO6. The optimal concentrations of NPs are 0.2 and 0.3 wt% depending on the parameter evaluated; overall, the best concentration is 0.2 wt% due to the excellent tribological reductions with less nanoparticle amount.
- There is a synergistic effect between the SiO$_2$-SA NPs and the SA dispersant, showing the combination of both additives the best reductions of friction and wear. In addition, the SA coating of NPs reduces friction and wear compared to the uncoated SiO$_2$ NPs.
- The PAO6 + 0.20 wt% SiO$_2$-SA + 0.20 wt% SA nanodispersion has proven to be an alternative to PAO6 + 0.20 wt% ZDDP.
- All the nanodispersions led to roughness reductions of the worn surfaces compared to that obtained with PAO6. This fact together with the presence of SiO$_2$ NPs in the worn surfaces shown through Raman microscopy (Figure 5.12) lead to the conclusion that polishing, mending, and tribofilm formation occur on the contact surface.

- Significant reductions of the COF were observed, not only under pure sliding conditions, but also in rolling-sliding conditions. As far as we know, this is the first time that strong friction reductions due the NPs were found under rolling-sliding conditions [26].

5.6 References

[1]   P. Wang, X. Wang, S. Yu, Y. Zou, J. Wang, Z. Chen, N.S. Alharbi, A. Alsaedi, T. Hayat, Y.J.C.E.J. Chen, Silica coated Fe_3O_4 magnetic nanospheres for high removal of organic pollutants from wastewater, 306 (2016) 280-288, https://doi.org/10.1016/j.cej.2016.07.068.

[2]   Y. Zhao, J. Li, S. Zhang, X. Wang, Amidoxime-functionalized magnetic mesoporous silica for selective sorption of U (VI), RSC Advances 4 (2014) 32710-32717, https://doi.org/10.1039/C4RA05128A.

[3]   M. Remzova, R. Zouzelka, T. Brzicova, K. Vrbova, D. Pinkas, P. Rőssner, J. Topinka, J. Rathousky, Toxicity of TiO_2, ZnO, and SiO_2 nanoparticles in human lung cells: safe-by-design development of construction materials, Nanomaterials 9 (2019) 968, https://doi.org/10.3390/nano9070968.

[4]   X. Zhang, K. Saravanakumar, A. Sathiyaseelan, Y. Lu, M.-H. Wang, Adsorption of methyl orange dye by SiO_2 mesoporous nanoparticles: adsorption kinetics and eco-toxicity assessment in Zea mays sprout and Artemia salina, Environmental Science and Pollution Research (2023), https://doi.org/10.1007/s11356-023-26173-4.

[5]   V. Cortes, K. Sanchez, R. Gonzalez, M. Alcoutlabi, J.A. Ortega, The Performance of SiO_2 and TiO_2 Nanoparticles as Lubricant Additives in Sunflower Oil, Lubricants 8 (2020) 10, https://doi.org/10.3390/lubricants8010010.

[6]   D.X. Peng, Y. Kang, R.M. Hwang, S.S. Shyr, Y.P. Chang, Tribological properties of diamond and SiO_2 nanoparticles added in paraffin, Tribology International 42 (2009) 911-917, https://doi.org/10.1016/j.triboint.2008.12.015.

[7]   D.X. Peng, C.H. Chen, Y. Kang, Y.P. Chang, S.Y. Chang, Size effects of SiO_2 nanoparticles as oil additives on tribology of lubricant, Industrial Lubrication and Tribology 62 (2010) 111-120, https://doi.org/10.1108/00368791011025656.

[8]   T. Sui, B. Song, Y.-h. Wen, F. Zhang, Bifunctional hairy silica nanoparticles as high-performance additives for lubricant, Scientific Reports 6 (2016) 1-9, https://10.1038/srep22696

[9]   T. Sui, B. Song, F. Zhang, Q. Yang, Effects of functional groups on the tribological properties of hairy silica nanoparticles as an additive to polyalphaolefin, RSC Advances 6 (2016) 393-402, https://doi.org/10.1039/C5RA22932D.

[10]   N. Zawawi, W. Azmi, M. Ghazali, Tribological performance of Al_2O_3–SiO_2/PAG composite nanolubricants for application in air-conditioning compressor, Wear 492 (2022) 204238, https://doi.org/10.1016/j.wear.2022.204238.

[11]   Y. Singh, E. Abd Rahim, N.K. Singh, A. Sharma, A. Singla, A. Palamanit, Friction and wear characteristics of chemically modified mahua (madhuca indica) oil based lubricant with SiO_2 nanoparticles as additives, Wear 508 (2022) 204463, https://doi.org/10.1016/j.wear.2022.204463.

[12]   M. Cai, R. Guo, F. Zhou, W. Liu, Lubricating a bright future: Lubrication contribution to energy saving and low carbon emission, Science China Technological Sciences 56 (2013) 2888-2913, https://doi.org/10.1007/s11431-013-5403-2.

[13]   I. Madanhire, C. Mbohwa, Mitigating environmental impact of petroleum lubricants, Springer (2016), https://doi.org/10.1007/978-3-319-31358-0.

[14]   I. Otero, E.R. López, M. Reichelt, M. Villanueva, J. Salgado, J. Fernández, Ionic liquids based on phosphonium cations as neat lubricants or lubricant additives for a steel/steel contact, ACS Applied Materials Interfaces 6 (2014) 13115-13128, https://doi.org/10.1021/am502980m.

[15]   R. Jafari, M. Farzaneh, A simple method to create superhydrophobic aluminium surfaces, Materials Science Forum 706 (2012) 2874-2879, https://doi.org/10.4028/www.scientific.net/MSF.706-709.2874.

[16]   Q. Hu, H. Suzuki, H. Gao, H. Araki, W. Yang, T. Noda, High-frequency FTIR absorption of SiO_2/Si nanowires, Chemical Physics Letters 378 (2003) 299-304, https://doi.org/10.1016/j.cplett.2003.07.015.

[17]   F. Kimura, J. Umemura, T. Takenaka, FTIR-ATR studies on Langmuir-Blodgett films of stearic acid with 1-9 monolayers, Langmuir 2 (1986) 96-101, https://doi.org/10.1021/la00067a017.

[18]   D.E. Gonçalves, J.M. Liñeira del Rio, M.J.P. Comuñas, J. Fernández, J.H. Seabra, High Pressure Characterization of the Viscous and Volumetric Behavior of Three Transmission Oils, Industrial Engineering Chemistry Research 58 (2019) 1732-1742, https://doi.org/10.1021/acs.iecr.8b05090.

[19]   E. Gadelmawla, M.M. Koura, T.M. Maksoud, I.M. Elewa, H. Soliman, Roughness parameters, Journal of Materials Processing Technology 123 (2002) 133-145, https://doi.org/10.1016/S0924-0136(02)00060-2.

[20]   G. Faraci, S. Gibilisco, P. Russo, A. Pennisi, G. Compagnini, S. Battiato, R. Puglisi, S. La Rosa, Si/SiO_2 core shell clusters probed by Raman spectroscopy, The European Physical Journal B-Condensed Matter Complex Systems 46 (2005) 457-461, https://10.1140/epjb/e2005-00274-4.

[21]   D.L. De Faria, S. Venâncio Silva, M. De Oliveira, Raman microspectroscopy of some iron oxides and oxyhydroxides, Journal of Raman Spectroscopy 28 (1997) 873-878, https://doi.org/10.1002/(SICI)1097-4555(199711)28:11<873::AID-JRS177>3.0.CO;2-B.

[22]   L. Zhang, L. Chen, H. Wan, J. Chen, H. Zhou, Synthesis and Tribological Properties of Stearic Acid-Modified Anatase (TiO_2) Nanoparticles, Tribology Letters 41 (2011) 409-416, https://doi.org/10.1007/s11249-010-9724-z.

[23]   Z. Zachariah, P.C. Nalam, A. Ravindra, A. Raju, A. Mohanlal, K. Wang, R.V. Castillo, R.M. Espinosa-Marzal, Correlation Between the Adsorption and the Nanotribological Performance of Fatty Acid-Based Organic Friction Modifiers on Stainless Steel, Tribology Letters 68 (2019) 11, https://doi.org/10.1007/s11249-019-1250-z.

[24]   S. Loehle, C. Matta, C. Minfray, T. Le Mogne, J.-M. Martin, R. Iovine, Y. Obara, R. Miura, A. Miyamoto, Mixed Lubrication with C18 Fatty Acids: Effect of Unsaturation, Tribology Letters 53 (2014) 319-328, https://doi.org/10.1007/s11249-013-0270-3.

[25]   R.R. Sahoo, S.K. Biswas, Frictional response of fatty acids on steel, Journal of Colloid and Interface Science 333 (2009) 707-718, https://doi.org/10.1016/j.jcis.2009.01.046.

[26]   J.M. Liñeira del Rio, E.R. López, M. González Gómez, S. Yáñez Vilar, Y. Piñeiro, J. Rivas, D.E.P. Gonçalves, J.H.O. Seabra, J. Fernández, Tribological behavior of nanolubricants based on coated magnetic nanoparticles and trimethylolpropane trioleate base oil, Nanomaterials 10 (2020) 683, https://doi.org/10.3390/nano10040683.

[27]   W. Shang, M. Ye, T. Cai, L. Zhao, Y. Zhang, D. Liu, S. Liu, Tuning of the hydrophilicity and hydrophobicity of nitrogen doped carbon dots: A facile approach towards high efficient lubricant nanoadditives, Journal of Molecular Liquids 266 (2018) 65-74, https://doi.org/10.1016/j.molliq.2018.06.042.

6 CONCLUSIONS AND FUTURE WORK

This work was carried out, under two national research projects, to contribute to the development of nanolubricants for two key applications: gearboxes in wind turbines and electric drivetrains systems in electric vehicles. The main conclusions of this PhD Thesis are:

1. *Selection, synthesis, and characterization of functionalized nanoadditives to design new potential nanolubricants*: From the preliminary work performed during this PhD Thesis and the in-depth analysis of the literature in the field of tribology of oil-based nanolubricants, we concluded that the best stability times and tribological results were achieved with spherical NPs with sizes below 20 nm coated with organic acids that contain aliphatic chains longer than 12 carbon atoms. Hence, spherical NPs of metal and ceramic oxides with diameters between 5 and 10 nm were selected. Two types of them were purchased, TiO_2 NPs (5 nm) and SiO_2 NPs (8 nm); and the others were synthesized, ZnO NPs (10 nm). The selected modifying agents were oleic acid (OA) and stearic acid (SA), both with an aliphatic chain of 18 carbon atoms. The selected NPs were surface modified on iMATUS laboratories, obtaining the following coated NPs: ZnO-OA, TiO_2-OA, and SiO_2-SA. The chemical modification of all the NPs weas obtained by esterification reaction, which was proven successful by subsequent analysis of the coated NPs via FTIR. To complete the characterization of these NPs, other techniques were used: the morphology was identified by SEM or TEM, and, in the case of ZnO NPs, the chemical composition was also verified by XRD.

2. *Obtaining long-term stable nanolubricants of coated nanoadditives in PAOs*: After preliminary work and the analysis of the literature on preparation methods, the evaporation method was chosen for all the nanodispersions. Without any dispersant, for the PAO40 + 0.25 wt% ZnO-OA nanolubricant a stability time of 29 days was obtained, against no dispersibility for the uncoated ZnO NPs. Using OA as dispersant at a concentration of 0.20 wt%, stability times are four weeks for the three PAO8 nanolubricants containing TiO_2-OA up to 0.35 wt%, in contrast to 48 h stability for the PAO8 + TiO_2 nanodispersions. In this PhD Thesis, the longest stability time was obtained for PAO6 + 0.20 wt% SiO_2-SA + 0.20 wt% SA, being 100 days, whereas for the PAO6 + 0.20 wt% SiO_2 the stability time was less than 24 h. The effectiveness of the coating in increasing the stability time has been verified.

3. *Evaluation of thermophysical properties of the potential nanolubricants*: the density and dynamic viscosity at atmospheric pressure and temperatures from 5 to 100 ºC, as well as the viscosity index, of the PAO base oils and the studied nanodispersions were analyzed:

- Regarding the density results, all nanodispersions studied led to low density variations with respect to the corresponding base oil. The density showed a concentration dependence: the higher the NP concentration, the higher the density value, being 0.5 % the highest average absolute deviation with respect to PAO40 for the PAO40 + 1.00 wt% ZnO-OA nanodispersion. Moreover, for these nanodispersions, the experimental results were compared with two predictive models: the Pak and Cho model provided the closest predictions, with a maximum

of 0.28 % average absolute deviation. All the other nanodispersions (PAO8 + 0.35 wt% TiO$_2$-OA + 0.20 wt% OA; and PAO6 + 0.20 wt% SiO$_2$-SA + 0.20 wt% SA) led to much lower deviations from net oil behavior (0.06 % and 0.012 %), which are close or lower than the density uncertainty of the set-up.

- For the dynamic viscosities the largest variations (around 15 %) were obtained for the nanodispersions also containing a dispersant (PAO8 + 0.35 wt% TiO$_2$-OA + 0.20 wt% OA or PAO6 + 0.20 wt% SiO$_2$-SA + 0.20 wt% SA). The nanodispersions containing only the functionalized NPs (PAO40 + ZnO-OA) showed smaller increases in the dynamic viscosity, around 4 %, showing a dependence on the concentration of the nanoadditive (similarly to the density behavior). As regard to the two predictive models applied to PAO40 + ZnO-OA, the best estimates were obtained with the Chen et al. equation (0.87 % AAD).

- The effect of the additive on the viscosity index was quite small for all the studied nanodispersions: the addition of ZnO-OA NPs resulted in a slight decrease of the viscosity index (4 %) and for the other studied nanodispersions a slight increment was found, reaching up to a 7% for PAO8 + 0.35 wt% TiO$_2$-OA + 0.20 wt% OA.

4. *Evaluation of the influence of concentration, type of functionalized nanoadditive, dispersant and comparison with commercial additives on the tribological behavior under pure sliding conditions*: All the tests performed under pure sliding conditions were carried out at high temperatures, 80 ℃ for lubricants containing PAO40 and 120 ℃ for those containing PAO8 or PAO6, and for sliding distances of 180 m for the former and 340 m for the latter. All other parameters (speed, distance, tribo-contact materials) remained constant. The coefficient of friction and wear parameters vary according to different specifications such as:

- Concentration effect: all the nanodispersions studied showed optimum concentrations at which the highest friction or wear reductions were obtained. For ZnO-OA and TiO$_2$-OA nanodispersions, the highest reductions of friction and wear were obtained at the same optimum concentration (0.25 wt% ZnO-OA and 0.35 wt% TiO$_2$-OA), whereas for SiO$_2$-SA nanolubricants, the highest reduction for COF corresponds to the optimum concentration 0.30 wt% SiO$_2$-SA and for all the wear parameters was 0.20 wt% SiO$_2$-SA. At the optimum concentrations, the COF reduction goes from 25 % (for ZnO-OA NPs) to 56 % (for SiO$_2$-SA NPs + SA), and the WTD reductions from 65 % (for TiO$_2$-OA + OA) to 86 % (for SiO$_2$-SA NPs + SA).

- The effect of the modifying agent was evaluated in the case of PAO6 + 0.20 wt% SiO$_2$-SA + 0.20 wt% SA nanodispersion. The corresponding unmodified SiO$_2$ did not improve the antifriction capability of the base oil. The SA coating was shown to improve the antifriction capability of the nanoparticle with a friction reduction of 15% compared with the COF of the nanodispersion containing unmodified SiO$_2$ NPs. Furthermore, uncoated SiO$_2$ NPs worsen wear compared to PAO6, whereas the SiO$_2$-SA NPs improve the antiwear capability of the base oil: 22 % in WTW, 30 % in WTD, and 50 % in cross-sectional area.

- The effect of the dispersant in the PAO6 + 0.20 wt% SiO$_2$-SA nanolubricant was also determined experimentally. The PAO6 + 0.20 wt% SA reduced the COF by up to 44 % compared to PAO6, but only reduced WTD by 2 %. In addition, the PAO6 + 0.20 wt% SiO$_2$-SA + 0.20 wt% SA nanolubricant reduced COF by up to 45 % compared to PAO6 + 0.20 wt% SiO$_2$-SA, and by 65 % WTD. Hence, there is a synergistic effect between the SiO$_2$-SA NPs and the SA dispersant, with the combination of both additives showing the greatest reductions of friction and wear.

- Furthermore, the tribological performance of PAO6 + 0.20 wt% SiO_2-SA + 0.20 wt% SA nanolubricant was compared with that of PAO6 + 0.20 wt% ZDDP, showing that the former lubricant led to the following reductions with respect to the latter: 30 % in COF, 16 % in WTW, 45 % WTD, and 51 % in cross-sectional area. Thus, the combined use of SiO_2-SA NPs and SA has proven to be an alternative to ZDDP.

5. *Study of the tribochemical processes occurring in the interface between the nanolubricant and the worn lubricated surfaces*: to identify the tribological mechanisms, the roughness and the mapping composition of the worn areas were analyzed using 3D profilometry and confocal Raman microscopy, respectively. For the nanolubricants at the optimal concentration, the R_a values of the worn pins were lower than that of the pin lubricated with the corresponding base oil and also lower than that of the unworn surface. Hence, the three NPs lead to polishing and/or mending mechanisms. According to the confocal Raman microscopy results, the presence of NPs is observed in the mappings, through the identification of OA (distinguishing it from PAOs due to its double bond) or through the presence of peaks corresponding to the NPs (SiO_2). During the tribotests, the NPs are also adsorbed on the rubbing surface through tribofilm formation. Due to the sphericity of all the used NPs, it is likely that rolling mechanism occurs at boundary conditions. Furthermore, for the PAO40 + ZnO-OA nanolubricant, it was proven by ICP-MS that the amount of Zn present in the sample after the tribological test was lower than before, i.e., part of the ZnO-OA NPs is adsorbed on the steel surface.

6. *Evaluation of the tribological behavior of EV nanolubricants under rolling-sliding conditions*: From the Stribeck curves obtained for PAO8 + TiO_2-OA +OA and PAO6 + SiO_2-SA + SA nanodispersions at 120 ºC and with a SRR of 5%, the conditions of lubrication regimes were identified. In the case of the optimal nanolubricants, PAO8 + 0.35 wt% TiO_2-OA + 0.20 wt% OA and PAO6 + 0.30 wt% SiO_2-SA + 0.30 wt% SA, boundary behavior occurs up to the specific film thickness value, Λ, of 0.07 for the first one, and 0.08 for the latter, whereas the mixed regime appears from 0.07 to 1, and from 0.08 to 0.6, respectively. For the last nanolubricant important friction reductions up to $\Lambda=0.6$ were found. Up to our knowledge so strong reductions have not been reported in the literature, in similar sliding-rolling conditions. The reductions found at sliding-rolling conditions is coherent with the 56% COF reduction found in pure sliding conditions which is due to the combined effect of the SiO_2-SA NPs and the SA dispersant. Taking into account the tribological and stability results PAO6 + 0.20 wt% SiO_2-SA + 0.20 wt% SA nanolubricant is the best nanolubricant designed in this PhD Thesis.

Taking into consideration the above conclusions, the following suggestions are proposed as future work:

1. 1. Based on the literature review presented in Chapter 1, NPs of diameters between 5 and 10 nm were analyzed in this PhD Thesis. It is needed to analyze even smaller NPs, such as carbon dots or other types of quantum dots.

2. The chemical modification of the NPs surface with amphiphilic molecules has been shown to improve stability in all the studied cases, further studies with different modifying agents are needed. Moreover, the synthesis of the NPs prior to (or at the same time as) the modification reaction instead of using commercial NPs should be further investigated to avoid aggregation and thus the stability of the nanodispersions.

3. The addition of SA as a dispersant showed an interesting synergy with the SiO$_2$-SA nanodispersion in PAO6; an in-depth study of this type of synergies of dispersants (amines or organic acids) and coated NPs (with the same amines or organic acids) should be performed.

4. NPs of metal and ceramic oxides have proven to be excellent antifriction and antiwear additives in PAOs, the combination of two or more of these NPs should be considered to search possible synergies. Additionally, the tribological study of these kind of NPs in formulated oils should be performed, especially with the SiO$_2$-SA NPs.

5. For the development of lubricants for gearboxes for wind turbines, additional tribological (elastohydrodynamic lubrication, Stribeck curves, film thickness and friction torque) experiments with loads and speeds conditions similar to those of these gearboxes should be envisaged. In addition, compatibility with other additives and with other materials as well as the oxidative resistance of the formulated nanolubricants should be evaluated. The environmental effect of PAO40 + ZnO-OA should also be investigated.

6. For the development of lubricants for electric drivetrains, it is needed to analyze other properties that were not considered as specific objectives of this PhD Thesis, such as thermal or electrical conductivities of the nanolubricants or the compatibility with components of the transmission system like copper or polymers. The toxicity of these new nanomaterials should also be investigated.

APPENDIX A. PUBLICATIONS AND CONFERENCES

List of publications used in this thesis with quality index and publication rights

1. Mariño, F., López, E. R., Arnosa, Á., Gómez, M. A. G., Piñeiro, Y., Rivas, J., Álvarez-Lorenzo, C., & Fernández, J. ZnO nanoparticles coated with oleic acid as additives for a polyalphaolefin lubricant. *Journal of Molecular Liquids*, **2022**, 348, 118401. https://doi.org/10.1016/j.molliq.2021.118401 **Research article**, ELSEVIER, ISSN; 0167-7322, EISSN: 1873-3166, Open Access

Journal quality index:

- Journal Rank (JCR in 2022): Physics, Atomic, Molecular & Chemical, 4/35 Q1 (6.0)
- Field-weighted citation impact*: 4.37
- Number of citations (publication): 16 (25/08/2023)

* Field-Weighted Citation Impact shows how well this document is cited when compared to similar documents. A value greater than 1.00 means the document is more cited than expected.

Publication rights:

2. Liñeira del Río, J. M., Mariño, F., López, E. R., Gonçalves, D. E., Seabra, J. H., & Fernández, J. Tribological enhancement of potential electric vehicle lubricants using coated TiO₂ nanoparticles as additives. *Journal of Molecular Liquids*, **2023**, *371*, 121097. https://doi.org/10.1016/j.molliq.2022.121097 **Research article**, ELSEVIER, ISSN; 0167-7322, EISSN: 1873-3166, Open Access

Journal quality index:
- Journal Rank (JCR in 2022): Physics, Atomic, Molecular & Chemical, 4/35 Q1 (6.0)
- Field-weighted citation impact*: 4.69
- Number of citations (publication): 3 (25/08/2023)

Publication rights:

3. Mariño, F., Liñeira del Río, J. M., López, E. R., & Fernández, J. Chemically Modified Nanomaterials as lubricant additive: time stability, friction, and wear. *Journal of Molecular Liquids*, **2023**, 382, 121913. https://doi.org/10.1016/j.molliq.2023.121913 **Review article** ELSEVIER, ISSN; 0167-7322, EISSN: 1873-3166, Open Access
Journal quality index:
- Journal Rank (JCR in 2022): Physics, Atomic, Molecular & Chemical, 4/35 Q1 (6.0)
- Field-weighted citation impact*: 4.69
- Number of citations (publication): 1 (25/08/2023)

Publication rights:

4. F. Mariño, J. M. Liñeira del Río, D. E. P. Gonçalves, J. H. O. Seabra, E. R. López, J. Fernández. Effect of the addition of coated SiO_2 nanoparticles on the tribological behavior of a low-viscosity polyalphaolefin base oil. *Wear*, **2023**, 350-351, 205025. (Open Access) https://doi.org/10.1016/j.wear.2023.205025 **Research article**, ELSEVIER, ISSN; 0043-1648, EISSN: 1873-2577

Journal quality index:
• Journal Rank (JCR in 2022): Engineering, Mechanical, 23/135 Q1 (5.0)
• Number of citations (publication): 0 (25/08/2023)

Publication rights:

5. F. Mariño, J. M. Liñeira del Río, E. R. López, J. Fernández. Influence of the nanoparticle coating agent on stability time and tribological performance on potential e-transmission nanofluids, *Proceedings of the eighth "International Conference on Lubrication, Maintenance and Tribotechnology", LUBMAT 2023*, Preston, UK, 17th to 19th of July 2023.

RE: authorisation of the publisher for the use of the tables of a procceeding in a Thesis

LUBMAT Conference <LUBMAT-Conference@uclan.ac.uk>
Vie 11/08/2023 13:58
Para:FERNANDEZ PEREZ JOSEFA <josefa.fernandez@usc.es>;Ian Sherrington <ISherrington@uclan.ac.uk>
CC:MARIÑO FERNANDEZ FATIMA <fatima.marino.fernandez@usc.es>;LOPEZ IGLESIAS ENRIQUETA <enriqueta.lopez@usc.es>

Hello Josefa,

Thank you for your enquiry.

I am pleased to confirm that we give authorisation for the use of the material in your LUBMAT paper in a thesis in the manner outlined in your email below.

Best regards,

The LUBMAT team.

Complementary publications

6. Villamayor, A., Guimarey, M. J., Mariño, F., Liñeira del Río, J. M., Urquiola, F., Urchegui, R., Comuñas, P. M. J., & Fernández, J. High-Pressure Thermophysical Properties of Eight Paraffinic, Naphthenic, Polyalphaolefin and Ester Base Oils. *Lubricants*, **2023**, *11* (2), 55. https://doi.org/10.3390/lubricants11020055 **Research article**

This complementary publication evaluates the thermophysical properties at high pressure of four mineral (paraffinic and naphthenic) and four synthetic (polyalphaolefin and ester) base oils. The two PAOs are PAO4 and PAO16, which could be used as transmission fluids in EVs.

Journal quality index:
• 	Journal Rank (JCR in 2022): Engineering, Mechanical, 46/135 Q2 (3.5)

Conference contributions

1. Mariño, F., Yañez S., Gómez, M. A. G., Piñeiro, Y., Rivas, J., Fernández, J., R López, E. R., Comuñas, P. M. J.; *Estudio tribológico de dispersiones de ZnO con recubrimiento de ácido oleico en PAO 40* (poster); VII Encontro da Mocidade Investigadora. Santiago de Compostela (Spain), 27th -29th May 2019.

2. Mariño, F., Fernández, J., R López, E. R.; *Nanolubricants based on silane-coated nanoparticles using supercritical CO₂* (poster); 1º Encontro Ibérico de Fluidos Supercríticos (EIFS2020). Santiago de Compostela (Spain), 18th -20th February 2020.

3. Mariño, F., Fernández, J., R López, E. R.; *Design and characterization of functionalized nanoparticle-based lubricants* (oral presentation); 10th International Seminar on Thermodynamic Engineering of Fluids. Tarragona (Spain) and online, 22nd-23rd July 2021.

4. Mariño, F., Fernández, J., R López, E. R.; *Estudio tribológico de nanolubricantes* (oral presentation); IX Encontro da Mocidade Investigadora. Santiago de Compostela (Spain), 20th -22nd Jun 2022.

5. Mariño, F., Fernández, J., R López, E. R.; *Lubricantes basados en nanopartículas funcionalizadas: diseño y caracterización* (oral presentation); Thesis Pitch, iMATUS. Santiago de Compostela (Spain), 21st July 2022.

6. Mariño, F., Fernández, J., R López, E. R.; *ZnO nanoparticles coated with oleic acid as additives for a polyalphaolefin lubricant* (oral presentation); IBERTRIB 2022. Setúbal (Portugal), 6th -7th October 2022.

7. Mariño, F., Liñeira del Río, J. M., López, E. R., Fernández, J. *Reviewing Stability over Time and Tribological Performance of Non-Aqueous Lubricants containing Chemical Modified Nanoadditives* (oral presentation); IBERTRIB 2022. Setúbal (Portugal), 6th -7th October 2022.

8. Liñeira del Río, J. M., Mariño, F., Gonçalves, D. E. P., Seabra, J. H. O., López, E. R., Fernández, J.; *Tribological behavior enhancement using coated TiO$_2$ nanoparticles as PAO8 additives* (oral presentation); IBERTRIB 2022. Setúbal (Portugal), 6th -7th October 2022.

9. Liñeira del Río, J. M., Castro Currás, A., Somoza, V., Mariño, F., Guimarey, M. J. G., Comuñas, M. J. P., Fernández, J.; *Effect of SiO$_2$ and coated SiO$_2$-SA nanoparticles on the lubricant properties of a paraffinic base oil* (poster); IBERTRIB 2022. Setúbal (Portugal), 6th -7th October 2022.

10. Guimarey, M. J. G., Liñeira del Río, J. M., Mariño, F., Castro Currás, A., Somoza, V., Comuñas, M. J. P., Fernández, J.; *The role of chemical modified SiO$_2$ nanoparticles in the tribological performance of a paraffinic oil* (poster); XXVI Encontro Galego-Portugués de Química. Santiago de Compostela (Spain), 16th-18th November 2022.

11. Liñeira del Río, J. M., Guimarey, M. J. G., Mariño, F., Comuñas, M. J. P., López, E. R., Fernández, J.; *Nanolubricants stability: surface modification of nanoparticles* (poster); XXVI Encontro Galego-Portugués de Química. Santiago de Compostela (Spain), 16th-18th November 2022.

12. Mariño, F., Liñeira del Río, J. M., López, E. R., & Fernández, J.; *Influence of the nanoparticle coating agent on stability time and tribological performance on potential e-transmission nanofluids* (oral presentation); LUBMAT 2023, Preston (United Kingdom), 17th-19th July 2023.

13. Mariño, F., López, E. R., & Fernández, J.; *On the stability of non-aqueous lubricants containing functionalized nanoparticles* (oral presentation); 12th International Seminar on Thermodynamic Engineering of Fluids. Tarragona (Spain) and online, 20th-21st July 2023.

14. Mariño, F., Liñeira del Río, J. M., López, E. R., & Fernández, J.; *Effect of the size and coating agents of the NPs and the dispersion method on the stability time of non-aqueous nanofluids* (accepted as oral presentation); ECTP 2023, Venice (Italy), 10th-13rd September 2023.

Awards

Prize for 1st Thesis Pitch (iMATUS) for the oral presentation of *Lubricantes basados en nanopartículas funcionalizadas: diseño y caracterización* in Santiago de Compostela (Spain), 21st July 2022. https://imatus.usc.es/en/we-already-have-the-imatus-thesis-pitch-winners-held-on-july-21/

APPENDIX B. PRELIMINARY RESULTS

This appendix summarizes the initial steps done during this thesis. This information can be classified, depending on the type of modifying agent and reaction method, into three categories organized in Tables B.1, B.2 and B.3.

Table B.1 includes failed experiments with organic acid modifiers. This coated inorganic NPs (ZnO, Fe_3O_4, Nd alloy, and TiO_2) showed good stability times in different base oils, however, the tribological tests were not promising: the reductions of wear and/or friction were small or non-existent. On the other hand, the organic acid modification of GnP with OA and dodecyl sulfate did not improve the stability of the nanodispersions in any of the tested base oils. Therefore, no tribological experiments were performed.

Table B.1 Failed experiments of organic acid modified nanoadditives

Base oil	Nanoparticle	Functionalization	Concentration (wt%)	Failed due to
PAO40	ZnO (77 and 118 nm)*	OA	0.10, 0.25, 0.50, 0.75, 1.00	Tribology
	Fe_3O_4 (6 and 10 nm)*	OA	0.015, 0.030	Tribology
	Nd alloy (19 nm)*	OA	0.015, 0.030	Tribology
	GnP (15 µm x 15 nm)	Dodecyl sulfate + OA	0.05	Stability
TMPTO	GnP (15 µm x 15 nm)	Dodecyl sulfate + OA	0.05	Stability
	TiO_2 (6 nm)*	OA	0.10, 0.25, 0.50, 0.75, 1.00	Tribology
G II Mineral oil	GnP (15 µm x 15 nm)	Dodecyl sulfate + OA	0.05	Stability

* Synthesis and functionalization made in collaboration with the NanoMag group from the USC

Table B.2 contains the functionalizations of two commercial carbon nanomaterials (GnP and GO) and of two commercial metal oxide NPs (MgO and NiO) which were silanized with trimetoxyoctylsilane via supercritical CO_2 as the reaction solvent. In the case of GO, the silanization did not improve enough the stability and no further analysis was made. Regarding the silanized GnP nanomaterial, the functionalization sufficiently improved the stability times and a tribological analysis of different nanodispersions at various concentrations (PAO40, a mixture of PAOs and TMPTO, and a G II mineral oil) were performed. Nonetheless, the tribological results were only slightly better than those of the base oils. As to the metal oxide NPs, the silanization reaction improved the stability times for the MgO NPs, but the tribological results were poor. The two most promising nanoadditives (GnP and MgO) were tested in the EHD2 tribometer of the University of Porto. Nevertheless, behavior of the nanodispersions was very similar to those of the base oils. Moreover, the GnP and MgO nanoadditives were also silanized via supercritical CO_2 with OTS, but the results (stability and tribology) were almost identical to those obtained with the trimethoxyoctylsilane.

Table B.2 Failed experiments of silanized nanoadditives via supercritical CO_2 **

Base oil	Nanoparticle	Functionalization	Concentration (wt%)	Failed due to
PAO6	GO (1.5-2 µm x 30 nm)	Trimethoxyoctylsilane	0.5	Stability
PAO40	GnP***	Trimethoxyoctylsilane	0.007, 0.015, 0.030, 0.050	Tribology
	GO		0.04, 0.10	Stability
	MgO (35 nm)***		0.015, 0.07, 0.1, 0.25	Tribology
	NiO (20 nm)		0.15, 0.25	Stability
75% PAO40 15% PAO100 10% TMPTO	GnP	Trimethoxyoctylsilane	0.015, 0.030, 0.050	Tribology
	GO		0.25, 0.50	Stability
	MgO		0.05, 0.10, 0.25	Tribology
	NiO		0.15	Stability
	GnP	OTS	0.015, 0.030, 0.050	Tribology
	MgO		0.05, 0.10, 0.25	Tribology
TMPTO	GnP***	Trimethoxyoctylsilane	0.015, 0.030, 0.050	Tribology
	MgO***		0.05, 0.10, 0.25	Tribology
G II Mineral oil	GnP***	Trimethoxyoctylsilane	0.015, 0.030, 0.050	Tribology
	MgO***		0.05, 0.10, 0.25	Tribology

** Silanizations via sCO_2 were made in collaboration with the USC group R+D Pharma

*** These nanodispersions were measured using the EHD2 tribometer during my research stay in INEGI, Porto.

Lastly, Table B.3 compiles the results of an unfinished work about Fe_3O_4-OTS NPs, which were silanized in our laboratory through a conventional silanization reaction of OTS and commercial Fe_3O_4 NPs of two diameters. The NPs were characterized through FTIR, Raman spectroscopy, TGA, and TEM. The two-step method was used to prepare the nanodispersions of each size of Fe_3O_4-OTS NPs. The stability of the PAO6 nanodispersions was analyzed visually and using the refractometer. The silanization improved the stability, but the best maximum stability time was 3 days. Pure sliding tribological test was performed to the NPs at three different concentrations, for the same conditions used in Chapters 4 and 5. Although the COF reductions were low, the wear reductions were high, especially for the larger Fe_3O_4-OTS NPs (up to 59 % reduction of the worn area). Soon this work will be completed with an analysis of the thermal and electrical conductivity of the silanized nanodispersions, which will be performed by other members of the laboratory.

Table B.3 Summary of the results of silanized magnetite nanodispersions in PAO6 for transmissions of EVs

NPs + PAO6	Fe_3O_4	Fe_3O_4-OTS	Fe_3O_4	Fe_3O_4-OTS
Commercial diameter		8 nm		20-30 nm
Measured mean diameter (TEM)		14 nm		20 nm
Concentrations (wt%)		0.007, 0.015, 0.030		
Stability	3 h	3 days	3 h	3 days
Coupling density (per nm^2 of NP)	Not performed	17 OTS molecules	Not performed	31 OTS molecules
Optimum concentration		0.015 wt%		0.015 wt%
COF reduction		8 %		3 %
WTW reduction		14 %		20 %
WTD reduction		15 %		41 %
Worn area reduction		33 %		59 %
Ra		30 %		58 %

APPENDIX C. INDEX OF TABLES AND FIGURES

Index of tables

Index of figures

APPENDIX D. RESUMO

A triboloxía é a ciencia que estuda a fricción, o desgaste e a lubricación, e a aplicación dos seus principios ten unha gran influencia no aforro enerxético. Un 23 % da enerxía consumida no mundo débese á fricción e ao desgaste dos contactos tribolóxicos de compoñentes mecánicos. Ademais, unha redución da fricción e do desgaste suporía unha redución nas emisións de dióxido de carbono de máis de 8 000 $MtCO_2$ ao ano. Unha das formas máis efectivas de reducir a enerxía consumida na maquinaria utilizada en distintos sectores e industrias é a lubricación dos seus compoñentes móbiles. Os lubricantes son unha mestura multicompoñente formada por diferentes aceites basee e aditivos.

Segundo o Instituto Americano do Petróleo (API), os aceites basee dos lubricantes líquidos pódense clasificar en cinco grupos dependendo das súas propiedades físicas e composición. O primeiros tres grupos (I, II e III) desta clasificación son aceites base minerais. Doutra banda, o grupo IV utilízase para designar aos aceites sintéticos de tipo polialfaolefina (PAO). Finalmente, o grupo V asígnase a aqueles aceites basee que non entran dentro das outras catro categorías, como aceites nafténicos, ésteres, siliconas, glicois, ou aceites vexetais. Os aceites das distintas categorías teñen diferentes propiedades, variando a súa viscosidade, estabilidade á oxidación, biodegradabilidade, etc. A selección dun aceite basee faise en función da aplicación na que se necesita utilizar, buscando a opción máis adecuada en función da temperatura de traballo, a carga, a velocidade ou outros factores.

Un lubricante comercial contén ao redor dun 10 % de aditivos, estes engádense ao aceite base con diferentes funcións como poden ser antioxidantes, antiespumantes, antifricción ou antidesgaste, entre outras. Moitos dos aditivos tradicionais demostraron ser malos para o medio ambiente, tal como no caso do dialquilditiofosfato de cinc (ZDDP), que é un dos tipos de aditivos máis comúns para reducir a fricción e o desgaste, ademais de mellorar as propiedades antioxidantes do aceite.

Recentemente, numerosos estudos demostraron que o uso dunha pequena cantidade de nanopartículas como aditivo, tamén chamados nanoaditivos, pode mellorar as propiedades triboloxicas dos aceites base, chegando a obter mellores resultados que cos aditivos tradicionais. Estas melloras débense ao seu pequeno tamaño. Así, os nanoaditivos poden entrar na área de contacto dando lugar a mecanismos triboloxicos favorables como: rodadura, formación de tribofilm, pulido ou reparación. Un dos maiores beneficios, en comparación con outros aditivos, é a súa baixa volatilidade, de modo que é posible utilizalos en condicións de altas temperaturas sen perda do mesmo. Ademais, son máis inertes quimicamente que o seu equivalente tradicional, o que os fai máis duradeiros no aceite base. Con todo, as nanopartículas presentan limitacións na súa aplicación como aditivos de lubricantes xa que unha vez suspendidas no

aceite, as nanopartículas tenden a agregarse e sedimentar co paso do tempo, podendo chegar a xerar problemas na maquinaria.

O desenvolvemento de nanodispersións estables é pois fundamental para a súa aplicación na industria. Para evitar a agregación das nanopartículas é necesario utilizar algún método que evite as forzas atractivas de Van der Waals que actúan entre elas. Existen dúas estratexias para evitar esta agregación, a primeira é o uso de dispersantes; e a segunda é a formación dun recubrimento afín ao medio no que se vai a dispersar. O uso de dispersantes permite mellorar a estabilidade das nanodispersións pero, normalmente, non consegue estabilidade a longo prazo. Ademais, nesta estratexia cámbiase a formulación do lubricante. En cambio, o uso de axentes modificadores da superficie da nanopartícula, recubríndoa, permite manter a formulación orixinal do lubricante e, así mesmo, mellora considerabelmente a estabilidade das nanopartículas en suspensión. Existen diferentes tipos de moléculas que se poden utilizar como axentes modificantes, os máis comúns son os ácidos orgánicos, aminas e silanos. As moléculas destes compostos son capaces de reaccionar coa superficie da nanopartícula a través do seu grupo funcional polar (ácido carboxílico, amina ou silano), quedando cara ao exterior das NPs as longas cadeas alquílicas, o que permite unha mellor dispersión nos aceites base, dado que xeralmente son apolares. Na primeira etapa desta Tese Doutoral, levaron a cabo traballos preliminares con nanopartículas de óxidos metálicos e nanoplaquetas de grafeno, entre outros nanomateriais de carbono, as cales foron funcionalizadas con ácidos orgánicos ou silanizadas mediante CO_2 supercrítico. Con todo, as nanodispersións preparadas coa maior parte destes nanoaditivos non conduciron a bos resultados en estabilidade ou triboloxía, debido a factores como o tamaño dos nanomateriais ou a densidade de axuste dos axentes modificadores. Así, e tendo en conta a bibliografía analizada no desenvolvemento desta Tese Doutoral, é posible concluír que os mellores resultados, tanto para estabilidade como para triboloxía, obtéñense cando a nanopartícula utilizada é esférica, menor a 20 nm de diámetro e cun recubrimento formado por un ácido orgánico que conteña unha cadea de 12 carbonos ou superior, sendo a máis común a de 18 carbonos, habitualmente acedo oleico (OA).

Deste xeito, o obxectivo principal desta Tese Doutoral é contribuír no desenvolvemento de novos e eficientes nanolubricantes formados por polialfaolefinas e nanopartículas recubertas con axentes modificadores que melloren a súa estabilidade temporal no aceite base. Para iso, primeiramente realizáronse os ensaios previos e o estudo en profundidade da bibliografía sobre a estabilidade no tempo de nanodispersións que conteñen nanoaditivos modificados quimicamente para analizar factores como a morfoloxía, o tamaño e o tipo de recubrimento. Seleccionáronse as bases en función da aplicación para a que se deseña o nanolubricante. Escolléronse tres polialfaolefinas con diferentes viscosidades (todas proporcionadas por Repsol). A máis viscosa é a PAO40, seleccionada para a súa aplicación en multiplicadoras de aeroxeradores; as outras dúas, de menor viscosidade, son PAO8 e PAO6, e teñen a súa aplicación en transmisións eléctricas de vehículos eléctricos. A continuación, seleccionáronse as nanopartículas tendo en consideración as probas preliminares e o estudo bibliográfico antes indicados. Por todo iso, optouse por nanopartículas esféricas de diámetro medio de entre 5 e 10 nm de óxidos metálicos ou cerámicos. Exceptuando as nanopartículas de óxido de cinc (ZnO, 10 nm) que foron sintetizadas, o resto das nanopartículas estudadas (TiO_2 de 5 nm e SiO_2 de 8 nm) foron adquiridas a través da empresa US Research Nanomaterials, Inc. A síntese de nanopartículas de ZnO realizouse a partir de una sal precursora de cinc, cos parámetros de

reacción axustados para obter a morfoloxía e tamaño desexados. Outro factor analizado foi o método de preparación do nanolubricante, atopándose que o método de evaporación conduce a dispersións de longa duración.

Ao longo desta Tese Doutoral estudáronse varios axentes modificadores, e en todos os casos a cadea alifática está formada por 18 carbonos. Utilizáronse dous ácidos orgánicos, ácido oleico (OA) e ácido esteárico (SA), cuxa diferencia é a presenza ou non dunha insaturación, respectivamente. Os dous axentes modificadores adquiríronse a través da compañía Sigma-Aldrich e utilizáronse sen realizar ningún proceso de purificación posterior. A reacción entre a superficie da nanopartícula e os ácidos orgánicos é unha esterificación no medio básico. A superficie das nanopartículas de óxidos metálicos ou cerámicos, en presenza de auga se hidratan dando lugar a grupos hidroxilo que permiten as reaccións de funcionalización cos grupos polares de axentes modificadores. Así, o procedemento consiste na dispersión das nanopartículas en auga ata formar unha mestura homoxénea e na adición, no medio básico, do ácido orgánico correspondente, deixando reaccionar a refluxo durante varias horas. As nanopartículas recubertas son ZnO-OA, TiO$_2$-OA e SiO$_2$-SA.

Os aceites base e as nanopartículas caracterizáronse mediante diversas técnicas. No caso das polialfaolefinas, caracterizáronse mediante espectroscopía infravermella de transformada de Fourier (FTIR) e por microscopía confocal Raman, en ambos os casos a través dos servizos da área de Infraestruturas de Investigación (RIAIDT) da Universidade de Santiago de Compostela (USC). As nanopartículas comerciais (TiO$_2$, SiO$_2$) caracterizáronse mediante o uso de microscopio electrónico de varrido (SEM) ou do microscopio electrónico de transmisión de alta resolución (TEM), para coñecer a súa morfoloxía e tamaño, ambos os instrumentos pertencentes ao RIAIDT. Ademais, para obter máis información sobre a súa composición química, analizáronse utilizando FTIR e microscopía confocal Raman. Para o caso das nanopartículas de ZnO sintetizadas durante a realización desta Tese Doutoral, así como das nanopartículas comerciais recubertas cos distintos axentes modificantes, realizóuselles tamén caracterización con FTIR e microscopía confocal Raman. Estas dúas técnicas permítennos recoñecer se a reacción de recubrimento ocorreu correctamente mediante a interpretación dos picos e bandas que aparecen nos seus respectivos espectros e comparándoos cos das nanopartículas sen recubrir e cos dos axentes modificantes comerciais. Outra técnica que se utilizou para coñecer o grao de recubrimento das nanopartículas foi a análise termogravimétrico xa que o recubrimento orgánico degrádase termicamente a menor temperatura que as nanopartículas, o que nos permite determinar a porcentaxe en masa de axente modificante con respecto ao de nanopartículas e calcular entón a súa densidade de axuste. Ademais, no caso do ZnO recuberto con ácido oleico, realizóuselle unha análise de difractometría por raios X (XRD) para coñecer a estrutura cristalina da nanopartícula e confirmar a correcta síntese das nanopartículas de ZnO a partir do seu sal precursora.

A continuación, preparáronse as nanodispersións. O método de preparación utilizado nesta tese, e que demostrou ter bos resultados na estabilidade a longo prazo, é a mestura dunha suspensión das nanopartículas nun disolvente orgánico volátil coa polialfaolefina e a posterior eliminación do disolvente, de modo que a nanopartícula non está seca en ningún momento, evitando así procesos de agregación.

Para avaliar a estabilidade das dispersións de nanopartículas utilizáronse dúas metodoloxías. A primeira implica o estudo da estabilidade visual das nanodispersións mediante fotografías tomadas regularmente ata observar a sedimentación das nanopartículas. En canto á segunda, utilizouse a análise do índice de refracción, a 25 °C, ao longo do tempo, unha dispersión estable ten un valor practicamente constante co tempo, con todo, en caso de sedimentación das nanopartículas, obsérvase un aumento do índice de refracción co paso do tempo. A estabilidade das nanopartículas recubertas comparouse coa súa equivalente sen recubrir para coñecer o efecto deste parámetro.

Tamén realizouse a caracterización termofísica dos aceites base e algunhas das súas nanodispersións. Mediuse a densidade, viscosidade (dinámica e cinemática) e índice de viscosidade utilizando un viscosímetro rotacional con cela de medida de densidade conectada. Este viscosímetro permite medir nun rango de temperaturas de -40 a 105 °C, nesta Tese Doutoral utilizouse no intervalo de temperaturas de 5 a 100 °C, tomando un dato cada 5 °C. Comparáronse os resultados obtidos para cada polialfaolefina cos dalgunhas das súas dispersións para así poder coñecer o efecto da nanopartícula nestas propiedades. Cabe destacar que, como para unha aplicación concreta requírese un rango específico de densidade e viscosidade, é preferible que a nanopartícula que se engada como aditivo ao aceite teña o menor efecto posible nestas propiedades. Ademais, no caso do ZnO recuberto con OA en PAO40, comparáronse os resultados experimentais de densidade e viscosidade dinámica con predicións de varias ecuacións empíricas para analizar cal delas é máis adecuada para predicir o resultado experimental.

A continuación, realizouse a caracterización tribolóxica dos aceites base e as súas nanodispersións, deste xeito podemos coñecer o coeficiente de fricción para os contactos tribolóxicos en presenza do lubricante seleccionado. Nesta Tese Doutoral avaliáronse contactos aceiro-aceiro utilizando dous tribómetros: a célula tribolóxica T-PTD200 do Laboratorio de Propiedades Termofísicas e Tribolóxicas da Universidade de Santiago de Compostela, que utiliza unha configuración de bóla en tres pins, e o tribómetro EHD2 da Facultade de Enxeñería da Universidade do Porto, que ten unha configuración de bóla en disco. A célula tribométrica é un módulo dun reómetro modular da firma Anton Paar MCR 302 que utilizamos en dous reómetros do mesmo modelo, un do grupo I+D Farma e outro do grupo de Materia Branda e Biofísica Molecular. A célula tribométrica permite realizar ensaios en condicións de esvaramento puro, que son aqueles en os que só un dos compoñentes está en movemento, neste caso a bóla rota sobre se mesma entrando en contacto cos tres pins estáticos. Este equipo pode realizar ensaios a temperaturas nun rango entre -40 e 300 °C, cunha forza tribolóxica máxima de 9.43 N. Para os experimentos deseñados para multiplicadoras de aeroxeradores utilizouse unha temperatura de 80 °C, unha carga tribolóxica de 9.43 N, velocidade de esvaramento constante de 0.1 m/s e unha distancia total percorrida de 180 m. Doutra banda, nos experimentos para transmisións eléctricas de coches eléctricos, utilizouse unha temperatura maior, de 120 °C, e aumentouse a distancia percorrida a 340 m, os outros parámetros mantivéronse igual para ambos os tipos de ensaios. O segundo tribómetro, que se utilizou durante a miña estancia doutoral na Universidade do Porto, permite medir ensaios de rodadura-esvaramento, que son aqueles en os que tanto o disco como a bóla están en movemento. Este tribómetro só utilizouse para os traballos realizados dentro do proxecto de lubricantes para transmisións eléctricas de coches eléctricos. Por ese motivo, os ensaios realizáronse á mesma temperatura, 120 °C, que co

outro tribómetro. Neste caso, a forza triboláxica foi de 50 N e a velocidade de ambas as partes do contacto triboláxico variou para obter sempre unha relación esvaramento-rodadura dun 5%, estando as velocidades dentro do rango de 0.05 a 2 m/s. Estes ensaios realizáronse para obter as curvas de Stribeck do aceite base e as súas dispersións modificando a rugosidade do disco que contacta coa bóla no tribómetro. Para obter as curvas de Stribeck foi necesario obter mediante unha estimación o valor do espesor de película dos diferentes lubricantes estudados. Estas curvas permítennos coñecer o réxime de lubricación dos nosos nanolubricantes e os seus aceites base para as condicións experimentais utilizadas.

No caso dos ensaios en condicións de esvaramento puro realizados coa cela triboláxica Anton Paar T-PTD200, non só estudouse a fricción dos contactos aceiro-aceiro, senón tamén se analizou o seu desgaste tras os ensaios triboláxicos. Este desgaste estudouse mediante o perfilómetro óptico 3D da marca Sensofar S Neox da Facultade de Física da Universidade de Santiago de Compostela. Este instrumento permítenos obter información sobre a topografía (profundidade, anchura, área ou volume) da pegada de desgaste que aparece tras os ensaios triboláxicos. Tamén é posible medir diferentes parámetros da rugosidade da superficie dos pins. Outra análise realizada ás superficies desgastadas foi a obtención dun mapeado da composición química mediante microscopía confocal Raman. Pódese desta maneira extraer información sobre os mecanismos triboláxicos máis probables para os nanolubricantes en comparación co aceite base.

Así, nesta Tese Doutoral analizouse a estabilidade temporal de dispersións de polialfaolefinas con concentracións en peso entre 0.05 e 1.0 wt% de nanopartículas, observándose en todos os casos unha mellería clara con respecto á nanopartícula sen recubrir. As nanopartículas de ZnO sen recubrir non chegan a dispersarse en PAO40. Para os aceites con menor viscosidade, PAO8 ou PAO6, ademais dos nanoaditivos (TiO$_2$-OA ou SiO$_2$-SA) conteñen un dispersante (OA ou SA, respectivamente) para mellorar aínda máis a estabilidade das nanodispersiones. A nanodispersión de PAO8 con TiO$_2$-OA con 0.20 wt% de OA presenta unha estabilidade de catro semanas fronte a tan só 48 h da correspondente dispersión das nanopartículas de TiO$_2$ comerciais. No caso de PAO6 con 0.20 wt% SiO$_2$-SA e 0.20 wt% de SA alcanzouse unha estabilidade de 100 días fronte a 24 h de estabilidade para as NPs comerciais de SiO$_2$.

Doutra banda, en todos os casos estudados os resultados triboláxicos das nanopartículas recubertas son mellores que os dos aceites base. Para o caso do ZnO-OA en PAO40 a concentración óptima foi de 0.25 wt%, na que reduciu o coeficiente de fricción un 25 % e a área desgastada ata un 82 %. Así mesmo, a rugosidade media tamén diminuíu un 43 % comparado co valor obtido para PAO40. Para os lubricantes estudados con polialfaolefinas de menor viscosidade, PAO8 e PAO6, obtivéronse reducións aínda maiores. Por unha banda, estudouse o efecto do TiO$_2$-OA en PAO8, cuxa nanodispersión óptima foi a de 0.35 wt% TiO$_2$-OA reducindo o coeficiente de fricción un 30 % e ata unha 73% a área desgastada para os ensaios de esvaramento puro. Tamén se realizaron ensaios de esvaramento-rodadura nos que se observa unha redución máxima do coeficiente de fricción con respecto ao PAO8 para a nanodispersión de 0.35 wt% TiO$_2$-OA cando está en réxime de lubricación límite. No caso das nanodispersiones de PAO6 con nanopartículas de SiO$_2$-SA e SA, a concentración óptima destas nanopartículas foi de 0.30 wt% para a fricción tanto nos ensaios de esvaramento puro (56 %) como nos de esvaramento-rodadura. A concentración óptima para a redución de desgaste foi de

0.20 wt%, alcanzando un 95 % de redución na área de desgaste. Ademais, observáronse sinerxías positivas entre a nanopartícula recuberta e o dispersante SA, obtendo mesmo resultados mellores que co ZDDP.

Analizáronse os mecanismos triboláxicos que ocorren durante os ensaios de fricción de esvaramento puro. Existen distintos tipos de mecanismos dependendo de como actúe a nanopartícula no contacto triboláxico, así se clasifican como: rodadura, formación de tribofilm, reparación, cizallamento, sinterización ou pulido. Ademais, tamén pode ocorrer que a nanopartícula teña un comportamento negativo no tribocontacto, se as nanopartículas teñen unha alta dureza é posible que actúen cun mecanismo de abrasión e danen a superficie de contacto empeorando ao aceite base. Para obter información sobre os devanditos mecanismos realizáronse mapeados da composición da superficie desgastada mediante microscopía Raman confocal aos pins ensaiados nos experimentos triboláxicos de fricción, tanto a pins lubricados só con aceites base como a aqueles lubricados coa nanodispersión de concentración óptima para fricción e desgaste. Para realizar esta análise é fundamental limpar correctamente os pins para evitar ter residuos dos lubricantes que non estean realmente adheridos quimicamente á pegada desgastada; esta limpeza realízase con hexano, e secando os pins con aire quente. No caso do ZnO-OA obsérvase a presenza de OA, indicando presenza da nanopartícula, posibelmente debida á formación dun tribofilm protector. E no caso de TiO$_2$-OA e SiO$_2$-SA, obsérvase a presenza das nanopartículas coincidindo coa dirección do desgaste indicando tamén a formación dun tribofilm na pegada de desgaste.

En conclusión, esta tese cumpriu os seus obxectivos, desenvolvendo potenciais nanolubricantes baseados en NPs formuladas con PAOs modificados quimicamente con moléculas anfifílicas que melloraron a estabilidade das nanodispersiones en comparación coas correspondentes con NPs sen recubrir e reducen eficazmente a fricción e o desgaste en ensaios baixo condicións de laboratorio. Tamén se comprobou que a adición do mesmo ácido orgánico como dispersante e como axente modificador dá lugar a excelentes sinerxías para melloras triboláxicas e estabilidades duradeiras.

The main objective of this PhD thesis is to design and characterize efficient nanolubricants based on three polyalphaolefins
(PAOs) and nanoparticles (NPs) of metal oxides or ceramics coated with organic acids for wind turbine gearboxes and electric transmissions of electric vehicles. First, preliminary tests and an in-depth literature survey on the time stability and tribological behavior of nanodispersions containing chemically modified nanoadditives were performed. Then, the thermophysical and tribological properties of PAO nanolubricants containing coated NPs (ZnO-OA, TiO2-OA, or SiO2-SA)
were evaluated; in addition, possible tribological mechanisms were analyzed by confocal Raman microscopy. All the coated NPs studied improve the tribological behavior of their base oil, being the best the SiO2-SA NPs.